1-1-2013

Cross Layer Optimizations Of Integrated Networks In Underground Mines

Wisam F. Farjow
Ryerson University

CROSS LAYER OPTIMIZATIONS OF INTEGRATED NETWORKS IN UNDERGROUND MINES

by

Wisam Faraj Farjow, P.Eng.
MASc. Ryerson University, Toronto, Ontario, Canada, 2009

A dissertation exhibition presented for Ryerson University
in partial fulfillment of the
requirements for the degree of
PhD in the Program of
Electrical and Computer Engineering.

Toronto, Ontario, Canada, 2013

Author’s Declarations

AUTHOR'S DECLARATION FOR ELECTRONIC SUBMISSION OF A DISSERTATION

I hereby declare that I am the sole author of this dissertation. This is a true copy of the dissertation, including any required final revisions, as accepted by my examiners.

I authorize Ryerson University to lend this dissertation to other institutions or individuals for the purpose of scholarly research.

I further authorize Ryerson University to reproduce this dissertation by photocopying or by other means, in total or in part, at the request of other institutions or individuals for the purpose of scholarly research.

I understand that my dissertation may be made electronically available to the public.

Abstract

Cross Layer Optimizations Of Integrated Networks In Underground Mines
Doctoral Program in Electrical and Computer Engineering, Ryerson University, 2013,
© Wisam Faraj Farjow, P.Eng.

Establishing reliable communication is a difficult task in underground mines due to the extreme environmental conditions. This work proposes novel approaches and architectures to optimize the reliability, scalability and power efficiency of the communication networks in the environment of underground mines.

Our research considers an integrated network architecture with three main elements that represent the common path of information flow from the surface of the mine to remote points deep in the underground. These three main elements are as follows: the backbone networks, the wireless channel of the confined spaces and the Wireless Sensors Networks (WSN).

The objectives of enhancing the network reliability, scalability and power efficiency are globally considered for the entire integrated network. As a first step, the backbone network of the mine is optimized with intelligent algorithms for maximum stability, scalability and power efficiency. These objectives were achieved by introducing our novel Prediction-based Adaptive Equalization Algorithm (PAEA) and The Power-aware Adaptive Charging Schedule Algorithm (PACSA). Furthermore, this research introduced a novel wireless channel model to characterize the performance of the wireless systems in underground mines. The new proposed model, called "Mine Segmenting Wireless Channels Model", is utilized by the wireless network as an added layer of intelligent network capacity. Lastly, with power efficiency and conservation in mind, the performance of the WSN in the underground is optimized for power efficiency, scalability and rapid development of applications. These objectives are achieved by introducing our novel Resources-Aware Sleep Scheduling Algorithm (RASSA) for the wireless sensor networks to provide an integrated platform, where new applications in mines can be rapidly developed to suit the operational requirements of the mine.

Acknowledgments

I would like to express my sincere thanks to my supervisor Dr. Xavier Fernando for his valuable guidance, encouragement and patience. His valuable direction and friendly manner of supervising the work made this project a reality. Dr. Fernando's support and guidance for long number of years starting with my Masters studies all the way through the PhD work have positively shaped my career and created a true and a rare expertise in the field of telecommunication engineering in underground mines.

I would also like to express my sincere thanks and gratitude to my co-supervisor Dr. Kaamran Raahemifar for his continuous support, encouragements and friendly manners all the way supervising my work. I am very grateful for his hard work and long hours helping to make this work reality.

I would also like to acknowledge and thank the Department of Electrical and Computer Engineering at Ryerson University and all the professors who provided the theoretical courses for their exceptional efforts. It was all a great experience.

Dedications

Thanks Lord for blessing me
with a wonderful family
to whom this achievement is dedicated

To my wife Rasha,
and our children
Matthew and Mark

Contents

List of Figures

List of Symbols

a_T	Tunnel's width
b_T	Tunnel's Height
CG_m	The Corrected Gain of the amplifiers, in dB
$CL_{n,m}$	The longitudinal cable losses in one section of the RCN, in dB
D_m	The Gain Correction Factor, in dB
E_{ac}	The energy consumed by the sensor for the period of one time slot
E_k	The normalized total energy consumed by the sensor r_k
E_{UP}	The normalized Power-Up energy consumed by the sensor in the WSN
E_w	The Power-Up Energy consumed by the sensor in the WSN
f_1	The frequency of the lower end of the $m = 1$ band, in MHz
f_2	The frequency of the upper end of the $m = 1$ band, in MHz
f_3	The frequency of the upstream $m = 3$ band, in MHz
f_{PL}	Low Pilot Frequency, in MHz
p_e	The probability of bit error
h	The mean square root of tunnel walls' roughness
Γ	Global Satisfaction Ratio
IL	The total insertion loss of all passive in the RCN, in dB
K	The ratio between the deterministic signal power and variance of the multipath
L	Path or System loss, in dB
M	The CCK modulation factor
m	The band index in the RCN system, or number of functions in the WSN
n	The cable section index in the RCN system, or number of sensors in the WSN
T	Sleep Schedule Time-Cycle, in sec

r	Distance between the center and out conductor of the radiating cable, in mm
t	Time, in sec
$L_{n,m}$	The total loss in dB for one section of the cable, n, at frequency band m,
PG_m	The Amplifier's Predicated-Gain, in dB
PH_o	High-Pilot level at the system Head-End, dBm
PL_o	Low-Pilot level at the system Head-End, in dBm
P_{MAX}	Maximum Permissible Power in the network, in dBm
$PMAX_m$	The maximum power outputs of the upstream amplifier, in dBm
$PMIN_m$	The minimum acceptable power at the amplifier, in dBm
PM_o	Midpoint -Pilot level at the system Head-End
$POUT_m$	The output envelope power, in dBm
R_D	The RCN cable losses ratio between PL and PH frequency
R_{U1}	The Cable Loss Radio at f_1
R_{U2}	The Cable Loss Radio at f_2
R_{U3}	The Cable Loss Radio at f_3
T_s	Sampling rate, sec
V_C	Control signal voltage, in Volte
V_O	Output signal voltage, in Volte
x	Binary variable referring to the sensor mode being active or asleep
y	Binary variable referring to the mode of the sensor transition
$Z_{i,t}$	Binary variable representing sensors status
α_p	The constant of propagation
θ_k	The total energy consumed by a sensor in the WSN
σ^2	The time-average power of the received signal before envelope detection
τ_i	Stratification Ratio for individual device a_i in the network

φ_k	The total Power-Up energy consumed by the sensor in the WSN
γ	The instantaneous SNR, in dB
σ	The rms value of the received voltage signal before envelope detection, in volte

List of Abbreviations

AAS	Application Administration Sub-layer
ACS	Application Composition Sub-layer
AGC	Automatic Gain Control
AOD	Amplification On Demand
AP	Access Point
APS	Application Processing Sub-layer
ASC	Automatic Slope Control
BDA	Bi-Directional Ampliforms
BER	Bit Error Rate
CCK	Complementary Code Keying
CMTS	Cable Modem Termination System
CTE	Components Tolerance Errors
DAS	Data Administration Sub-layer
DBPSK	Differential Binary Phase Shift
DOCSIS	Data Over Cable Service Interface Specification
DPS	Data Processing Sub-layer
DQPSK	Differential Quaternary Phase-Shift Keying
DV	Distance Vector
FEC	Forward Error Correcting
FTP	File Transfer Protocol
GAF	Geographical Adaptive Fidelity
IL	Insertion Loss
ILP	Integer Linear Programming
LFT	Leaky Feeder Technology
LOS	Line-of-Sight
MAC	Media Access Control
MSHA	Mine Safety and Health Administrations
NLOS	Non-Line-Of-Sight
NSC	Network Self Configurations
NSR	Network Self Recognition
PAEA	Prediction-based Adaptive Equalization Algorithm
PACSA	Power-aware Adaptive Charging Schedule Algorithm

PDF	Probability Distribution Function
PFO	Power Feed Opportunity
PH	High Pilot
PL	Low Pilot
PLOS	Partial-Line-Of-Sight
PM	Midpoint Pilot
QoS	Quality-of-Service
RCN	Radiating Cable Networks
RF	Radio Frequency
RSL	Receive Signal Level
SMTP	Simple Mail Transfer Protocol
SON	Self-Organized Networks
TCS	Tasks Composition Sub-layer
TDMA	Time Division Multiple Access
VGA	Variable Gain Amplifier
VOD	Ventilation On Demand
VoIP	Voice over IP
WSN	Wireless Sensors Networks

Chapter 1

1. Communication Systems for Underground Mines

1.1 Introduction

Along with agriculture, mining is considered to be one of the oldest endeavors of mankind. Despite its long history, mining still maintains an important role in modern life by supporting humans with energy (e.g., coal and uranium) and valuable resources (e.g., copper, iron and gold). In the broader sense, a mine is defined as "an excavation made in earth to extract minerals," whereas mining is defined as "the activity, occupation, and industry concerned with the extraction of minerals". Mining can be generally divided into these two groups according to the excavation type: 1) Surface mining, and 2) Underground mining.

Underground mining is one of the most extreme occupations from several perspectives. First of all, mining operations are carried out in very hazardous environments. Some major hazards are in–mine vehicle accidents, roof falls, fires, explosions, toxic gases, and floods. Any accident might end up with fatalities within such environments. Secondly, when a serious accident occurs during mining operations, the emergency response for underground mines is much more difficult than those for other types of working environments. This stems from the fact that the structure of underground mines does not allow immediate response to accidents. In spite of these extreme environmental conditions, efficiency and productivity are two essential concerns that must always be maintained during mining operations [1].

Communication is the intersection point for all of the aforementioned concerns and considerations, since it is used at every stage of mining operations. Day–to–day operations, extracting and moving the product are all handled with the aid of communications, which increases productivity. The vital importance of communication for underground mining is most

evident when an accident occurs. Information flow, including coordination of the workers and locating them, is carried out by communications during emergency conditions [2, 3].

1.2 Integrated Network Architecture

In general, the objective for the communication systems in the mines is to provide links of communications among points on the surface of the mine and points within the confined spaces of the underground galleries. Figure 1.1 shows the main components of a typical communication network in mines. As we are optimizing the entire network, this block diagram will be repeated a few times in this research to highlight the major areas of the optimizations.

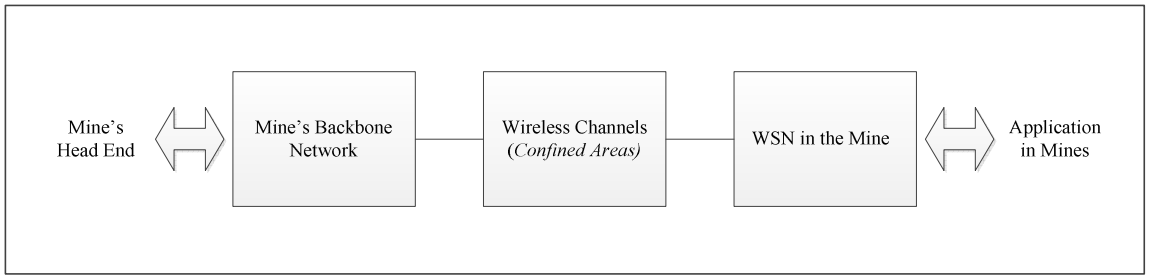

Figure 1.1: Networks' Components in Underground Mines

An interesting characteristic of underground mines is that the environment is dynamic. As long as products are taken out, mines expand. From the general perspective of communications, expansion of a mine means that the coverage area of communications will also expand. Thus, the expansion of the operating environment necessitates having a bigger communication infrastructure. Specifically, when radio communication is considered, the dynamic operating environment creates extra challenges to communication. The dynamic operating environment introduces not only the coverage problem, but also a change in radio propagation behavior since radio signals are prone to changes in the physical environment. Apart from general characteristics of underground mines, there are some other characteristics peculiar to each mine. First and foremost, mines differ from each other by the minerals (e.g., coal, rock, or iron) excavated. This is very important from the perspective of radio communications, since the electromagnetic characteristics of each mineral, such as dielectricity and conductivity, are different. In addition to the type of mineral extracted, the style of excavation might differ from one mine to another. For instance, some mines are excavated by leaving pillars to support the roof of the mine, whereas others are excavated through "long-wall mining", without any pillars. The difference between

excavation styles is an important factor in both the installation of the communication infrastructure and the behavior of radio propagation inside mine galleries. Structures of the upper layers of underground mines are not the same either. Therefore, the physical characteristics of underground mines have a great impact on which communication system will be selected for underground mining.

In our study for the underground mines system, we have built our analyses and research on a system architecture that is an integrated combination of wired and wireless networks, as shown in Figure 1.2. This integrated network is constructed from Radiating Cable Networks (RCN) and Wireless Sensors Networks (WSN). This selection was based on both the popularity of RCN which commonly provide communication services in underground mines and the promising new wireless technology of WSN.

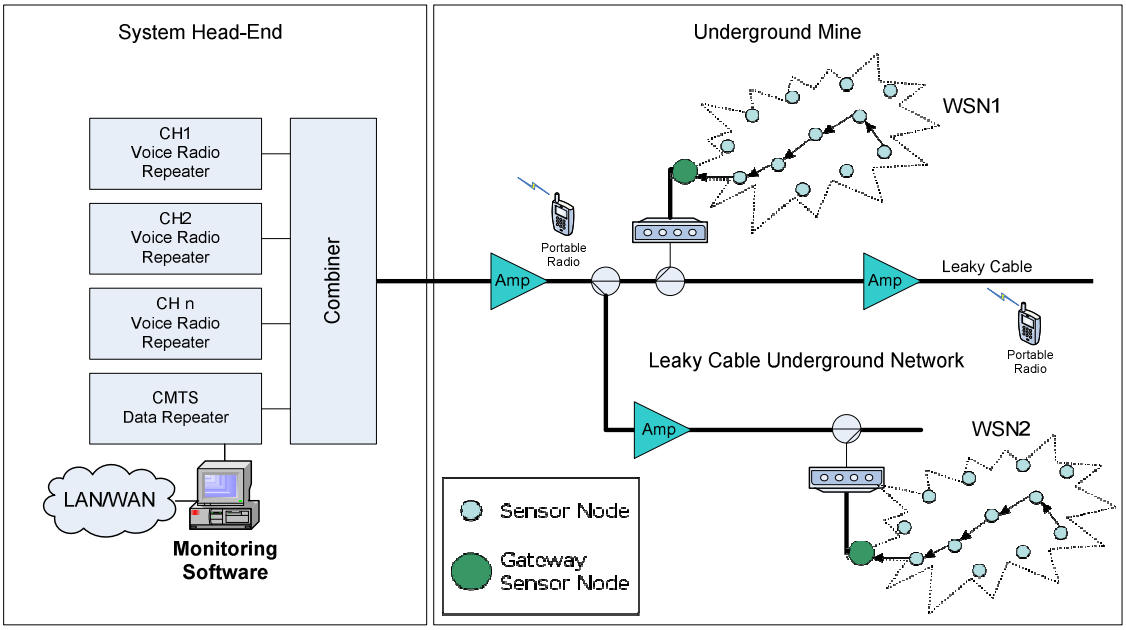

Figure 1.2: Integrated Network for Underground Mines

1.3 Challenges of Current Systems

Deploying reliable communication systems in mines is a challenging task due in part to the unique and difficult environments of the underground mine. One of the challenges that are addressed in our research is the propagation channels in the mine. Due to the randomized structure and roughness of the mine, predicting the performance of a system is a difficult process. Physical phenomena such as multipath transmissions, reflections, diffractions and scattering are among the challenges in characterizing the wireless channels in mines. The second challenge is the availability of power as well as the permissible amount of power that can be safely distributed in the mine networks. In our research this very critical area is exposed, and novel solutions are presented to safely prolong the life of the network in the mine. The third main challenge addressed in our research is the scalability of the network in the mines. To respond to the dynamic nature of the mine, the networks are required to grow constantly with the mine. Therefore, the networks in the mine are required to be reliably self-organized, scalable and dynamic with respect to the mine's ever-changing size and layout. These major challenges are presented in the sub-sections that follow.

1.3.1 Wireless Channel Characteristics

The wireless channel characteristics in mines are different from those in free space because of the harsh underground environment. This is due to physical phenomena such as severe signals' reflections, scatterings and diffractions in the confined spaces of the underground mines [4, 5]. The most important factor in characterizing the wireless channels in the mines is the randomized and irregular shapes of these environments. Underground mines have no definite size and shape. Based on the physical structure, areas in the mine can be divided into the following two major areas: a) open areas where the extraction activities take place and b) tunnel areas, which include passageways and shafts.

Many researchers have investigated the characteristics of the underground mines wireless channels based on mine shapes and layouts. Few studies have characterized the wireless channels in the open areas of the mines by utilizing generic models, such as Ray-Tracing techniques. Other studies have analyzed the wireless channels in the tunnel areas (canonical areas) by utilizing the theories of the guided wave propagation model. None of the previous works have resulted in a comprehensive and generic channel model for all the confined areas of mines. In this study, we

are proposing a comprehensive approach to characterize the performance of wireless communication systems in the underground. This approach is presented in detail in Chapter 6.

1.3.2 Power Limitations in Underground Mines

The network life is a primary consideration in the design of any communication system in the underground. Given the harsh environment and complex structure of the mine, the availability of the power is restricted. For the WSN for example, the nodes of the network operate on batteries installed in the units. It is impractical to replace or recharge the batteries frequently in such a complex structure and operation in the mines [6]. One major power conservation technique in wireless sensor networks is to design adaptive sleep schedules to minimize the energy consumption. However, a sensor in sleep mode is not able to communicate; therefore, it affects the operations at both the network layer and the application layer. Thus, a cross-layer sleep scheduling design is desired to devise sleep scheduling, which considers the requirements at other layers such as sensing coverage, delay efficiency, energy consumption and network connectivity. For the backbone networks of the mines, the cost of operating such networks as the RCN in the underground mines can be very expensive. This cost is due the high power consumption of the active components such as the repeaters and bi-directional amplifiers. Furthermore, this equipment is powered directly from the radiating cable itself. This means that the power signal (i.e. DC power) that exists in the radiating cable can be of high magnitude. Many regulations have been established to control the permissible amount of power in the radiating cable. For example, the regulating agency, Mine Safety and Health Administrations (MSHA), dictates very stringent rules for the safe system deployments in North American coal mines. One of these stringent regulations is limiting the magnitude of allowable power in the systems to absolute minimum values. The constraint in allowable power is one of the most difficult challenges for powering underground communication systems. Therefore, solutions must provide reliable and efficient power utilizations for the underground mine systems. Chapter 5 presents a novel algorithm for optimizing the power consumption of the RCN and Chapter 7 presents a new approach for optimizing the power utilization of the WSN in the mines.

1.3.3 Mines' Networks Scalability and Stability

As mentioned before, the environments of the mines are dynamic. Mines expand on a daily basis as long as the ore is taken out. The backbone networks in mines are required to be adaptive and scalable to the mine's expansion. Therefore, the daily expansions in these networks as more

cables and branches are added to the systems require automatic and intelligent methods for loss compensations and expansions. Equalization circuits have been introduced to automatically compensate for the changes in the networks, such as the variations in the levels of Radio Frequency (RF) signals. The quality of the radio communications may vary with the level variations in the signals traveling through the networks in the mine. In the case of the RCN, variations in signal level can be caused by temperature variations, which change the longitudinal loss characteristics of the cable. The level variations can also be caused by external noise generated by machinery in the mines. Many equalization algorithms and schemes for the Automatic Gain and Slope Control (AGC/ASC) systems have been developed to overcome the problems of level variations and slope corrections in the backbone networks of the mines; however, these approaches have not offered fully reliable system performance. The most common approach in deploying AGC/ASC is by utilizing reference RF carriers normally referred to as "pilots." These reference pilots propagate through the entire system and are used by each amplifier as a measuring tool to correct the gain and slope of the amplifier.

One of the major scalability problems in the existing systems is due to the stability of the AGC circuits. Most of the systems utilize AGC/ASC circuits based on closed loop gain topology. The AGC loop depicted in Figure 1.3 consists of a Variable Gain Amplifier (VGA), a peak detector, and a loop filter. The AGC loop is generally a nonlinear system, having a gain acquisition settling time that is dependent on the input signal level.

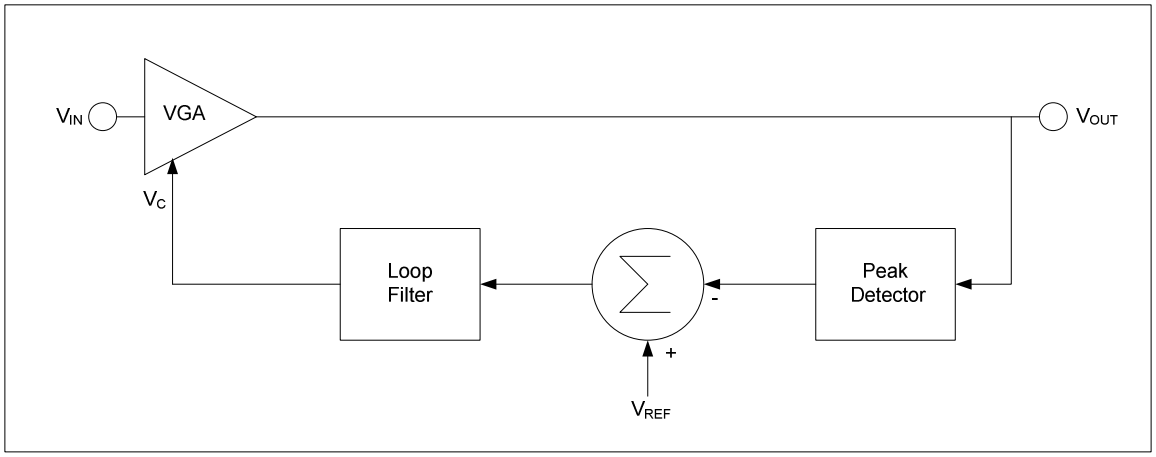

Figure 1.3: Closed Loop Automatic Gain Control Circuit

In general, the time to adjust the gain in response to an input amplitude change should remain constant, independent of the input amplitude level and, hence, the gain setting of the amplifier. Achieving a constant gain settling time permits the AGC loop's bandwidth to be maximized for fast signal acquisition while maintaining stability for all operating conditions. In actual practice, the AGC loop time constant of each amplifier differs, due to the tolerances in component values. Therefore, overshoot is evident in cascaded amplifier systems. The magnitude of the overshoots increases with the number of amplifiers in the system. This implies that the stability of the cascade decreases as the number of AGC/ASC amplifiers used increases. As a result, signal levels in the cascade exhibit random fluctuations. Transients that are to some degree repetitive cause periodic variations in levels that affect the stability of the entire system.

Another problem in most of the current RCN is the misleading reference pilot level. From the system point of view, reliance on the reference pilots by the equalization circuits creates major problems, especially for multi-branched large leaky cable systems. In these types of systems, multiple reference pilot generators must be installed at the system head-end and at the end of each branch in the system, as shown in Figure 1.4. At the points of the system branching where the pilot carriers from each branch superimpose, the accuracy of detecting the reference pilots are affected by the superimposition of multiple pilots. This, of course, affects the operations of the equalization circuits in the subsequent amplifiers and it results in unstable system operations.

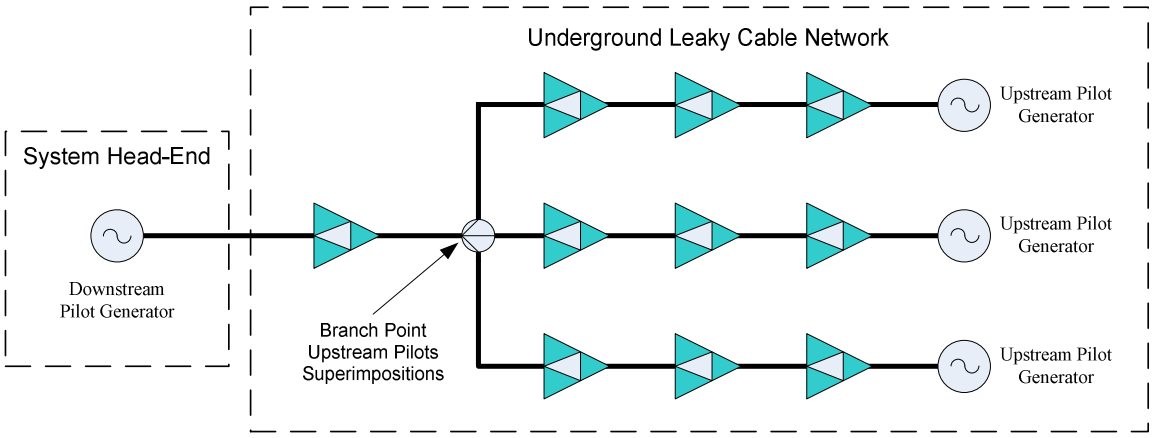

Figure 1.4: Multiple References Equalizations Topology

Within the context of the Self-Organized Networks (SON), in Chapter 4, we are proposing optimized algorithms to provide scalable and reliable system operation for the RCN of the underground mines.

1.4 Objective

The following list highlights our intended objectives in optimizing the performance of the integrated network in the mines.

1.4.1 Optimized Backbone Networks in Underground Mines:

Within the context of the SON, an intelligent algorithm will be developed to mitigate the problems of network stability and scalability in the RCN of the mines. Our intention is to have the network in the mine to be self-configured and optimized for enhanced stability and scalable performance.

1.4.2 Intelligent Power Management for Green Communication in Mines:

Within the context of Green Communication the constraint of the permissible power in the mines will be addressed. We will be proposing a novel algorithm and scheme to enable the backbone network to be self-organized and operate in a minimized power that meets the mine's safety restrictions. Ultimately, this approach will result in an effective green communication networks that will be optimized for a higher level of scalability and stability for the use in underground mines operations.

1.4.3 Novel Wireless Channels Modeling:

We will be proposing a novel modeling scheme to characterize the wireless channels in the underground. Our approach will adopt a performance-based strategy to predict the performance of the nodes in the mine. Regardless of the general shape and layout of the mine, the proposed model will characterize the wireless channels in the mines by dividing the mine's galleries into a number of segments. Furthermore, the nodes in the wireless network will use this model to evaluate their wireless channels and therefore optimize their performance and power consumption in the network.

1.4.4 WSN Power Optimization in Underground Mines:

Targeting longer network life and optimized power utilization, the performance of the WSN in the underground will be optimized for power efficiency, scalability and rapid application developments. We will be proposing a new algorithm to integrate number of schemes that offer advanced approaches in deploying WSN in the mines.

1.5 Outline of the thesis

This thesis is organized in the following manner:

Chapter 1: Communication Systems for Underground Mines
This Chapter gives a general overview of the communication systems in the confined spaces of underground mines. Integrated system architecture is presented as a model for the research. This Chapter also presents the challenges that exist in the communication systems of underground mines. The proposed contributions are summarized as possible solutions to the problems encountered in the mines' communications system.

Chapter 2: Propagation in the Underground Mine: Literature Review
This Chapter highlights the theories of wave propagation in the confined areas of the mines. Literatures survey is presented for the two main mediums of signal propagations in the mines i.e. the wireless channels and the RCN.

Chapter 3: WSN in Mines: Opportunities and Challenges
This Chapter describes the theories of the WSN as one of the promising wireless networks that can provide important and modern applications in underground mines. A review for the OSI layers model is be presented in conjunction with the application of the WSN in the confined spaces of the mines.

Chapter 4: The proposed optimized Backbone Networks for Underground Mines
The RCN, is considered in this Chapter. The challenges in using the RCN are explained by emphasizing the problems of the network scalability and power consumption in the mines. This Chapter presents our novel algorithm called, "Prediction-based Adaptive Equalization Algorithm (PAEA)" to solve the challenges encountered in the network. Simulation analyses are presented

to demonstrate the performance of the algorithm. This Chapter also presents our prototype model validating the operation of the algorithm.

Chapter 5: Intelligent Power Management for Green Communication in Mine

In this Chapter, the optimization of the backbone networks in the mine continues by proposing an optimized scheme for the network power management. The optimization problem is formulated mathematically and explained with examples to demonstrate the philosophy of the algorithm. The optimized algorithm is simulated and analyzed to illustrate the operation of the algorithm under different conditions in improving the power utilizations of the backbone networks of mines.

Chapter 6: Novel Wireless Channels Modeling

This Chapter proposes a novel approach for characterizing the wireless channel in underground mines. The new modeling approach, called "Mine Segmenting Wireless Channel Model", is explained in detail. Simulation results are presented to validate the model. The test procedure and results for a test conducted in an actual mine environment are presented and compared with the simulation analyses.

Chapter 7: RASSA: The Proposed WSN Power Optimization for Underground Mines

This Chapter presents new concepts to prolong the life of Wireless Sensor Networks in the mines. This Chapter also presents a novel "Adaptive Topology-Aware Scheme," for an improved network operation where the nodes have the intelligence of estimating their wireless channel characteristics. These concepts are formulated mathematically with a number of constraints. Simulation analyses are then presented to demonstrate the performance of the proposed algorithm.

Chapter 8: Conclusions and Future Work

This Chapter summarizes the results and conclusions of the thesis. The major contributions are highlighted to demonstrate the effectiveness of the proposed schemes and algorithms in optimizing the Integrated Networks of the underground mines for improved reliability, scalability and efficient utilization of the available power in underground mines.

1.6 Summary

Mining has an important role in our daily life as it supports the civilizations with essential needs such as energy and valuable resources. Mining operations are carried out in very hazardous environments and under very challenging conditions. Reliable communication systems in the mines are considered of the most important infrastructures that support the mining operations. All the mining operations, such as the extracting and moving the product are handled with the aid of communications, which increases the productivity. The vital importance of communication for underground mining is most evident when an accident occurs.

In general, the communication networks in the mines are hybrid systems with a number of integrated segments. The most common network architecture is made of a backbone of certain propagation mediums such as the RCN and other network segments such as wireless based networks. A number of unique challenges in deploying reliable communication in the mines were presented to demonstrate the difficulties encountered in these types of environments. Among these challenges is the characterization of the wireless channels in the mine where physical phenomena such as multi-path reflections and scatterings are considered very difficult and randomized type of analyses. The limitation of power availability in the mines is considered another type of the challenges that affect deploying reliable communication networks in the mines. This Chapter highlights the major contribution of the thesis to optimize the performance of the network in the underground given the challenges of mines' environments.

Chapter 2

2. Propagation in the Underground Mine: Literature Review

2.1 Introduction

The communication system in underground mines is a very complex structure made of multiple physical layers of networks and protocols. As shown in
Figure 2.1 the network in the mine may contain topologies composed of a wired network, such as coaxial and radiating cable networks, integrated in a complicated manner with wireless networks, such as WSN or Mesh Network.

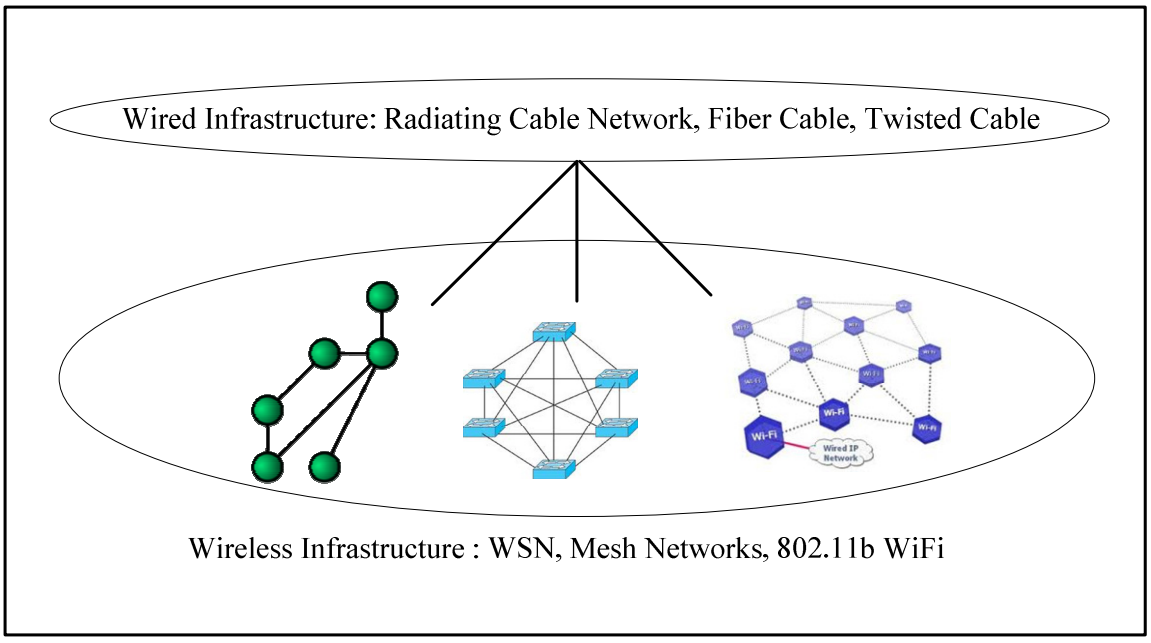

Figure 2.1: Underground Mine Integrated Network Topology

This combination better be observed as *one* entity of an integrated network. This is especially necessary to provide higher level of network management and resource optimizations. As a background introduction to the nature of the systems in the underground mines, this chapter presents a brief overview for the propagations' theories in the mines' common channel mediums. This chapter also presents a literature survey for research on the modeling and characterization of wireless channels and radiating cable networks of the mine.

2.2 Wireless Channel Characterizations in Underground Mines

The propagation characteristics of electromagnetic waves in an underground mine are different from those in free space because of the harsh underground environment. This is due to physical phenomena such as severe reflection, scattering, and diffraction along the mine's rough wall. Wireless communications in confined environments have been widely studied for years, and numerous experimental results have been presented in the literature. However, none of the previous works have resulted in a comprehensive channel model.

The two main existing approaches for mines' channel models are the Geometrical Optical model (GO model) and the waveguide model [7]. In the Geometrical Optical model which is a ray-tracing technique, EM waves are approximately modeled as optical rays. The EM field is obtained by summing the contributions of rays undergoing reflections on the tunnel walls. In [8, 9], the rays diffracted near tunnel wedges are considered to improve the accuracy of the GO model. Except in some very idealized situations, e.g., the waveguide with two perfectly reflecting side walls [10], the GO model depends on computer simulations to obtain numerical solutions, and the computational burden increases dramatically as the signal path is prolonged. In the waveguide model, the tunnel behaves as an oversized waveguide with imperfectly lossy walls. Maxwell's equations are solved by taking consideration of the boundary conditions. In addition, the waveguide model assumes that there is only the lowest mode signal propagation in the tunnel.

In [11], a model combining the GO model and waveguide models is presented. A free-space model is utilized in the near region, and a waveguide model is used in the far region. The near and far regions are divided by the breakpoint (or turn-point), which is viewed as the intersection of the two different models. However, the change from near region with multiple modes to the far

region with single mode is a continuous process. An exact break-point cannot exist. In addition, it cannot characterize the fast signal fluctuation of the multi-mode channel in the near region.
Based on the physical structure, underground mines can be divided into the following two major areas [12]:

1. Open Area (Room and Pillar): The mining area can be viewed as a big room with some randomly shaped pillars, as shown in Figure 2.2(a).
2. Tunnel areas: For cut-and-fill mining as shown in Figure 2.2(b) and long-wall mining as shown in Figure 2.2 (c), the mining area consists of several types of tunnels, e.g. mining tunnel and transport tunnel.

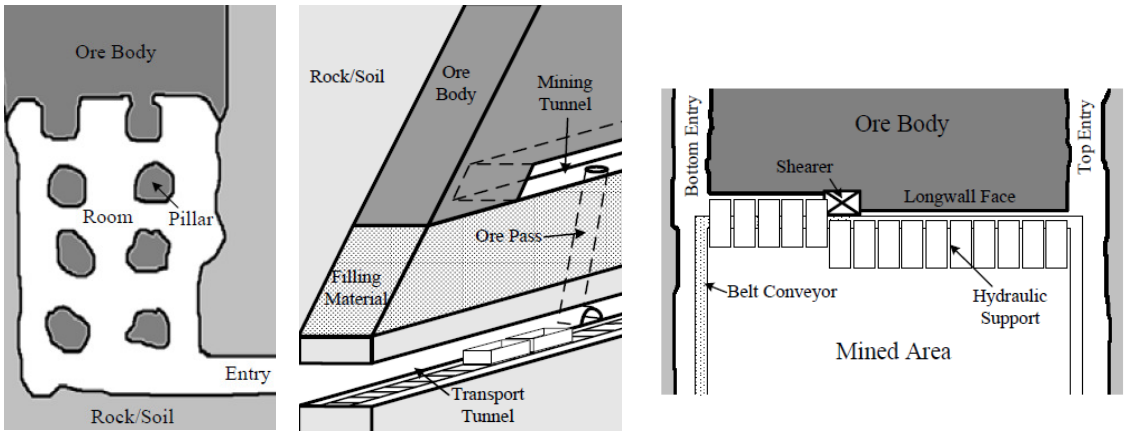

(a) Plan of room-and-pillar mining (b) Cut-and-fill mining (c) Plan of longwall mining

Figure 2.2: Mine structure of different mining methods

Therefore, underground mines require two types of channel models. The open areas in the mines are generally analyzed by utilizing generic models, such as ray-tracing techniques, since there is no known model that explicitly describes the characteristics of the open area. For the tunnel area, there are several studies related to the channel modeling based on the guided wave propagation model. In the following two subsections, a brief overview of the ray-tracing techniques and the channel model for tunnel areas are presented.

2.2.1 Open Areas Model (Ray-Tracing Technique)

In [13] the ray tracing technique was demonstrated for modeling an Ultra Wide Band (UWB) indoor channel. The performance of the channel was analyzed in terms of channel impulse response; power delay profile and RMS delay spread. The model was developed for an indoor environment which comprises a typical single room. There is a single transmitter and single receiver with multiple antennae in the room apart from each other at a variable distance. Reflection and refraction phenomena have been taken into account in this approach.

G.Y. Delisle [14] showed that the Ray Tracing Technique enables the estimation of the received signal in a mobile system, taking into account the reflection from the rough sidewalls, as well as the diffraction and the scattering of the signal from the corners and from the obstacles. Figure 2.3 represents a mine area with seven access points linked in a random topology.

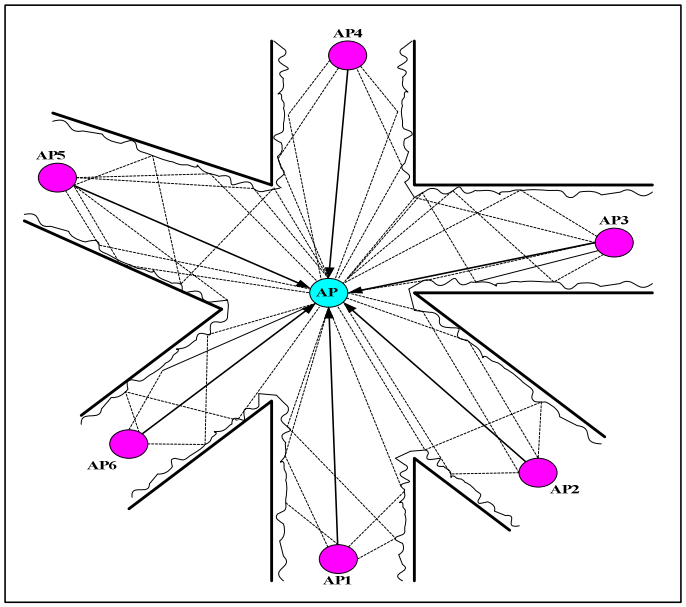

Figure 2.3: Ray-Tracing Technique [7]

G.Y. Delisle [14] presented the following equation to illustrate the components of signals received at the transceiver (AP):

$$S = F + R + RS + RSD + RD \quad , \tag{2.1}$$

where;

S: Received signal level at the receiving AP in dBm,

F: Represents all the direct paths from the transmitters to the receiver AP in dBm,

R: Represents the reflected components of the signals that reach the receiver AP without involving scattering or diffracting phenomena. It is measured in dBm,

RS: Represents all the reflected paths, which will reach the receiver AP after scattering against the obstacles, measured in dBm,

RSD: Represents all the reflected paths, which will reach the receiver AP after scattering and diffracting against the obstacles and rough corners of mine corridors, measured in dBm,

RD: Represents all the components of the signal that will reach the receiver AP after encountering the reflection and the diffraction from the rough sidewalls and on the corners, measured in dBm.

The Ray Tracing Technique is a generic model that can be used in open area environments to predict the characteristics of the wireless channels. This section illustrates the utilization of the Ray Tracing Technique in an underground mine's open areas.

2.2.2 Tunnel Areas Models (Tunnel Galleries)

The propagation model in the "tunnel area" can be approximated by using the theories of waveguide propagations as shown in Figure 2.4. Several research studies have made use of this idea but with different approaches. The basic idea is that the propagation exhibits the guided wave characteristic, and in some cases the propagation loss can be even smaller than in free space.

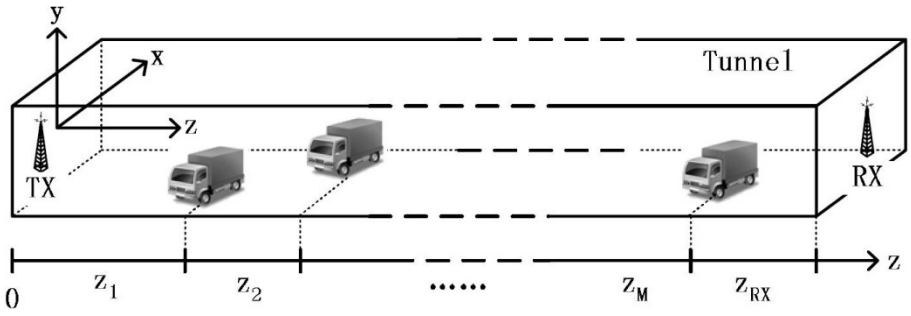

Figure 2.4: RF Propagation in Tunnels

In [7], Zhi and Akyildiz, have presented a modeling approach for the wireless channels in the tunnels based on multimode propagations, which provides an analytical expression for the received power and the power delay profile at any position in a tunnel. They demonstrated that the propagation of EM waves in tunnels can be viewed as the superposition of multiple modes with different field distribution and attenuation coefficients. By solving the Maxwell's equations, the field distribution of each mode can be derived in the form of eigenfunctions;

$$E_{m,n}(x,y) = \sin(\frac{m\pi}{2a}x + \varphi_x) \cdot \cos(\frac{n\pi}{2b}y + \varphi_y), \tag{2.2}$$

were $\varphi_x = 0$ if m is even; $\varphi_x = \frac{\pi}{2}$ if m is odd; $\varphi_y = 0$ if n is odd; $\varphi_y = \frac{\pi}{2}$ if n is even

The field at any position (x, y, z) inside the tunnel can be obtained by summing up the field of all significant modes, which is given by:

$$E^{R_x}(x,y,z) = \sum_{m=1}^{\infty}\sum_{n=1}^{\infty} C_{m,n} \cdot E_{m,n}(x,y) \cdot e^{-(\alpha_{m,n} + j\beta_{m,n})z}, \tag{2.3}$$

were $C_{m,n}$ is the mode intensity on the excitation plane; $\alpha_{m,n}$ and $\beta_{m,n}$ are the attenuation coefficient and the phase-shift coefficient, respectively.

Emsile *et al* [15] provided the first comprehensive theoretical study of propagation characteristics in underground mines. This work has a particular focus on the loss of signal strength along a tunnel. As shown in Figure 2.5, Emsile models a straight section of a tunnel as a dielectric waveguide with rough surfaces, and he derives expressions relating the attenuation of radio waves in terms of wave polarization, radio frequency, and tunnel dimensions.

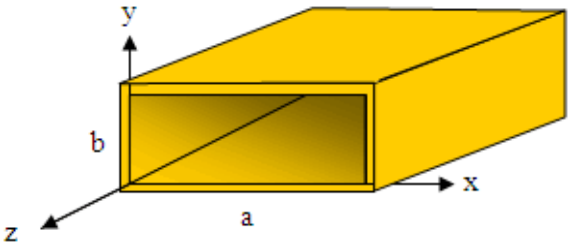

Figure 2.5: Waveguide Cross Section

It is evident that the loss due to surface roughness increases with wavelength. Assuming a Gaussian distribution roughness h, the loss in dB is defined by the following equation (z is the coordinate along the tunnel):

$$L = 4.343\pi^2 h^2 \lambda \left(\frac{1}{a_T^4} + \frac{1}{b_T^4} \right) Z, \tag{2.4}$$

where a_T , and b_T are the tunnel dimensions and h is the mean square root of tunnel walls' roughness.

Another model by Sun *et al.*[16] used a multimode model to analytically characterize the natural wave propagation in both near and far regions of an antenna. In this model, the tunnel area is divided into two regions based on their distance from the transmitter. These regions are the near and far regions.

The channel model indicates that in the near region of the transmitter, the received power attenuates quickly and fluctuates very rapidly, as shown in Figure 2.6. This behavior is attributed to the combined effect of multiple modes near the transmitter antenna. In contrast, the decline in the received power is gradual in the far region due to the fact that the higher order modes attenuate faster as the distance increases. The operating frequency has a clear effect on the propagation constants. Signals with higher frequency attenuate slower. Therefore, as frequency increases, the signal attenuation decreases and the fast fluctuating region persists.

Hence, the field in distant regions is governed by the few low-order modes that remain. The mode attenuation is mainly determined by the tunnel size and operating frequency, while the mode intensity is controlled by the position of the excitation antenna. Physical factors, such as the humidity, pressure and temperature of the tunnel air, as well as the composition of the tunnel walls influences the signal propagation in the tunnels.

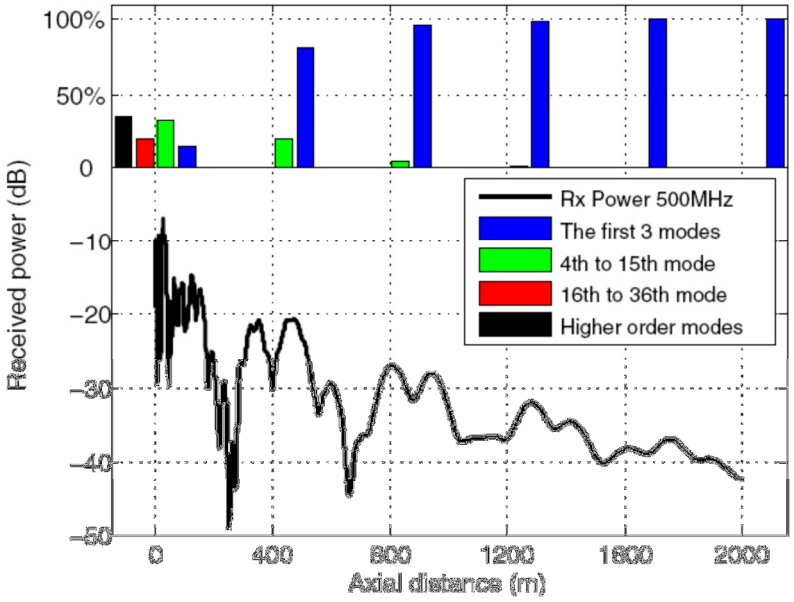

Figure 2.6: Sun Model for Tunnel Areas

In practical applications, tunnels are usually filled with obstructions, e.g. traffic in a road tunnel or a train in a subway tunnel. Obstructions will cause additional loss for each mode. The attenuation rates are different for different modes. In addition, the obstructions may also cause mode coupling between different modes. The position and size of the obstructions, as well as the shape and size of the tunnel determine the attenuation and coupling coefficients of the modes [17].

In [18], Zhang offers a different view in waveguide modeling of underground mines. The results are based on experiments conducted in two underground coal mines at 900 MHz with horizontal and vertical polarization. A hybrid tunnel propagation model consisting of the free space propagation model and the modified waveguide propagation model is used to explain the measurement results. In the tunnel area, it is noted that propagation exhibits guided wave characteristics in the region after a so-called "breakpoint" and free space propagation characteristics before the "breakpoint". Zhang in [19] proposed an equation to calculate the location of the breakpoint for propagation along a LOS (line-of-sight) in tunnels. The breakpoint is located in the propagation path, where the propagation loss from two models in the far region (L_f) and the near region (L_n) are equal;

$$L_n = L_f \,. \tag{2.5}$$

Figure 2.7 shows the test results for the relative received power as a function of distance for a passageway in the Wang Tai Po coal mine, where the breakpoint is 45 m [18].

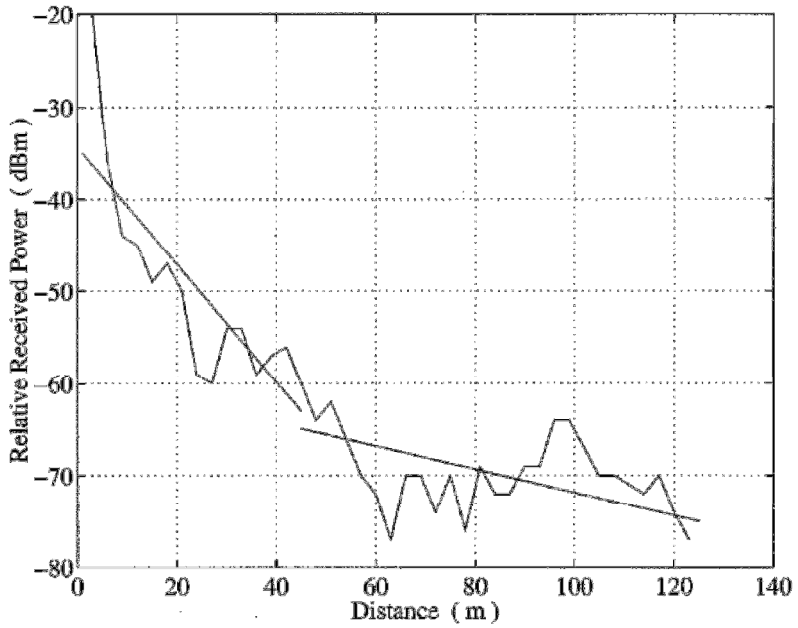

Figure 2.7: Zhang Breakpoint Model

2.3 Radiating Cable Channel Characterizations

There are various methods available for providing radio frequency coverage in underground environments. The most versatile and reliable system is the "Leaky Feeder" system. The leaky feeder, also called “Radiating Cable”, functions both as a transmission line and as an antenna [20-22]. RF energy is simultaneously transmitted down the radiating cables and radiated from all points into the surrounding space. Slots cut into the outer conductor of the coaxial cable allow controlled levels of electromagnetic energy to be radiated both out of and into the cable. The amount of radiation is quantified by the coupling loss. Coupling loss is defined as the difference between the power transmitted into the cable and the power received by a λ/2-dipole antenna located at a distance of 2 meters from the cable. The structure of a typical leaky cable is shown in Figure 2.8 [23]. The Leaky Feeder Technology (LFT) is a combination of leaky feeder cables and amplifiers. Other components can be added, but the backbone of the system comprises of only

these two elements. It is necessary to compensate for the inherent loss of the signal, and this is achieved by the insertion of line amplifiers. Correct installation of the system ensures a consistent signal level is maintained throughout the network, and hence throughout the mine [21]. The Leaky Feeders have already been in use for decades under various conditions to assure communication in confined areas. It appears that the need for secure communications in mines forced the development in this area, starting with very early experiments during the middle of the last century.

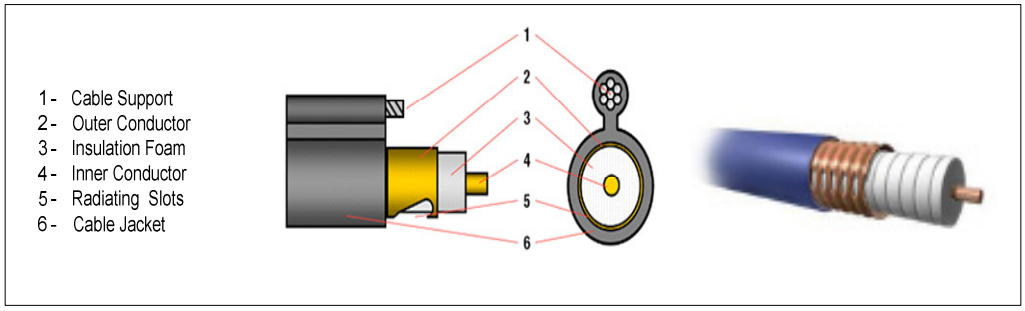

Figure 2.8: Leaky Cable Structure

Advances in technology can be used in mine environments, but many factors make it a challenging proposition. This special discipline began at very low frequencies, but the spectrum of applications has grown, especially in recent years, at a great speed, from AM-rebroadcast up to PCN at 1900 MHz and 3G and Wi-Fi applications at 2.4 GHz. Digital modulation technology, e.g. in telephony systems, imposes particularly stringent requirements on regular field strengths along the cable trunk and low system dynamics in combination with optical systems. Humidity and street salt in tunnels and the need for flame retardant cables in mines and subways demonstrate just a few obstacles to developing communication systems in the mine environment. However, solutions must be explored. The objective of this section it to explain the theory of the radiating cable models and to give an overview of various application possibilities based on this type of technology.

2.4 Radiating Cable Systems Theory of Operation

In this section the theory of operation of the radiating cable is explained as follows:

2.4.1 Coupled mode

All the different types of leaky feeders employ a basic mechanism, i.e. the effects of two types of waves, excited by leakages in the outer conductor of an RF-cable, as shown in Figure 2.9:

- Spherical waves and their higher order modes
- Cylindrical surface waves propagating along the cable in both directions.

The resulting field at a certain distance from the cable consists of interferences between all these various fields. Figure 2.9 shows the envelope of the resultant field along the cable. It demonstrates that each of the field types is excited at distinctive field strengths, which decrease at different rates with the distance r from the center of the cylinder or sphere, by $1/r^2$ for spherical and by $1/r$ for cylindrical waves. The field strength, which can be received along the cable by an antenna, is the sum of all interferences caused by the nearby leakages. The amount depends upon the distance and on the size of the leakage related to the wavelength. These phenomena exist in every case, if no special mode is dominant. This field constitution is called the coupling mode. Typically, the field level along the cable is very irregular due to the effects of interference [20].

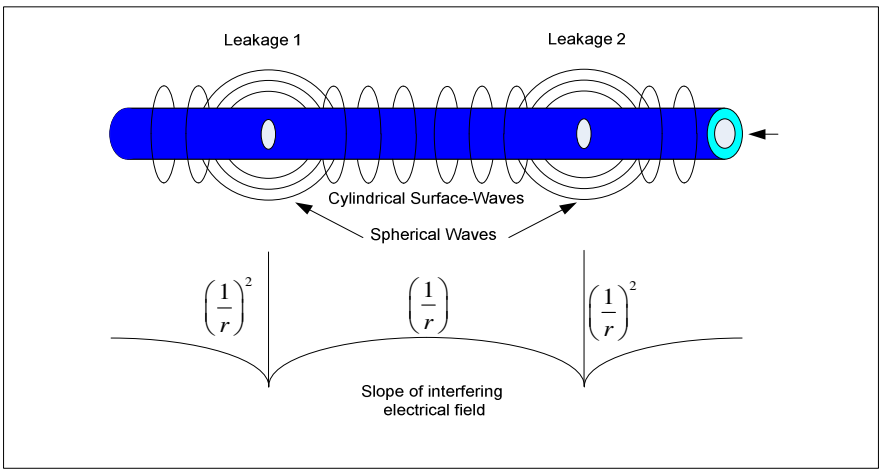

Figure 2.9: Characteristics of the Coupled Mode

2.4.2 Radiating mode

One of the operating modes of radiating cable is the radiating mode, which is characterized by coherent interference of the spherical waves directly excited by the leakages as shown in Figure 2.10. This effect predominates against the previously described interferences of surface waves, which still exist. In this mode the transverse wave leads to higher field strengths, resulting in more radiated energy. Of course, this will result not only in lower coupling loss but also higher cable losses [20,21].

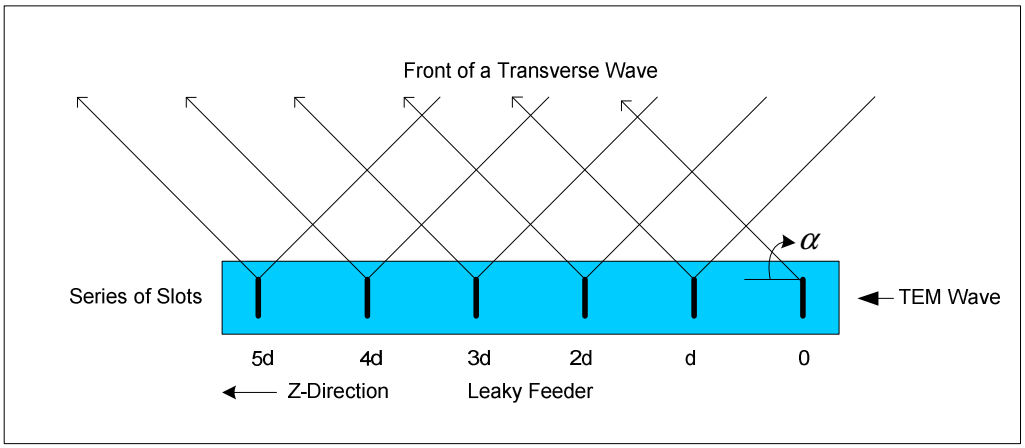

Figure 2.10: Radiating Mode Electrical Field

This mode has a lower and an upper cut-off frequency, due to the physical limitations of coherent interferences. The basic mode propagates at its lowest frequency, when half of the wavelength is shorter than the distance between leakages.

The direction of propagation of the transverse wave depends on the phase progress of the inner TEM-wave inside the cable and, in particular, on relation of wavelength to leakage distances. The main lobe can be observed in the geometrical plane corresponding to the cable axis. Since the outer surface of the cable is relatively small, the directivity around the cable is very low as shown in Figure 2.11.

Therefore, by increasing the frequency over a greater range, the main lobe of the basic mode rises from being parallel to the cable at the lower cut-off and rotates against the direction of the inner

TEM-wave of the feeder, disappearing in the opposite direction at the upper cut-off. Thus the radiating mode passes over from one coupled mode to another.

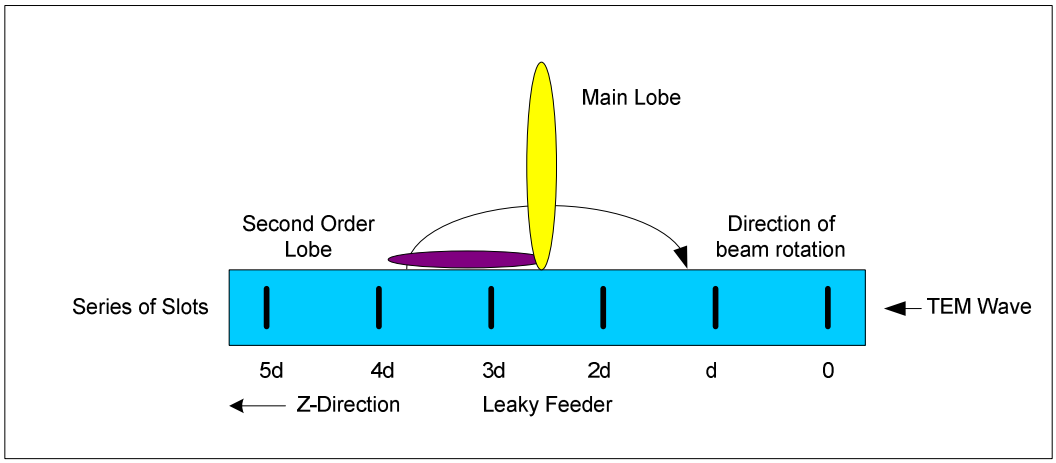

Figure 2.11: Linear Array Model

2.5 Typical Networks Layout in the Mines

Normally, the leaky feeder system consists of the surface portion and the underground portion. The system head-end equipment, which includes the radio repeaters for all communication channels and any other system peripherals, is typically installed on the surface. The underground portion of the system consists of the leaky cable network and bi-directional amplifiers installed periodically at regular distances to act as repeaters to boost the RF signal in both directions of the communication system (upstream and downstream directions).

Traditionally, leaky feeder systems were capable of only voice and low speed data communications. In these systems, two bands of communications were required to enable full-duplex voice and data communications. Nowadays, the leaky feeder system can transport high speed data communications by utilizing DOCSIS standards to deliver Ethernet connectivity based on the Cable Modem Termination System (CMTS). Typically, there are four bands of amplification in each amplifier to compensate for the system losses. In the CMTS system, there are two bands dedicated to providing full-duplex voice communication (upstream and downstream) and two bands to provide the CMTS high-speed data communication in the upstream and downstream directions [24,25]. A typical layout for the leaky feeder communications system is shown in Figure 2.12.

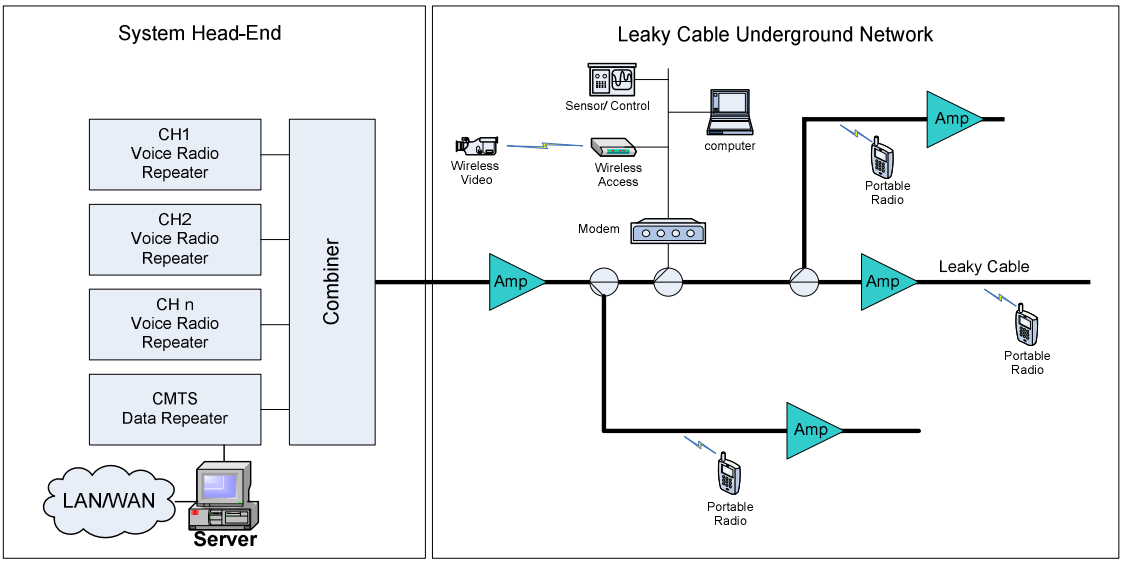

Figure 2.12: Leaky Feeder System Block Diagram

In this research, our analyses have been applied and demonstrated on the CMTS leaky cable. There are four distinct RF bands in the system. These bands are required to provide RF paths for the voice and data communications. Table 2.1 lists the four bands of the system and their frequency ranges.

Band No.	Band Name	Frequency (MHz)
1	Upstream Data	5-42
2	Downstream Voice	155-158
3	Upstream Voice	172-175
4	Downstream Data	220-232

Table 2.1: System Frequency Plan

2.6 Summary

Typically, the communication networks in the underground mines are complicated infrastructures that are made of a number of components. The transportation of information in the mines can follow a number of media for the message to arrive at its final destination. Through these transportation paths, the mediums can change from one type to another. The most common propagation paths and channels in the mines are the wireless channels and radiating cable networks. The characterizations of these channels are essential for the evaluation and prediction of performance of the communication systems in the mines.

While the analysis for radiating cable is very deterministic and is explained in the literature, the analyses of the wireless channels of mine can be very challenging as it is a randomized exercise and requires extensive efforts. Although there are many previous works in this area, they are lacking comprehensive models to explain the confined space galleries of mines in a unified manner. All the models that were researched in the past have focused on particular mine topologies (either canonical or open area topologies). In Chapter 6, we are presenting a simplified and novel model to analyze wireless channel characteristics that can be applied to both types of topology. These analyses are important to the research of the cross layers' optimizations since they establish the foundation of the reliable networks. The knowledge obtained from our comprehensive wireless channel model is used to develop an integrated algorithm to optimize the performance of the mines' networks.

Chapter 3

3. WSN in Mines: Opportunities and Challenges

3.1 Introduction

Wireless Sensor Networks are one of the today's most interesting emerging technologies. WSN is made up of a large number of inexpensive devices that are networked via low power wireless communications. It is the networking capability that fundamentally differentiates a sensor network from a mere collection of sensors, as it allows cooperation, coordination, and collaboration among sensor assets. By harnessing advances in the past decade in microelectronics, signal processing, wireless communications, and networking, wireless sensor network technology is expected to have a significant impact on our lives in the twenty-first century [26]. Unlike the centralized networks, wireless sensor networks work in an *ad-hoc* fashion. Their self-configuring, self-healing characteristics make WSN autonomous; therefore they have a great advantage in a multitude of situations.

The development of this attractive network has opened many doors for several "new and exciting" applications, in which flexibility, easy deployment and configuration are important properties. Among a diverse set of applications for sensor networks, some of the fields where this technology is most applicable include agriculture, inventory monitoring, intrusion detection, motion tracking, machine malfunction, toys, and in the military. In the mining industry, the WSN has very quickly emerged as one of the most promising technologies that can meet many of the underground mine's requirements.

Within mines, the WSN can provide the following features: prompt response to identification of workers entering or leaving a mine, control of personnel traffic into hazardous areas by providing warning indication signals, identification of vehicles entering or leaving production areas or

passing specific locations in the mine, tracking of supplies and materials, reducing fatal accidents due to collisions, monitoring of underground gases, and scheduling maintenance [27, 28].

Generally speaking, the measurement of physical parameters makes sensors the most suitable technology for monitoring and reporting important quantifiable measurements. Sensors, though, are not just limited to environmental sensing. Any application involving the sensing of physical parameters, such as sound, humidity, pressure, temperature, etc., might use a sensor network [29].

The choice of WSN deployment in an underground mine requires considerations for conflicting requirements. The priority is to ensure a robust global network with battery-operated nodes. Therefore, these types of networks are usually developed with the following goals in mind. First, the nodes, in most cases, are tiny devices and often battery-powered. Some applications have stringent QoS requirements in terms of timely delivery of packets (bounded delay), high packet delivery ratio, and low jitter. Packet delay is directly related to the number of hops traversed by the packets and the congestion level of the network. In contrast, other networks might have a required system lifetime [30].

Secondly, the distributed and the mobile nature of the wireless sensor network combined with the QoS requirements make traditional protocols unsuitable. So, an alternative analysis should be adopted for the design of WSN. Recent technological advances allow us to envision a future where large numbers of low-power and inexpensive sensor devices are densely embedded in the physical environment and operating together in a wireless network.

The envisioned applications of these wireless sensor networks in the confined spaces of the mines are wide ranging. For example, Ventilation On Demand (VOD) schemes would allow energy savings by having a smart network of WSN to be responsible for the mine's ventilation systems. As well, WSN could be deployed in the mines to provide RFID and tracking solutions for the personnel and assets in the mines.

3.2 WSN Applications in Underground Mines

WSN has found a very welcome position in being utilized in underground mine applications. As the name suggests, the wireless sensor network can be thought of as a combination of two functionalities; they are the collection (or sensing) of information and the transportation of information in a wireless network.

To enhance safety and increase productivity in the operations of underground mines, it is very important to continuously monitor the miners and environmental conditions such as temperature, carbon monoxide levels, and methane levels. When underground mine accidents occur, the availability of the following applications could enhance rescue efforts:

- Location of trapped miners,
- Two-way communication with the miners, and
- Environmental conditions (for example, temperature, carbon monoxide level, presence of methane, or other undesirable gases) along the rescue path to the trapped miners.

The general working principle of the WSN made of dual-element functionalities (sensing and wireless communications) has been translated into many applications in underground mines. Among these applications are the WSN-based Localization System, Environmental Data Collection System, Automated Mines Operations, and Ventilation on Demand Systems. In this Section the following two applications of WSN in underground environments are presented: the WSN based Localization Systems and Monitoring and Control Systems.

3.2.1 Localization Systems

Localization is among the important applications for which WSN can be implemented. With wireless sensor networks, the personnel and assets in the mine can be located by simply labeling them with a small node. This task is important for many applications such as traffic management in underground mines, tracking, or rescue operations [31, 32].

To implement a successful WSN-based location application, it is important to locate the nodes accurately, at least within an acceptable range, to pin-point the user's positioning. In practice, two types of location techniques are used: the first one is based on information contained by the

received signal such as the angle of arrival (AoA), the received signal strength (RSS) and the time of arrival (ToA). The second technique is the fingerprinting technique [33]. This technique assumes that the characteristics of the propagation signal are different at each location of the zone of interest. In other words, each location has a unique fingerprint or signature in terms of propagation characteristics. A fingerprinting technique determines the unique pattern features and then this knowledge is used to develop the rules for recognition [33].

In addition, many algorithms have been developed to enable the localizations in the mines. Sensor network localization algorithms estimate the locations of sensors by utilizing given information about special reference sensors and their locations in the mine [34]. Sensors with known location information are called anchors, and their positions can be obtained by installing anchors at points with recognized coordinates. These anchors define the local coordinate system to which all other sensors refer. The other types of sensors are called non-anchor nodes or, simply, tags. The coordinates of these non-anchor nodes can be estimated by utilizing special algorithms developed for the localization function of personnel and assets in the mine.

Two main philosophies of developing these algorithms have been established. The first is based on using connectivity information only. With this philosophy, nodes with unknown positions can localize themselves with respect to reference nodes from which they receive the anchor signal. The estimated position of the node is computed by solving a linear program at the central location. For this method to work well, the anchor nodes must be placed at the perimeter of the network. Otherwise, the position estimation of the outer nodes can easily collapse toward the center, leading to large estimation errors [35, 36].

The second type of algorithms is based upon measurements. These include the DV-hop, DV-distance, and Euclidean methods. The DV-hop (Distance Vector-hop) approach begins with all anchors sending their locations to other nodes in the network. As shown in Figure 3.1, the messages are propagated hop-by-hop, and there is a hop-count in the message. Each node maintains an anchor information table and determines the shortest route to an anchor. When an anchor receives a message from another anchor, it estimates the average distance of one hop using the locations of both anchors and the hop-count, and then sends it back to the network as a correction factor. When receiving the correction factor, a non-anchor node is able to estimate its distance to anchors and performs triangulation to estimate its location [37].

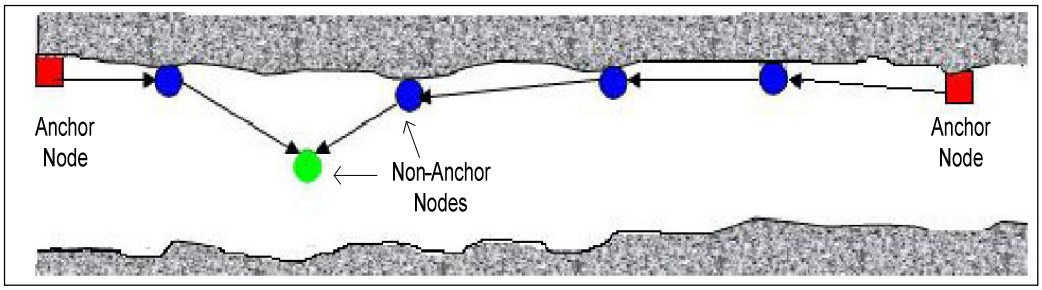

Figure 3.1: Distance Vector DV-hop destination node

Furthermore, in the DV-hop method, anchors propagate their positions inside the network. Each node relates the information of posted anchors with its neighbors and builds a table, which comprises the ID of the anchor, its position, and the hop distance. When an anchor receives one of the propagated packets with the position of different anchors, it uses this information to compute the average hop distance between the two anchors. The computed average hop is again propagated in the network. The nodes that receive this information can estimate their distances from the beacons. The DV-distance approach is similar to DV-hop, but it uses received radio signal strength measurements to estimate the distance between two neighboring nodes in order to reduce the location estimation error. The Euclidean distance method uses the local geometry relationship of the nodes for position estimation.

3.2.2 Environmental Monitoring

Monitoring systems in underground mines are crucial to ensure safe working conditions because many environmental factors, including the amount of gas, water, and dust, need to be monitored. To obtain comprehensive monitoring results in the mine environment, an adequate number of data samples need to be collected at different places. Precise and sufficient knowledge of the mine environment requires a high sampling density, which involves a large number of sensing devices. The existing underground mine safety monitoring systems are of these two kinds: wired and wireless systems. Utilizing wires to connect sensing devices to a processing server requires a large amount of wire deployment; poor working conditions and high maintenance costs within the underground mine make this task difficult. Moreover, the wired communication method makes the system less scalable; as the mine advances, more sensing devices need to be deployed.

Although the wireless systems take advantage of convenient deployment and flexible adjustment; it is often impossible to maintain direct wireless communication channels between sensing devices and the processing server.

Figure 3.2, shows an integrated system combining Leaky Feeder technology and WSN. In this case, the leaky cable system operates a CMTS all through the mine. This system can provide multiple Ethernet access points via CMTS modems. These modems can be installed in different areas of the mine. Typically, the Leaky Cable (or any other communication infrastructure) already exists in the mine to provide other communication facilities, such as voice communications. Therefore, in this case, no additional cost is needed to create a an integrated system that can interface the WSN.

The WSN can be integrated to the Leaky Feeder System via gateway sensor nodes. In this scheme, clusters of nodes can be integrated into a large-scale system via Leaky Cable. In each cluster of nodes, the WSN employs multi-hop routing to implement data gathering. Each sensor node plays the role of data collector as well as the message forwarder in the network [30]. The gateway nodes at each cluster will then relay the information into the Leaky Cable network via the CMTS modems. Once interfaced with the IP network of the Leaky Cable, the data can be transported a long distance to a central processing facility, where data can be monitored, analyzed, and possibly processed further for automation actions.

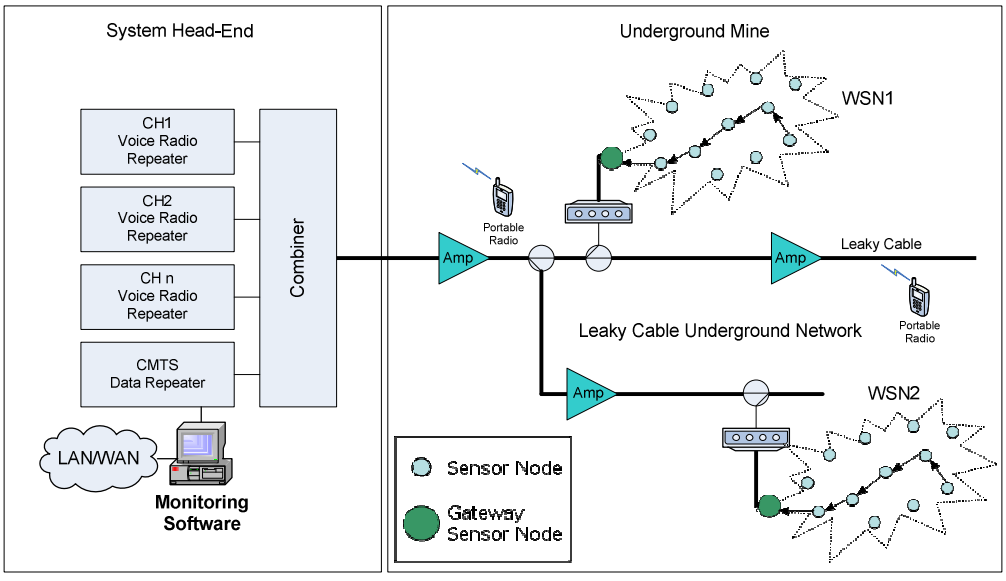

Figure 3.2: WSN-Leaky Cable Integrated System

3.3 WSN Components

As shown in Figure 3.3, there are several key components that make up a typical wireless sensor network device [38]:

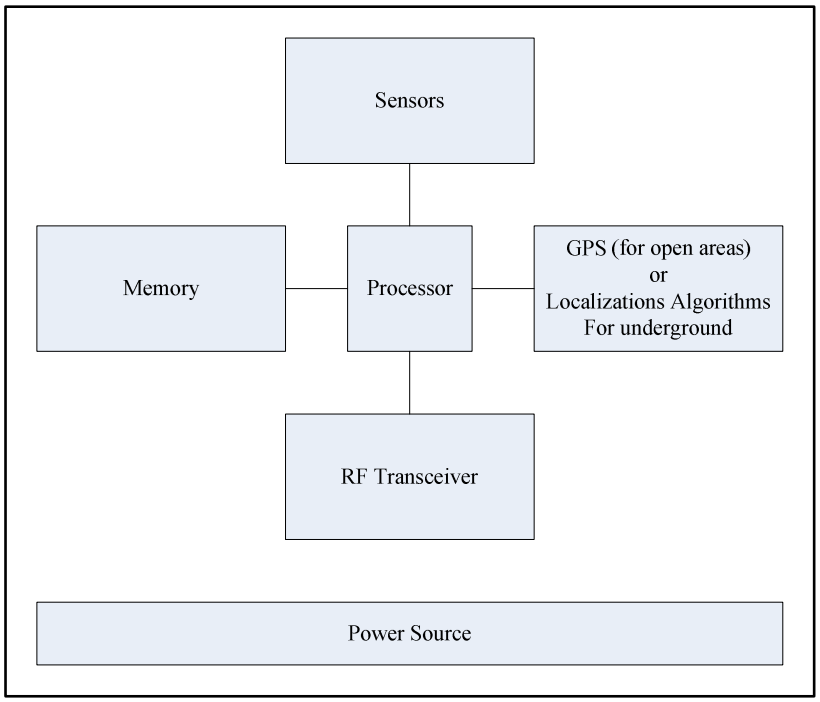

Figure 3.3: Wireless Sensor Block Diagram

3.3.1 Low-power embedded processor:

The computational tasks on a WSN device include the processing of both information locally sensed as well as information communicated by other sensors. At present, primarily due to economic constraints, the embedded processors are often significantly constrained in terms of computational power (e.g., many of the devices currently used in research and development have only an eight-bit 16-MHz processor) [38]. Due to the constraints of such processors, devices typically run specialized component-based embedded operating systems. However, it should be kept in mind that a sensor network might be heterogeneous and include at least some nodes with significantly greater computational power.

3.3.2 Memory:

In general, the storage elements of the WSN nodes have the form of random access and read-only memory that include both program memory (from which instructions are executed by the processor), and data memory (for storing raw and processed sensor measurements and other local information). Due to economic considerations, the quantities of memory and storage on the WSN device are often limited.

3.3.3 Radio transceiver:

WSN devices include a low-rate, short-range wireless radio (10–100 kbps, <100 m). While presently quite limited in capability, these radios are likely to improve in sophistication over time – including improvements in cost, spectral efficiency, tunability, and immunity to noise, fading, and interference. Radio communication is often the most power intensive operation on a WSN device, and hence the radio must incorporate energy-efficient sleep and wake-up modes.

3.3.4 Sensors:

Due to bandwidth and power constraints, WSN devices primarily support only low-data-rate sensing. Many applications call for multi-modal sensing, so each device may have several sensors on board. The specific sensors used are highly dependent on the application; for example, they may include temperature sensors, light sensors, humidity sensors, pressure sensors, accelerometers, magnetometers, chemical sensors, acoustic sensors, or even low-resolution imagers [39].

3.3.5 Geo-positioning system:

In many WSN applications, it is important for all sensor measurements to be location stamped. The simplest way to obtain positioning is to pre-configure sensor locations at deployment, but this may be feasible only in limited deployments. Particularly for outdoor operations, when the network is deployed in an *ad hoc* manner, such information is most easily obtained via satellite-based GPS. However, even in such applications, only a fraction of the nodes may be equipped with GPS capability due to environmental and economic constraints. Thus, other nodes must obtain their locations indirectly through the network localization algorithms.

3.3.6 Power source:

To enable flexible deployment the WSN device is likely to be battery powered (e.g. using LiMH AA batteries). Some of the nodes may be wired to a continuous power source in some applications, and energy harnessing techniques may provide a degree of energy renewal in some cases. Nevertheless, the finite battery energy is likely to be the most critical resource bottleneck in most WSN applications.

3.4 Cross Layer Design

The philosophy of the cross-layer design, and optimization in general, states that the different layers of the protocol stack are allowed to couple, integrate, and exchange information with one another to a much higher degree than what was originally intended when the layered architecture was designed, as shown in Figure 3.4 [40]. The operation of each layer, from the power used by the physical layer hardware to the quality of the source coding employed on the application layer, can be optimized with tremendous performance and efficiency gains when knowledge about the other layers, such as channel quality, traffic patterns, user needs, Quality-of-Service (QoS) constraints, is taken into account. Typically, the network can react and adapt much more intelligently and efficiently to the dynamic behavior of the radio environment and the traffic load instead of being designed for "worst-case" conditions. It has been well established that such co-optimization can significantly enhance the performance and lifetime of wireless networks in general as well as for *ad hoc* and sensor networks, and wireless networks communicating over short ranges.

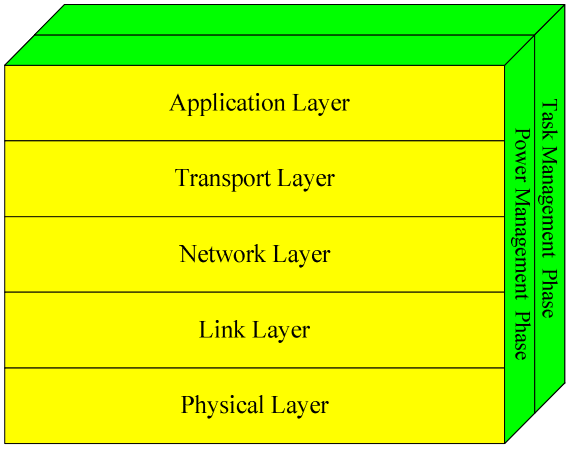

Figure 3.4: WSN protocol stack

3.5 Challenges of WSN in Underground Mines

Two design criteria are very important in creating WSN applications for underground mines. The first is to ensure that the wireless sensor network has a long life of operation, and the second is to achieve a prescribed QoS. These requirements are always conflicting and require a careful compromise between them.

The life of a WSN is a direct function of the battery life of nodes in the network. Battery life of the nodes is affected by the node deployment, power management scheme, routing mechanism as well as by the RF transceiver and antenna characteristics. QoS is defined in terms of message delay, bit error rates, packet loss, economic cost of transmission, and so on. QoS can be affected by network topology (node deployment) and the routing mechanism of the WSN.

This section presents brief analyses and descriptions for a few of the challenges faced in the design and deployments of the WSN in underground mine.

3.5.1 Power management and conservation

An important feature that distinguishes sensor networks from traditional monitoring systems is their limited energy reservoir system, where the sensors nodes are battery-power limited. It is commonly accepted that the main design goal in wireless sensor networks is the reduction of energy costs.

Energy consumption can be affected by all layers of the network, ranging from physical to application layer. Several energy management strategies have been investigated of a WSN. These strategies have focused on certain areas such as efficient topology design, link adaptation, energy efficient MAC, energy aware routing protocol and suitable power preserving physical layer by using green modulation and power control [41, 42].

In [43], an interesting approach, based on cross layer design, has been proposed to improve the whole network performance. The main idea behind the cross-layer design is the transparency behaviour between two or more layers. The interactions and information exchange between various protocol layers can achieve, generally, a good networks performance.

The node deployment and distribution affect the scheme of the power management. Thus, the power management scheme for a tunnel area with uniform node distribution may not be suitable for an open area with non-uniform distribution and vice versa. When a message is relayed via WSN in the tunnel area, only a few nodes are active and exchanging information at a given moment while the rest of the nodes are idle. Different power management schemes were presented in the literature, such as the one proposed by [44]. This scheme switches nodes between the two states of "transfer state" and "monitoring state". Data are forwarded only in the transfer state. In the monitoring state, nodes keep their radio transmitters off and will switch into a transfer state to become an initiator node on event detection.

The "Geographical Adaptive Fidelity" (GAF) algorithm by Xu et al. [45] was presented as one of the power management schemes. In this approach, nodes use location information to divide the field into fixed square grids. The size of each grid remains constant, regardless of node density. Nodes within a grid switch between sleeping and listening mode, with the guarantee that one node in each grid stays active so that a dynamic routing backbone is maintained to forward packets. GAF conserves energy by identifying nodes that are equivalent from a routing perspective and turning off the unnecessary nodes, thereby keeping a constant level of routing fidelity. Conservation can also be achieved by utilizing power-efficient hardware. There are a number of strategies that can be considered to reduce the average power supply of the radio including the following:

- Reduce the amount of data through data compression,
- Reduce transceiver duty cycle,
- Reduce the frame overhead, and
- Implement an event-driven transmission (i.e., only when a sensor event occurs).

3.5.2 Node Deployment

Node deployment is a major challenge to the successful implementation of a large-scale wireless sensor network. The number, position, and type of nodes determine many intrinsic properties of a WSN system such as power consumption, and these factors have a direct impact on the overall cost of the sensor network [46]. Generally, the distribution of nodes can be divided into two major subclasses of uniform and non-uniform distribution. In a uniform distribution, the nodes are equally spaced and have approximately the same coverage [47]. In a non-uniform

distribution, the nodes are randomly distributed in the area, and nodes may differ in terms of functionality and coverage at different locations. In terms of functionality, nodes can be classified into the three subclasses of sensing node, relay node and sensing/relay node.

For an underground application, the fundamental question is: “How should we deploy the nodes in order to minimize the WSN deployment and operation cost?”. As mentioned in previous sections, the underground mine can be divided into two major areas, which are the tunnels and open areas. The tunnel shaped areas are generally long hallways where the uniformly distributed nodes are the likely candidate for node deployment. Based on the channel properties of the tunnel area, the maximum distance between the two relay nodes can be estimated. Since nodes are arranged along the tunnel path, their failure can cause a complete interruption of communication. Thus, the deployment must take into account the possibility of redundancy to combat such a failure, as shown in Figure 3.5.

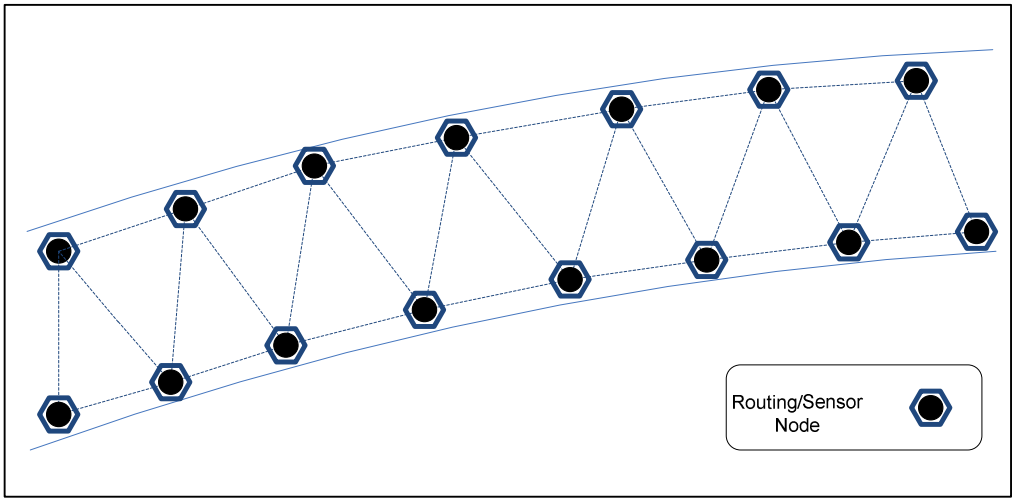

Figure 3.5: Uniform node distribution in tunnels

The open area generally has higher activity because it is the site of mining operation and ore extraction and thus requires a greater number of nodes to provide adequate node coverage. For the open area, non-uniform distributions of nodes are more desirable, as shown in Figure 3.6. Most of the nodes are involved in sensing and monitoring while a few of them are used for relaying the acquired information. Therefore, in the open area, each node may act either as a data

collector or a traffic relay. The maximum distance among relay nodes must be defined based on the channel properties and communication traffic in the area.

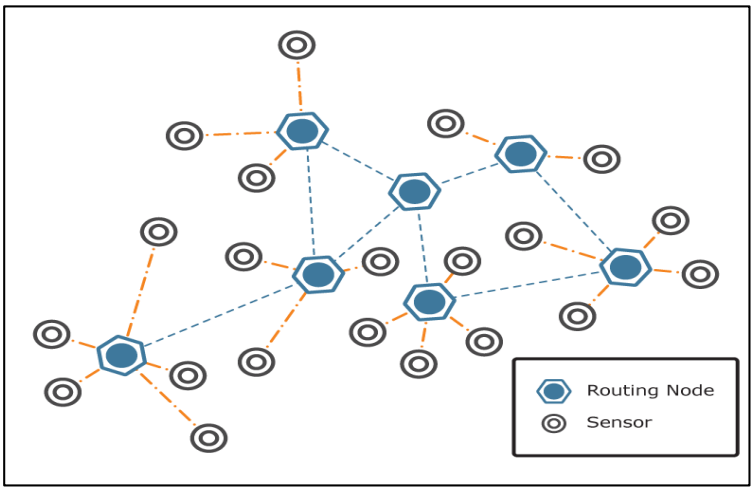

Figure 3.6: Non-uniform node distribution in an open area

3.5.3 Routing

The task of finding and maintaining routes in WSN is essential since energy restrictions, latency, and sudden changes in the node status (e.g., failure) cause frequent and unpredictable topological changes. Many algorithms have been proposed for the routing, considering the inherent features of WSN along with the application and architecture requirements [48, 49].

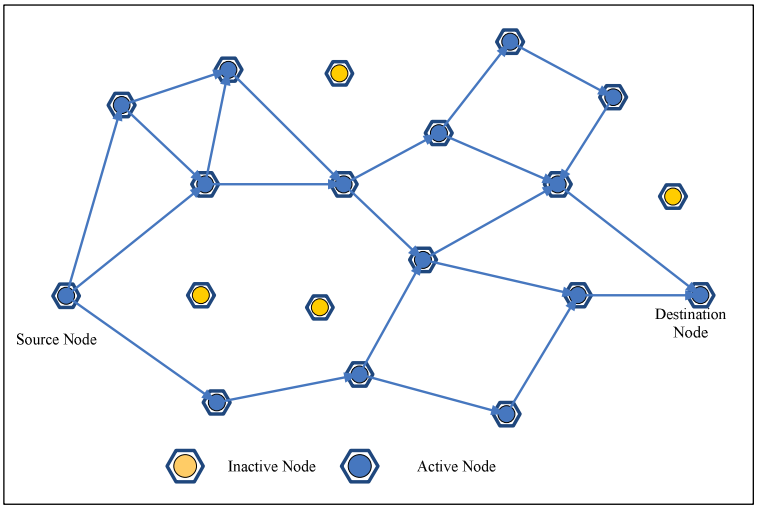

Figure 3.7: Possible paths between source and destination node

In general, the objective of the WSN routing algorithms is to find the "optimum" path between two nodes, the source node (n_s) and the destination node (n_D), while the optimality is defined by criteria such as minimum latency or power consumption.

Assume that $r = n_D, n_1, \dots, n_{k-1}, n_S$ is a path between n_s and n_D that has $k-1$ intermediate nodes $n_1, n_2, \dots, n_{k-1}$ and R_S^D is the set of all possible paths between n_s and n_D, as shown in Figure 3.7. The total power consumption associated with a path like r is given by:

$$P(r) = \sum_{i=0}^{k} (p(n_i, n_{i+1}) + c(i+1)) \tag{3.1}$$

where $n_0 = n_S$, $n_k = n_D$, and $c(i+1)$ is the receiver power consumption at node n_{i+1}, and the power required to transmit data between two nodes n_i and n_j is:

$$p(n_j, n_k) = \alpha_p . d(n_j, n_k)^L \tag{3.2}$$

L is the path loss, α_p is a constant of propagation and $d(n_i, n_j)$ is the distance between n_i and n_j. Therefore, a routing optimization problem can be defined as:

$$\min_r P(r) = \sum_{i=0}^{k} (p(n_i, n_{i+1}) + c(i+1)) \quad \forall r \in R_S^D \tag{3.3}$$

The underground mine wireless sensor network has its own restrictions. In addition to being a power constrained network, it has various latency limits for different types of data. For example, reporting some emergency events, such as the toxicity level in some parts of a mine is delay-sensitive while the air temperature or humidity is not. Therefore, emergency traffic could compromise energy efficiency to minimize delay. If $T(n_i, n_j)$ is the communication delay between the nodes n_i and n_j, and T_{max} is the maximum latency, then routing optimization can be modified as follows:

$$\min_{r} P(r) = \sum_{i=0}^{k} (p(n_i, n_{i+1}) + c(i+1))$$

$$\sum_{i=0}^{k} T(n_i, n_{i+1}) \leq T_{Max} \tag{3.4}$$

$$\forall r \in R_S^D$$

3.5.4 Fault Tolerance

In an underground mine, some sensor nodes may fail or be blocked due to lack of power or physical damage. The failure of individual sensor nodes should not affect the overall task of the wireless sensor network. However, when many nodes fail routing protocols must accommodate the formation of new links and routes to the data collection base stations. This may require either actively adjusting the transmission power or rerouting packets through regions of the network where more energy is available. Therefore, multiple levels of redundancy may be needed in an underground wireless sensor network. Fault tolerance routing techniques are still one of the areas that require continuous research and further investigations [50].

3.5.5 Network Scalability & Dynamics

As the tunnels expand in the underground mine, the number of sensor nodes increases. Routing protocols are mostly concerned with excessive routing message overhead caused by the increase of network size. Any routing scheme must be able to work with this addition to the network. In the underground, the WSN nodes can be stationary or mobile. The scalability is more challenging in the presence of both large numbers of nodes and mobility. Routing messages to or from moving nodes is more challenging since route stability becomes an important issue.

3.5.6 Latency

There are some types of data (toxicity level, alarm signal) that should be delivered within a certain period of time from the moment it is sensed. Therefore latency becomes an additional constraint on the routing algorithm [50]. The routing algorithm for these time sensitive WSN applications must address the latency issue and establish a route between an event and a sink within a short interval of the event.

3.6 Summary

The promise that WSN brings to the mining industry is very significant for the enhancements of safety and productivity for the operations of mines. A number of applications and features can be offered by the WSN in the mines; this includes the identification of workers in the mines through the deployments of localization solutions based on the WSN. The control of personnel traffic into hazardous areas can also be achieved by WSN that provides warning indication signals. The WSN can also be used for reducing fatal accidents due to collisions, monitoring of underground gases, and scheduling maintenance.

Deploying WSN in the mines is associated with number of challenges that requires exceptional efforts to achieve reliable and economical operating outcomes. The limitations of power availability to power up the nodes of the WSN in the underground is one of the major issues that confronts those efficiently deploying WSN for any type of application. To ensure that the WSN has a long life of operation, the utilization of available power needs to be optimized and managed carefully within the networks of the mines. Other types of challenges are related to the structure and layout of the mines themselves. The complex characteristics of the wireless channel in the mines added another layer of complication to the design and deployments' processes of the WSN.

Traffic routing can be another challenging task in the design of the WSN for the mines. The optimization of the best route in the mine will need to consider a number of constraints due to the difficult nature and layouts of the mines. Fault Tolerance, Network Scalability and Latency are among other challenges that can affect the reliable deployments of the WSN in the mines.

Chapter 4

4. The Proposed Optimized Backbone Networks for Underground Mines

4.1 Introduction

As mentioned in the previuse chapters, the communication networks typically deployed in underground mines are integrated networks consisting of three main elements. As Figure 4.1 shows, these elements are the mine network's backbone; the wireless channel of the mine and the wireless and mobile networks such as the WSN or mesh networks that are wirelessly related to the rest of the integrated network in the mine.

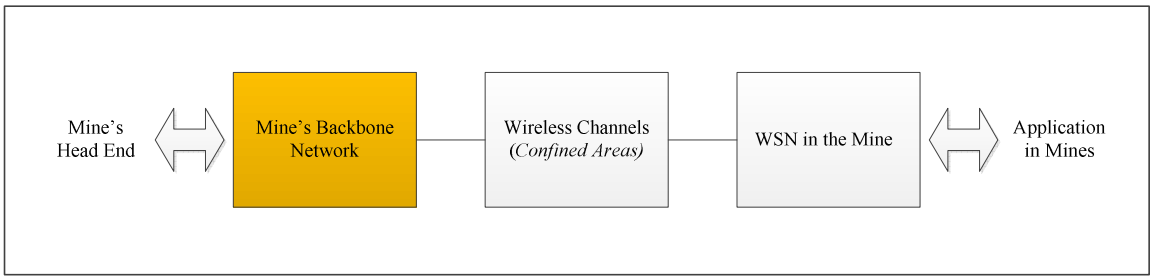

Figure 4.1: Mines Networks Components

In this Chapter the backbone element is optimized for improved reliability, scalability within the context of self-organized networks and green communication in the mines. The backbone network is the main transmission line through which the information travels back and forth from the surface of the mine to different locations and branches all through the mine. These networks are typically connected to other secondary networks through special gateways or similar devices. The backbone network can be any kind of transmission line or the combination of a few selections such as fiber networks, coaxial transmission lines, Radiating Cable Network, etc. The

RCN is considered to be the most common type of backbone networks in underground mines [2,3]. It is the mine's main transmission line through which all the communication RF traffic travel between the surface and different areas in the mine. The RCN also acts as long piece of antenna that enables homogeneous RF coverage in all the areas where the RCN is installed in the mine. The RCN is also used as the power grid to power up all the active devices in the backbone network. The amplifiers, repeaters, wireless nodes and gateways are powered directly from the RCN. This communication network and power grid is required to be very robust to resist the harsh environmental conditions in the mine. Mine size is very dynamic as it grows constantly with the progress of excavations and the removal of the ore from the ground. Therefore, the RCN is required to grow with the mine itself. The mine's backbone network is required to be very scalable and flexible to accommodate the growth and dynamic expansion of the mine layout. The flexibility and scalability requirement brings about an important challenge in the design of such networks in the mines. In this Chapter, we are presenting new approaches and algorithms to optimize the operation of the RCN in the mines and to increase scalability and reliability.

4.2 Radiating Cable Systems Challenges

As mentioned in Chapter s1 and 2 a number of fundamental challenges and difficulties exist in the RCN of underground mines. These issues can be summarized in the following subsections.

4.2.1 System Scalability and Stability Problems

The signal level varies as it travels through the system. The variations in signal level can be caused by temperature variations or by external noise generated by mining machinery. Therefore it is important to employ equalization mechanisms to equalize the levels within the system and to ensure adequate system performance. As explained in Chapter 1 many equalization techniques have been developed to overcome the problems of level variations and slope corrections in the leaky feeder systems; however, these approaches have not yielded fully reliable and stable system performance. In general, the system equalization is achieved via the reliance on closed-loop control circuits to equalize the system gain. These approaches were associated with stability and level variation problems. Overshoot is evident in cascaded amplifier systems. The overshoot magnitude increases with the number of amplifiers in the system. This implies that the stability of the cascade decreases as the number of amplifiers in use increases. In this Chapter, we are presenting a novel technique for optimizing the stability and scalability capacities of the RCN in the mine. The developed algorithm was designed within the context of self-organized networks

to produce a high level of power management to enhance the power consumption and utilization of the mines' backbone networks [51].

4.2.2 Power Availability Problems

The active components of the radiating cable system, namely the system repeater, bidirectional amplifiers and wireless gateway nodes are relatively high in power consumption. Moreover, this equipment is powered directly from the radiating cable itself. This means that the power signals (i.e. DC power) that exist in the radiating cable can be of high magnitude. The expense associated with the high power consumption is obviously a big concern for the mine's operators as these systems can be very costly to operate on a continuous basis.

Furthermore, a higher power signal is not permitted in the mines especially when explosive gases, like methane, exist. Many regulations have been established to control and minimize the amount of power in the radiating cable. The constraint in allowable power is one of the most difficult challenges the mines' operation faces today. Of course, the combination of low permissible power and its availability in the mines create a major constraint that limits the scalability of the mine's backbone networks. Therefore, innovative solutions are needed to provide reliable and efficient power utilizations for the system in the underground mines. In the next Chapter, a charging schedule algorithm is presented to mitigate the problem of the power availability and distribution. This will open the door to a new era of green commendation in the confined areas of the underground mines.

4.3 The proposed Prediction-based Adaptive Equalization Algorithm (PAEA)

Within the overall scheme of the Self-Organized Network (SON), an intelligent algorithm is developed to mitigate the problems of network stability and scalability in the RCN. The algorithm optimizes the performance of the system in two stages. The First stage, called Network Self Recognition (NSR), the network will discover its own parameters. Based on this learned knowledge the network will optimize the performance by adjusting the network configurations during the second stage of the PAEA algorithm which is called Network Self Configuration (NSC). To achieve higher network stability, the amplifiers in the mine's RCN will be able to predict the losses in the network even before they happen.

This prediction is based on some preliminary information and parameters determined by the network during the NSR phase. The developed algorithm, called "Prediction-based Adaptive

Equalization Algorithm (PAEA)," will then apply certain configuration parameters to the network during the Network Self Configuration (NSC) phase that result in an optimized system stability and maximized scalability of the network. The algorithm was applied to a typical Radiating Cable Network in the mine as shown in Figure 4.2. There are four distinct RF bands in the system. These bands are required to provide RF propagation paths for voice and data communications.

Table 4.1 lists the four bands of the system and their frequency ranges. The upstream and downstream orientations of the system bands are shown in Figure 4.2. This type of reading cable network is normally known as the CMTS. These types of networks are capable of providing analogue voice communication and high-speed digital data communications [23, 51].

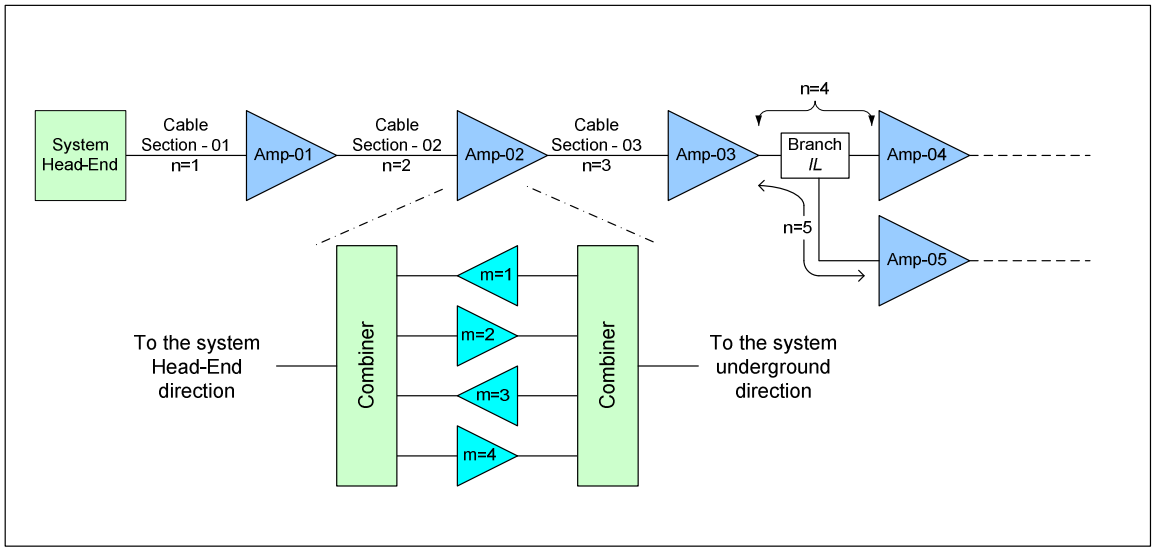

Figure 4.2: RCN Frequency Bands Layout

Band No.	Band Name	Frequency (MHz)
1	Upstream Data	5-42
2	Downstream Voice	155-158
3	Upstream Voice	172-175
4	Downstream Data	220-232

Table 4.1: System Frequency Plan

The algorithm utilizes three reference carriers, also called pilots, which are generated at the system Head-End. These pilots can be referred to as Low-Pilot (PL), Midpoint-Pilot (PM), and High-Pilot (PH). The frequencies of these pilots are selected to be within the downstream voice and data bands (i.e. m=1 and 3). The PL propagates within the downstream voice band. The PM propagates at the lower end of the downstream data band and the PH propagates at the upper end of the downstream data band. A graphical representation of these reference pilots is shown in Figure 4.3. The amplitude of these pilots can be set at the system head-end to reference power level, PL_o , PM_o and PH_o, for the Low Pilot, Midpoint Pilot and High Pilot, respectively.

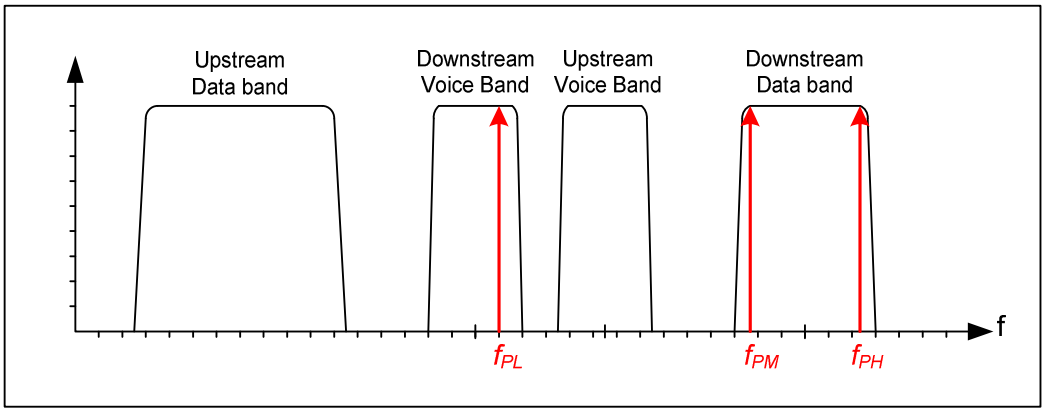

Figure 4.3: Graphical Representations of the Reference Pilots.

4.3.1 Network Self Recognition (NSR)

As a first stage and within the phase of Network Self Recognition (NSR), the network collects the necessary information and parameters such as system losses in different sections of the RCN. The fact that we have reference pilots traveling across the network in only one direction on only a certain frequency that makes it difficult to know the channels' characteristics and losses of the RCN for other frequency bands of the network. Therefore, the algorithm needs the intelligence to adaptively model the channel characteristics of the RCN in the other frequency bands of the network. Moreover, the System Loss, *L*, of each section (i.e. between two nodes) consists of two components. The first component is called the Cable Longitudinal Loss (CL), which is due to the loss of the leaky cable itself. The amount of this component is, in fact, a function of frequency and cable length. Frequency response to this type of loss constitutes a negative slope since the frequency terms in the high spectrum suffer higher losses than the lower frequency terms. The second component of the system loss is called the Insertion Loss (IL). This component is not

frequency dependent, and it is caused mainly by the insertion loss of miscellaneous active and passive units installed on the system. The frequency response of these units is typically flat, where the attenuations are almost the same over the entire frequency spectrum. An example of these units is found in cable branch units (power dividers or splitters) and cable splice boxes for joining two sections of cables [51].

To determine the relative positions between two nodes, it is very important to differentiate between these two types of losses and to quantify their values in order to determine the nature of the losses between two nodes in the system. The system loss in each cable section, $L_{n,m}$, can be calculated by the following:

$$L_{n,m} = CL_{n,m}(x_n, f_m) + IL_n \ , \tag{4.1}$$

where,

$L_{n,m}$: The total loss in one section of the cable, n, at frequency band m,

$CL_{n,m}$: The longitudinal cable losses in one section. This loss is a function of cable length, x_n, and the frequency, f_m, for each frequency band. (Negative slope loss),

IL_n: The total insertion loss of all passive units in section, n , of the system. (Flat repose loss),

n : The cable section index in the system,

m : The band index in the system.

During the NSR phase, the reference pilots, PL, PM and PH, propagate through the RCN and losses occur as a result. As previously mentioned, the losses are of two components, namely, the cable longitudinal loss and the insertion loss of units installed on the system. When these two carriers arrive at the first node (i.e. amplifier), the RF detector at the input stage detects (measure) the levels of these carriers. For the first amplifier in the system, $(i.e. n = 1)$, the measured levels, PL_1, PM_1 and PH_1, will be stored in the amplifier's microcontroller memory.

Thus far, the actual total system loss of the first cable section, $n = 1$, for the two downstream bands ($m = 2 \ and \ m = 4$)can be calculated. The system loss is essentially the difference in the pilots' levels at the head-end and the measured levels of these pilots when they are detected (i.e. measured) at the amplifier's input stage.

The system loss at PL frequency, f_{PL} , is:

$$L_{n,2} = PL_o - PL_n \,, \tag{4.2}$$

and the system loss at PH frequency, f_{PH} , is:

$$L_{n,4} = PH_o - PH_n \,. \tag{4.3}$$

So far, only the total system loss, L, of the first cable section has been measured in the two downstream bands of interest. The values of CL_n and IL_n are yet to be determined. Let's rewrite Eq. 4.1 to define the total system loss for any cable section, n , in downstream bands $m = 2$ and $m = 4$.

$$L_{n,2} = CL_{n,2} + IL_n \,, \tag{4.4}$$

$$L_{n,4} = CL_{n,4} + IL_n \,. \tag{4.5}$$

It will be advantageous to define a relationship between the longitudinal losses of leaky cable at the downstream frequency bands, $m = 2$ and $m = 4$. This relationship helps in defining the loss of PL in terms of PH loss or vice versa. We can define the Downstream Cable Loss Ratio, R_D , to be the ratio between the cable losses at PL frequency (which represent the cable loss at $m = 2$) to those at PH frequency, which represent the cable loss at $m = 4$:

$$R_D = \frac{Cable\ Loss\ @\ f_{PL}}{Cable\ Loss\ @\ f_{PH}} \,,$$

$$R_D = \frac{CL_{n,2}}{CL_{n,4}} \,, \tag{4.6}$$

therefore,

$$CL_{n,2} = R_D\ CL_{n,4} \,. \tag{4.7}$$

In Practice, cable loss ratios for different frequencies and types of cables can be obtained from the cable manufacturer and are also available in many reference manuals. A sweep test was conducted on one type of leaky cable commonly used in underground communication systems. The result of this test is shown in Figure 4.4.

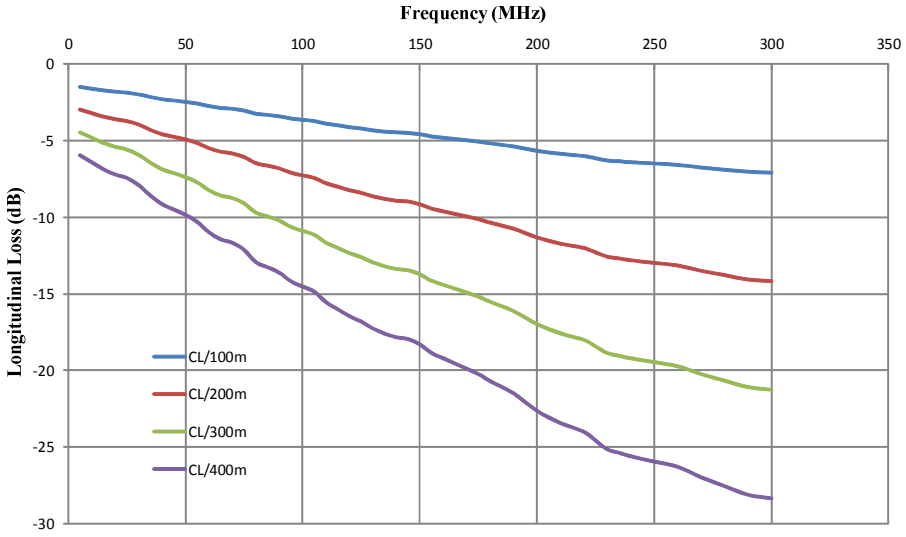

Figure 4.4: Leaky Cable Longitudinal Loss Chart

Substituting Eq. (4.7) into (4.4) and rearranging the equation will arrive at:

$$L_{n,2} = R_D \; CL_{n,4} + IL_n \; ,$$

$$IL_n = L_{n,2} - R_D \; CL_{n,4} \; . \qquad (4.8)$$

Substituting Eq. (4.8) into (4.5) and solving for $CL_{n,4}$ results in:

$$L_{n,4} = CL_{n,4} + L_{n,2} - R_D \; CL_{n,4} \; ,$$

$$L_{n,4} = CL_{n,4}(1 - R_D) + L_{n,2} \; ,$$

$$CL_{n,4} = \frac{L_{n,4} - L_{n,2}}{1 - R_D}. \quad (4.9)$$

IL_n can be calculated by substituting Eq. 4.9 into Eq. 4.5 as follows:

$$IL_n = L_{n,4} - CL_{n,4}. \quad (4.10)$$

The insertion loss in cable section n, IL_n is the same for all frequency bands. The Longitudinal loss $CL_{n,2}$ of the cable section, n, in band $m = 2$, can be easily calculated by using the Downstream Cable Loss Ratio defined in Eq. 4.6. Therefore, at the end of the NSR stage, we could obtain the following parameters:

- System losses for only the band in the downstream direction where reference carriers are available,
- Cable sections lengths in the network,
- Passive devices losses in the network.

4.3.2 Networks Self Configuration (NSC)

The self - discovered network parameters during the NSR phase are used in this phase to provide system gain and slope equalizations. Thus far, both components of the system loss, the leaky cable longitudinal loss, CL, and insertion loss, IL, have been determined for the system bands $m = 2$ and $m = 4$. Therefore, the gains of these bands can be found and adjusted to compensate for the system losses incurred in system section, n, previous to the amplifier as follow:

$$G_{n,m} = L_{n,m}. \quad (4.11)$$

Since there are no reference carriers in the upstream directions, the algorithm will use the information provided during the NSR phase to model and then predict the required equalization parameters of the amplifiers in this direction. Eq. 4.1 can be used to define the system loss in the upstream bands, $m = 1$ and $m = 3$ respectively:

$$L_{n,1} = CL_{n,1} + IL_n, \quad (4.12)$$

$$L_{n,3} = CL_{n,3} + IL_n \ . \qquad (4.13)$$

Recall that the insertion loss component, IL_n, was already determined during the calculations of the downstream system losses.

Let's define some reference points in the upstream bands as shown in Table 4.2.

Reference Points	Frequency (MHz)
f_1	5.00
f_2	42.00
f_3	174.00

Table 4.2: Upstream Bands reference points-frequencies

f_1 represents the frequency of a reference point at lower end of the $m = 1$ band.

f_2 represents the frequency of a reference point at upper end of the $m = 1$ band.

f_3 represents the frequency of a reference point within the upstream $m = 3$ band.

These points are used in calculating the predicted signal losses in these bands. A graphical representation of these reference points is shown in Figure 4.5

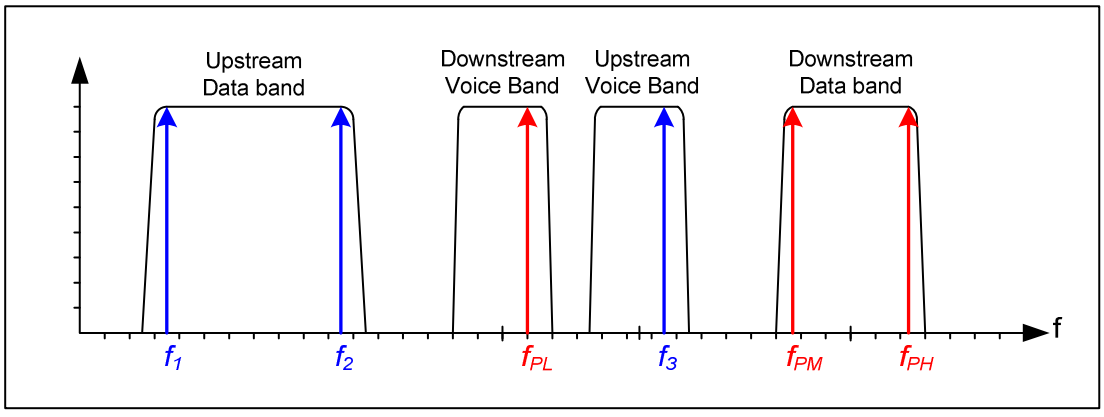

Figure 4.5: Graphical Representations for the Reference Points

Similar to the Downstream Cable Loss Ratio, R_D, that defined a relationship between the two downstream bands, m= 2 and m= 4, more cable loss ratios are required to define relationships between the cable longitudinal loss at $m = 2$ and $m = 1$ and between $m = 2$ and $m = 3$ as follows:

Let R_{U1} be the Cable Loss Radio between the cable losses at f_{PL} and the cable losses at f_1

$$R_{U1} = \frac{Cable\ Loss\ @\ f_{PL}}{Cable\ Loss\ @\ f_1},$$

$$R_{U1} = \frac{CL_{n,2}}{CL_{n,f_1}}. \tag{4.14}$$

Let R_{U2} be the Cable Loss Radio between the cable losses at f_{PL} and the cable losses at f_2 as in the following:

$$R_{U2} = \frac{Cable\ Loss\ @\ f_{PL}}{Cable\ Loss\ @\ f_2},$$

$$R_{U2} = \frac{CL_{n,2}}{CL_{n,f2}}. \tag{4.15}$$

Let R_{U3} be the Cable Loss Radio between the cable losses at f_{PL} and the cable losses at f_3 as in the following:

$$R_{U3} = \frac{CL_{n,2}}{CL_{n,f3}}. \tag{4.16}$$

We know that, $CL_{n,1} = CL_{n,f2}$. Substituting for $CL_{n,1}$ in Eq. (4.15) , we obtain:

$$CL_{n,1} = CL_{n,f_2} = \frac{CL_{n,2}}{R_{U2}}. \tag{4.17}$$

The total system losses in the upstream data band, $L_{n,1}$ can be calculated from Eq. 4.1

$$L_{n,1} = \frac{CL_{n,2}}{R_{U2}} + IL_n \,. \tag{4.18}$$

Similarly, the total system loss in the upstream $m = 3$ band, $L_{n,3}$ can be found as following

$$L_{n,3} = \frac{CL_{n,2}}{R_{U3}} + IL_n \,. \tag{4.19}$$

At this point, all the components of the system loss have been determined for all the four bands in the system. Eq. 4.11 can be used to calculate the gains of the upstream amplifiers in the system. Next, the algorithm will provide Slope Equalization to the network. The slope control is required only for the data bands as these bands have broad bandwidths, 12 MHz for the downstream data band and 37 MHz for the upstream data band. The RF response of any cable section has the shape of a negative slope (Tilt). The longitudinal loss in the cable at higher frequencies is greater than the loss at lower frequencies. Figure 4.6 shows the proposed system equalization block diagram.

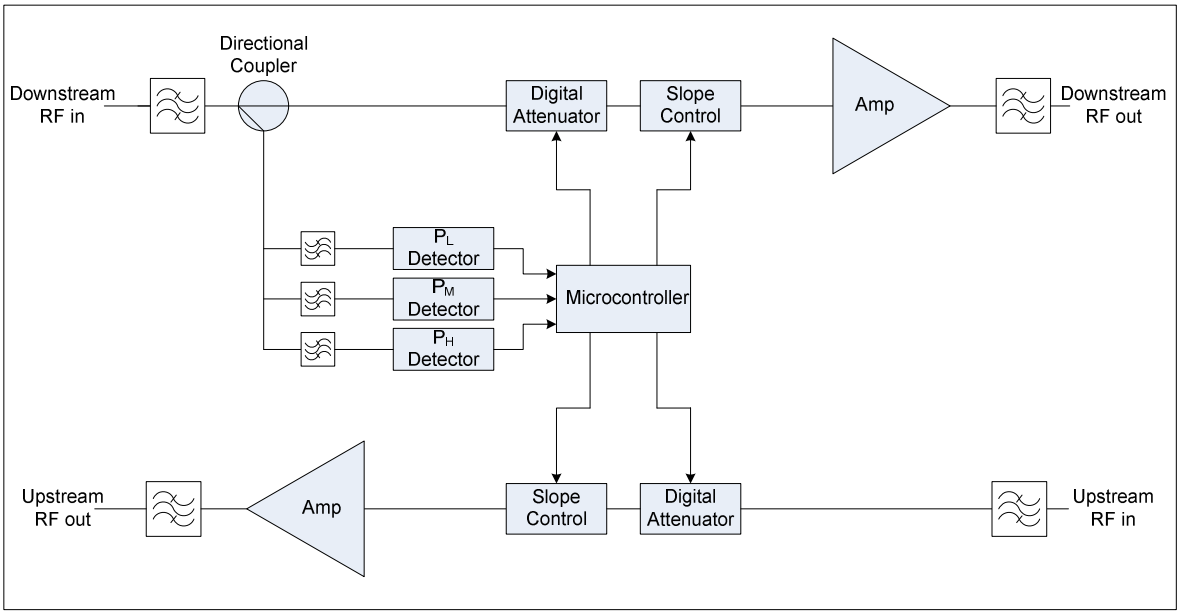

Figure 4.6: System Equalization Block Diagram.

To calculate the slope in the downstream data band, the system losses at the frequencies of PM (f_{PM}) and PH (f_{PH}) need to be determined. The losses at f_{PH} were calculated in Eq. 4.3.

The losses at f_{PM} can be calculated as follows:

$$L_{n,PM} = PM_o - PM_n \,. \tag{4.20}$$

The Slope in the downstream data band can be calculated as follows:

$$T_4 = L_{n,4} - L_{n,PM} \,. \tag{4.21}$$

T_4 is the slope in the data downstream band, m= 4. Next we need to calculate T_1 the slope in the upstream data band, $m = 1$. To calculate this slope, the cable longitudinal losses $CL_{n,f1}$ and $CL_{n,f2}$ at the two reference points, f_1 and f_2 respectively are required.

From the Cable Loss Ratio equations RU_1 and RU_2, the cable longitudinal loss at the lower end of band m=1 can be calculated as in the following;

$$CL_{n,f1} = \frac{CL_{n,2}}{R_{U1}} \,. \tag{4.22}$$

The cable longitudinal loss at the higher end of band m=1 was calculated in Eq. 4.18. Therefore, the slope, T_1, in the upstream data band can be calculated as follows:

$$T_1 = CL_{n,f2} - CL_{n,f1}. \tag{4.23}$$

Thus far, the algorithm could calculate all the required equalization parameters Figure 4.7 shows the flowchart of the Prediction-based Adaptive Equalization Algorithm (PAEA).

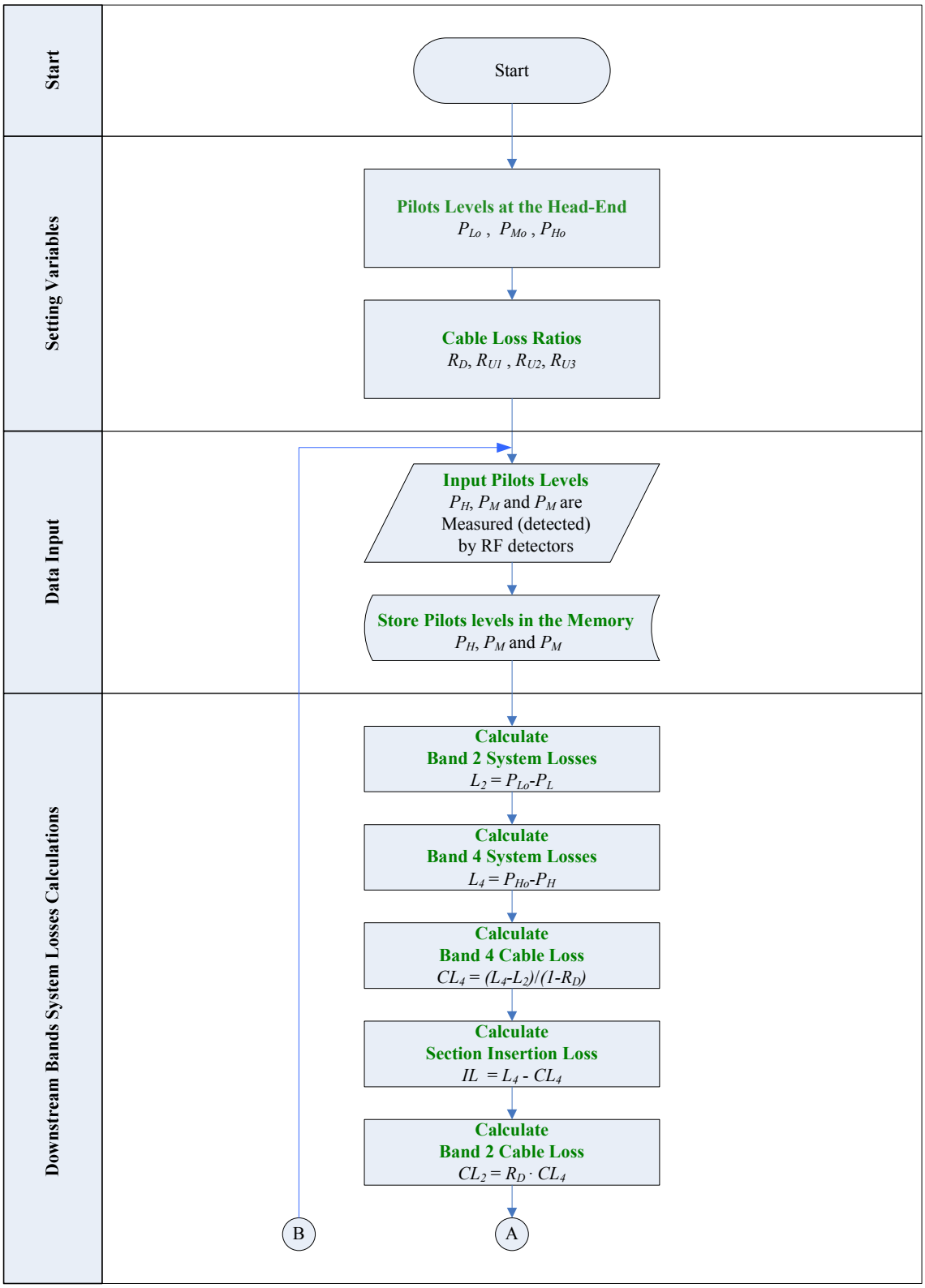

Figure 4.7: Prediction-based Adaptive Equalization Algorithm (PAEA)
(Part 1 of 2)

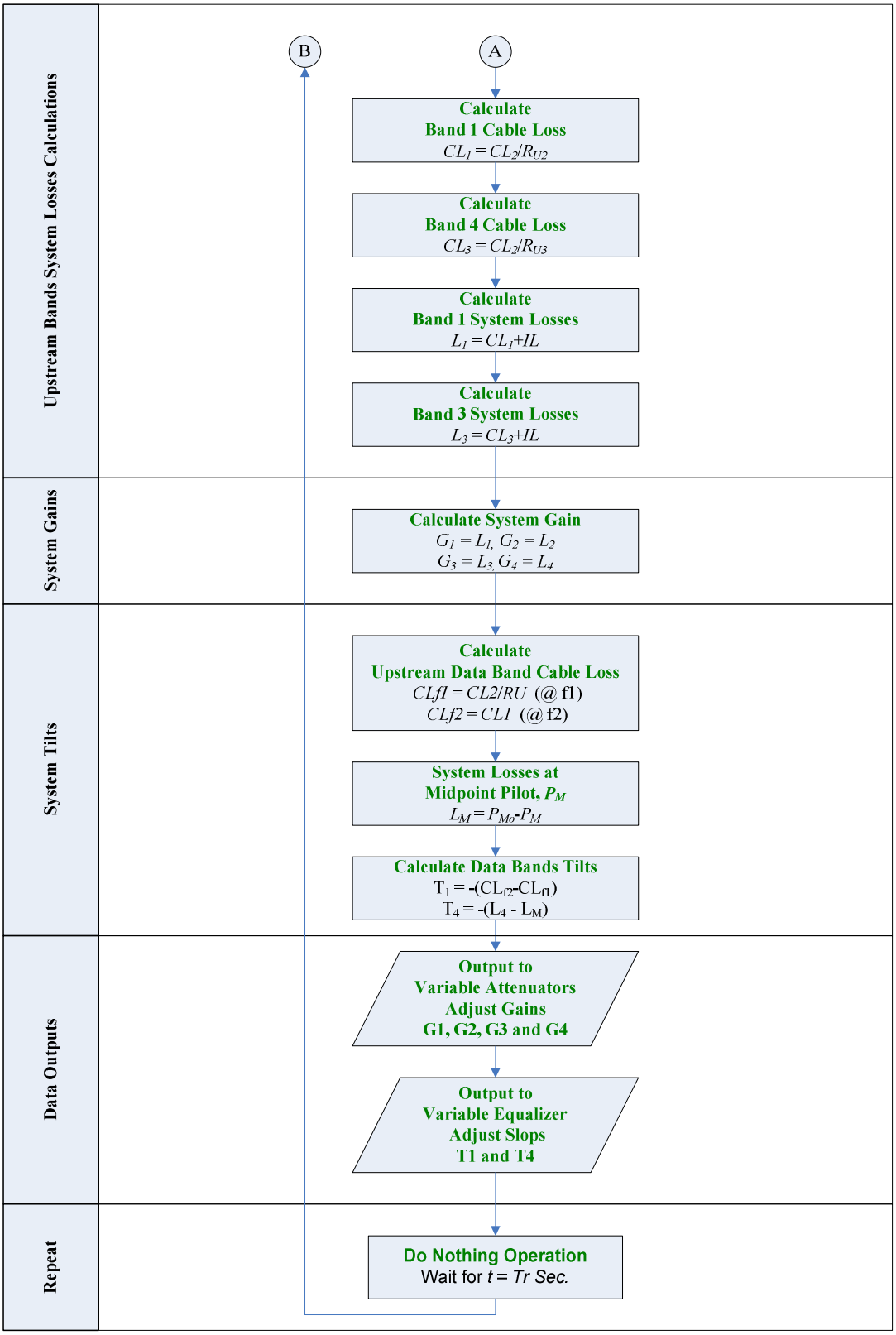

Figure 4.7: Prediction-based Adaptive Equalization Algorithm (PAEA)
(Part 2 of 2)

4.4 Simulation results

The PAEA algorithm was simulated using MATLAB simulation software. A typical leaky cable system layout with 10 amplifiers was assumed for the purpose of the simulations, as shown in Figure 4.8. The output results of the simulations are summarized in
Table 4.3.

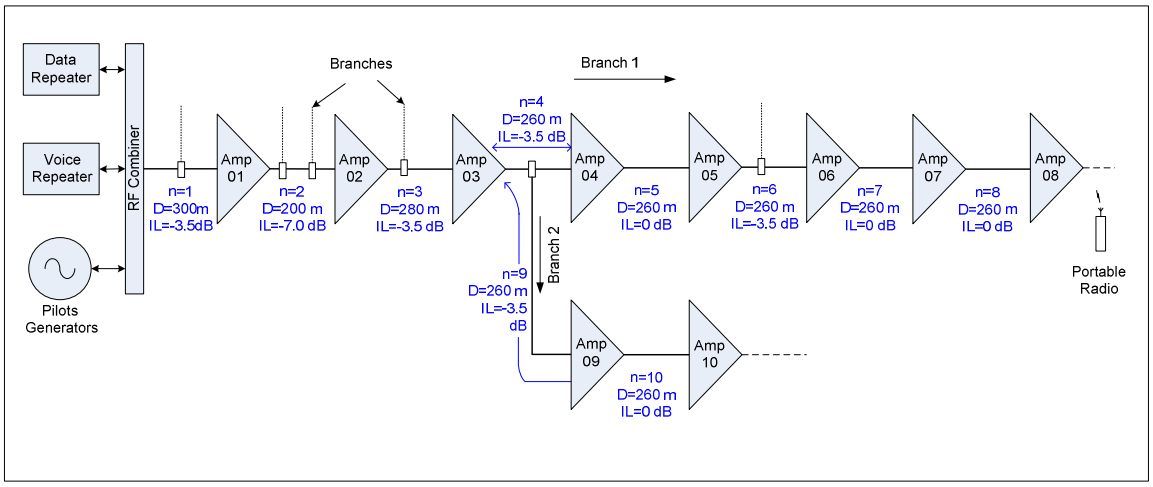

Figure 4.8: Typical Leaky Feeder System Layout

To evaluate the simulation results, the following system operating conditions were considered in the evaluations of the algorithms.

1. Amplifier's Maximum Power Output: Each of the four amplification bands of the amplifier has a maximum power output rating. A wrong gain or slope decision might result in higher output levels that could potentially saturate the amplifiers and generate unstable system behaviors. In our simulation, it was assumed that the maximum power rating for the downstream voice band, m=2, is (+ 5.00 dBm). The maximum power rating for the other three bands was assumed to be equal to (-10.00 dBm). These assumptions reflect the typical system levels requirements normally used in a similar network in the mines. The simulation analyses show acceptable results for the maximum power outputs.

2. Actual System Losses vs. Calculated Amplifier's Gains: The calculated gain of the amplifier should match the actual system loss for each section. The analyses have verified that the calculated gain is adequate to compensate for the system loss.

3. Actual Cable Tilt vs. Calculated Amplifier's Slopes: The calculated slope should match the actual slope or tilt caused by the cable sections in the system. The analyses have verified that the calculated equalizations are adequate to correct the slopes in the system.

As per
Table 4.3, the PAEA algorithm has aligned the system to produce the proper gain and slope for each amplifier in both directions of the communication. After the amplifiers are aligned by the algorithm, the actual RF traffics for all bands in the network are applied to propagate through the system. These RF carriers need not be confused with the reference pilots used by the algorithms for the system gains and slopes alignments.

For the downstream direction, the RF levels of the voice and data carrier start from the surface Head-End. Therefore, the simulation output table should be followed from the top to the bottom. For the upstream direction, the RF levels of the voice and data carrier start from the end of the system. Therefore, the simulation table should be followed from the bottom to the top. In the simulation, the upstream RF carriers were injected at the output of the amplifier # 8.

Head-End	Band Name	DST Voice	DST Data	UST Voice	UST Data
	Bands Number	2	4	3	1
	Channel's Level @ Head End, dBm	25.00	-10.00	-60.00	-49.98
	Head-Ed Filtering Loss, dB	-20.00	-10.00	-20	-10
	Channel's Level @ Head End, dBm	5.00	-20.00	-40.00	-39.98
	Channel's Tilt @ Head End, dB		0.00		-0.01
n=01	Cable Length, m	300.00	300.00	300.00	300.00
	Actual Cable Loss, dB	-13.71	-17.31	-13.97	-7.11
	Actual Insertion Loss in the Section, dB	-3.50	-3.50	-3.50	-3.50
	Actual Section System Loss, dB	-17.21	-20.81	-17.47	-10.61
	Actual Cable Tilt, dB		-0.77		-4.37
Amp – 01	Measured Channels Level @ Amplifier Input, dB	-12.21	-40.81	-22.53	-29.37
	Calculated Equalizer, dB		0.77		4.37
	Calculated Gain, dB	17.21	20.81	17.47	10.62
	Measured Level @ Amplifier Output, dBm	5.00	-20.00	-40.00	-39.99
	Measured Flatness (Tilt) @ Amplifier Output, dB		0.00		-0.01
n=02	Cable Length, m	200.00	200.00	200.00	200.00
	Actual Cable Loss, dB	-9.14	-11.54	-9.31	-4.74
	Actual Insertion Loss in the Section, dB	-7.00	-7.00	-7.00	-7.00
	Actual Section System Loss, dB	-16.14	-18.54	-16.31	-11.74
	Actual Cable Tilt, dB		-0.51		-2.91
Amp – 02	Measured Channels Level @ Amplifier Input, dB	-11.14	-38.54	-23.69	-28.24
	Calculated Equalizer, dB		0.51		2.91
	Calculated Gain, dB	16.14	18.54	16.31	11.74
	Measured Level @ Amplifier Output, dBm	5.00	-20.00	-40.00	-39.99
	Measured Flatness (Tilt) @ Amplifier Output, dB		0.00		-0.01
n=03	Cable Length, m	280.00	280.00	280.00	280.00
	Actual Cable Loss, dB	-12.80	-16.16	-13.04	-6.64
	Actual Insertion Loss in the Section, dB	-3.50	-3.50	-3.50	-3.50
	Actual Section System Loss, dB	-16.30	-19.66	-16.54	-10.14
	Actual Cable Tilt, dB		-0.72		-4.08
Amp – 03	Measured Channels Level @ Amplifier Input, dB	-11.30	-39.66	-23.46	-29.85
	Calculated Equalizer, dB		0.72		4.08
	Calculated Gain, dB	16.30	19.66	16.54	10.14
	Measured Level @ Amplifier Output, dBm	5.00	-20.00	-40.00	-39.99
	Measured Flatness (Tilt) @ Amplifier Output, dB		0.00		-0.01

Table 4.3: System Simulation Results
(Part 1 of 4)

Branch 1	Band Name	DST Voice	DST Data	UST Voice	UST Data
	Bands Number	2	4	3	1
n=04	Cable Length, m	260.00	260.00	260.00	260.00
	Actual Cable Loss, dB	-11.88	-15.01	-12.11	-6.17
	Actual Insertion Loss in the Section, dB	-3.50	-3.50	-3.50	-3.50
	Actual Section System Loss, dB	-15.38	-18.51	-15.61	-9.67
	Actual Cable Tilt, dB		-0.67		-3.79
Amp – 04	Measured Channels Level @ Amplifier Input, dB	-10.38	-38.51	-24.39	-30.32
	Calculated Equalizer, dB		0.67		3.79
	Calculated Gain, dB	15.38	18.50	15.61	9.67
	Measured Level @ Amplifier Output, dBm	5.00	-20.00	-40.00	-39.99
	Measured Flatness (Tilt) @ Amplifier Output, dB		0.00		-0.01
n=05	Cable Length, m	260.00	260.00	260.00	260.00
	Actual Cable Loss, dB	-11.88	-15.01	-12.11	-6.17
	Actual Insertion Loss in the Section, dB	0.00	0.00	0.00	0.00
	Actual Section System Loss, dB	-11.88	-15.01	-12.11	-6.17
	Actual Cable Tilt, dB		-0.67		-3.79
Amp – 05	Measured Channels Level @ Amplifier Input, dB	-6.88	-35.01	-27.89	-33.83
	Calculated Equalizer, dB		0.67		3.79
	Calculated Gain, dB	11.88	15.00	12.11	6.17
	Measured Level @ Amplifier Output, dBm	5.00	-20.01	-40.00	-39.99
	Measured Flatness (Tilt) @ Amplifier Output, dB		0.00		0.00
n=06	Cable Length, m	260.00	260.00	260.00	260.00
	Actual Cable Loss, dB	-11.88	-15.01	-12.11	-6.17
	Actual Insertion Loss in the Section, dB	-3.50	-3.50	-3.50	-3.50
	Actual Section System Loss, dB	-15.38	-18.51	-15.61	-9.67
	Actual Cable Tilt, dB		-0.67		-3.79
Amp – 06	Measured Channels Level @ Amplifier Input, dB	-10.38	-38.51	-24.39	-30.33
	Calculated Equalizer, dB		0.67		3.79
	Calculated Gain, dB	15.38	18.50	15.61	9.67
	Measured Level @ Amplifier Output, dBm	5.00	-20.01	-40.00	-40.00
	Measured Flatness (Tilt) @ Amplifier Output, dB		0.00		0.00

Table 4.3: System Simulation Results
(Part 2 of 4)

Branch 1	Band Name	DST Voice	DST Data	UST Voice	UST Data
	Bands Number	2	4	3	1
n=04	Cable Length, m	260.00	260.00	260.00	260.00
	Actual Cable Loss, dB	-11.88	-15.01	-12.11	-6.17
	Actual Insertion Loss in the Section, dB	-3.50	-3.50	-3.50	-3.50
	Actual Section System Loss, dB	-15.38	-18.51	-15.61	-9.67
	Actual Cable Tilt, dB		-0.67		-3.79
Amp – 04	Measured Channels Level @ Amplifier Input, dB	-10.38	-38.51	-24.39	-30.32
	Calculated Equalizer, dB		0.67		3.79
	Calculated Gain, dB	15.38	18.50	15.61	9.67
	Measured Level @ Amplifier Output, dBm	5.00	-20.00	-40.00	-39.99
	Measured Flatness (Tilt) @ Amplifier Output, dB		0.00		-0.01
n=05	Cable Length, m	260.00	260.00	260.00	260.00
	Actual Cable Loss, dB	-11.88	-15.01	-12.11	-6.17
	Actual Insertion Loss in the Section, dB	0.00	0.00	0.00	0.00
	Actual Section System Loss, dB	-11.88	-15.01	-12.11	-6.17
	Actual Cable Tilt, dB		-0.67		-3.79
Amp – 05	Measured Channels Level @ Amplifier Input, dB	-6.88	-35.01	-27.89	-33.83
	Calculated Equalizer, dB		0.67		3.79
	Calculated Gain, dB	11.88	15.00	12.11	6.17
	Measured Level @ Amplifier Output, dBm	5.00	-20.01	-40.00	-39.99
	Measured Flatness (Tilt) @ Amplifier Output, dB		0.00		0.00
n=06	Cable Length, m	260.00	260.00	260.00	260.00
	Actual Cable Loss, dB	-11.88	-15.01	-12.11	-6.17
	Actual Insertion Loss in the Section, dB	-3.50	-3.50	-3.50	-3.50
	Actual Section System Loss, dB	-15.38	-18.51	-15.61	-9.67
	Actual Cable Tilt, dB		-0.67		-3.79
Amp – 06	Measured Channels Level @ Amplifier Input, dB	-10.38	-38.51	-24.39	-30.33
	Calculated Equalizer, dB		0.67		3.79
	Calculated Gain, dB	15.38	18.50	15.61	9.67
	Measured Level @ Amplifier Output, dBm	5.00	-20.01	-40.00	-40.00
	Measured Flatness (Tilt) @ Amplifier Output, dB		0.00		0.00

Table 4.3: System Simulation Results
(Part 3 of 4)

Branch 2	Band Name	DST Voice	DST Data	UST Voice	UST Data
	Bands Number	2	4	3	1
n=09	Cable Length, m	260.00	260.00	260.00	260.00
	Actual Cable Loss, dB	-11.88	-15.01	-12.11	-6.17
	Actual Insertion Loss in the Section, dB	-3.50	-3.50	-3.50	-3.50
	Actual Section System Loss, dB	-15.38	-18.51	-15.61	-9.67
	Actual Cable Tilt, dB		-0.67		-3.79
Amp – 09	Measured Channels Level @ Amplifier Input, dB	-10.38	-38.51		
	Calculated Equalizer, dB		0.67		3.79
	Calculated Gain, dB	15.38	18.50	15.61	9.67
	Measured Level @ Amplifier Output, dBm	5.00	-20.00		
	Measured Flatness (Tilt) @ Amplifier Output, dB		0.00		
n=10	Cable Length, m	260.00	260.00	260.00	260
	Actual Cable Loss, dB	-11.88	-15.01	-12.11	-6.16571
	Actual Insertion Loss in the Section, dB	0.00	0.00	0.00	0.00
	Actual Section System Loss, dB	-11.88	-15.01	-12.11	-6.17
	Actual Cable Tilt, dB		-0.67		-3.79
Amp – 10	Measured Channels Level @ Amplifier Input, dB	-6.88	-35.01		
	Calculated Equalizer, dB		0.67		3.79
	Calculated Gain, dB	11.88	15.00	12.11	6.17
	Measured Level @ Amplifier Output, dBm	5.00	-20.01		
	Measured Flatness (Tilt) @ Amplifier Output, dB		0.00		

Table 4.3: System Simulation Results
(Part 4 of 4)

4.5 Algorithm's Performance under Error

Errors in calculating and predicting the gains and slopes might occur within the scheme of the proposed algorithm. There are many areas within the scheme of the algorithm operation where errors could be generated. From the system-level point of view, errors could accumulate in cascaded amplifier systems. The accumulated errors could, in some cases, be of a significant magnitude that they would result in producing intolerable operating conditions. Therefore, the analyses of the accumulated errors are very important exercises that help in producing quantifiable figures required to evaluate the effects of the errors on the performance of the system. The scale of the system (i.e. the number of amplifiers in the system) is an important contributing factor in the accumulation of errors.

This section highlights three distinct types of errors that could affect the accuracy of calculating the gains and slopes of the amplifiers in the system. In general, these errors are of a probabilistic nature. The analyses will help in quantifying the magnitude of errors and estimate the accumulated effects of the errors on the systems.

System simulations have been conducted in analyzing the effects of errors on a typical system's operations. Based on these error analyses, suggested remedies and modifications have been presented to help reduce the errors in the systems. Three types of errors were identified as factors potentially affecting the accuracy of the algorithms in calculating and predicting the gains and slopes of the amplifiers in the system.

4.5.1 Pilot's Levels Precision Errors (LPE):

At the inputs' stages of the system amplifiers, the levels of the reference pilots are detected by the RF detectors. These levels are expected to be stable at the points where they are measured to provide stable and accurate inputs needed for the calculations of the system losses. However, this is not the case. There might be some variations in the pilots' levels over a short period of time. The variations in levels could be caused by the operational instability of the RF generators that are producing the pilots at the system head-end. The variations in the pilots' levels could also be caused by external noise generated by mining machineries or any other types of external noise sources within the proximity of the leaky cable. As a result, the precision and accuracy of the detected levels might include some errors.

The errors or variations in pilot levels are random in magnitude. They can be modeled with a Normal (Gaussian) distribution function. In our case, the average or the mean (μ) of the normal distribution function represents the average level of the pilot (i.e. the average of PL, for example, when detecting the Low Pilot) .The standard deviation (σ) is the variation in the pilot levels away from the mean. In this algorithm, it is assumed that the first standard deviation (1σ) is 1.0 dB away from the mean.

Pilot Levels Averaging Technique:

The Probability Density Function, PDF, for a normal distribution function is given by the formula [33]:

$$p(x) = \frac{1}{\sigma\sqrt{2\pi}} \exp\left(-\frac{(x-\mu)^2}{2\sigma^2} \right). \tag{4.24}$$

The Level-Averaging can be achieved by sampling the pilot levels over a period of time. The levels of these samples can then be stored in the memory of the microcontroller. The average value of the samples can be computed by calculating the means (μ) of the discrete Gaussian function.

$$\mu = \sum_{i=1}^{N} x_i \cdot p(x_i) , \tag{4.25}$$

where N is the number of samples over one cycle of sampling time, TS. The Averaging Technique is explained in the flowchart of Figure 4.9.

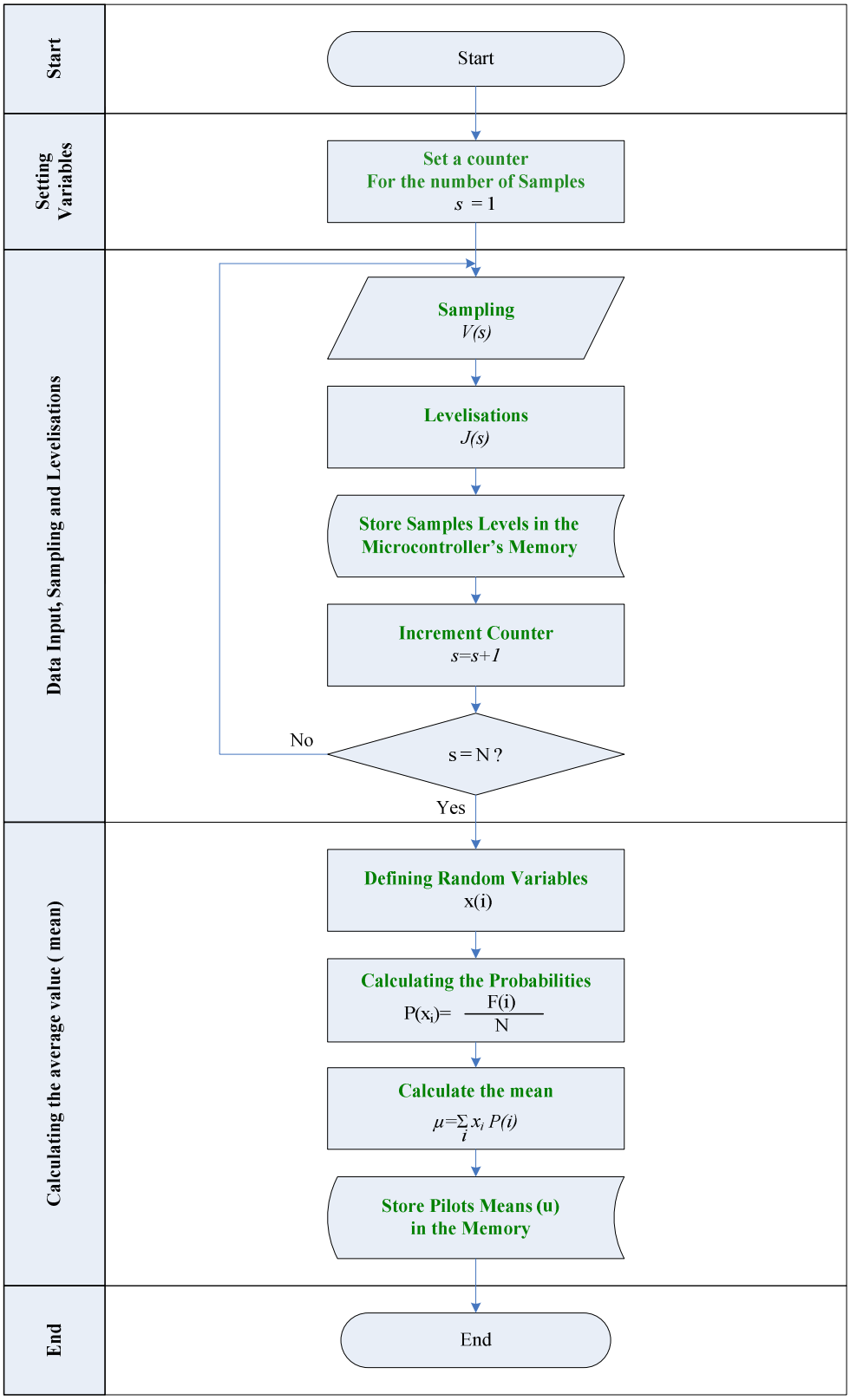

Figure 4.9: Reference Pilots Averaging- Technique Flowchart

Averaging Technique Simulations

The Level Averaging Technique was simulated to verify its effectiveness in reducing the Pilots Levels Precision Errors, LPE. In this analysis, the pilot signal is sampled 50 times over the sampling cycle of 100 units. Figure 4.10 shows the hypothetical pilot signal and the samples taken for the signal. It was concluded that an accuracy of less than 1 dB could be obtained from this averaging technique.

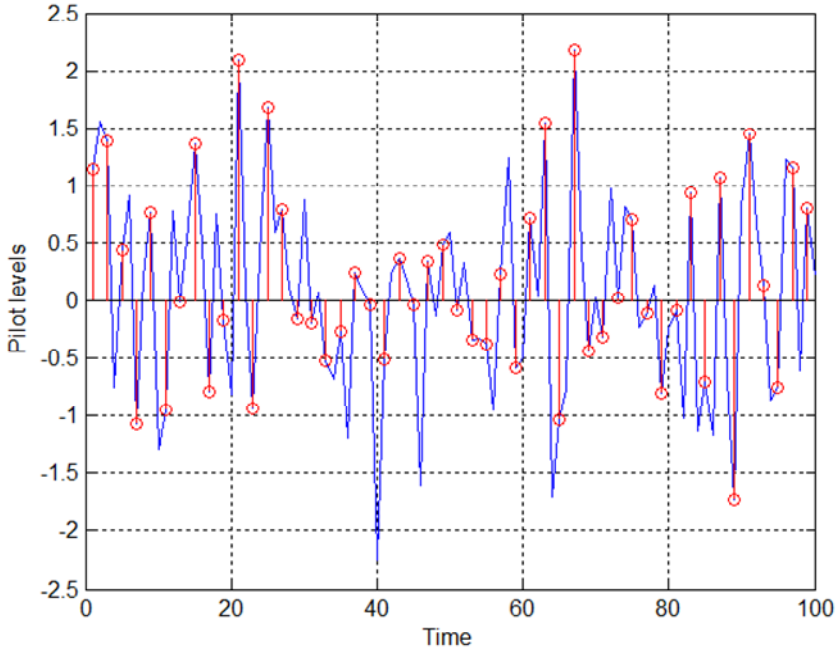

Figure 4.10: Pilot Signal Sampling Simulations.

Ideal Number of Samples N

The precision in calculating the average (μ) of the pilot levels generally improves by increasing the number of the samples N within the sampling time cycle T_S. The increase in the number of the samples also increases the calculation time needed by the microcontroller in order to obtain a result. Therefore, it is important to obtain an ideal number of samples to satisfy the precision requirements while not impeding the calculation speed.

Simulation analyses were conducted to evaluate the ideal number of sample vs. precisions in averaging the pilot levels, as shown in Figure 4.11. In the simulations, the expected value of the

pilot level at the input of the amplifier with no variations occurring was expected to be 0 dBm. However, errors occur with the variation in the pilot level. The averages of the detected signal were analyzed vs. the number of samples used in the averaging technique. It was found that the precision improves by increasing the number of samples, N. The simulations showed that the precision reaches a certain limit of improvements with increasing the number of samples. An ideal number of samples could be determined. The simulation analysis shows an ideal number of N = 20 samples when the precision of the pilot level reached a limit of a little or no further improvements.

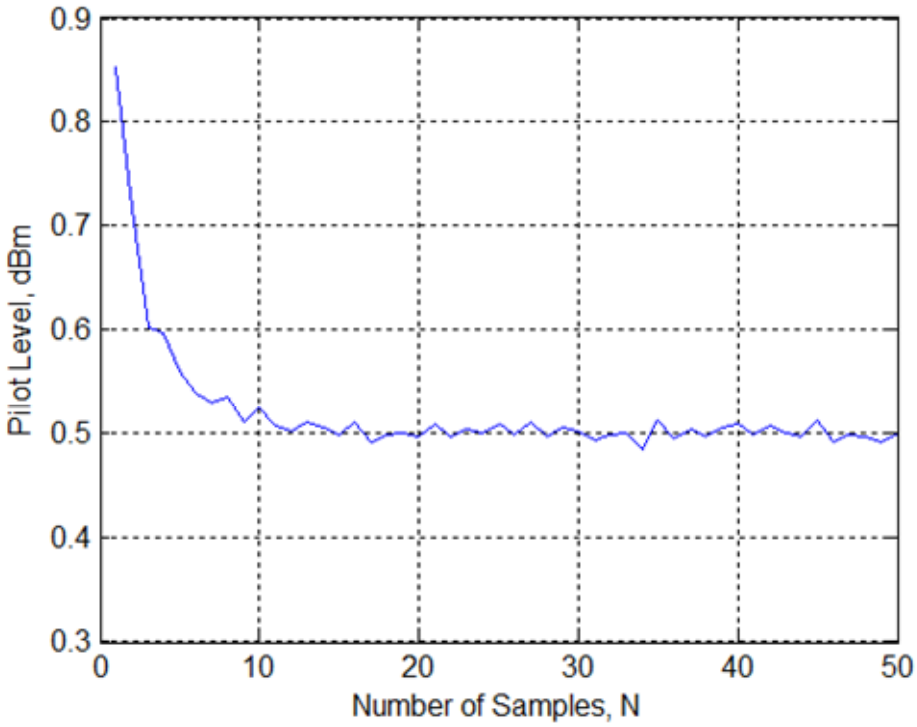

Figure 4.11: Number of Averaging Samples vs. Precision.

4.5.2 Components Tolerance Errors (CTE):

The accumulations of components' tolerance in electronics circuits can cause parts of the circuits to operate outside their nominal operating range. This will, of course, affect the functionality and the outputs of the algorithms. The levels of the reference pilots at the output of the downstream amplifiers are required to be exactly the same as their levels at the Head-End. However, the CTE can affect the accuracy of these levels.

The errors related to the tolerances of the circuits components can be controlled and reduced to a good extent by properly calibrating the amplifiers during the manufacturing process. However, the tolerances of some components might change after the installation of the system or by the effects of temperature variations. These errors will result in imprecise reference pilots levels leaving the amplifiers (i.e. unequal to the level of the pilots at the system head-end). Mostly, these errors affect the operation of amplifiers in the downstream direction.

The Components Tolerance Errors factor (E_{CTE}) can be defined as the percentage of errors in the gains of the amplifiers caused by the CTE.

$$PG_m = G \cdot (1 + E_{CTE}), \tag{4.26}$$

where,

PG_m: Is the Predicted-Gain of the amplifier. This is the gain estimation produced by the algorithm that might include error,

G_m: Is the Nominal (error free) gain of the amplifier,

E_{CTE}: Is the Components Tolerance Errors factor (in ± percentage figures).

The E_{CTE}, can be either positive or negative. Positive E_{CTE} makes the gain of the amplifier higher than the proper level of the error-free gain. Negative E_{CTE} makes the amplifier's gain lower than the error-free gain.

CTE Simulation Analysis:

Obviously, CTE can affect the operation of the PAEA algorithm and thereby could generate inaccurate gain and slope figures. To evaluate the effects of the CTE, simulation analyses were conducted. In these analyses, the (E_{CTE}) was assumed to be a discrete uniform random

distribution function of a maximum value of 5% (or ± 2.5 %). The analyses were conducted on a system with 100 cascaded amplifiers, as shown in Figure 4.12.

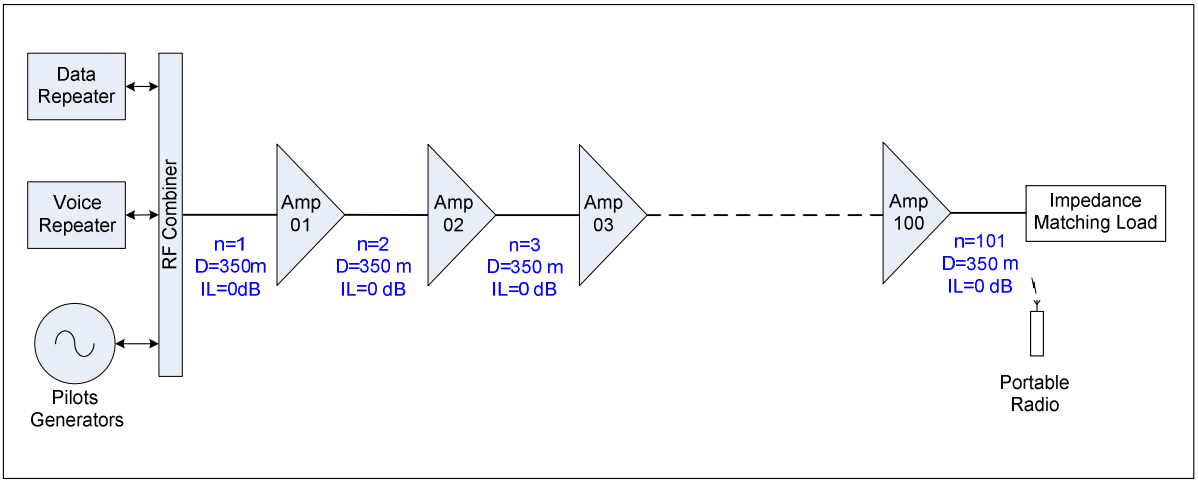

Figure 4.12: Multi-Cascaded Amplifiers Simulation Network

For the downstream voice band ($m = 2$), the voice carrier level leaving the system head-end was assumed to be 0 dBm. When this carrier propagates through the first section of the system, it will be attenuated by a factor equivalent to the losses of this section. Typically, the next amplifier in the system will compensate for the losses with a gain of ($G_2 = L_2$). This way the signal level will be boosted to its level at the head-end. However, errors occur where the CTE affects the operation of the algorithm in calculating the downstream system gain.

Figure 4.13 shows the output of the simulation analyses of 100 amplifiers in cascaded configurations. The trace in green shows the output levels of the downstream voice carrier with no error assumed by the CTE. The trace in red shows the output levels of the downstream voice carrier with 5% of uniformly distributed random CTE error affecting the gains of the system in band $m = 2$. Figure 4.14 shows the output of the simulation analyses for the downstream data band ($m = 4$).

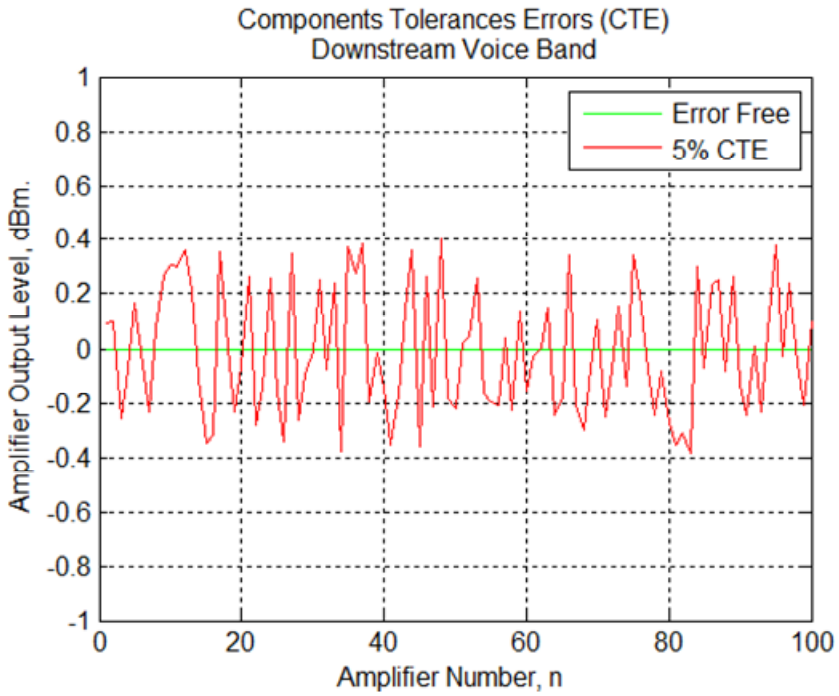

Figure 4.13: Downstream Voice Band CTE Simulations

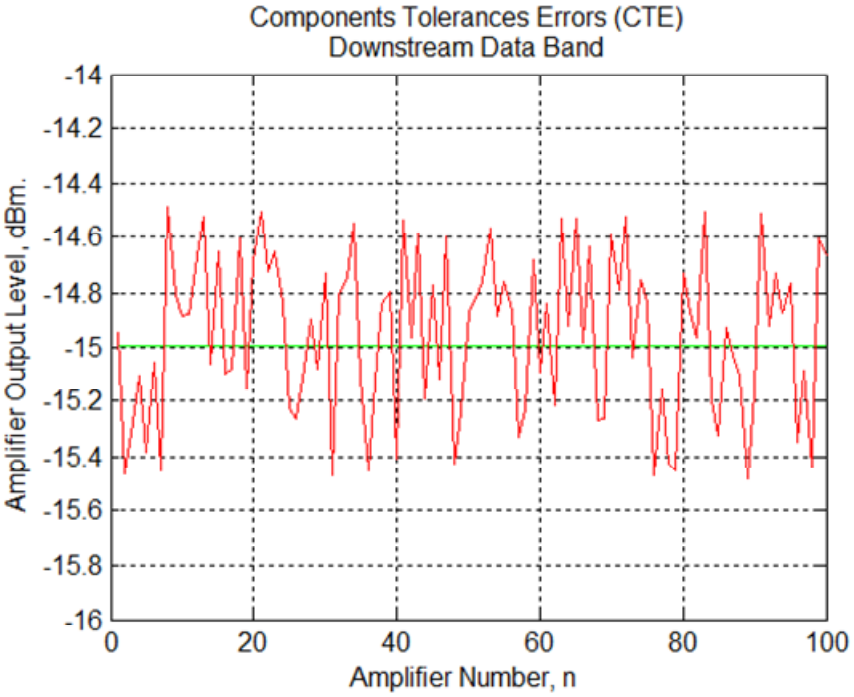

Figure 4.14: Downstream Data Band CTE Simulations

CTE Corrections:

Although, CTE is not expected to be more than ± 2.5 %, but to ensure higher levels of precision, additional RF detectors can be added at the output stages of the downstream amplifiers. The output RF detectors will feed the algorithm with two additional inputs (entries) for the levels of downstream pilots at the outputs of the amplifiers. Based on these additional inputs, the algorithm will be informed about any deviations in the amplifiers' gains caused by CTE. Therefore, the algorithm will adjust the gain of the downstream amplifiers to keep the output levels of the pilots to their constant reference levels at the system head-end. This technique will offer high precision in controlling the levels of the pilots to exactly match the levels at the head-end (100% corrections).

A correction factor is introduced to the algorithm to obtain the deviation factor of the predicated gain from the error free gain, as follows:

$$D_m = \begin{cases} PL_O - PL_{out} & for\ m = 2 \\ PH_O - PH_{out} & for\ m = 4 \end{cases} . \qquad (4.27)$$

By adding the correction factor to the amplifier's Predicted-Gain (PG), the Corrected-Gain can be determined as below:

$$CG_m = PG_m + D_m , \qquad (4.28)$$

where,

CG_m: Is the Corrected Gain. In the case of the CTE corrections, the corrected gain is only applicable to the downstream bands ($m = 2\ and\ m = 4$),

D_m: Is the gain Correction Factor,

PG_m: is the Amplifier's Predicted-Gain of band m,

PL_o: is the Low-Pilot level at the system Head-End (i.e. the reference level),

PH_o: is the High-Pilot level at the system Head-End (i.e. the reference level),

PL_{out}: is the Low-Pilot level at the output stage of amplifier,

PH_{out}: is the High-Pilot level at the output stage of the amplifier.

Simulation analyses for the CTE corrections technique on a system of 100 amplifiers were conducted. The output results of these analyses are shown in Figure 4.15 and Figure 4.16. The analyses have demonstrated that the proposed correction technique is very effective in correcting errors caused by CTE to almost 100 %.

The blue traces in the figures indicate the corrected RF signals at the amplifiers output ports. The red traces show the output of the amplifiers with CTE components added as a uniform distribution function with a maximum value of 5 %. The green trace (behind the blue trace) is the original, error free, output levels. It is clear that the CTE has been corrected completely.

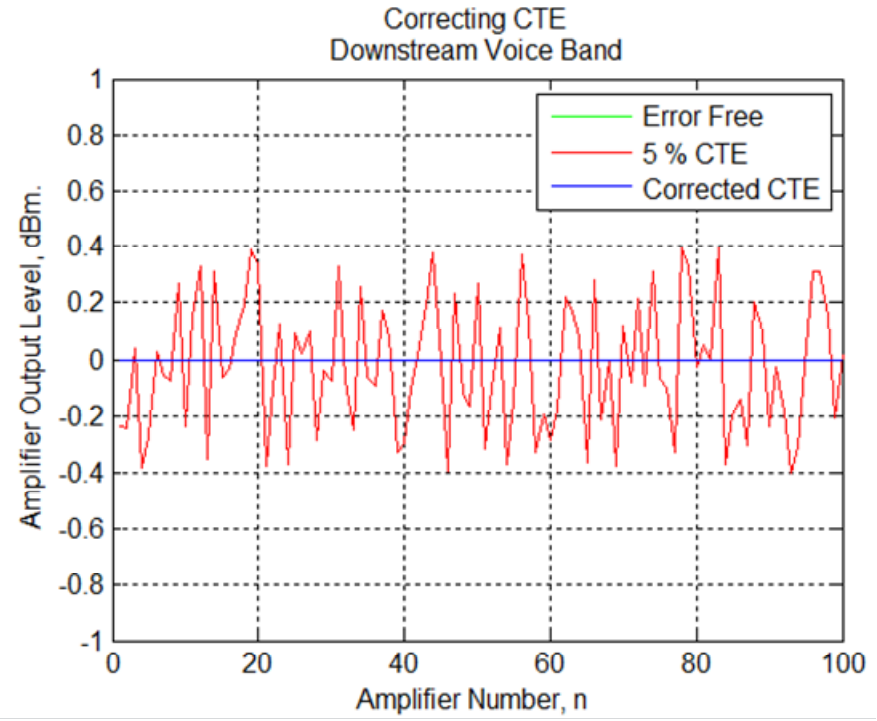

Figure 4.15: Downstream Voice Band CTE Corrections

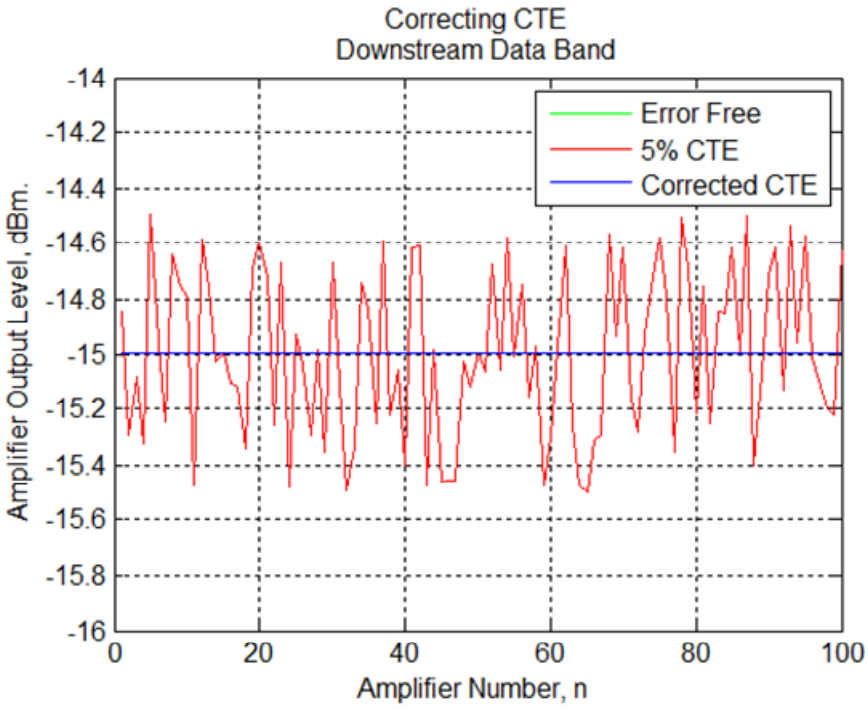

Figure 4.16: Downstream Data Band CTE Corrections

4.5.3 Gain Estimation Errors (GEE)

According to the PBAEA algorithm, calculating the gains of the amplifiers in the upstream bands is achieved totally by predicting (estimating) the losses in the system section ahead of the amplifier. These estimations are based on the inputs provided to the algorithm during the calculation of system losses in the opposite downstream directions of the system. In the algorithm, there are few pre-defined variables and parameters specific to the type of the leaky cable. These cable parameters are very important variables in calculating the system gains and slopes, especially for the upstream bands where there are no reference pilots used to measure the actual system losses. It is very important for these parameters to be accurate and consistent all through the system. These parameters are normally obtained from the data sheets of the cable. Faulty cables or bad installation practices could cause the cable characteristics to change from the predefined parameters. Therefore, errors occur in estimating the gains of the amplifiers. These errors are referred to as Gain Estimation Errors (GEE).

The GEE can be defined as a percentage of gain estimation errors in the upstream bands (band 1 and 3). These errors are not expected to be a significant factor (about 5%). However, for bigger systems, with large a number of amplifiers, the accumulation of these errors should be considered. GEE can be either positive or negative. A positive percentage of GEE occurs when the estimated gain is higher than the nominal gain required for the compensations of the upstream system losses. A negative percentage of GEE happens when the estimated gain is lower than the nominal gain required by the system for the compensation of the upstream losses. For m=1 and m= 3, GEE errors can be calculated as follows:

$$PG_m = G_m \cdot (1 + G_{GEE}), \tag{4.29}$$

where,

PG_m: is the Predicted-Gain of the amplifier.

G_m: is the Nominal (error free) gain of band m amplifier.

G_{GEE}: is the Gain Estimation Errors factor (in ± percentage figures)

GEE Simulation Analyses

Two important operating conditions must always be satisfied when analyzing the operation of the algorithm. The first condition is that the output of the amplifiers must not exceed their rated maximum output power; otherwise the amplifiers might become saturated and produce unstable system operations. The second operating condition is that the signal levels at the amplifiers' output should not be less than a specific value allowed by the receiver's sensitivities; otherwise, the signals received at the system head-end cannot be detected. Low output levels also result in a low Signal-to-Noise Ratio (SNR). The effects of the GEE were analyzed using MATLAB system simulation software. The circuit of Figure 4.12, Multi-Cascaded Amplifiers Simulation Network, was considered during the analyses.

Figures 4.17 and 4.18 show the output results of analyzing the effects of the GEE when estimating the gains of the upstream bands of the amplifier. In these analyses, a uniform randomly distributed error with a maximum value of 5% was assumed. For the system to operate properly, the levels of the data signals at the outputs of amplifiers must be maintained below (-10 dBm), which is the maximum output power of the amplifiers in this band. The other operating condition is that the data signal levels must be higher than (- 40 dBm) at the output of the

amplifiers. In this simulation, the input signal level of the data carrier in the upstream direction was assumed to be (-40 dBm) at the inputs of the system's last amplifier. Typically, the gain of the amplifiers in this case should be (8.3 dB) according to the algorithm estimations. This means that the output of the amplifiers in this band should be (-31.7 dBm) when no error was assumed. The trace in green in Figure 4.17 shows the nominal (error free) amplifier's output levels in the upstream data band. The trace in red shows the output with 5% of GEE included. The simulations show acceptable results to satisfy the operating conditions of the system.

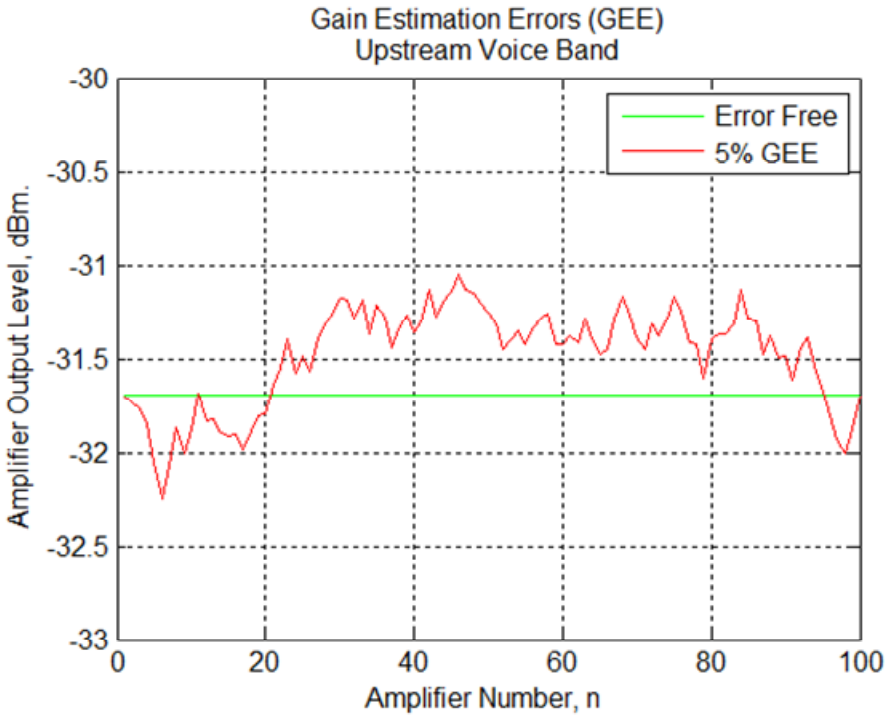

Figure 4.17: Upstream Data Band GEE Simulations

Figure 4.18 shows the results of simulating the system in the upstream voice bands. The maximum output power of the amplifiers in these bands is (-10 dBm); therefore, the output of the voice carriers in the upstream direction must be kept below (-10 dBm). The minimum level at the amplifier's output in these bands must be higher than (-80 dBm). These parameters consider the receiver's sensitivities and the filter losses at the head-end as well as the cable losses at the cable section immediately following the head-end. These simulations assumed a single voice carrier of

(-40 dBm) power input to the last amplifiers in the system. The error-free gain in this case is (16.3 dB). The output of the amplifier is (- 23.7 dBm) when no GEE is assumed. As shown in Figure 4.18, the trace in red is the output of the amplifiers when 5% of randomly distributed GEE is introduced to the system. The simulation results show acceptable system operating conditions.

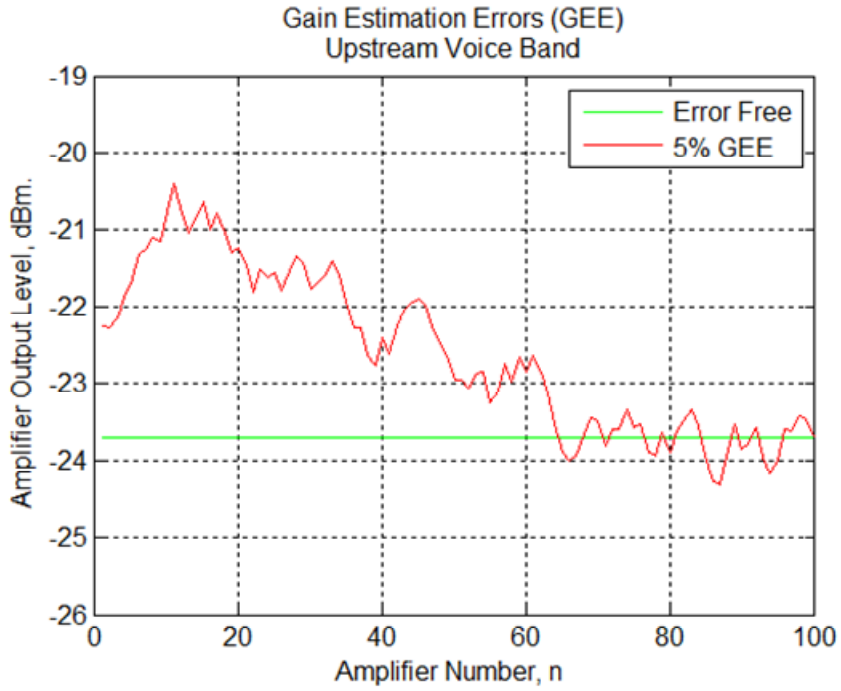

Figure 4.18: Upstream Voice Band GEE Simulations

GEE Errors Corrections

Although the GEE is not expected to be significant, the accumulation effect of these errors should be seriously considered, especially for bigger systems (50 amplifiers or more). Therefore, some measures to correct these errors are required. As a solution for this problem, a wide-band RF detector can be added to the output of the upstream amplifiers as shown in Figure 4.21. These detectors will be able to measure the envelope power of the upstream bands and feed these measurements as additional inputs to the AGC algorithm. With these additional inputs, the algorithm will be able to adjust the estimated gain of the upstream amplifier in order to maintain acceptable system operating conditions. A correction factor, D_m, will be calculated by the

algorithm to obtain the deviation factor of the Predicated-Gain from the error free gain, as follows:

$$D_m = \begin{cases} \text{PMIN}_\text{m} - \text{POUT}_\text{m} & \text{for POUT}_\text{m} < \text{PMIN}_\text{m} \\ \text{PMAX}_\text{m} - \text{POUT}_\text{m} & \text{for POUT}_\text{m} > \text{PMAX}_\text{m} \\ 0 & \text{Otherwise} \end{cases}. \tag{4.30}$$

By adding this correction factor to the Predicated– Gain (PG) of the amplifier, the Corrected Gain (CG) can be determined by:

$$CG_m = PG_m + D_m \,, \tag{4.31}$$

where,

CG_m: The Corrected Gain of the amplifiers in band m,

D_m: The Gain Correction Factor,

PG_m: The Amplifier's Predicated-Gain of band m,

$POUT_m$: The envelope power at the output of the amplifier for band m,

$PMAX_m$: The maximum power outputs of the upstream amplifier of band m,

$PMIN_m$: The minimum acceptable power at the amplifier outputs to satisfy the receivers' sensitivities.

This correction technique was analyzed by MATLAB simulations software. To illustrate the GEE correction effects, more stringent and narrow dynamic ranges for the PMIN and PMAX were assumed. For the upstream data band, $m = 1$, the PMIN was assumed to be -32.5 dBm and PMAX was assumed to -31.5 dBm. Of course, in reality the system will have a much wider dynamic range of operation (-10.00 dBm to -40 dBm). Figure 4.19 shows the simulation results when applying the GEE correction technique to the algorithm operation. The trace in green shows the error free levels of the upstream data carrier at the output of the amplifiers. The trace in red shows the levels of upstream data carrier when 5% of GEE is introduced. The corrections of these levels are shown in blue. The levels are clipped to maintain the output levels within the required dynamic range and to meet the operating conditions of the system. Figure 4.20 shows the effect of the correction technique on correcting GEE in the upstream voice bands.

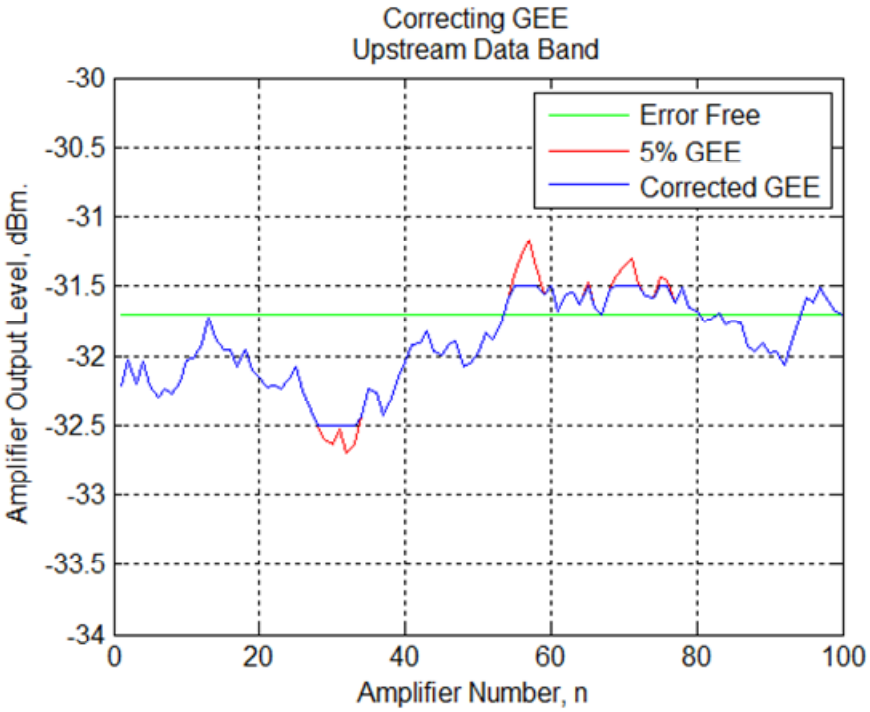

Figure 4.19: Upstream Data Band GEE Corrections

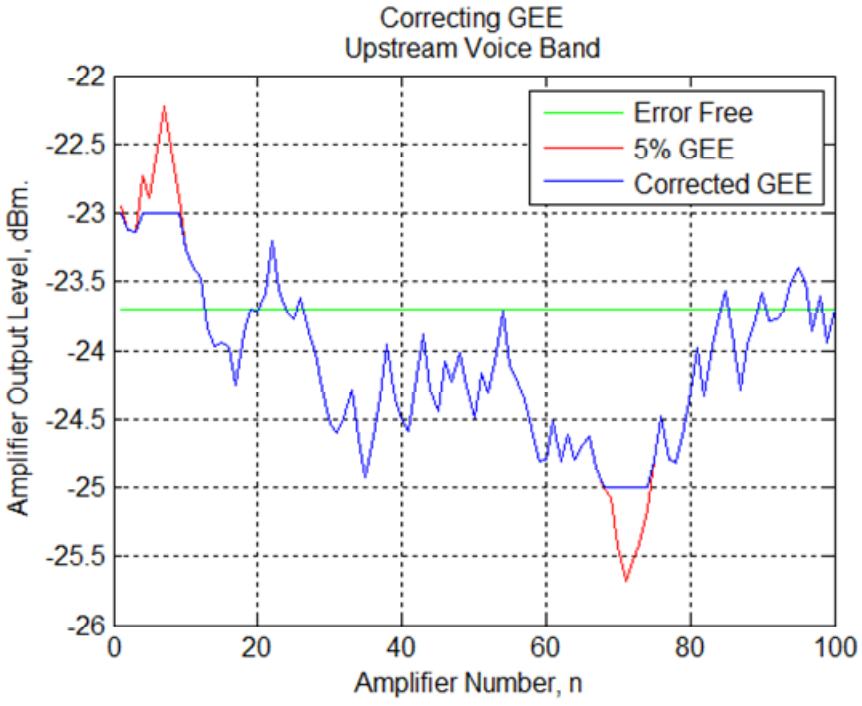

Figure 4.20: Upstream Voice Band GEE Corrections

4.6 Algorithm Prototyping

Prediction-based Adaptive Equalization Algorithm (PAEA) was prototyped to verify and evaluate the operation the algorithm to optimize the system performance and enhance stability. The prototype system was tested in both a lab environment and an actual mine environment to verify the operation of the algorithm. Figure 4.21 shows the block diagram of the prototype. The prototype system consists of a number of circuits built to analyze the performance of the algorithm. The following circuits were designed and prototyped to evaluate the performance of the algorithm.

- **PAEA Controller Board:** This is the main and critical board in the system that features a microcontroller circuit (PIC24 from Microchip Technology) programmed with a firmware running the PAEA algorithm. The "Controller Board" prototype is shown in Figure 4.22-A.

- **PAEA Pilots Receiver Board:** This board is responsible for receiving the three pilots and averages their levels using the developed averaging technique of the PAEA. The averaged levels are fed to the microcontroller of the controller board for utilization by the PAEA algorithm. The "Receiver Board" prototype is shown in Figure 4.22-B.

- **PAEA Pilots Generator Board:** The Pilots Generator Board generates the three reference pilots used by the algorithm. The level of the pilots can be changed and configured via a software application we developed, to simulate the effect of varying RF levels in the RCN of the mine. This application is called "PAEA Simulator". The Pilots Generator Board prototype is shown in Figure 4.22-C.

- **PAEA Main Amplifier Board:** The algorithm was applied on typical bi-directional amplifiers that are normally used in the mine RCN. Figure 4.23 shows a picture of the CMTS mine's amplifier. The controller and receiver boards were interfaced to these amplifiers in order to control their equalization responses. We developed a software application, called "PAEA Response Monitor" to control and monitor the response of the algorithm.

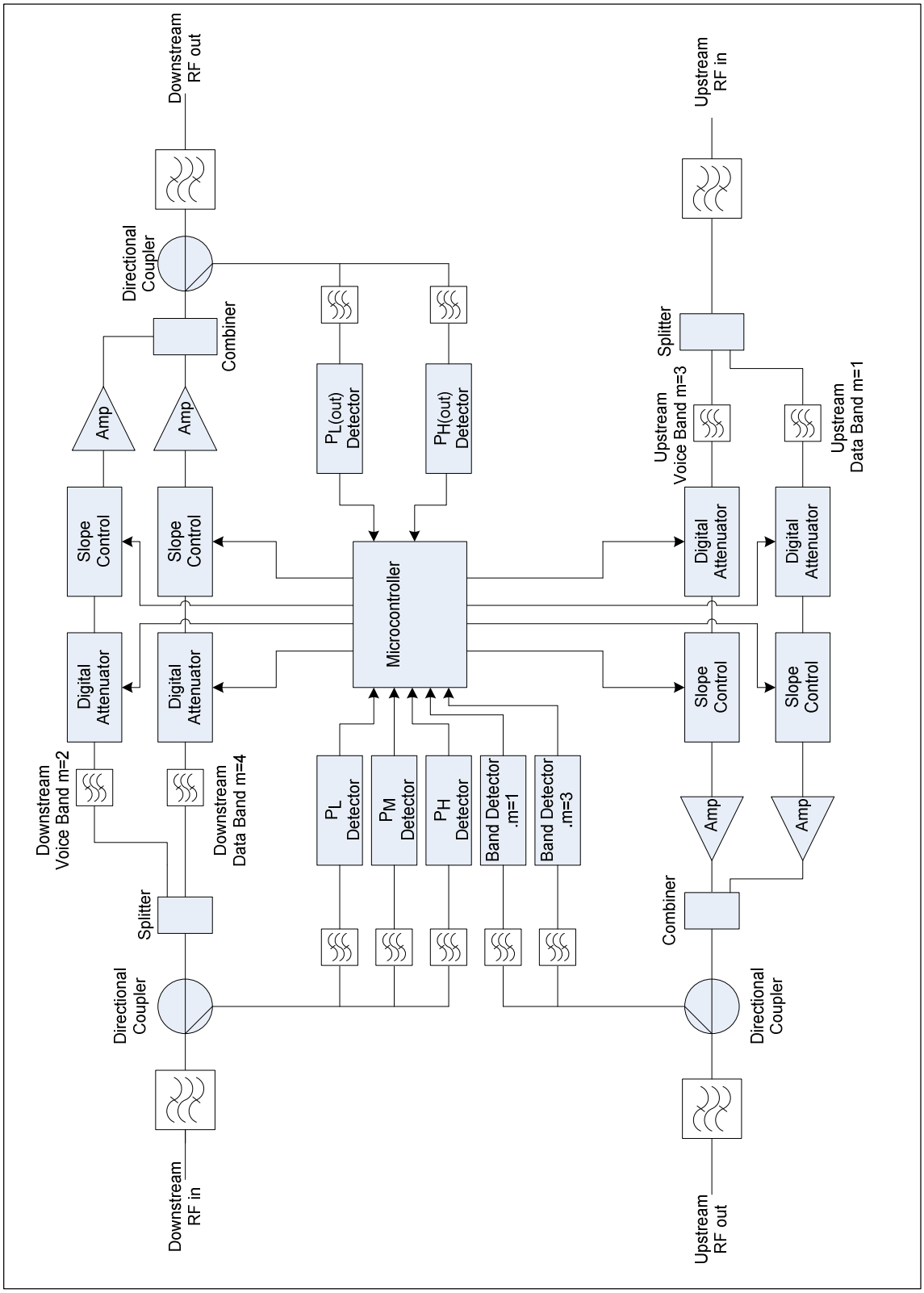

Figure 4.21: Prototype Block Diagram

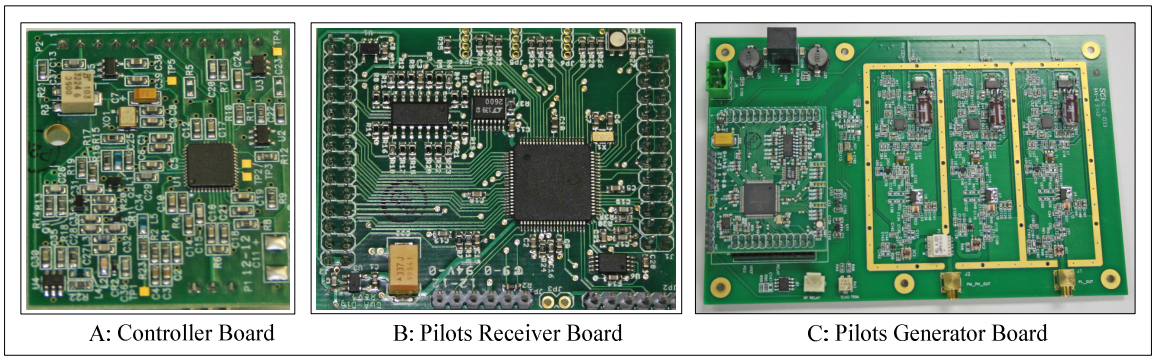

A: Controller Board B: Pilots Receiver Board C: Pilots Generator Board

Figure 4.22: Controller Circuit Board

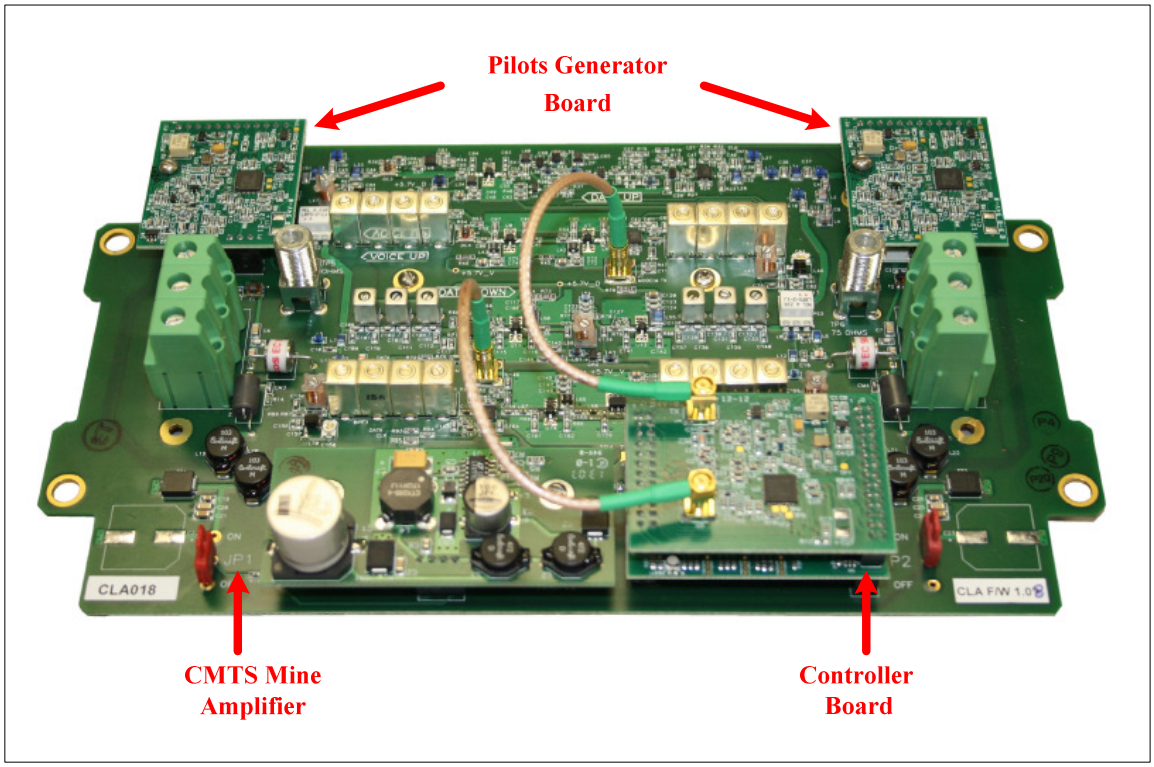

Figure 4.23: Amplifier Prototype

4.6.1 Algorithm Performance Test

The prototype was first evaluated in a lab environment. Figure 4.24 shows the test configuration for the prototype. The Pilots Generator Board was used to generate the references pilots (PL, PM and PH). The specially developed application software, "PAEA Simulator", was used to generate simulated cases and scenarios of Radiating Cable Longitudinal Losses and Insertion Losses (i.e. CL and IL). The algorithm response was monitored by the specially developed software application "PAEA Response Monitor."

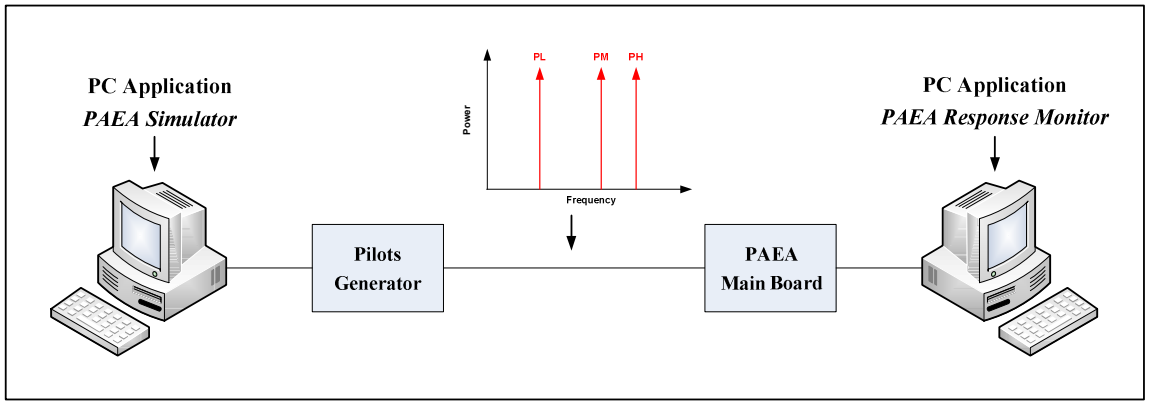

Figure 4.24: Beach Test Configuration

To test the equalization response of the PAEA algorithm, the Pilots Generator Board was configured to generate two cases of RCN scenarios. Switching between these two scenarios represent a sudden change in the RF levels of the system that requires equalizations by the PAEA algorithm. It was observed that when the power level of the reference pilots change to mimic time variant channels in the mine network, the algorithm could compensate for the system losses and equalize the system gain and slope accurately. Obviously the sampling technique implemented in the algorithm succeeded in measuring the level of the incoming reference pilots and then reported the average values to the memory of the microcontroller in the system. Figure 4.25 shows the time-response of the algorithm with respect to changes in the input levels of the pilots. It is obvious that PAEA algorithm could equalize the system performance when pilots' inputs levels change.

In the particular example of Figure 4.25, when the pilot levels changed by -10 dB, the system gain could be equalized and stabilized after 1.5 ms. The stabilization time is configurable parameters that can be changed to faster or slower response depending on the pilot level averaging time and network behaviour. In this prototype, faster time response (close to 100μsec) could be obtained, however given the very slow dynamic variations in the mine network such as mines expansion, we believe faster time response is not required for the RCN in the mine.

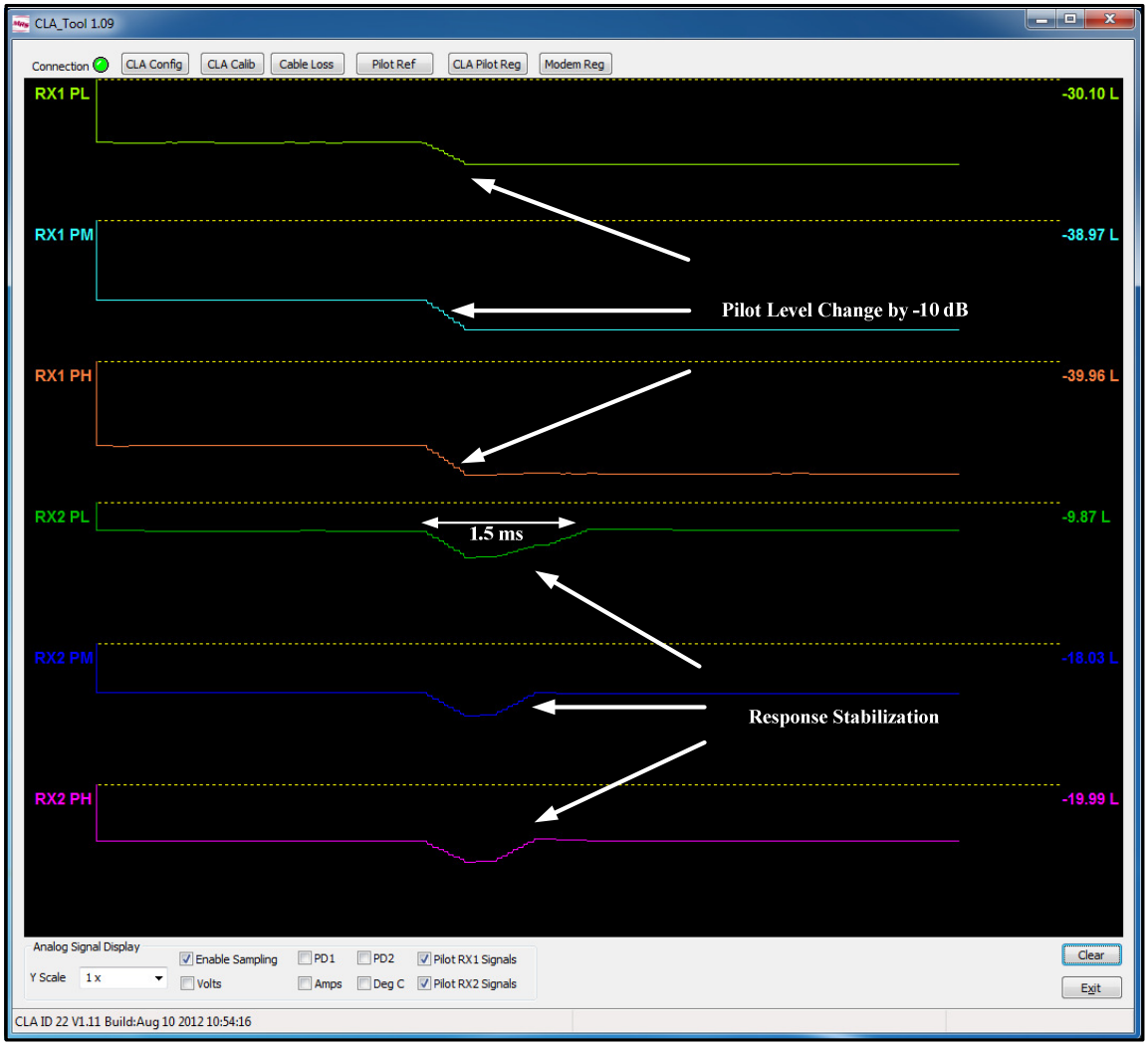

Figure 4.25: PAEA Time Response

4.6.2 Cascade Analysis in NORCAT mine

A cascade analysis was performed in NORCAT Mine, Sudbury, Ontario. Figure 4.27 shows the network layout in the mine. The analysis included four amplifiers cascaded in the mine's RCN. Figure 4.26 shows the test block diagram in the mine. The Pilot Generator Board was installed in the system head-end. The reference levels of the three pilots were set as 0 dBm leaving the system head-end (i.e. $P_L = P_M = P_H = 0\ dBm$). As shown in Figure 4.26 the length of the first section of the network is 150 m with no passive devices installed in between the head-end and the first amplifier (i.e. IL=0 dB). The second section is 110 m with one passive combiner unit that has an Insertion Loss of 4 dB (IL=4dB). The third section is 140 m and has three passive devices with an Insertion Loss of 4 dB each (i.e. IL= 12 dB). The fourth section of the RCN is 160 m of cable with no passive devices (i.e. IL=0 dB). Table 4.4 shows a comparison study between the actual test results and simulation analysis.

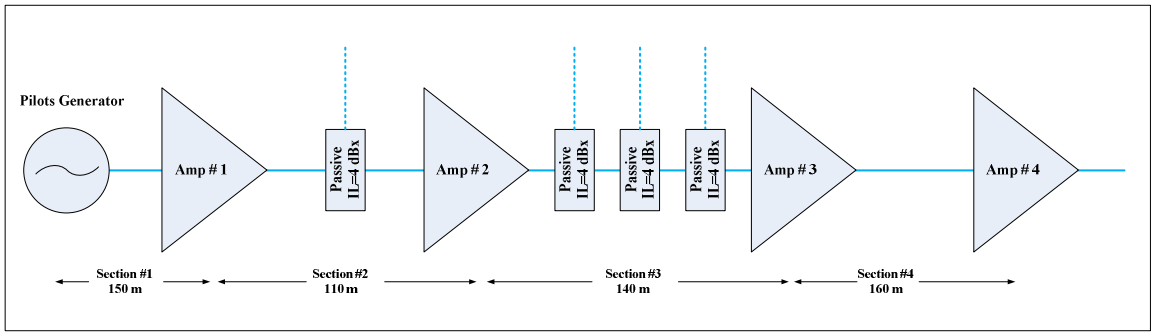

Figure 4.26: Mine Test Block Diagram

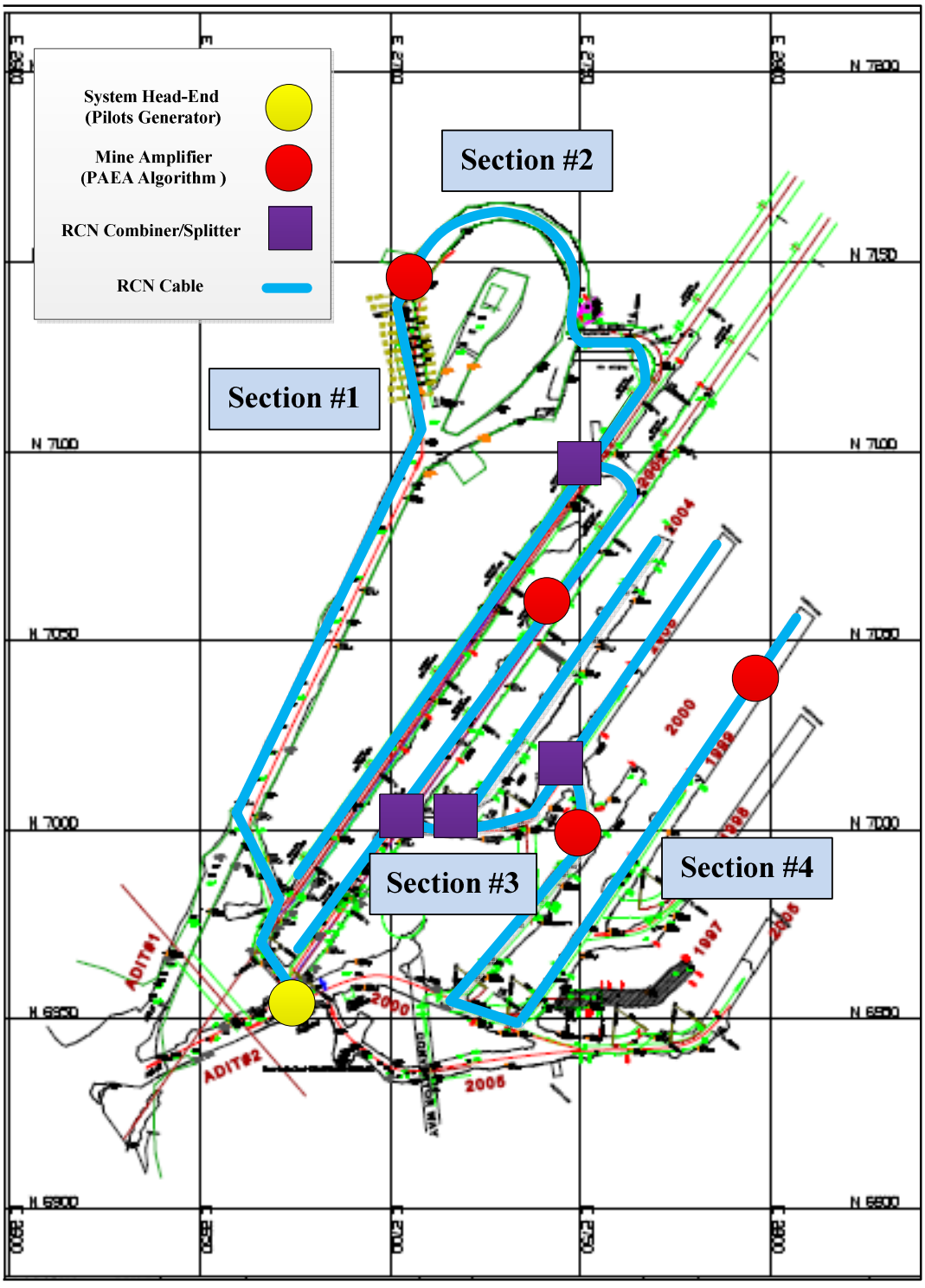

Figure 4.27: System Layout in NORCAT Mine, Sudbury, Ontario

	Band Name	DST Voice		DST Data		UST Voice		UST Data	
		Simulation	Test	Simulation	Test	Simulation	Test	Simulation	Test
Head-Eend	Bands Number	2		4		3		1	
	Channel's Level @ Head End, dBm	25.00		-10.00		-60.00	-56.51	-50.00	-48.50
	Head-Ed Filtering Loss, dB	-20.00		-10.00		-20.00		-10.00	
	Channel's Level @ Head End, dBm	5.00		-20.00		-40.00	-36.51	-40.00	-38.50
	Channel's Tilt @ Head End, dB	NA		0.00		NA	NA	0.00	-0.10
Section # 1	Cable Length, m	150.00		150.00		150.00		150.00	
	Calculated Cable Loss, dB	-6.71		-9.51		-7.59		-3.44	
	Calculated Insertion Loss in the Section, dB	0.00		0.00		0.00		0.00	
	Calculated Section System Loss, dB	-6.71		-9.51		-7.59		-3.44	
	Calculated Cable Tilt, dB	NA		-0.51		NA		-1.20	
Amp # 1	Channel Levels @ Amplifier Input, dBm	-1.71	-2.40	-29.51	-32.50	-32.41	-28.92	-36.57	-35.07
	Slope Equalization, dB	NA	NA	0.51	0.64	NA	NA	1.20	1.10
	Gain Equalization, dB	6.71	7.40	9.51	12.50	7.59	8.20	3.44	3.52
	Channel Level @ Amplifier Output, dBm	5.00	5.00	-20.00	-20.00	-40.00	-37.12	-40.00	-38.59
	Flatness (Tilt) @ Amplifier Output, dB	NA	NA	0.00	0.00	NA	NA	0.00	0.34
Section # 2	Cable Length, m	110.00		110.00		110.00		110.00	
	Calculated Cable Loss, dB	-4.92		-6.97		-5.57		-2.52	
	Calculated Insertion Loss in the Section, dB	-4.00		-4.00		-4.00		-4.00	
	Calculated Section System Loss, dB	-8.92		-10.97		-9.57		-6.52	
	Calculated Cable Tilt, dB	NA		-0.37		NA		-0.88	
Amp # 2	Channel Levels @ Amplifier Input, dBm	-3.92	-5.40	-30.97	-33.20	-30.43	-27.55	-33.48	-32.07
	Slope Equalization, dB	NA	NA	0.37	0.45	NA	NA	0.88	1.22
	Gain Equalization, dB	8.92	10.40	10.97	13.20	9.57	10.43	6.52	7.32
	Channel Level @ Amplifier Output, dBm	5.00	5.00	-20.00	-20.00	-40.00	-37.98	-40.00	-39.39
	Flatness (Tilt) @ Amplifier Output, dB	NA	NA	0.00	0.00	NA	NA	0.00	0.18
Section #3	Cable Length, m	140.00		140.00		140.00		140.00	
	Calculated Cable Loss, dB	-6.26		-8.88		-7.08		-3.21	
	Calculated Insertion Loss in the Section, dB	-12.00		-12.00		-12.00		-12.00	
	Calculated Section System Loss, dB	-18.26		-20.88		-19.08		-15.21	
	Calculated Cable Tilt, dB	NA		-0.48		NA		-1.12	
Amp # 3	Channel Levels @ Amplifier Input, dBm	-13.26	-16.40	-40.88	-43.70	-20.92	-18.90	-24.79	-24.18
	Slope Equalization, dB	NA	NA	0.48	0.66	NA	NA	1.12	1.30
	Gain Equalization, dB	18.26	21.40	20.88	23.70	19.08	21.10	15.21	15.82
	Channel Level @ Amplifier Output, dBm	5.00	5.00	-20.00	-20.00	-40.00	-40.00	-40.00	-40.00
	Flatness (Tilt) @ Amplifier Output, dB	NA	NA	0.00	0.00	NA	NA	0.00	0.00

Table 4.4: PAEA Mine Test Results

4.7 Summary

In this Chapter the scalability and reliability challenges in the backbone component of the mine's network were addressed and optimized for improved performance within the context of self-organized networks and green communication in the mines.

The analyses of the transient behavior of AGC amplifiers in cascade systems have demonstrated that overshoot and ringing are evident at the output of amplifiers in the cascade. It was also concluded that the magnitude of the overshoot is directly proportional to the number of amplifiers in the system. Our novel algorithm, "Prediction-based Adaptive Equalization Algorithm (PAEA)", provided a new scheme in controlling the gain and the slope in the leaky cable system of underground mines was presented. It was concluded from the simulation analyses of the algorithm that, when applied in a typical mine layout, the performance of the algorithm in predicting the gain is very reliable for the operation of the system.

Error analyses for the developed PAEA algorithm have considered three types of errors that affect the operations of the algorithm. The first type of error in the algorithm is the "Pilots Levels Precision Errors, LPE. It was concluded that a precision of less than 1 dB is achievable in measuring the reference pilot level. The second type of error that was analyzed is the CTE. These are the errors in calculating the gains and the slopes of the amplifiers due the tolerance of the amplifier's components. It was concluded that errors corrections up to 100% is possible by adding RF detectors at the output stages of the amplifiers. The third type of error that was considered is the GEE. These are the errors in estimating the gain and slopes for upstream amplifiers bands. It was concluded from the simulation analyses that the algorithm can ensure reliable predictions for the gain and slope of the amplifiers in the cascade. The amplifiers in the system will be operating in acceptable dynamic ranges of operation.

To validate the operation of the algorithm and evaluate its performance, the PAEA was prototyped with hardware and software applications. The prototype system was tested in both a lab environment and an actual mine environment. The test results showed agreeable outcomes in comparison to the expected and simulated analyses.

Chapter 5

5. Intelligent Power Management for Green Communication in Mines

5.1 Introduction

The subject of power consumption minimization has unique challenges when addressing the communication networks in underground mines. In addition to the normal objectives of Green Communication such as power savings and reduced cost in a friendly approach to the environment, green communication in underground mines requires further explorations and expansion because of its special location. In the mines, the permissible amount of power must be minimized to levels that ensure safe operation especially in the areas where gases are present which could be ignited from sparks caused by high power signals in the networks. Normally, active devices such as amplifiers, repeaters and WSN-sink nodes are powered by the radiating cable network. This is due in part to the limitation of power availability and the difficult access to the power networks in the mines. In Chapter 4, the backbone network of the mine was addressed to optimize the scalability and reliability of the RCN. In this Chapter, as shown in Figure 5.1, the optimization of the backbone network in the mine continues by proposing a novel algorithm to optimize the power management in the mine given the constraints of power availability.

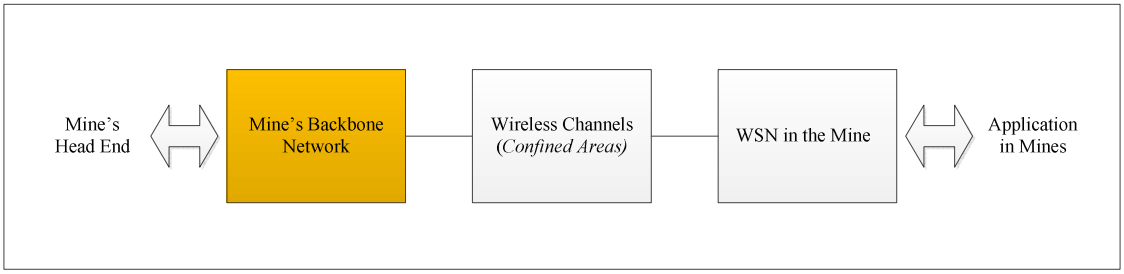

Figure 5.1: Mines Networks Components

5.2 RCN Powering System

Typically in the radiating cable systems, the in-line repeaters or Bi-Directional Ampliforms (BDA) in the system receive their power directly from the radiating cable itself [6,24]. These amplifiers are constantly powered regardless of whether they are participating in any useful action. In other words, they are consuming power whether they are amplifying RF signal or not.

A new approach and algorithm to solve the power problem of the radiating cable network in mines is presented in this chapter. We refer to the new algorithm as "Power-aware Adaptive Charging Schedule Algorithm" or simply (PACSA). The system model is twofold. The first part is to operate all the amplifiers in the system in the idle mode. In the event of RF signal presence at the input of any amplifier, the unit switches on to operate in the active mode to service the RF signal (signal processing, amplifications equalizations, etc.). This way, the system operates only when it is needed; we can refer to this approach as Amplification On Demand (AOD). See Figure 5.2 for a block diagram representation.

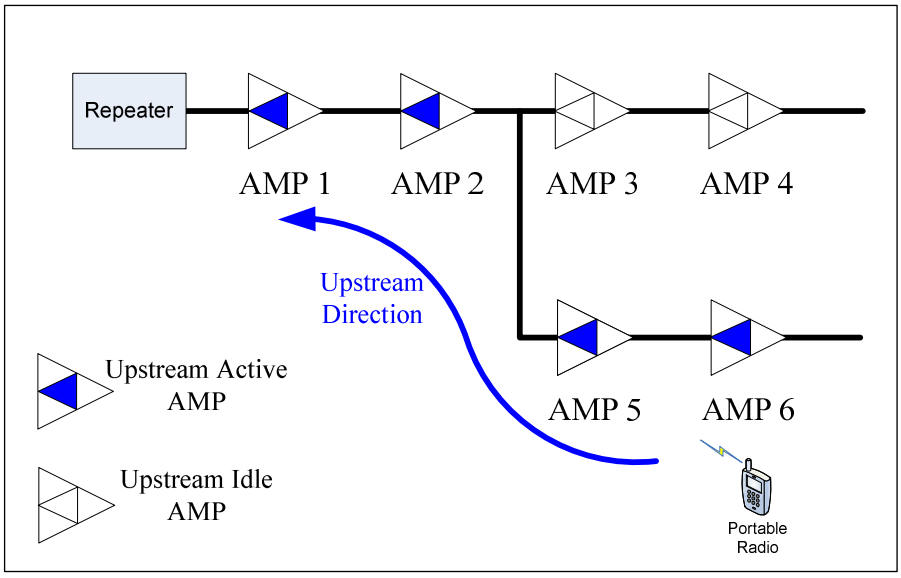

Figure 5.2: Amplification-On-Demand Architecture

The second part of the proposed architecture is to develop an algorithm that controls the power consumption of the system. Rechargeable batteries are installed in each amplifier in the system. These batteries are charged directly from the leaky feeder system. Through this approach, the amplifiers in the system are not powered directly from the RCN but from the individual onboard

batteries installed in the amplifiers. This research presents a charging scheduling algorithm to control the charging schemes of the amplifiers in the system.

In simple terms, if the system is composed of a straight line of amplifiers as shown in Figure 5.3, then a scheduling scheme for charging the batteries of network's devices can be achieved simply by periodically charging the batteries in a cyclic sequence. In this approach, we can define the Time-Cycle, T, as a unit that is made of a number of time slots. In each time slot, one or more of the system amplifiers are charged from the main power supply. Therefore, the maximum power present in the radiating cable network at any given time is limited to the minimum amount needed to maintain enough charge in only the few active devices as per certain schedule.

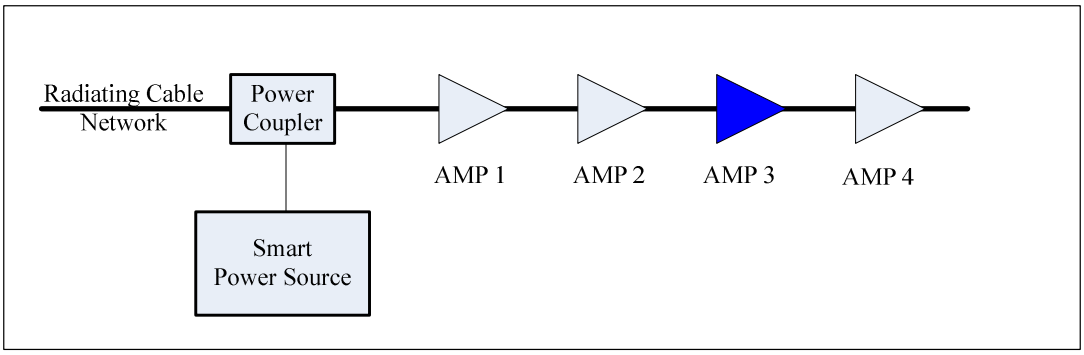

Figure 5.3 : RCN Charging scheduling scheme

For the simple system layout shown above, where the system is made of four amplifiers, the time schedule can easily be designed as a loop of periodically repeated successive time slots that are equally assigned to all the amplifiers in the system, as shown in Figure 5.4.

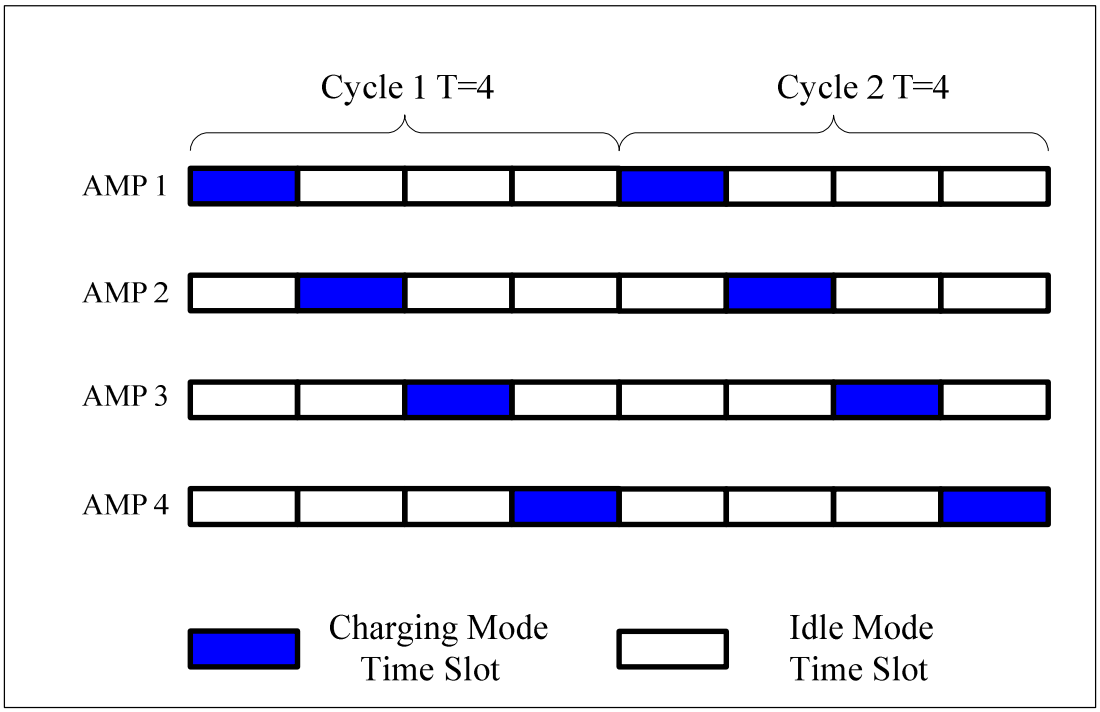

Figure 5.4: Simple RCN charging time schedule

However, the layout of typical mines can be a complex configuration with a number of branches. Different branches in the system can be busier than others. In other words, the power consumption is not homogeneous throughout the system. Therefore, there are some amplifiers that require more frequent charging than others. For example, if we consider the system of Figure 5.5, the branch of AMP 1, AMP 2, AMP 5, and AMP 6 is busier (i.e. used more frequently) than the other branch where AMP 3 and AMP 4 are installed. Therefore, the charging scheduling algorithm needs to be optimized to provide an adaptive scheduling solution that provides longer charging time to the first set of the amplifiers. Figure 5.6 shows a possible time schedule for this situation. In this schedule, AMP 1, AMP 2, AMP 5, and AMP 6 receive more charging time than AMP 3 and AMP 4 to correspond to actual power consumed by these units.

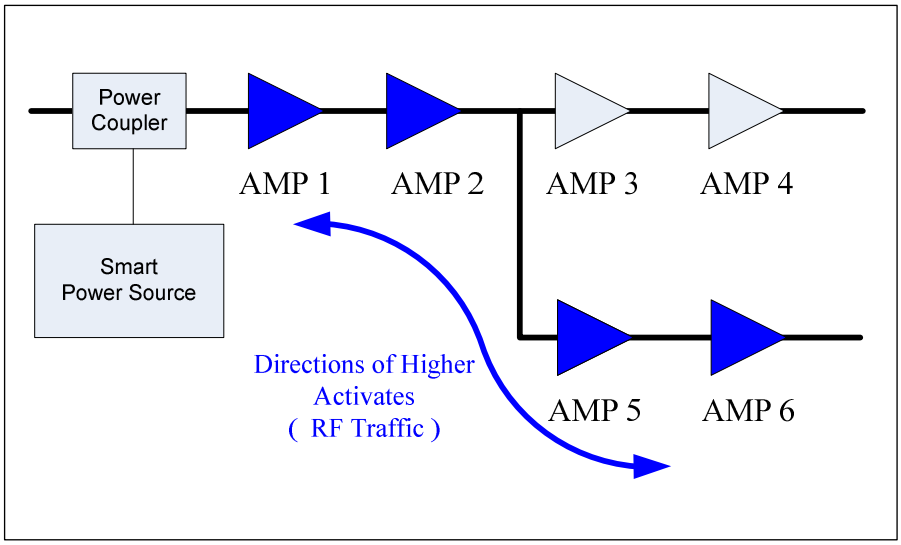

Figure 5.5: Branched RCN layout

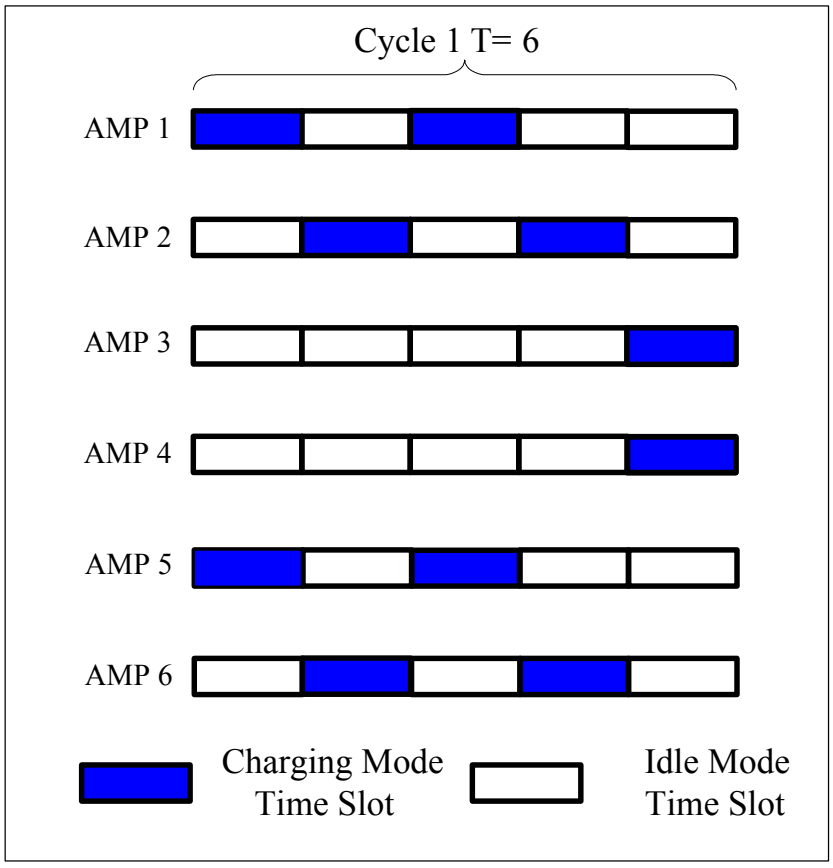

Figure 5.6: Charging scheduling scheme example

5.3 Optimization Problems Formulizations

Let's assume that the Radiating Cable Network has M active devices and nodes powered in-line from the system, $A = \{ a_1, a_2, \ldots\ldots, a_M \}$. Each of these devices are powered by internal batteries. The radiating cable network provides charging power to these batteries. Our objective is to determine a charging schedule for each amplifier "a_i" in "A" so that the total network power (P_N) at any network section in the system does not exceed certain permissible amount called Permissible Power of the network (P_{MAX}) at any time.

The charging schedule will provide time opportunities for the devices in the network to receive power to charge their batteries. We will refer to these powering units as Power Feed Opportunity (PFO). The time-cycle (T) of the charging schedule, is the time duration of one complete schedule. We will refer to the total amount of the PFO delivered to the entire devices in the network during one time–cycle (T) as the Network Global Power (θ_N). Our objective is to minimize θ_N to ensure maximum utilization of the power available in the network. Minimize θ_N also mean optimized time-cycle (T) to a minimum period with a minimum amount of power wasted (Lost Opportunities) due to providing unnecessary charging power to devices that do not require it.

Let $z_{i,t}$ be a binary variable, where $z_{i,t} = 1$ indicates that device (a_i) is in active charging mode at time slot (t) and $z_{i,t} = 0$ indicates that device (a_i) is in standby mode at time slot (t).

$$z_{i,t} = \begin{cases} 1 & \text{When } a_i \text{ is at active charging mode at time slot } t \\ 0 & \text{When } a_i \text{ is at standby mode (not charging)at time slot } t \end{cases} \quad (5.1)$$

As explained earlier the Time-Cycle, T, is the time required by the charging schedule to ensure adequate power distribution to the devices in the network. Each of these devices has different power requirements, $PR(i)$. The power requirement for each device is the amount of power required by that device to maintain enough charge in its battery (i.e. above certain threshold) for continuous network operation.

As a first constraint, this optimization is required to limit the amount of total power in the network to a certain safe level to ensure the safe operation of the mines. Therefore, the

optimization must consider the constraint of the maximum Permissible Power (P_{MAX}) allowed in the network. Thus at any time slot (t), we need to guarantee that;

$$\sum_i z_{i,t} \le P_{\max} . \tag{5.2}$$

The second optimization constraint is to provide adequate PFO to each active device in the network to ensure continuous network power availability. Thus, according to a specific charging schedule { $Z_{i,t}$}, the total PFO that each device (a_i) receives can be calculated as follow;

$$p_i = \sum_{t=1}^{T} z_{i,t} , \tag{5.3}$$

where p_i is PFO of a_i which is the total power received by a_i from the network during one time-cycle (T). It is important to provide each component in the network with an adequate energy supply to maintain enough charge in the units' batteries and keep the network alive all the time.

We can define τ_i to be the "Power Satisfaction Ratio" of an individual device (a_i) in the network. The Power Satisfaction Ratio is the ratio of the device PFO (i.e. p_i) to the total power required by that device (i.e. Power Requirements PR_i);

$$\tau_i = \frac{PFO \text{ for } a_i}{\text{Power Requirement for } a_i} = \frac{p_i}{PR_i} . \tag{5.4}$$

To fully satisfy the power requirements for each device in the network, the Power Satisfaction Ratio, τ_i , for any device must be greater than or equal to one (i.e. $\tau_i \ge 1$). Therefore, it is important that the PFO for each device in the system to be equal or greater than the power requirement, PR_i , of that device;

$$\sum_{t=1}^{T} z_{i,t} \ge PR_i . \tag{5.5}$$

It is also important that we fully utilize the available power in the network by using the maximum of the P_{MAX} at any time;

$$\sum_i z_{i,t} \geq P_{\max} - 1 \ . \tag{5.6}$$

In summary our objective is to minimize the maximum Network Global Power (θ_N) delivered to the network per one time cycle (T) as follows:

$$\min \quad \theta_N = \sum_{i=1}^{M} \sum_{t=1}^{T} z_{i,t} \ , \tag{5.7}$$

subject to

$$\sum_{t=1}^{T} z_{i,t} \geq \ PR_{(i)} \ , \tag{5.8}$$

$$\sum_i z_{i,t} \leq P_{\max} \ , \tag{5.9}$$

$$\sum_i z_{i,t} \geq P_{\max} - 1 \, , \tag{5.10}$$

where;

θ_N: Network Global Power,

T: Charging Schedule Time-Cycle,

a_i: Device in the mine network {A},

$z_{i,t}$: Binary variable representing a_i status at time t,

PR_i : Power Requirements of a_i,

p_i : PFO received by a_i during a complete Time-Cycle (T),

P_{MAX}: Maximum Permissible Power in the network,

τ_i : Satisfaction Ratio for individual device a_i in the network.

5.4 Power-Aware Charging Schedule Algorithm for Underground Networks

Based on Linear Programming (LP) and Branch and bound (B&B) algorithm, our proposed scheme, Power–Aware Adaptive Charging Schedule Algorithm (PACSA), will optimize the utilization and distribution of the power in the radiating cable network. This algorithm consists of a systematic enumeration of all candidate solutions, where large subsets of fruitless candidates are discarded, by using upper and lower estimated bounds of the quantity being optimized. The algorithm ensures continuous power availability to all nodes and devices powered by the RCN of the mine

In this optimization, the PACSA algorithm assumes global network synchronization. The schedule is generated at a centralized node level that could be located at the mine head-end on the surface underground or any other gateway node in the underground. The schedule will then be distributed to the rest of the devices in the network to coordinate their power schedule. The optimization takes place in two stages. The first stage, which is the most critical one, is the generation of the charging schedule that coordinates the power distribution in the mine's network. The charging schedule provides an optimized Network Global Power (θ_N) at a minimized time cycle (T).

The second stage of the algorithm is to order the schedule that was generated in the first stage. It is desirable to feed each device with continuous PFO. This ensures an ideal charging cycle for the batteries in the network. The optimization of the continuous PFO is achieved by trying to switch the network's devices between the charging and standby modes less frequently.

5.4.1 Power-Aware Charging Schedule Generations

In our PACSA algorithm we consider the schedule time slot by time slot. In each time slot, t_s , we select a device or node in the network that we refer to as the "anchor" of that time slot. The anchor device is switched to the active mode if it requires power (i.e. $PR_i > P_i$). The selection of the anchor sensor follows certain criteria that guide the process of generating the schedule to an optimized maximum number of active devices and yet ensuring the total network power is less than the permissible power available in the network at any time slot (i.e. $P_N < P_{MAX}$). The device in the RCN is identified by a unique ID address; the schedule selects the anchor device at each time slot based on the ID sequence of the devices in the network. At each time slot there might be enough PFO to supply to more than one device; therefore more devices can then be

switched to the active mode in addition to the anchor. After evaluating the anchor device power requirements, the algorithm evaluates all the other devices in the network starting with the devices with an ID before the anchor and then with the devices that follow the ID of the anchor in a cyclic manner.

Figure 5.7 shows an example for RCN network with five devices powered from the network. In this example the first device, a_1, requires 3 units of power, the second device, a_2, requires 4 units of power, the third device, a_3, requires 2 units of power, the fourth device, a_4 , requires 4 units of power and the fifth device, a_5, requires 3 units of power (i.e. $PR_{(1)} = 3,\ PR_{(2)} = 4,\ PR_{(3)} = 2$, $PR_{(4)} = 4$, $PR_{(5)} = 3$ respectively).

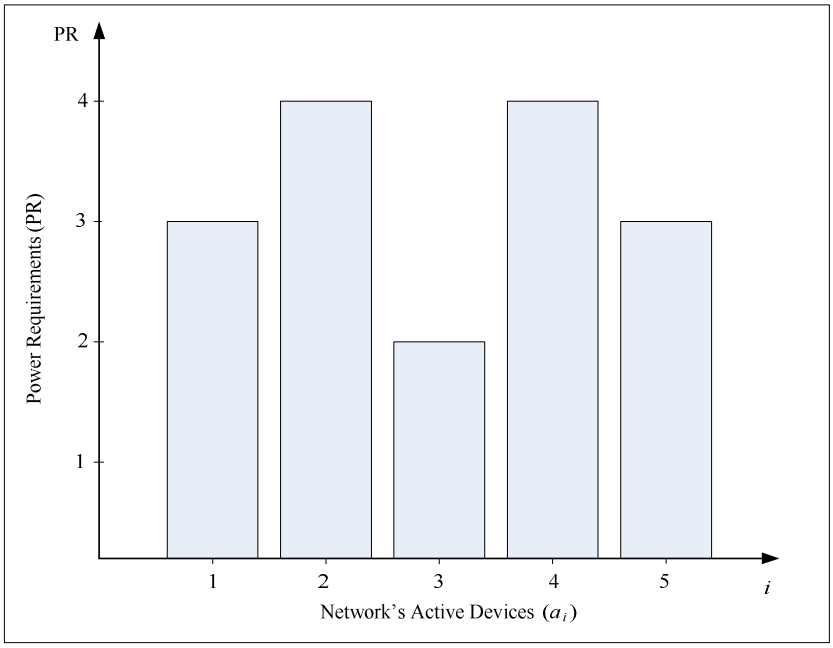

Figure 5.7: Network Power Profile

The network power requirements can be satisfied by a simple schedule where power units are delivered to the devices in the network one unit at a time (i.e. one PFO at each time slot). In this case, the time-cycle is equal to the total network power requirements (i.e. $T = PR_A$) as shown in Figure 5.8. Obviously, this is not an effective method for assigning a schedule since the time-cycle can be optimized for shorter time duration.

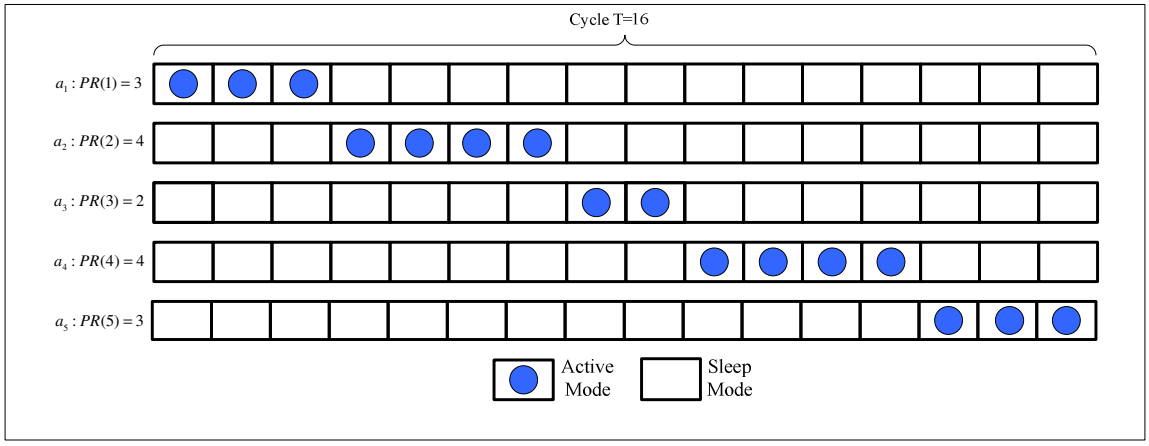

Figure 5.8: Un-optimized Charging Schedule

To demonstrate our Power-Aware Charging Schedule Algorithm, let's start by having the time-cycle fixed to predetermined time duration. In this case we select T=8 time slots. The algorithm starts generating the schedule by assigning the first device in the network to be the anchor at the first time slot of the time-cycle (T). The anchor is evaluated for Power Requirements. If the anchor device requires power it is set to the active mode (i.e. $z_{i,t} = 1$ for $i = 1$ and $t = 1$). If the anchor device does not require power, it is set to standby mode (i.e. $z_{i,t} = 0$ for $i = 1, t = 1$). It is possible that the network can provide power to more than one device at each time slot. This is true if the permissible power is greater than the instantaneous current of the network. Therefore more PFO can be delivered to other devices in the network. In this example, we have assumed that the maximum permissible power is 2 units (i.e. $P_{MAX} = 2$ units of power). Therefore, we can afford to provide a second PFO to another device in the network as shown in Figure 5.9. In the second time slot, the anchor device will be assigned to the second device in the network. The anchor will again be evaluated for its power requirements and, in case it requires power, a PFO is provided to this device. The power evaluation will then continue in the same manner for the rest of the devices in the network until the power required by the network is satisfied.

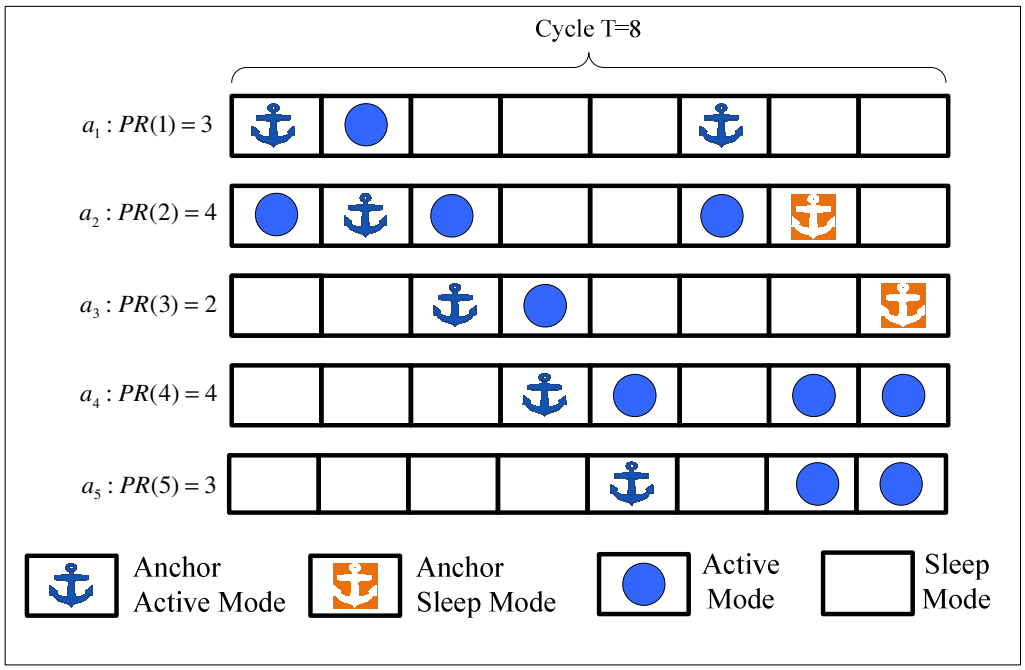

Figure 5.9: PACSA Charging Schedule

If for some time slots, the anchor device does not require power or has already acquired its required power, then the anchor device in this case will be in the standby mode. This is the case for a_2 and a_3 at $t_s = 7$ and $t_s = 8$ respectively. Therefore, other devices in the network could benefit from this unused PFO and the time cycle of the schedule could be further optimized to a shorter time period for efficiently providing the network with the required power. The resultant charging schedule matrix at this stage $[Z]$ is shown in Eq. 5.11.

$$Z = \begin{bmatrix} 1 & 1 & 0 & 0 & 0 & 1 & 0 & 0 \\ 1 & 1 & 1 & 0 & 0 & 1 & 0 & 0 \\ 0 & 0 & 1 & 1 & 0 & 0 & 0 & 0 \\ 0 & 0 & 0 & 1 & 1 & 0 & 1 & 1 \\ 0 & 0 & 0 & 0 & 1 & 0 & 1 & 1 \end{bmatrix}. \tag{5.11}$$

At this stage $[Z]$ is not optimized for the best order of minimum number of switches between active and standby modes. In the next Section, the PACSA algorithm is improved to optimize the order of the schedule for a minimum number of mode switching for each device in the network.

5.4.2 Power-Aware Charging Schedule Ordering Optimization

The second stage of PACSA is to order the schedule generated in the first stage for an improved continuous power delivery in the network. As explained before, continuous power delivery improves the charging cycle of batteries powering the device in the network, and therefore improve the utilization of the devices' battery for longer operating life. The charging schedule ordering algorithm is based on two stages. The first is to perform preliminary ordering upon the optimized schedule generated in the first stage. We initially count the number of ones in each column and then sort the schedule $[Z]$ in descending order. The result of the preliminary ordering is a new matrix $[\bar{Z}]$. In the second stage, we calculate the differences between each adjacent column in matrix $[\bar{Z}]$ and then sort the matrix in an ascending order with respect to the sequences of the differences between the adjacent columns. The result of the second stage of the ordering technique is a new matrix $[\bar{\bar{Z}}]$ that is optimized to a minimum number of transitional switches in the rows of the matrix. Figure 5.10, shows an example of sorting a charging schedule to produce an optimized minimum number of switches from standby mode to active mode for each device in the network. In this example, we have equal numbers of 1s in all columns. Therefore, $Z = \bar{Z}$. For illustration purpose, we will perform the second stage in two steps. In the first step the position of columns 3 and 6 in $[\bar{Z}1]$ is exchanged to produce $[\bar{Z}2]$. In the second step of the second stage, column 5 in $[\bar{Z}1]$ will be shifted to the position of column 4 while column 4 will be shifted to the position of column 5, and column 5 will be shifted to the position of column 6. The result of the second stage of the ordering technique is a new matrix $[\bar{\bar{Z}}]$ that has a minimum number of transitional switches in the rows of the matrix.

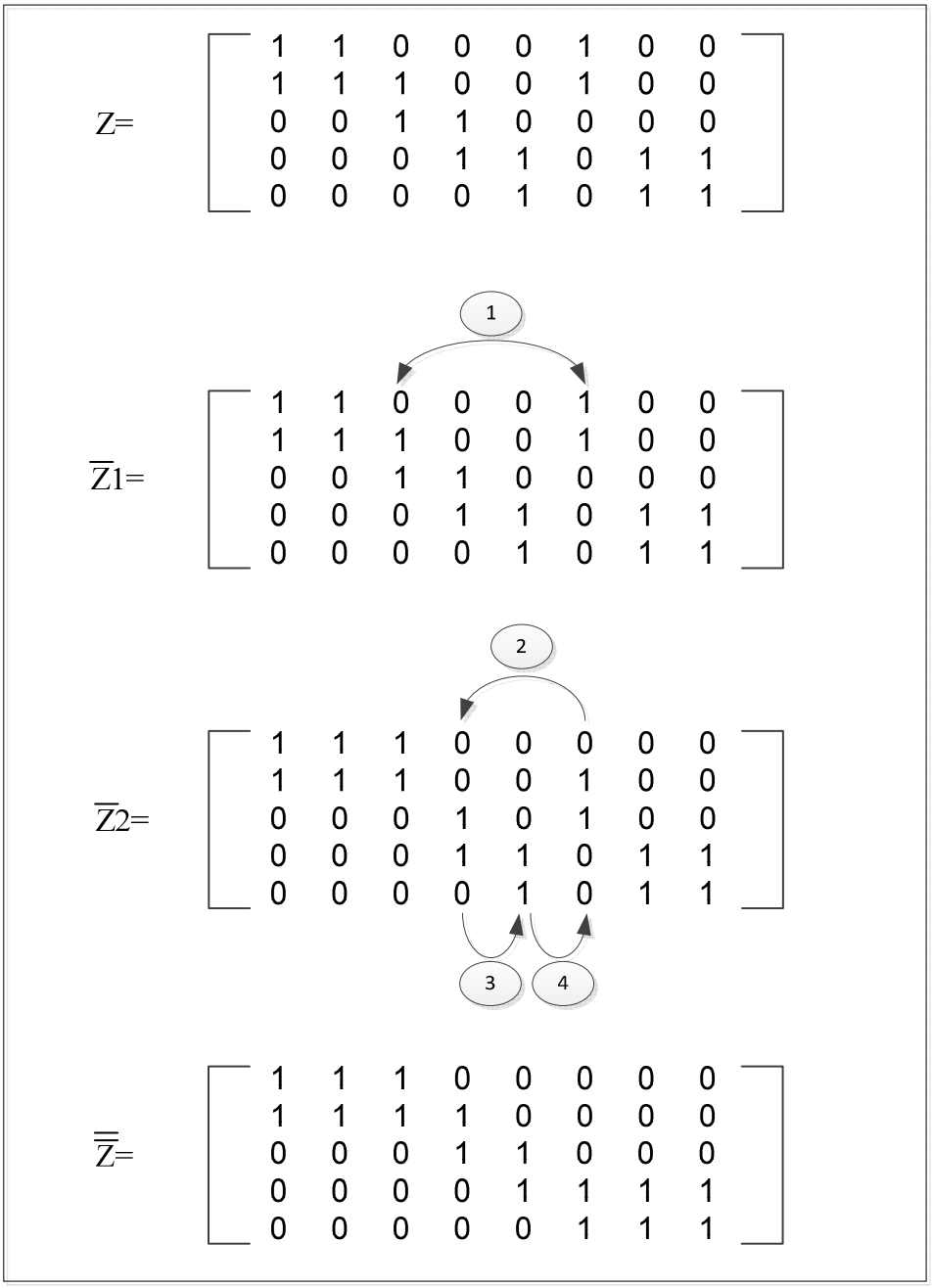

Figure 5.10: Charging Schedule Ordering Technique

The ordered charging schedule is shown in Figure 5.11. It is obvious that all of the devices receive continuous PFO, thus satisfying the Power Requirements (PR) of the network.

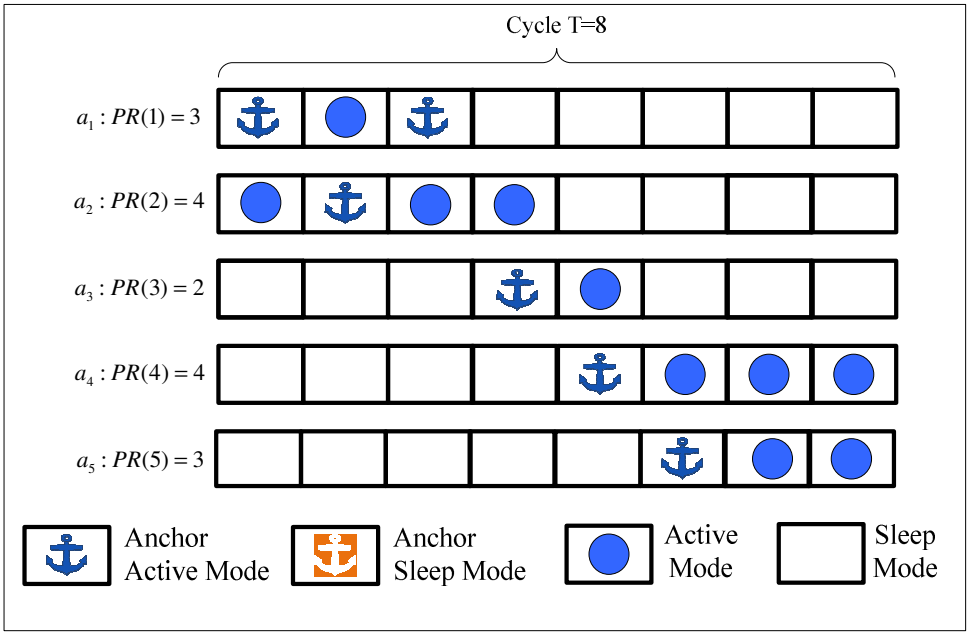

Figure 5.11: Ordered Schedule Example

5.5 Adaptive Time-Cycle Optimization

In the previous example we assumed a fixed and predetermined length of time-cycle (T) for the charging schedule to provide a satisfactory power distribution to the nodes and devices in the network. Our example illustrated a case where the time-cycle consisted of eight time slots (i.e. T=8). Within this time the algorithm could design a schedule that satisfied the power requirements of the network. We can define a ratio that quantifies the percentage of network satisfaction in obtaining the required power. This ratio can be referred to as "Global Satisfaction Ratio" and can be defined as follows:

$$\Gamma = \frac{PFO \text{ for } A}{\text{Power Requirement by } A} = \frac{P_A}{PR_A} = \frac{\sum_{i=1}^{M}\sum_{t=1}^{T} z_{i,t}}{\sum_{i=1}^{M} PR_{(i)}}. \qquad (5.12)$$

In the previous example we could achieve a Global Satisfaction Ratio of 100% when the time-cycle was eight time slots in length (i.e. $\Gamma = 1$ for $T = 8$). If the duration of allowed time for the schedule was shorter, for example if T= 6, the algorithm might not be able to produce an

optimized solution for the problem. Figure 5.12 shows an example when the time-cycle was selected to have a duration shorter than an optimum value (such as T=6). In this case the Global Satisfaction Ratio is less than 1. Subsequently, this means the network power requirements is not fully provided. When, T=6, the PFO for the entire network can be calculated as follows:

$$P_A = \sum_{i=1}^{M} \sum_{t=1}^{T} z_{i,t}\,, \tag{5.13}$$

$$PR_A = \sum_{i=1}^{M} PR_{(i)}\,, \tag{5.14}$$

where M= 5 and T= 6. Therefore, $P_A = 12$ and $PR_A = 16$ and $\Gamma = 0.75$

This means, only 75% of the network power requirements could be delivered to the devices in the network. Obviously the time-cycle was too short for the algorithm to provide optimized solution that satisfies the power requirements of the network.

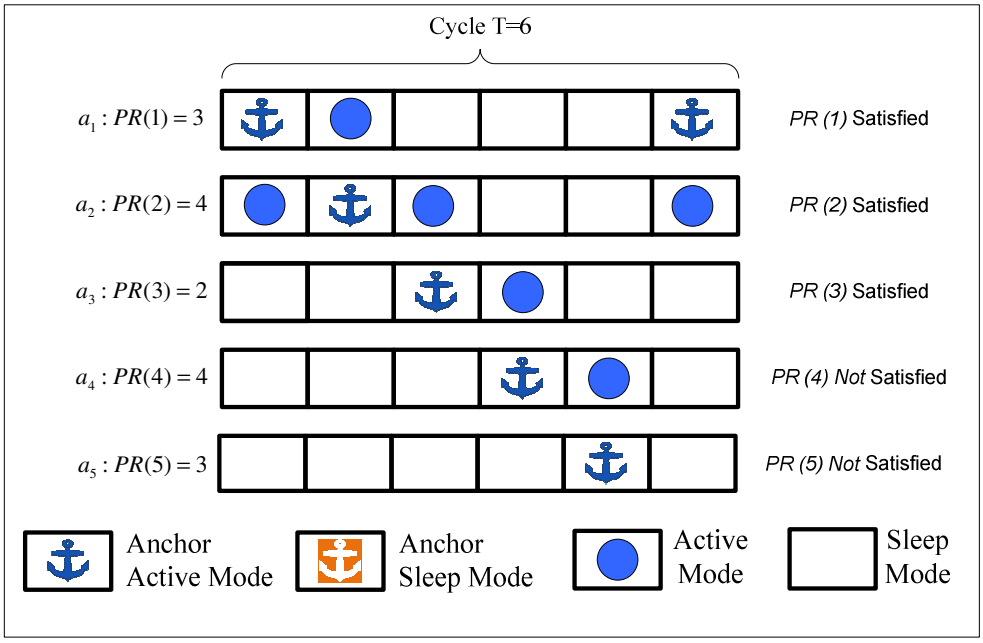

Figure 5.12: Clipped Charging Schedule

If a longer time-cycle was selected, such as T=12, then the schedule would have enough time to generate a schedule that satisfies the power requirement. However, a longer time-cycle can also result in an undesirable state where the schedule can deliver the required power units to all the devices in the network and then go into a waiting period until the next cycle. During the waiting period, no device can receive any PFO from the network. Obviously, this is another "Lost Opportunity" in utilizing the time to provide an optimized schedule. Waiting too long for another schedule to start is undesirable not only because no power is delivered to the devices in the network during the idle time but also a longer waiting time can cause a heavier schedule load during the next cycle. The time of idle waiting increases the network power requirements for the following schedule as the devices will continue consuming power during the idle time; therefore, the requirements for power will increase during the following time-cycle. Figure 5.13 shows an example for "Lost Opportunity" when the time-cycle chosen is too long such as T=12.

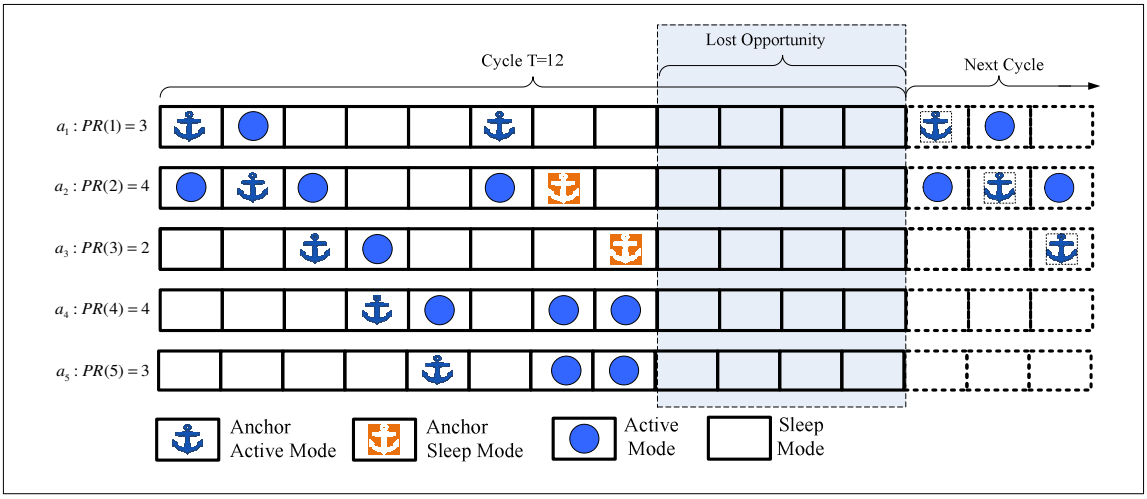

Figure 5.13: Lost Opportunity due to excessively long Time-Cycle (T)

For an optimized time-cycle duration, T must be selected so that it is neither short to the point that it results in less than an adequate amount of power being delivered to the network nor too long that it results in an idle period of "Lost Opportunity," where devices are waiting for the next time-cycle to start. The optimized duration of a time cycle should be long enough to merely satisfy the power requirement of the network (i.e. $\Gamma = 1$). Figure 5.14 shows the flowchart of the algorithm in optimizing the charging schedule of the network power.

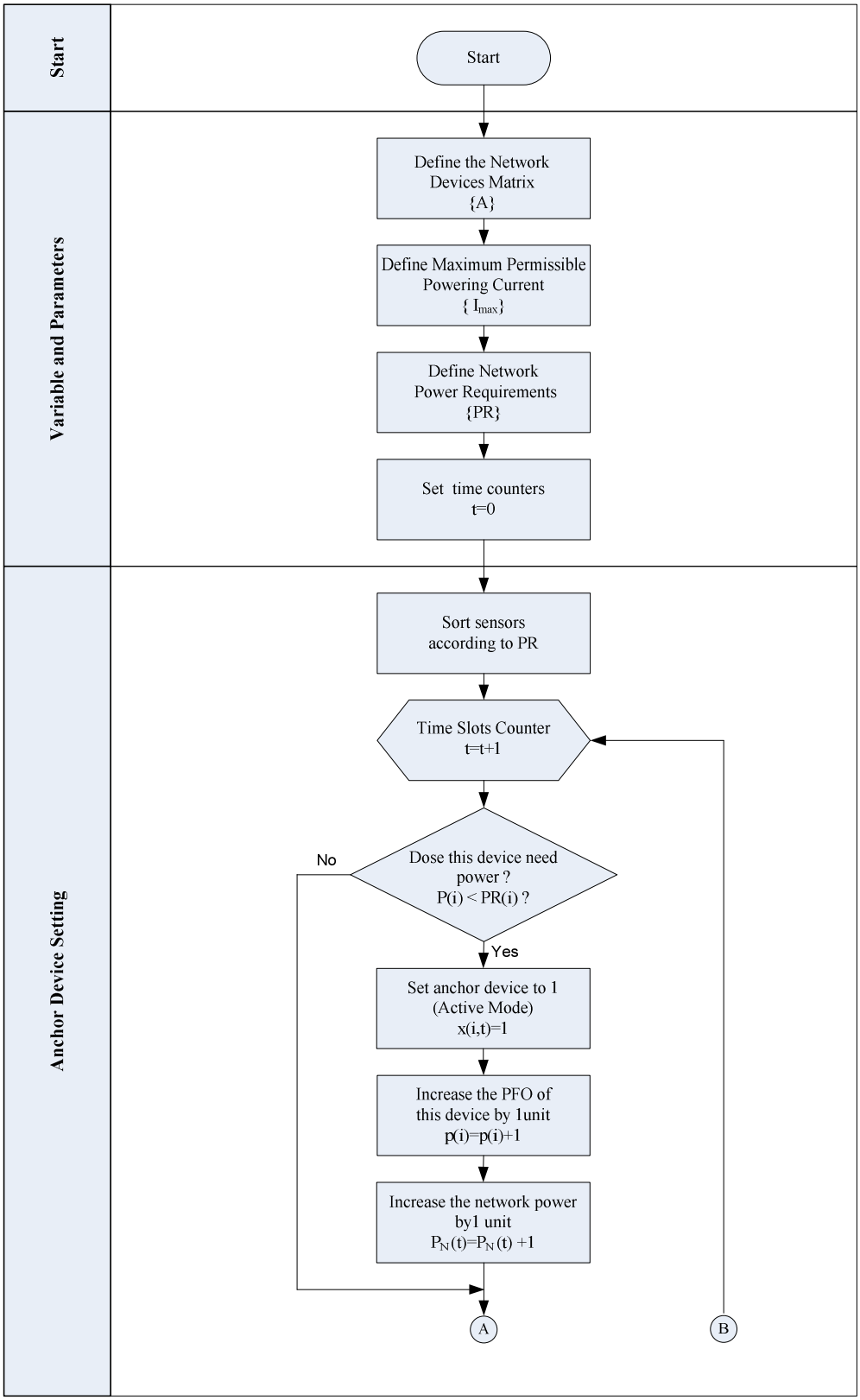

Figure 5.14: PACSA optimization flowchart
(Part 1 of 2)

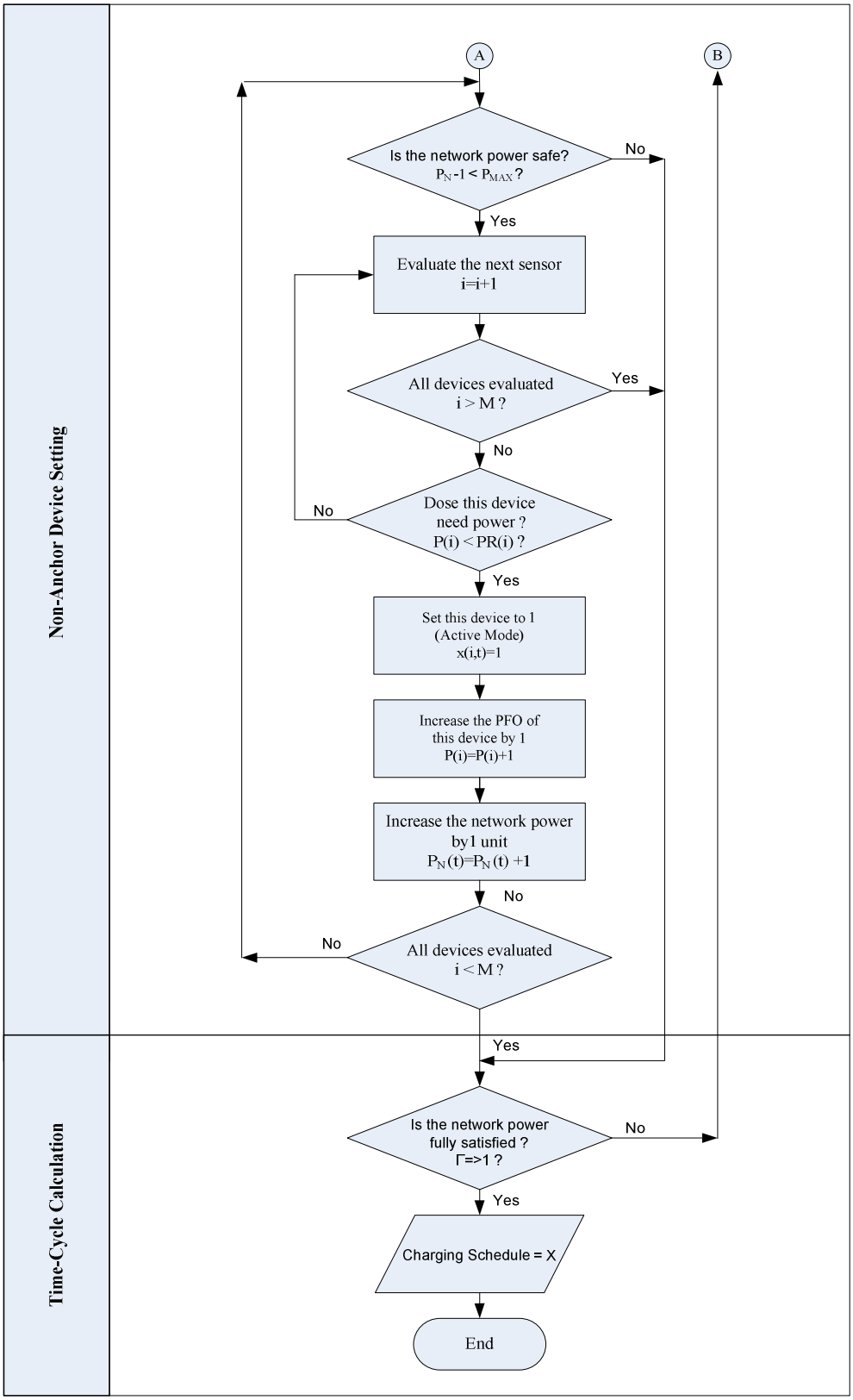

Figure 5.15: PACSA optimization flowchart
(Part 2 of 2)

5.6 Simulation results

5.6.1 Charging schedule generations

In this simulation we assumed a radiating cable network made of 10 devices and nodes. We started by randomly generating a Power Requirements (PR) profile for the network as shown in Figure 5.15. The generation of the power requirement profile was based on a uniformly distributed random function. We assumed that the devices in the network can demand a number of power units that range from PR=0 to PR =6. Obviously, when PR = 0 for any active device, it means that device does not require power during that time cycle. A higher number of PR means that the device was active for a longer time and therefore it requires a bigger number of PFO to maintain its operation.

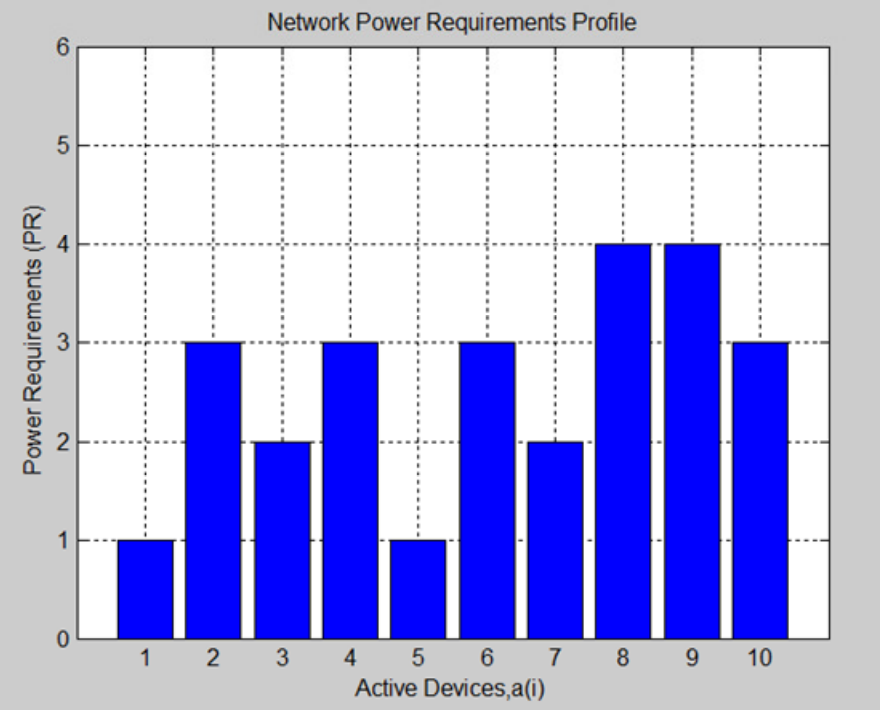

Figure 5.15: Network Power Profile

The Power Requirements profile shows that the total amount of the network PR is 25 units of power (i.e. $PR_A = 25$). Without optimization, we could have supplied the network with the required power over 25 time slots (T=25) by simply setting the time cycle to the same amount of power units required by the network (i.e. $T = PA_A$). However that would not be efficient. When

PACSA is applied, the Time-Cycle required to provide the same amount of power was optimized to a shorter duration of only 14 time slots (i.e. T=14). In this simulation we have assumed the permissible amount of power to be two units ($P_{MAX} = 2$ units) . This ensures that the instantaneous total distributed power in the network (P_N) is kept below the maximum permissible current (P_{MAX}) allowed in the system while satisfying the Global Satisfaction Ratio (i.e. $\Gamma = 1$ for $T = 14$). Figure 5.16 shows the charging schedule output of the algorithm. At this stage the schedule is optimized to a shorter duration of T. However, it is not yet optimized and ordered for the minimum number of mode switches (i.e. between standby and active modes) that provide optimized power delivery and longer battery and network life. In the next section the improved PACSA algorithm for ordering the schedule is simulated and analyzed.

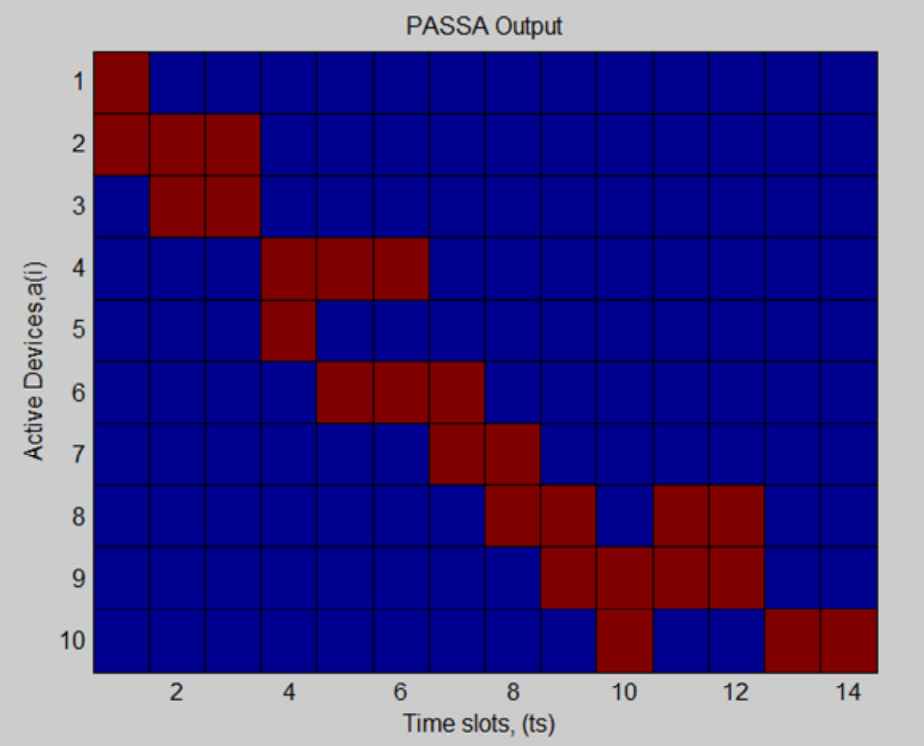

Figure 5.16: Optimized Charging Schedule

5.6.2 PACSA Ordering Improvement

During the second stage of the PACSA algorithm, the charging-schedule is ordered to optimize the power delivery within the network. In this simulation, the schedule of the previous section as

shown in Figure 5.16 was ordered by sorting the schedule in two stages. The first stage is to perform the preliminary ordering on the optimized schedule generated by PACSA. At the outset, the algorithm counts the number of ones in each column and then sorts the schedule in descending order. The result of the preliminary ordering is a new "preliminary-optimized" matrix that is ordered in descending order with respect to the number of ones per column. In the second stage of the ordering algorithm, all of the similar columns are sorted to be placed next to each other. We calculate the differences between each adjacent column and then sort the matrix in an ascending order. The result of the second stage of ordering is a new matrix as shown in Figure 5.17. The schedule is optimized to have less frequent transitional switching between ones and zeros. In this example, to reach an optimized schedule, columns 11 and 12 in Figure 5.17 were shifted to the left one step each, and column 10 was shifted to the right two steps.

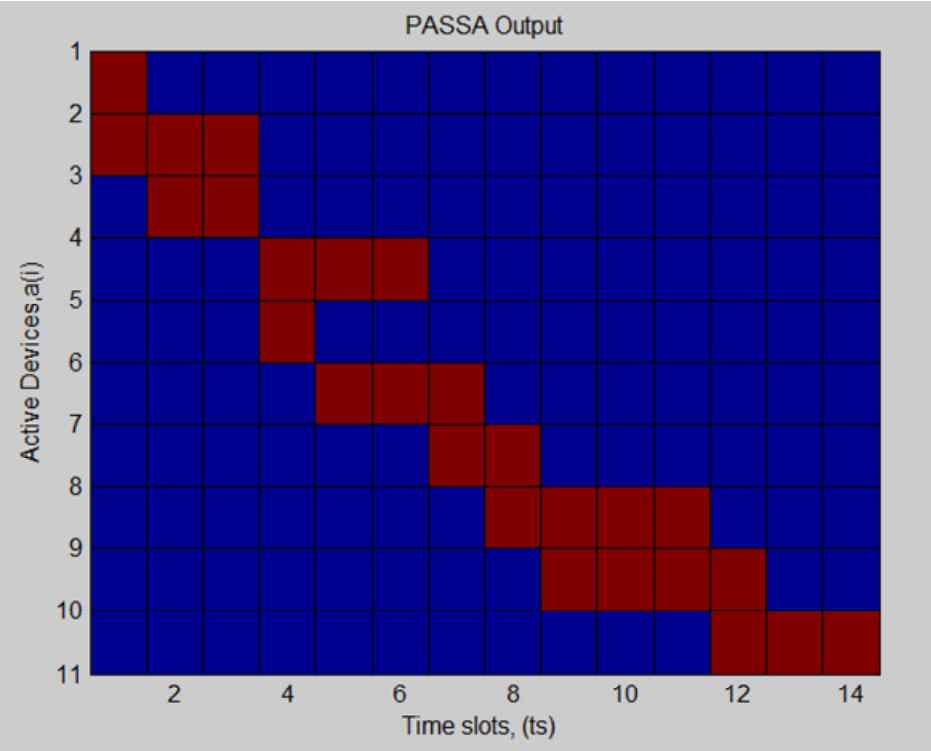

Figure 5.17: Optimized and Ordered Charging Schedule

5.6.3 Effect of Number of Network Devices on the Length of Time-Cycle (T)

To fully stratify the network power requirements, the PACSA should generate a schedule where the Global Satisfaction Ratio reaches unity (i.e. $\Gamma = 1$). To analyze the effects of increasing the

number of the nodes and devices in the network upon the length of the T, five scenarios of networks sizes have been simulated. It is obvious that the larger the network, the longer it takes to satisfy the network power requirements.

Figure 5.18 shows the simulation results for five different scales of networks. First, the network was assumed to have five devices (i.e. M=5). To reach a Global Satisfaction Ratio of unity, the optimized Time-Cycle was required to be 10 time slots (i.e. $T = 10$ for $\Gamma = 1$ and $M = 5$). When the devices in the network increased to 10 devices, the Time-Cycle was increased to 18 time slots (i.e. $T = 18$ for $\Gamma = 1$ and $M = 10$). When the devices in the network increased to 15 devices, the Time-Cycle was increased to 24 time slots (i.e. $T = 24$ for $\Gamma = 1$ and $M = 15$). When the devices in the network increased to 20 devices, the Time-Cycle was increased to 32 time slots (i.e. $T = 32$ for $\Gamma = 1$ and $M = 20$). When the devices in the network increased to 25 devices, the Time-Cycle was increased to 40 time slots (i.e. $T = 40$ for $\Gamma = 1$ and $M = 25$).
In this simulation we have assumed the permissible power in the network is ($P_{MAX} = 2$ units) and the simulations was averaged over 1000 samples.

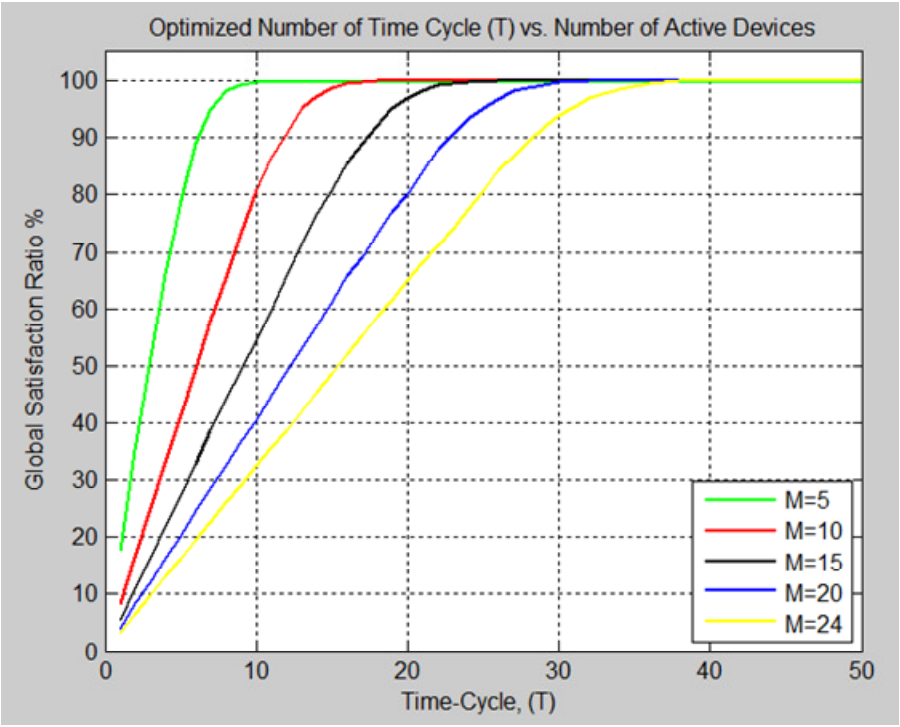

Figure 5.18: Effect of Number of Network Devices on the Length of Time-Cycle (T)

5.6.4 Effect of Permissible Power Limit on the Length of optimized Time-Cycle (T)

The amount of power permitted in the network is one of the very critical elements. It limits the operation of the RCN in the underground mines. Networks in coal mines especially are very limited in the amount of power allowed to be distributed to the devices. A higher power signal can cause dangerous sparks when methane and coal dust are present in the environment. Therefore, the objective of the optimization is to minimize the Time-Cycle (T) with the constraint of deriving the network power with a schedule that allows only a limited amount of power in the network (i.e. $P_N < P_{MAX}$). In this analysis we have simulated four cases of distributing PFO to the network's devices with different permissible power limits. The permissible power was varied for P_{MAX} = 2, 3, 4 and 5 units of PFO that are distributed in the network at the same time slot. For each of the four cases, the simulations were repeated 1000 times. The average was taken for the simulations results and plotted as shown in

Figure 5.19. In the first case, the permissible power of the network was selected to be 2 units of PFO delivered to the devices in the network at the same time (i.e. $P_{MAX} = 2$) . In this case, to reach a Global Satisfaction Ratio of unity, the optimized Time-Cycle was required to be 18 time slots (i.e. $T = 18$ for $\Gamma = 1$ and $P_{MAX} = 2$). When the permissible power of the network was increased to 3 units of PFO per time slot, the Time-Cycle was reduced to 13 time slots (i.e. $T = 13$ for $\Gamma = 1$ and $P_{MAX} = 3$) . When we increased the permissible power of the network to 4 units of PFO per time slot, the Time-Cycle was reduced to 10 time slots (i.e. $T = 10$ for $\Gamma = 1$ and $P_{MAX} = 4$).

Finally, when we increased the permissible power of the network to 5 units of PFO per time slot, the Time-Cycle was reduced to 8 time slots (i.e. $T = 8$ for $\Gamma = 1$ and $P_{MAX} = 5$). Obviously, the average of the optimized Time-Cycle of the schedule decreases when the amount of the permissible power in the network, P_{MAX} increases. There will be a trade-off between the allowed amount of P_{MAX} and the acceptable duration of the schedule that keeps the network operative all the time.

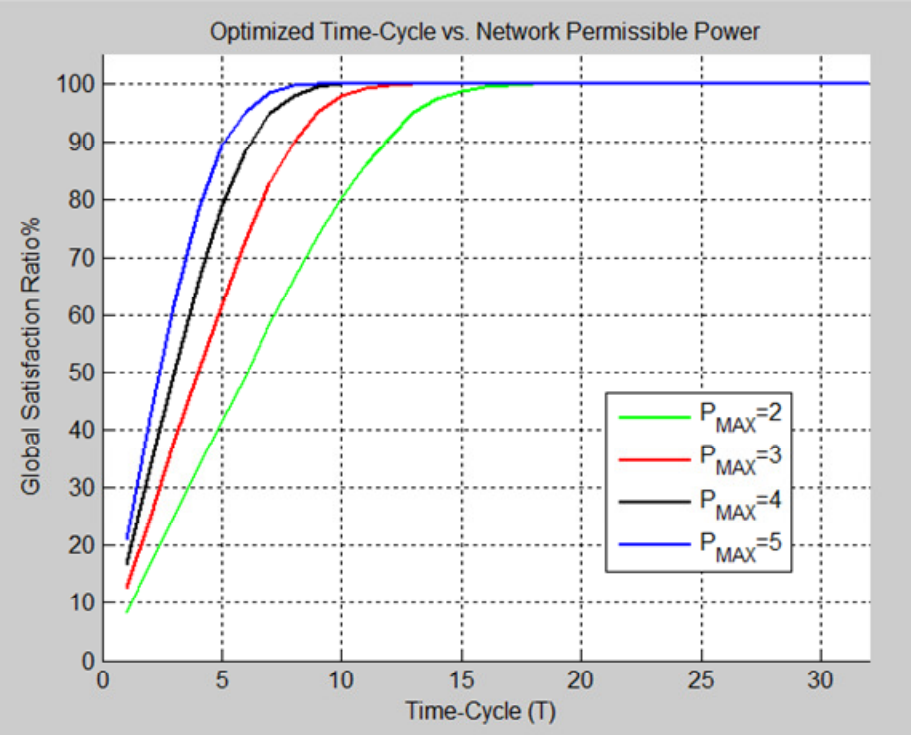

Figure 5.19: Effect of Permissible Power Limit on the Length of optimized Time-Cycle (T)

5.7 Summary

In this chapter, the backbone network of the mine was optimized for improved power utilization and management. The limitation of power availability in the mine and the constraint of the low allowable level of power in the network are considered among the important and difficult challenges that limit the operation of mines' networks.

Within the context of the Green Communication, this chapter presented a novel algorithm to solve the power problem of the backbone networks in mines. The proposed algorithm, PACSA, has improved the power utilization and distribution within the mine's network for a minimized power consumption that ensure safe operational conditions utilizing low permissible amount of power in the network.

The problem of power availability in the mine was formulated into an optimization problem with an objective function targeting the minimization of the Network Global Power (θ_N) and the Time-Cycle (T) of the charging schedule for each amplifier so that the total network power (P_N) does not exceed certain permissible amount of P_{MAX} at any time. The optimization also considers the constraint of providing adequate Power Feed Opportunity (PFO) to each device in the network to ensure continuous network power availability.

The simulations analyses of the proposed algorithm, PACSA, have demonstrated that an optimized schedule could be generated with a minimized duration of T. A Global Satisfaction Ratio of 100% could be obtained to fully satisfy the power demand of the network given the limitations and constraints of power availability. It was also demonstrated by the simulation analyses that the number of switches between the active and standby modes could be minimized for an efficient power utilization and longer battery life in the network's units.

Number of scenarios have been investigated and analyzed to evaluate the performance of the algorithm. When the effect of increasing the network's devices on the length of T was analyzed, it was determined that the larger the network, the longer it takes to satisfy the network power requirements. On the other hand, the average duration of the optimized Time-Cycle of the schedule decreases when the amount of the permissible power in the network, P_{MAX}, increases.

Chapter 6

6. Novel Wireless Channels Modeling

6.1 Introduction

The unprecedented success of wireless connectivity in our daily life has led to the emergence of this new technology in the mining industry. Increasingly more applications are becoming viable, and more industrial wireless products are becoming available. In the last decade, the use of wireless network solutions in underground mines has become essential. The arrival of these wireless solutions in the mining industry brought liberation from wired limitations, but initially presented its own challenge: an unreliable and unpredictable wireless link. The propagation characteristics of electromagnetic waves in an underground mine are different from those in free space because of the harsh underground environment. This is due to physical phenomena like severe reflection, scattering, and diffraction along the mine's rough wall. In this chapter the second block of the mine integrated network is addressed as shown in Figure 6.1.

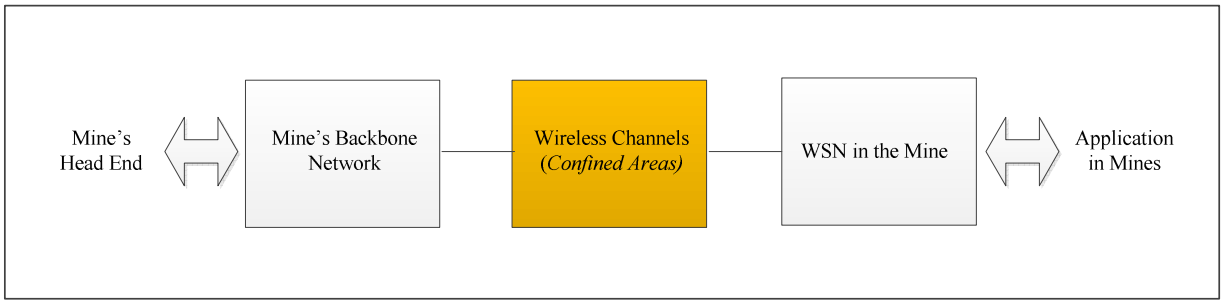

Figure 6.1: The Wireless Channel Element of the Mine's Integrated Network

For reliable wireless communication in an underground mine, the channel predictions are crucial in optimizing the performance of these networks. Although there are several channel prediction techniques, most of these approaches are very difficult and time consuming. An accurate and applicable channel model is needed to predict the wireless propagation characteristics in underground mines. The need for a generalized model that can be applied in an underground mine, regardless of whether the mine's topology is canonical or open, is required to form the foundation for developing an integrated and optimized mine systems. Deriving a universal channel model for an underground mine is a very challenging task as several factors are involved when such an environment is considered. First, there is no definite size and shape for an underground mine; it is generally irregular with rough surfaces. Second, the type of ore body could change the propagation property as well as the channel model. Lastly, most approximate channel models may be valid for a specific frequency range and are not suitable for a wide range of frequency [52, 53].

This chapter presents a new approach for the modeling of wireless channels in confined areas of the underground mines. The model is generated by adopting a performance-based approach rather than a classical coverage-based approach. This new model, called "Mine Segmenting Wireless Channel Model," divides the mine areas into three mains segments: (1) Line-of-Sight (LOS), (2) Partial-Line-Of-Sight (PLOS), and (3) Non-Line-Of-Sight (NLOS). The model combines these segments to produce performance-based analyses for the wireless channel in the mines. Different fading models are statistically combined to characterize a general area or areas in the mine

Detailed simulation analyses were conducted to demonstrate the performance of the new model in different mine layouts and with different fading channels. In addition, the model was evaluated in a real underground mine (NORCAT Mine, Sudbury, Ontario, Canada). The collected field test results showed very similar outcomes when compared to the model simulation. In addition to being a modeling method for characterizing the wireless channels in the underground mines, the developed "Mine Segmenting Wireless Channel Model" is utilized in our research for optimizing the performance of the wireless communication systems. This aspect is further demonstrated in the following chapter for optimizing the operation of the Wireless Sensors Network (WSN) in the mines.

6.2 Mine Segmenting Wireless Channel Model

For reliable wireless communication in an underground mine, there is a need for a generic scheme of communication that takes into account the environmental conditions of the mines as part of the universal and adaptive protocol to reach an optimal point of reliable communication and longer network life. Reaching that advancement, the wireless devices will have adequate information about their environments (i.e. the severity of multipath and the degree of Line-Of Sight). The devices can adaptively structure their transmission protocols accordingly. The nodes in the network will have the intelligence to characterize the wireless channels around them at any moment in time as they move in the mine. Therefore, there is a need for an adaptive method for modeling the wireless channel in the underground.

Rather than estimating the channel parameter for each region with one characterization model, our model divides the confined areas of the mine between the transmitting and receiving nodes into a number of segments, as shown in Figure 6.2. The wireless channel in each of these segments can be described using different distribution functions. This will form a combination of statistical models acting together to characterize a general area or areas in the mine. The main challenge in characterizing the wireless channels in the confined areas of the mine is due to the randomized multipath propagation phenomena. Therefore, our model's focus has been to select probability distribution functions that contain enough information about the multipath behaviors inside the mine. The statistical descriptions used in our model employ some factors that represent the ratio between direct-path (line-of-sight) power and diffuse power, which ultimately provide the information about different multipath scenarios in the mine. We are using a variable, factor (K factor), as a scaling element that maps the different mine segments to a number of approximate points between the Rayleigh and Rician models.

To demonstrate the theory, we have selected the wireless networks to be based on 802.11b. As mentioned before, our model follows a performance-based approach in characterizing the wireless channels in the mine. We start the modeling work by performing a series of BER analyses for different fading conditions at different data rates. In the next Section the mathematical model will be described in detail.

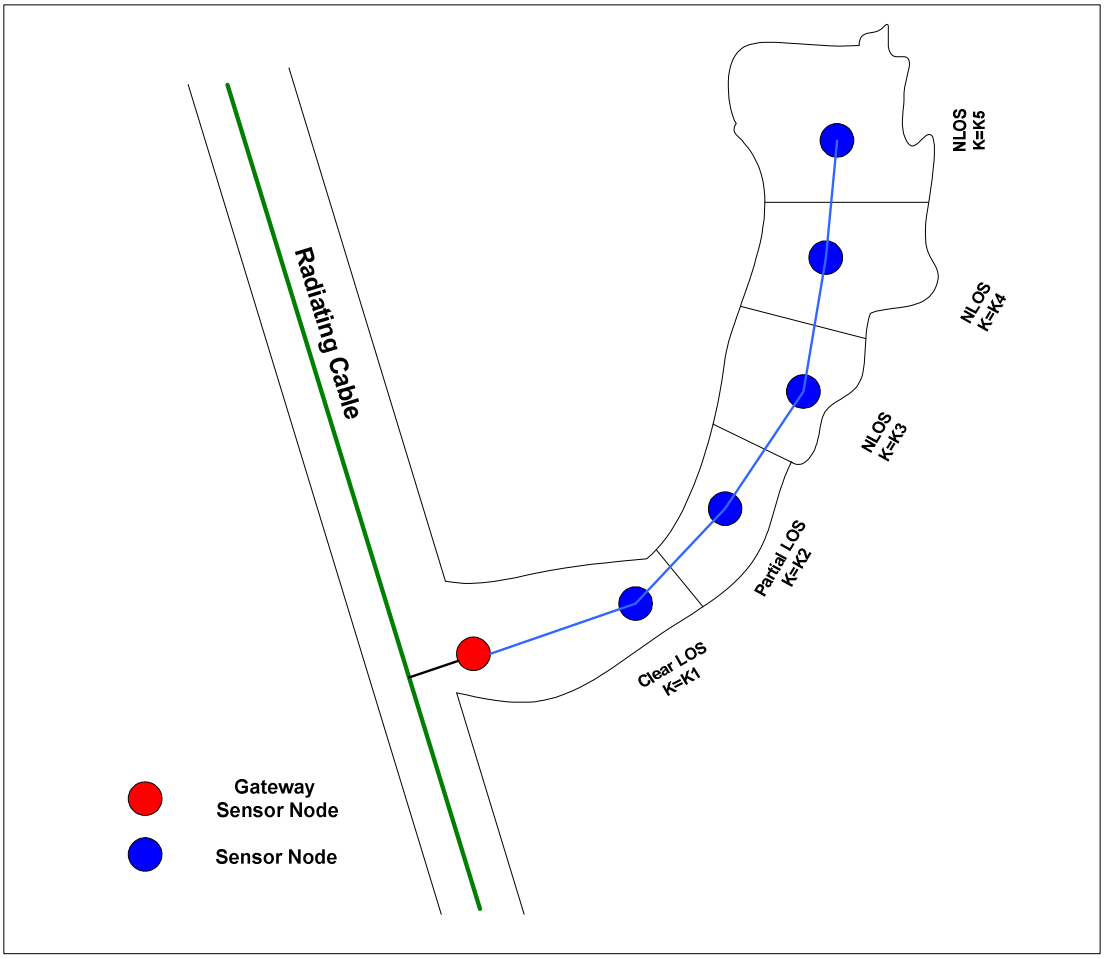

Figure 6.2: Mine Segmenting Wireless Channel Model

6.3 Fading Channels Statistical Combination

Our model considers two types of probability distribution functions representing two extremes between the cases of LOS and NLOS scenarios. These models are the Rician and Rayleigh fading distribution functions. Different segments in the mine will be mapped to number of distribution function depending on the multipath reflection scenarios in that particular segment in the mine. A combination of distribution functions will describe a larger area in the mine.

The Rayleigh probability density function (pdf) represents the worst case of fading with NLOS component in the signal. The Rayleigh distribution has a Probability Density Function (PDF) given by [33]:

$$p_{Ray}(r) = \begin{cases} \frac{r}{\sigma^2}\exp\left(-\frac{r^2}{2\sigma^2}\right) & 0 \le r \le \infty \\ 0 & r < 0 \end{cases}, \tag{6.1}$$

where r is the envelope amplitude of the received signal, σ is the rms value of the received voltage signal before envelope detection, and σ^2 is the time-average power of the received signal before envelope detection. For the Rayleigh distribution the Mean can be obtained by [5, 33]:

$$r_{mean} = E[r] = \int_0^\infty r\, p(r)\, dr = \sigma\sqrt{\frac{\pi}{2}} = 1.2533\,\sigma, \tag{6.2}$$

and the Mean Squared value;

$$E[r^2] = \int_0^\infty r^2\, p(r)\, dr = 2\,\sigma^2,$$

therefore ;

$$\sigma^2 = \frac{E\left[r^2\right]}{2}. \tag{6.3}$$

The Rayleigh probability density function with respect to the instantaneous SNR (γ) is obtained by [5, 54]:

$$p_{Ray}(r) = \begin{cases} \frac{1}{\gamma}\exp\left(-\frac{\gamma}{\overline{\gamma}}\right) & 0 \le r \le \infty \\ 0 & r < 0 \end{cases}. \tag{6.4}$$

When there is a dominant non-fading signal component present, such as LOS propagation path, the small-scale fading envelope is described by Rician fading distribution. The Rician probability density function is given by [33]:

$$p_{\text{Ric}}(r) = \begin{cases} \dfrac{r}{\sigma^2}\exp\left(-\dfrac{r^2+A^2}{2\sigma^2}\right) I_o\left(\dfrac{Ar}{\sigma^2}\right) & 0 \le r \le \infty \\ 0 & r < 0 \end{cases}, \tag{6.5}$$

where the parameter A denotes the peak amplitude of the dominant signal and $I_o(\cdot)$ is the modified Bessel function of the first kind and zero-order. The Rician distribution is often described in terms of K which is defined as the ratio between the deterministic signal power and variance of the multipath.

$$K = \frac{A^2}{2\sigma^2}. \tag{6.6}$$

The Rician pdf can be written with respect to γ as [33]:

$$p_{\text{Ric}}(r) = \begin{cases} \dfrac{2(1+K)}{\overline{\gamma}} e^{-K} e^{-\frac{(1+K)\gamma}{\overline{\gamma}}} I_0\left(\sqrt{\dfrac{4K(1+K)\gamma}{\overline{\gamma}}}\right) & 0 \le r \le \infty \\ 0 & r < 0 \end{cases}. \tag{6.7}$$

As shown in Figure 6.3 when the peak amplitude A decrease the value of K also decrease indicating that the dominate path decreases in amplitude value. This is the case when the Rician distribution degenerates to a Rayleigh distribution.

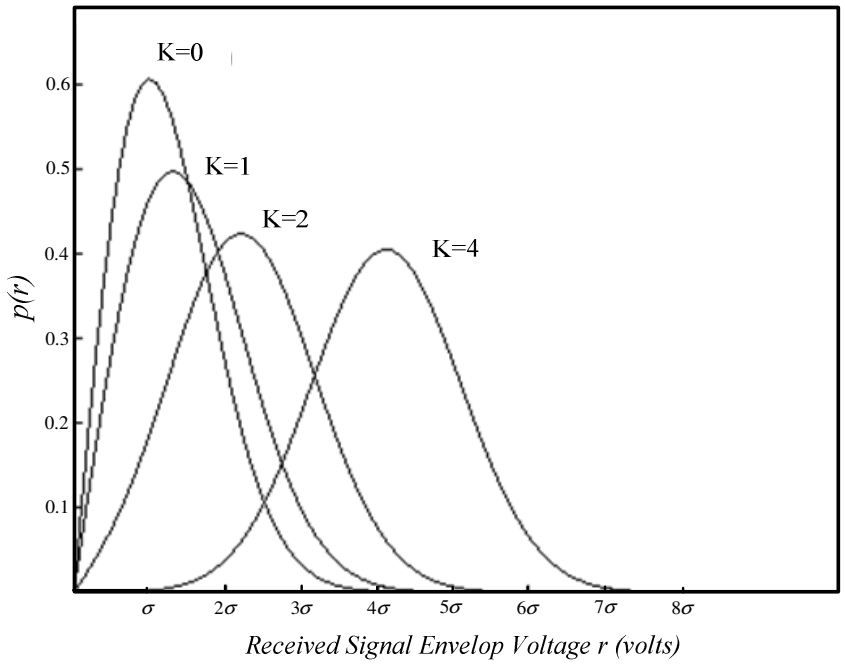

Figure 6.3: Rician and Rayleigh Distribution Degeneration

As mentioned earlier, our aim is to develop a wireless channel model in the mine based on the performance of wireless systems. Therefore, we are utilizing the BER as a metric to measure the performance. The average error probability in the presence of fading is obtained by averaging the conditional error probability over one of the selected fading Probability Density Functions (PDF) [6]:

$$p_e = \int_0^\infty p_e\left(x|\gamma\right) f\left(\gamma\right) d\gamma, \tag{6.8}$$

where $p_e(x|\gamma)$ is the conditional probability of bit error given by instantaneous SNR (γ) and $f(\gamma)$ represents the PDF of a particular fading channel.

In our analyses we have selected the wireless systems based on 802.11b standards. These standards are diverse with four levels of possible data rates and modulation schemes as demonstrated in the following sections:

6.3.1 DBPSK Performance over the fading channel

When the Differential Binary Phase Shift (DBPSK) modulation is selected the data rate of the communication link can achieve 1 Mbps of data transportation.

The probability of bit error over Rayleigh fading channel for DBPSK can be expressed as [54]:

$$p_{e\_DBPSK+Ray} = \frac{1}{2 \cdot (1+\overline{\gamma})}. \tag{6.9}$$

Similarly the, probability of bit error in Rician fading channel for DBPSK is given by:

$$p_{e\_DBPSK+Ric} = \frac{1+K}{2 \cdot (1+K+\overline{\gamma})} \exp\left(-\frac{K\overline{\gamma}}{1+K+\overline{\gamma}} \right). \tag{6.10}$$

6.3.2 DQPSK Performance over fading channel

When the Differential Quaternary Phase-Shift Keying (DQPSK) is used, the wireless channel can provide up to 2 Mbps of data rate.

The probability of bit error over Rayleigh fading channel for DQPSK can be expressed as [57]:

$$P_{b\_DQPSK+Rayleigh} = \int_0^{\infty} \frac{1}{\overline{\gamma}} \exp(-\frac{\gamma}{\overline{\gamma}}) \cdot \left[Q_1(a,b) - \frac{1}{2} I_o(ab) \exp\left(-\frac{1}{2}(a^2+b^2) \right) \right] d\gamma, \tag{6.11}$$

where $Q_1(a,b)$ is the Marcum Q-function, $I_o(ab)$ is the modified Bessel function of the first kind and zero order, and parameters a and b are defined as:

$$a = \sqrt{2\gamma.\left(1-\sqrt{\frac{1}{2}} \right)}, \quad b = \sqrt{2\gamma.\left(1+\sqrt{\frac{1}{2}} \right)}. \tag{6.12}$$

Similarly the, probability of bit error in Rician fading channel for DQPSK is given by:

$$P_{b\_DQPSK+Ric} = \int_0^{\infty} \left[Q_1(a,b) - \frac{1}{2} I_0(ab) e^{\left(-\frac{1}{2}(a^2+b^2)\right)} \right] . \frac{2(1+K)}{\bar{\gamma}} e^{-K} e^{\frac{(1+K)\gamma}{\bar{\gamma}}} I_0\left(\sqrt{\frac{4K(1+K)\gamma}{\bar{\gamma}}} \right) d\gamma. \quad (6.13)$$

6.3.3 CCK Performance over fading channel

Finally, the probability of bit error for Complementary Code Keying (CCK) over AWGN channel is defined as [55, 56]:

The total p_e of the system in the Rayleigh fading channel is given by:

$$P_{b\_CCK+Ray} = \int_0^{\infty} \frac{1}{\gamma} \exp\left(-\frac{\gamma}{\bar{\gamma}} \right) . \left[1 - \int_{-\sqrt{2\gamma}}^{\infty} \left(\frac{1}{\sqrt{2\pi}} . \int_{-(z+\sqrt{2\gamma})}^{z+\sqrt{2\pi}} e^{-\frac{y^2}{2}} dy \right)^{\frac{MD}{2}-1} . e^{-\frac{z^2}{2}} dz \right] d\gamma . \quad (6.14)$$

And for the Rician fading channels, the average BER can be obtained as in the following:

$$P_{b\_CCK+Ric} = \int_0^{\infty} \frac{2(1+K)}{\bar{\gamma}} e^{-K} I_0\left(\sqrt{\frac{4K(1+K)\gamma}{\bar{\gamma}}} \right) . e^{\frac{(1+K)\gamma}{\bar{\gamma}}} \left[1 - \int_{-X}^{\infty} \left(\frac{1}{\sqrt{2\pi}} . \int_{-(z+X)}^{z+X} e^{-\frac{y^2}{2}} dy \right)^{\frac{MD}{2}-1} . e^{-\frac{z^2}{2}} dz \right] d\gamma, \quad (6.15)$$

where MD is the CCK modulation factor. MD is 4 for 5.5 Mbps and 8 for 11 Mbps

6.4 Model Simulations

The BER performance over different fading channels has been simulated with various SNR and *K* – factor. MATLAB was used in these analyses. In this environment the BER performance of 802.11b was simulated by varying the SNR and *K* – factor of the distribution function to count for environment changes with respect to reflections in the mine. As shown in Figure 6.4, starting with one extreme, K was selected to have a small value. Starting with $K = 0$, the Rayleigh fading channel was simulated. This scenario shows the case of mine environments with many

surrounding objects. It is a case of NLOS between the transmitter and receiver. It represents one of the worst cases for wireless communication channels in the mine.

After this point, we started to increase the value of K to mimic areas in the mines with fewer reflections. With K=5, the performance of the wireless signal is poor. High transmission levels might be required to achieve a Signal to Noise Ratio (SNR) that corresponds to certain acceptable performance BER. This scenario represents Non-Line-Of-Sight propagations with high signal reflections. With the K-factor of 10, it is noticed there is a slight improvement in the wireless system performance. This scenario represents a case of PLOS with heavy reflections of signals on the walls of the mine. When K was increased to 15, the performance of the wireless system is further improved, however we still can see it is affected by moderate multi-path phenomena of the signal reflecting on the walls of the mine. This scenario represents a condition of PLOS.

With K = 20, we can observe a performance close to that of the AWGN channel with very strong LOS component. In this scenario, the degradation in performance for higher data rates in comparison with the lower data rates is not very obvious due to the LOS condition and reduced multipath phenomena. This is the case when the wireless transmitting and receiving nodes are in close proximity of each other. Further increase in K value, will result in further improvement in link performance. However, given the limited scales and sizes of the mine areas, the range of K can be limited to certain domain. Therefore, and to adopt a realistic range for values of K in the mine, we considered the value of K =20 as a maximum range for K.

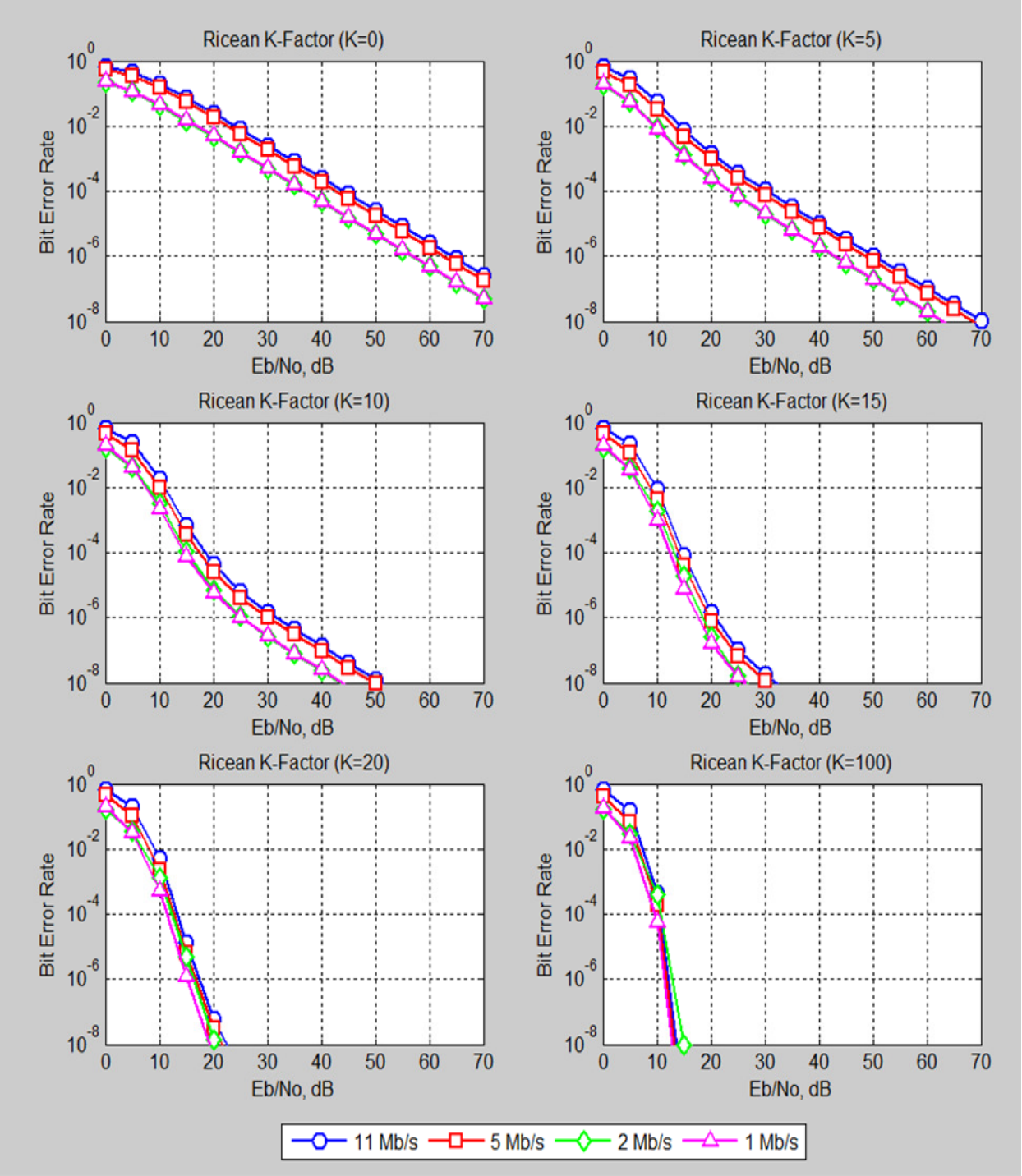

Figure 6.4: Mine segmenting performance curves

It is obvious the as the value of K gets bigger the channels characteristics tend to get closer to the Rician model. Different modulation/demodulation techniques were employed in the simulation to analyze different data rates; these are as follows: BPSK (1Mbps), DQPSK (2 Mbps) and CCK (5.5 Mbps and 11 Mbps).

Wireless networks in the underground mine can operate in mobile conditions. Wireless nodes (such as WSN) can transmit and receive while in motion. Therefore, the value of K can fluctuate which adds complications to the time varying wireless channels in the mine. Figure 6.5 shows simulation results for evaluating the performance of 1Mbps wireless channels. Different fading conditions are considered by varying the value of K in the simulation.

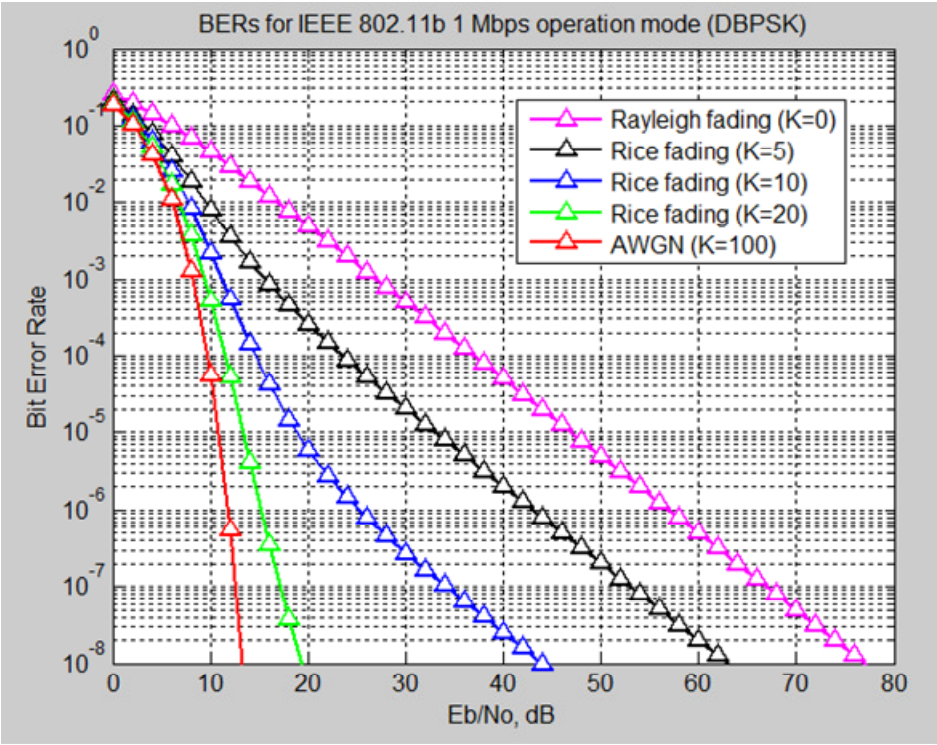

Figure 6.5: *K* factor Variations

6.5 Validation Measurements System

Real field test data were collected to validate the model. The test was conducted in the NORCAT mine in Sudbury, Ontario. The mine layout is shown in Figure 6.6. This mine is the NORCAT mine, located in Sudbury, Ontario, Canada.

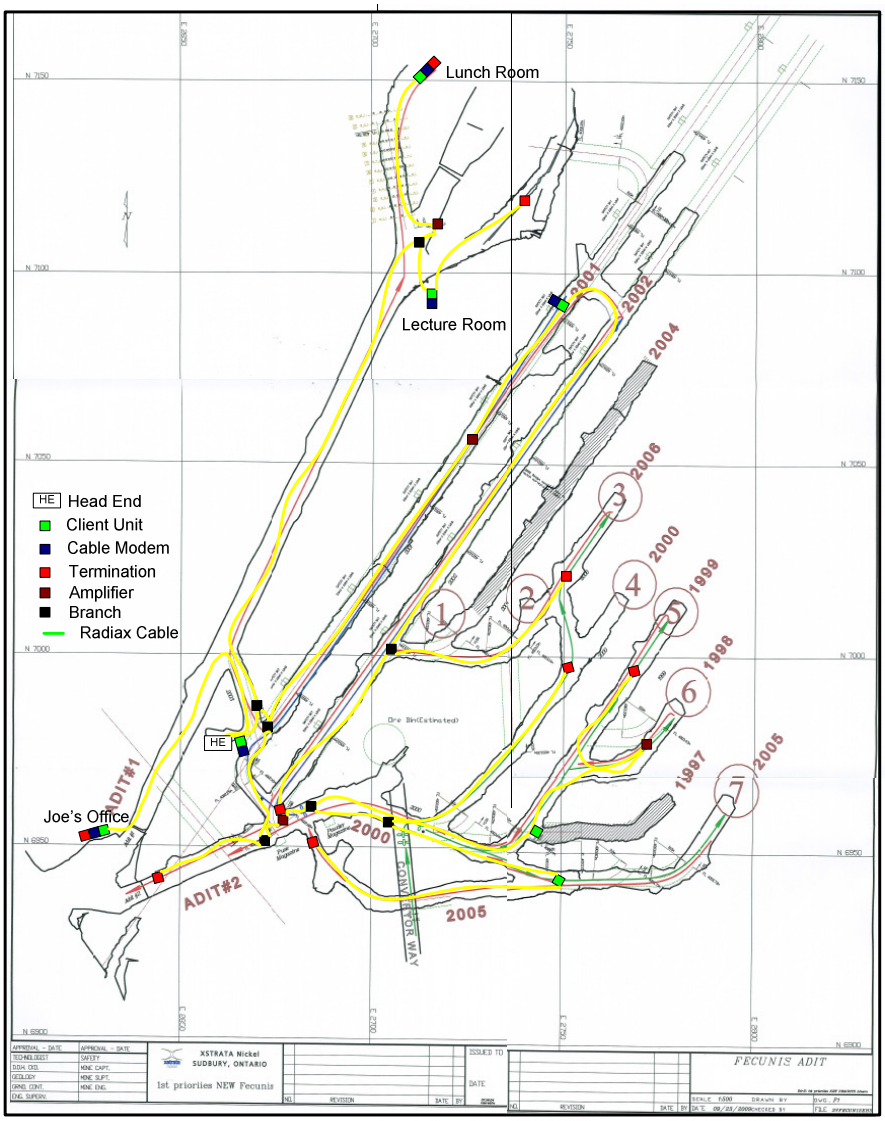

Figure 6.6: NORCAT mine, Sudbury, Ontario.

The area that was chosen to run the test is separated into the following three areas: LOS area, PLOS area and NLOS area. Each of these areas is about 30 meters in length. Figure: 6.7, shows the test layout of the NORCAT mine.

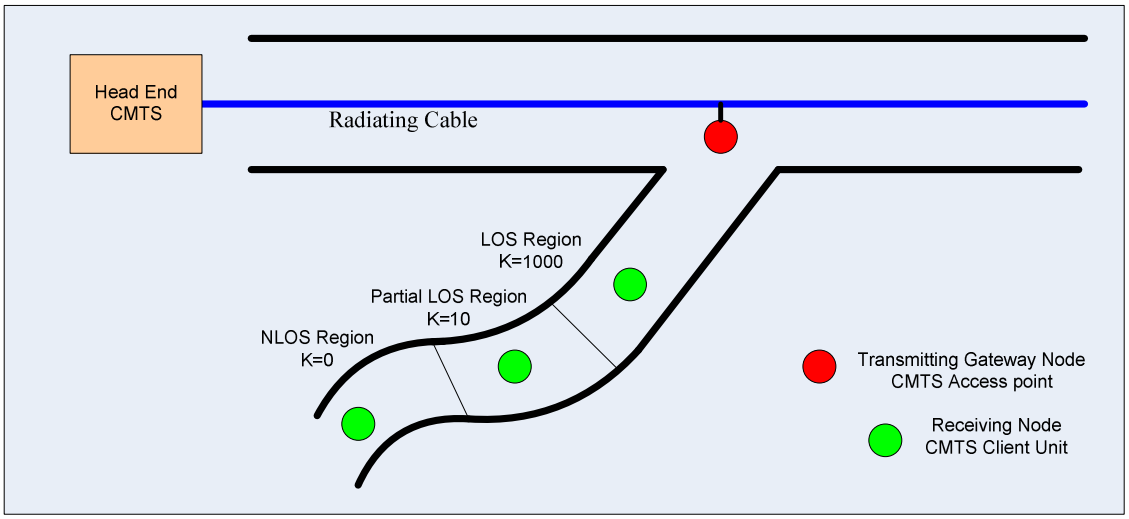

Figure: 6.7: Mine Segmenting Model Test Layout

In the test, we have used two access point transceivers to establish a point-to- point link in the mine galleries. The first unit used is an access point from ValuePoint (Model Multi AP 700). As a transmitting unit, this unit was configured as a fixed gateway Access Point (AP). This node was connected to the mine leaky feeder system via CMTS modem. This gateway Access Point has a maximum transmitting power of 400 mW (26 dBm). The output power of this unit is adjustable to enable transmission at different levels. The receiving unit was another AP from ValuePoint (Model Multi AP 570G). This unit was configured as a client node. Figure 6.8 shows the test block diagram. Outdoor Directional antennas from ValuePoint were used in the test. The antennas had a gain of 14dBi. As shown in the bock diagram 1 Mbps of data was transmitted from the AP 700 to AP570G access points. A BER tester from RAD Communications was used in the test. A data stream of 1 Mbps was sent from BER Tester –A to the BER Tester-B. The RSSI and SNR readings as reported by the test utility of the Access Point were measured and recorded as shown in Table 6.1.

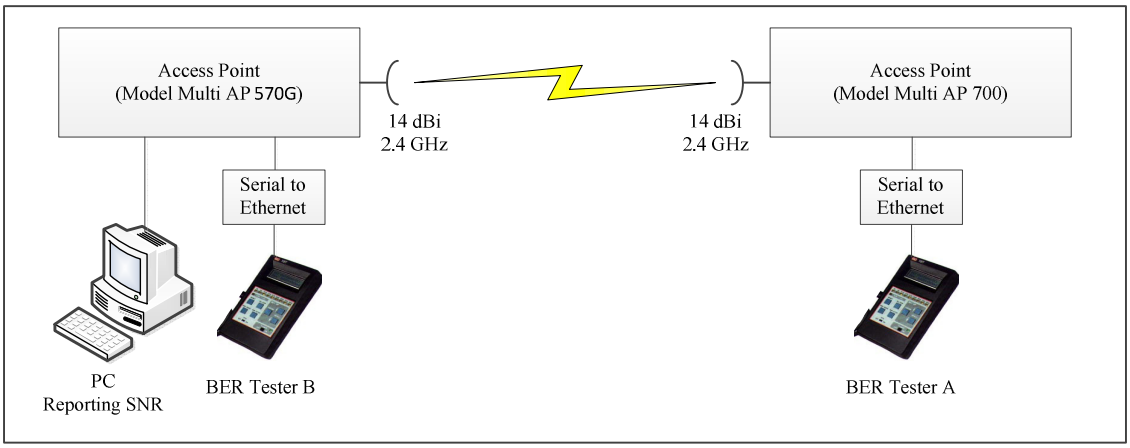

Figure 6.8: BER Test Block Diagram

During the test, the transmitting power of the AP-700 was varied in steps to obtain pre-determines levels of SNR at the receiving nods. Figure 6.9 shows the ValuePoint system used in the test and its test utility. The BER was measured at the receiving node by the BER Tester-B for each value of SNR. Table 6.1 shows the results of the tests in the three areas. This table also shows the comparison analyses between the measured and theoretical expected results. The comparison analyses are shown graphically in Figure 6.10. The test results converge with the expected theoretical results for the three segments of the tested area.

Figure 6.9: ValuePoint System

	Region 1 (LOS)		Region 2 (PLOS)		Region 3 (NLOS)	
	Theoretical	Test Data	Theoretical	Test Data	Theoretical	Test Data
E/N	BER	BER	BER	BER	BER	BER
15	1.20E-06	5.00E-06	7.74E-05	1.77E-04	1.53E-02	2.53E-02
20	5.75E-09	1.00E-08	6.06E-06	9.06E-06	4.95E-03	2.00E-02
25	2.23E-10	8.00E-10	1.07E-06	4.07E-06	1.58E-03	2.58E-03
30	3.20E-11	1.50E-10	2.75E-07	1.75E-07	5.00E-04	1.50E-03
35	7.76E-12	6.00E-12	8.15E-08	1.50E-07	1.58E-04	5.58E-04
40	2.25E-12	1.20E-11	2.52E-08	5.50E-08	5.00E-05	1.30E-04
45	6.93E-13	9.00E-13	7.92E-09	8.00E-09	1.58E-05	1.98E-05
50	2.17E-13	9.00E-13	2.50E-09	5.00E-09	5.00E-06	2.00E-05
55	6.90E-14	2.00E-13	7.90E-10	3.00E-09	1.58E-06	2.58E-06

Table 6.1: 802.11-b performance test

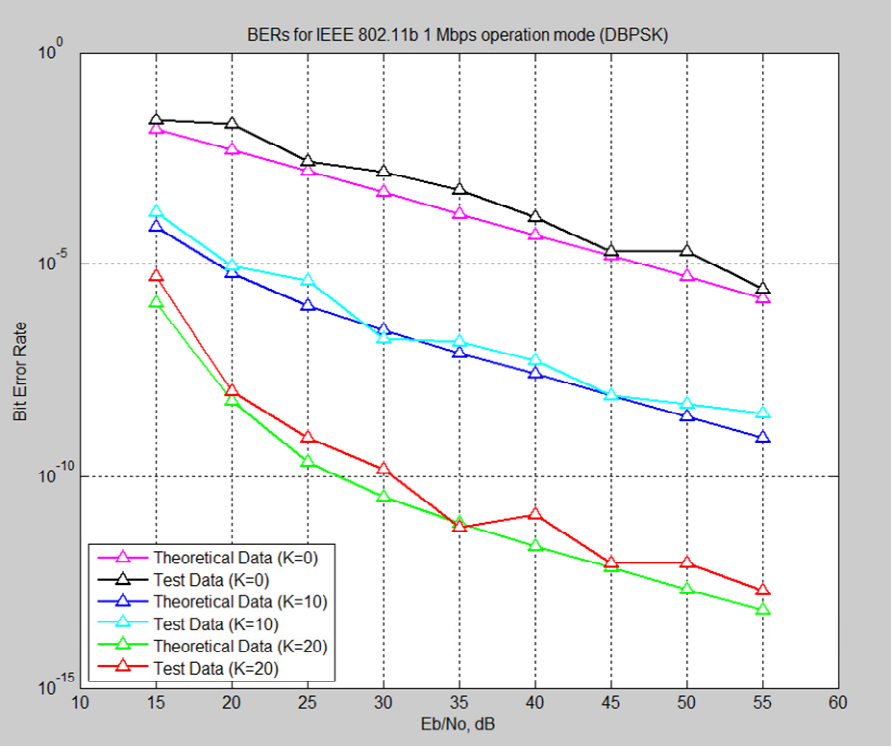

Figure 6.10: Comparison analyses 802.11-b, 1 Mbps

6.6 Summary

The *new Mine Segmenting Wireless Channels* Model offers a simplified and generic approach to characterizing the wireless channels in underground mines. This model can be applied in different areas of the mine regardless of the layout (tunnel channel and the room-and- pillar channel). The model demonstrates a new approach of combining different statistical models in order to formulate a performance-based approach in characterizing the wireless channels in underground environments. The combinations of the statistical models were mapped to the layout of the mine's galleries that have different wireless channel characteristics. Thus three general areas or segments were designated, namely, LOS, PLOS and NLOS.

Since this is a performance- based technique, the probability of bit error (p_e) was used to demonstrate the simulated performance of different modulation techniques associated with each 802.11b; these are; BPSK (1Mbps), QPSK (2 Mbps) and CCK (5.5 Mbps and 11). MATLAB was used to simulate the BER performance of 802.11b by varying SNR and K-factor of the distribution function. Starting with one extreme, K was first selected to have small value (K=0). In this case, the Rayleigh fading channel was simulated. This scenario is equivalent to the NLOS propagation path. For the case when K has a very large value (K=100), the performance was simulated to be close to that of an AWGN channel (very strong LOS path). For the range for values of K between 20 and 100, similar results were obtained. We have also mapped and compared results for values of K within the range of 0-20. This range gives a realistic figure to map a range of K values to an area in the mine (approximately less than a radius of 100 m). To validate the model, a real field test was conducted in the NORCAT mine in Sudbury, Ontario. During the test, the BER performance was verified when the Data Rate was fixed to 1 Mb/Sec. The test results showed very promising outcomes when compared to the simulation results. In the next Chapter, this model will be used to develop an adaptive communication scheme by which the characteristics of the wireless channels can be estimated from the performance of the network. In this scheme, the wireless nodes in the mine can determine values for K based on instantaneous performance (i.e. BER and SNR). Therefore, the nodes in the system will have information about their physical environments, such as the level of multi path reflection. Knowledge of the environmental conditions in the mine can benefit the nodes in the wireless network to better estimate their transmit power levels and improve their schedule algorithms. Therefore this model can be utilized to enhance the reliability and network life of wireless networks in underground mines.

Chapter 7

7. RASSA: The Proposed WSN Power Optimization for Underground Mines

7.1 Overview

This Chapter presents an optimized architecture for integrating WSN in underground mines. With power efficiency and conservation in mind, the performance of the WSN in the underground is optimized for power efficiency, scalability and rapid application developments. The developed algorithm called "Recourses-Aware Sleep Scheduling Algorithm" (RASSA) integrates a number of schemes that offer an advanced and novel approach. The algorithm targets the deployments of the wireless sensors' network in the mines' environments to ensure more reliable and scalable behaviours where new applications can be rapidly developed through flexible tasks compositions. The WSN in the mine is also be optimized for longer operating life in the environments. Figure 7.1 shows the wireless elements of the mine's integrated network.

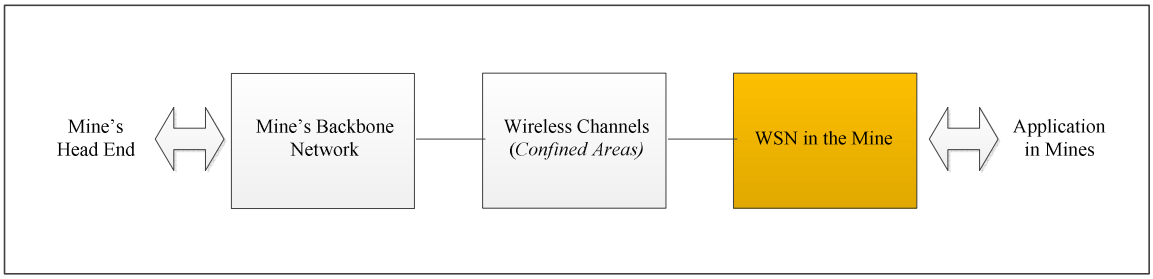

Figure 7.1: The Wireless Element of the Mine's Integrated Network

In wireless sensor networks, sensors are periodically switched into sleep mode for energy savings. This, however, causes the unavailability of nodes, which, in turn, means the possibility of disruptions to the application compositions requested by a particulate solution initiator [57-59]. Thus, it is desirable to maintain enough active sensors in the system to provide the required services at any time in order to achieve dependability for various applications. The developed algorithm offers a scheme for a cross-layer sleep scheduling optimization, which aims to prolong the network lifetime while satisfying the requirements of the application compositions in the application layer.

Furthermore, the wireless channel characteristics of the mines' confined spaces are part of the optimized algorithm for improved performances and power saving. By utilizing the developed wireless channel model "Mine Segmenting Wireless Channel Model" as demonstrated in Chapter 6, the nodes in the WSN are able estimate their environmental locations with respect to reflections, scatterings and other multi path phenomena. Therefore, further optimization can be obtained while maintaining acceptable performance characteristics.

The developed "Recourses-Aware Sleep Scheduling Algorithm (RASSA)" integrates three main schemes in optimizing the WSN in the underground mines for longer network life and flexible rapid applications deployments. The three schemes of the algorithm are listed below:

- Adaptive Cross-Layer Scheme for Rapid Applications-Compositions,
- Adaptive Recourses-Aware Scheme for Sleep Schedule Optimizations,
- Adaptive Topology Aware Scheme for Underground Mines.

These schemes are explained in detail in the following three Sections.

7.2 Adaptive Cross-Layer Scheme for Rapid Applications-Compositions

In our new approach, the algorithm presents a scheme where sensors in the WSN can be rapidly configured to provide new applications by composing a number of available services and functions the sensors in a certain WSN cluster can provide. Application-Composition WSN architecture treats software components provided by sensors as functions and services [64]. By composing a number of these functions into applications, adaptive solutions can be provided. Examples of the functions that can be provided by the sensors to compose an application are as

follows: data processing functions, time synchronization functions, wireless characterization functions, node localization functions and data aggregation functions.

In our creative scheme, each function can be provided by multiple nodes. A typical application consists of a set of required services that need to be coordinated through application composition. The task of the application composition is to assign each required function to an appropriate node according to certain criteria. In this scheme, the task of application compositions brings unique challenges to sensor sleep scheduling. For example, let us consider the Ventilation On Demand (VOD) application in mines. In this application, the WSN is responsible of controlling the ventilation system in the mine depending on air quality [24]. This application uses gas sensors to detect the air quality in the mine. The collected data is processed to control the ventilation system in order to provide acceptable air quality for the miners and the equipment to operate safely in the mine. At the same time, it saves power in running the ventilation equipment when they are operating only when needed and at the speed that provides acceptable air quality. Let us assume there are few sensors deployed in an area of the mine where a great deal of mining activity is happening and, therefore, the air quality is constantly changing. The WSN is required to report the level of toxic gas to the ventilation control center. The control center optimizes the speed of the fan depending on the gas level and the actual need for the ventilations. To compose this application, three functions are required: function f_1 senses the level of the toxic gas (i.e. data collection function), function f_2 processes the collected data and prioritizes them to the proper route (i.e. data processing and aggregation functions), and function f_3 transports the information to the sink node (i.e. synchronization and transportation functions). As shown in Figure 7.2, suppose that there are four sensors which can provide $\{f_1, f_2\}$, $\{f_2\}$, $\{f_3\}$, and $\{f_2, f_3\}$ respectively.

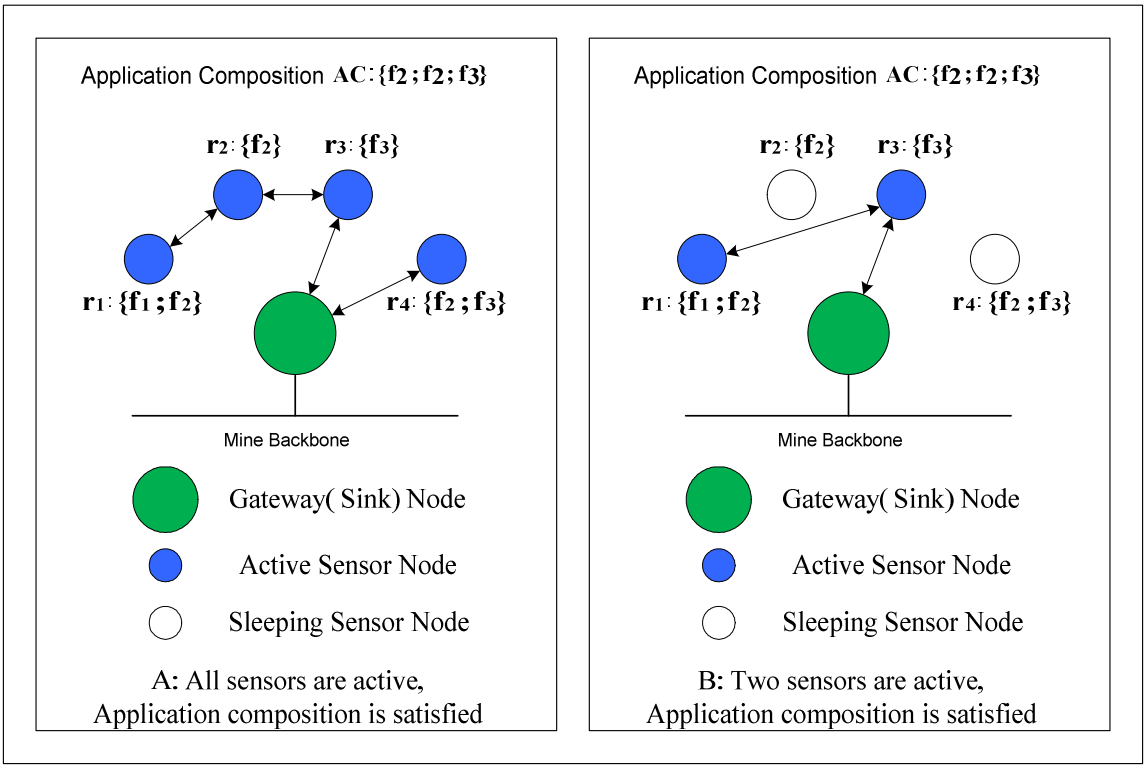

Figure 7.2: WSN Application -Compositions for underground mines

If each of these four sensors is active simultaneously $(r_1 + r_2 + r_3 + r_4)$, the network can accommodate the service composition request as shown in Figure 7.2- A. The application composition can be satisfied if only the first sensor, r_1, and the third, r_3, are active at the same time $(r_1 + r_3)$ as shown in Figure 7.2-B. Likewise, the application can be composed successfully if the first sensor r_1 and the fourth r_4 sensor are active at the same time $(i.e.\ r_1 + r_4)$. Other combinations do not satisfy the application composition requirements.

In this Section, the architecture of the Cross Layer Model for WSN in Underground Mines is presented. In this approach, the layers of the network can be crossed and divided into a number of sub-layers. Figure 7.3 shows an example for mine's network architecture, where the application layer of the WSN is divided to three sub-layers as follows:

1- Application Composition Sub-layer (ACS): This sub-layer composes of a number of functions into an application. The functions elements that are necessary for the application-composition are required to be available and provided by a number of sensors within the sink node cluster. The

ACS in the sink node maps an application into a composition of functions, which specifies the required solution. For our VOD example, the ACS composes a number of services to achieve the required application. In this case the application composition is made up of three functions (f_1 , f_2 and f_3).

2- Application Administration Sub-layer (AAS): This sub-layer administers the composition of the applications. This sub-layer provides application coordination and further break down structure for the applications

3- Application Processing Sub-layer (APS): This sub-layer supervises the execution of the applications to ensure successful applications deployments. This sub-layer utilizes the information provided by the other sub-layer (i.e. the ACS and AAS sub-layer.)

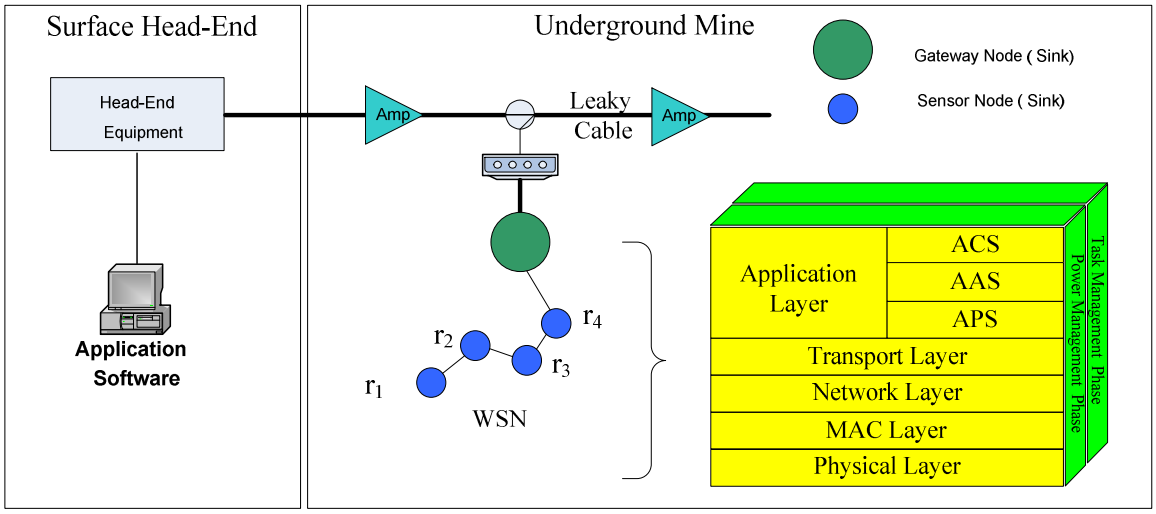

Figure 7.3: Cross Layer Model for WSN in Underground Mines

7.3 Adaptive Recourses-Aware Scheme for the Sleep Schedule Optimizations

Prolonging network life is a primary consideration in the design of WSN. A major power conservation technique in wireless sensor networks is to design adaptive sleep schedules at the MAC layer to minimize the energy consumption for sensors that are not effective parts of the application. However, a sensor in the sleep mode is not able to communicate, thereby affecting the operations at both the network layer and the application layer [60-64]. Thus, a cross-layer

sleep scheduling design is desired to devise sleep scheduling which considers the requirements at other layers and guarantee the availability of adequate number of active sensors providing certain functions. To demonstrate the process, imagine a cluster in a WSN with five sensors. Each sensor is capable of providing certain types and number of functions. Figure 7.4, shows an example for a profile of five sensors providing a number of function $\{f_1, f_2\}, \{f_2, f_4\}, \{f_3, f_4\}, \{f_1, f_3, f_4\}$, and $\{f_1, f_2, f_3, f_4\}$, respectively. Assuming a time-cycle of 8 time slots, T=8, a sleep schedule can be generated and then optimized to coordinate each sensor's activity and ultimately optimizing the average sensor power consumption to a minimum level. This optimization approach considers a number of constraints that ensure enough active sensors are available to satisfy the application composition requirements.

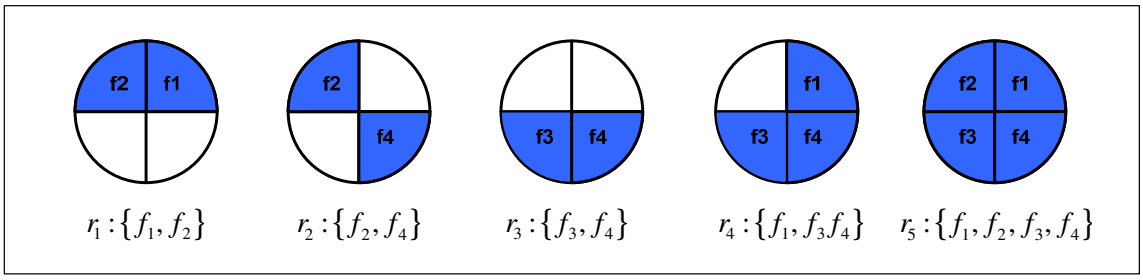

Figure 7.4: WSN cluster profile

For example, a sleep schedule can be developed for the five sensors to provide a certain application. Let us assume this application requires one of each function to be available at every time slot during the time-cycle , T. An example of such a schedule is shown in Figure 7.5. Under this sleep schedule, r_1 needs to be active in three time slots per cycle, r_2 also needs to be active in three time slots per cycle, r_3 needs to be active in two separate time slots of a cycle, r_4 needs to be active in three time slots per cycle and r_5 needs to be active in three time slots per cycle. Obviously, this schedule guarantees continuous service availability.

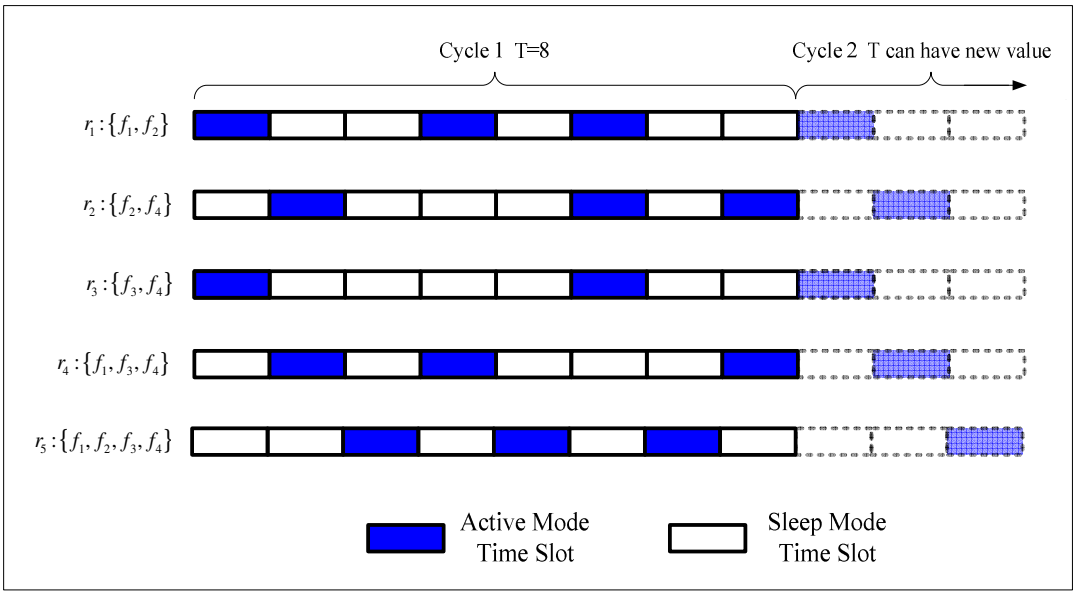

Figure 7.5: WSN sleep scheduling scheme example

In our scheme, multiple application- composition requests may exist concurrently. As a result, some functions may be required by multiple application-composition requests during the same time slot. Therefore, more active sensors may be required to accommodate the application requirements. In particular, we assume that each type of functions f_j needs C_j active sensors at any time slot in order to process the application-composition requests in the system. Statistical and historical information can help in estimating the number of the functions that are expected to be required at any given time[63,64]. For example, according to the historical information, if there are at the maximum three applications simultaneously requesting function f_1 at any time in the system, then we have to have more than three sensors providing this function (i.e. $C_1 \geq 3$).

Our scheme is adaptive in a way that the application –compositions can change from one time cycle to another. Figure 5.5 shows an example for the sleep schedule for three time cycles. The first time cycle is the sleep schedule to accommodate VOD application-composition. In the second time-cycle, the application-composition is changed to environmental monitoring. In the third time-cycle, both applications are required by the application- composition at the same time. In the first two time-cycles, only one application is required in every time-cycle. In these time-cycles, only one function of each type is required at each time slot $AC = \{f_1, f_2, f_3\}$ and ($C_1 = C_2 = C_3 = 1$). To accommodate both applications in the third time-cycle simultaneously, more

sensors are required to be in the active mode. In this case, each type of function is required twice at every time slot [i.e. $AC = \{f_1, f_2, f_3\}$ and ($C_1 = C_2 = C_3 = 2$)].

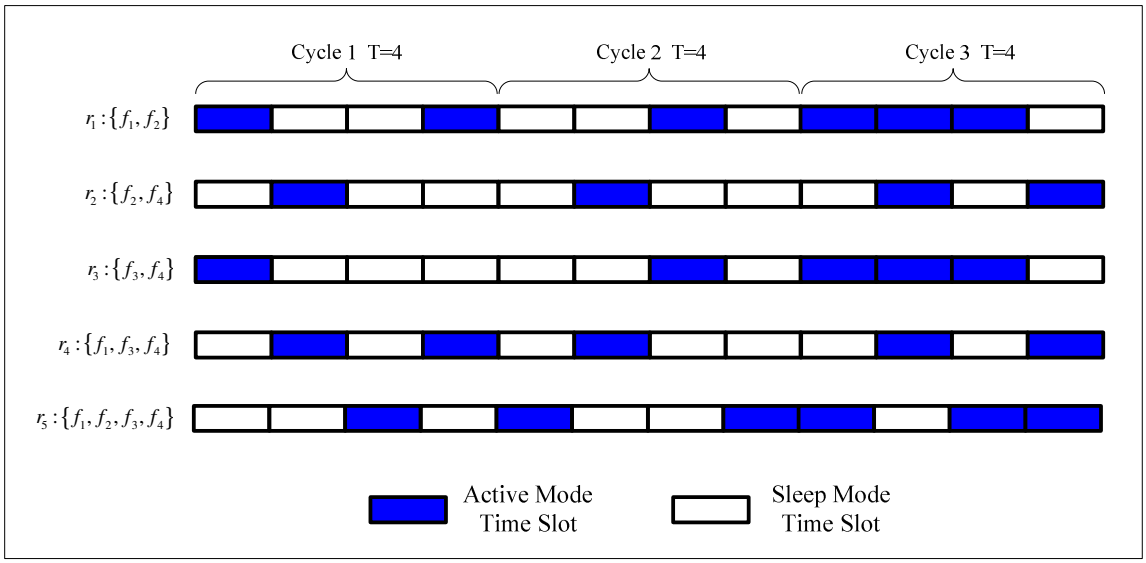

Figure 7.6: Adaptive sleep schedule example

7.4 Adaptive Topology-Aware Scheme for Underground Mines

Based on the wireless channel modeling analyses as demonstrated in Chapter 6, our theory of "Mine Segmenting Wireless Channel Model" is utilized to provide the sensors in the mines with very valuable information about the sensor's environmental location in terms of the severity of multi-path reflection and similar physical phenomena that can affect the performance of the wireless link between the sensors in the mine (i.e. Wireless channel characteristics). Within this scheme, the developed sleep schedule algorithm of the WSN is further optimized by having the sensors in the mine adaptively adjust their transmission RF power level to an optimized value that meets the wireless channel performance requirement. The performance requirements are defined in terms of Bit Error Rate (BER) that is required to maintain adequate data transportation integrity. Although the analyses were based on a Wi-Fi based WSN sensor, the same principle can also be applied to other types of sensors in the mine such as Zigbee-based WSN. The sensors can normally measure their BER and SNR at any given time. However, the crucial information needed is the type of instantaneous channel fading at any point in time for the sensors to estimate the proper RF power levels required to achieve a certain preference (i.e. BER). When the sensor is aware of the wireless channel characteristics of its communication channel or, in other words,

the K factor and the corresponding curve, it will be able to move on that curve to arrive at the SNR that corresponds to the target BER required by the WSN in the mine. When the sensor is made aware of its curve it can move up and down on the curve by adjusting it transmit power to a certain SNR and therefore to the BER that corresponds to that SNR on the curve.

Figure 7.7 shows the wireless channels performance curves for sensors communicating in underground WSN. Each curve corresponds to wireless channel characteristics with a different K factor. As mentioned before, the K factor is the ratio of the directly transmitted power to the total reflected power as received by the sensor. As it was explained in Chapter 6 a larger value of K corresponds to a wireless channel closer to AWGN or LOS. In these cases, lower RF transmission levels can achieve the required BER at lower SNR values. As values of K decrease, the wireless channel will have PLOS behaviour, which is closer to Rician fading characteristics. Obviously, it is harder for the sensors to achieve the target BER when K factors decrease, as it requires more RF power to arrive at the required SNR.

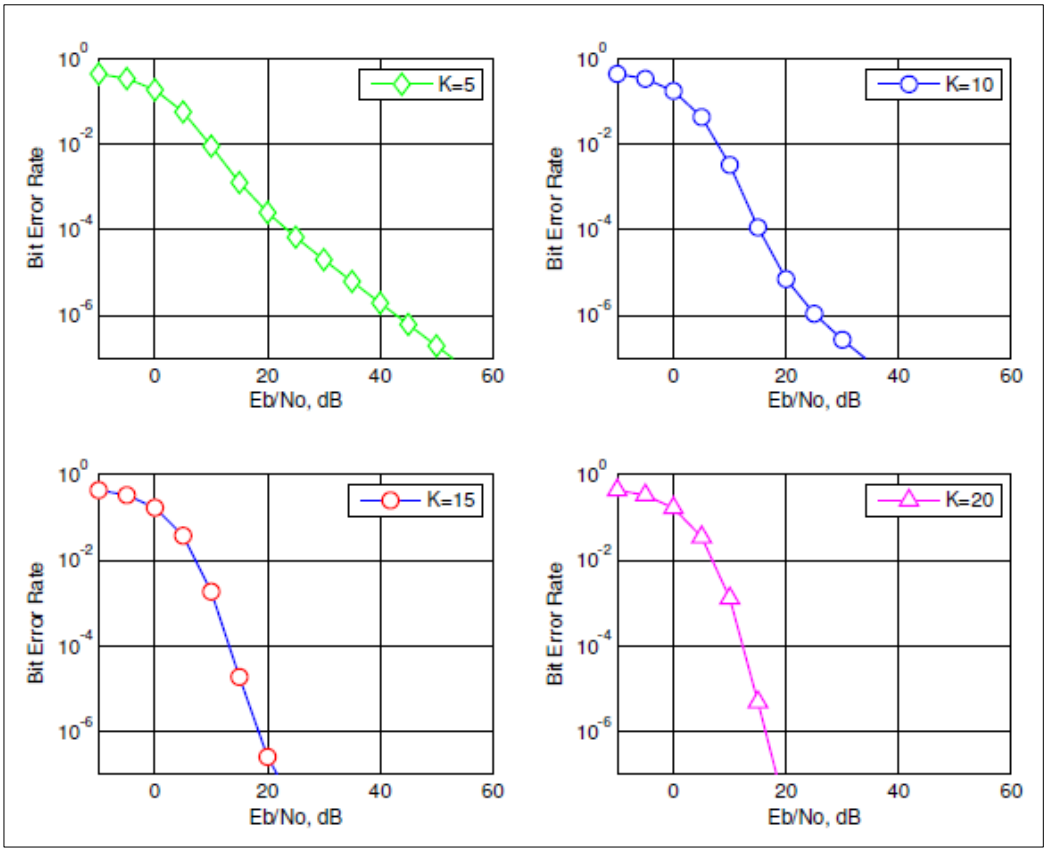

Figure 7.7: Wireless Channel Characteristics for area in the mine

7.5 WSN Optimization Problems Formulations

In a Multi-Objective optimization environment, the optimization problems are formulated to express the objective functions and constraint. We are presenting a new Hierarchy-based Multi-objective Optimization algorithm to solve the problem of prolonging the WSN network life while maintaining enough resources to satisfy the application-composition requirements. In this approach, the optimization is broken down into two stages. The first stage is considered to be the most critical and important one to produce an optimized sleep schedule with a minimum number of active sensors in each Time-cycle, T. At this stage, we relax the constraints of the second objective to achieve the best optimized results for the first objective without limiting the optimization to the constraint of the second objective.

We consider two sources of energy consumption for the sensors that can be reduced through sleep scheduling and ordering algorithms. The first source, also the dominant one, is the energy consumed (or wasted) when the sensor is fully powered but not performing any function in the network. We can also refer to this problem as "Lost Opportunities" when the sensors are fully powered but not utilized to be part of any useful Application-Composition. To minimize such energy consumption, we try to switch the sensors into the sleep mode as much as possible. The second source is the energy consumption caused by the power-up operations when a sensor is switched from the sleep mode to the active mode. In this case a sequence of operations must be performed when a sensor becomes active again. Such operations include initializing the radio and waiting for the radio's crystal oscillator to stabilize. The energy consumed by all these operations is referred to as "Power-Up" energy consumption. Clearly, in order to minimize the power-up energy consumption, we prefer less frequent mode changes for a sensor. Our sleep scheduling algorithms addresses both sources of energy consumption. The sleep schedule design aims to prolong the network longevity while maintaining enough active sensors for each required task from the application layer.

Suppose that in a WSN, there are m functions $F = \{f_1, f_2, \dots\dots\dots, f_m\}$ provided by n sensors $R = \{r_1, r_2, \dots\dots\dots, r_n\}$. We assume that each sensor r_k can provide a number of tasks or functions. We use $[F_k]$ to denote the set of functions that sensor r_k can provide, and $[R_l]$ be the set of sensors that can provide function f_l. If a sensor r_k is active, it can provide all functions in $[F_k]$; if it is sleeping, it cannot provide any function. We rotate the active/sleep modes of the sensors based on a cyclic schedule, where each cycle contains T equal-length time

slots. In each time slot t_s a sensor r_k is either active or asleep. We can assume that all sensors in one local network are locally synchronized.

7.5.1 First Optimization Problem Formulation (Lost Opportunities Minimization)

We first formulate the problem into an Integer Linear Programming (ILP) problem, which minimizes the maximum energy consumption among all sensors without considering the wake-up energy consumption in a given cycle with length T. At this stage, we are considering the Lost Opportunities energy minimization only. Our objective here is to determine a sleep schedule for each sensor in $[R]$ so that there are enough active sensors for each function f_j at any time.

Let $x_{k,t}$ be a binary variable, where $x_{k,t} = 1$ indicates that sensor r_k is active at time slot t. If we assume that the energy consumed by the sensor for the period of one time slot, t to be E_{ac}, then the total energy consumed by each sensor for being active for the number of time slots for the entire length of time-cycle, T, can be calculated as in the following:

$$\theta_k = E_{ac} \sum_{t=1}^{T} x_{k,t}, \tag{7.1}$$

where θ_k is the total energy consumed by the sensor r_k for the entire length of the time-cycle, T. To simplify the calculations, E_{ac} is normalized to one energy unit as in the following:

$$\theta_k = \sum_{t=1}^{T} x_{k,t}. \tag{7.2}$$

Therefore, the number of active time slots within a cycle indicates the energy consumption for r_k. Our first objective is to reduce θ_k to save energy from the sensors' being in active mode.

The constraint that needs to be considered is that at each time slot there must be enough active sensors to satisfy the application composition requirements. In other words, the number of sensors that can perform function f_1 must equal c_1. For example, if the application requires at least two active sensors that are capable of performing function (f_1) then function c_1 must be equal or greater than 2 ($i.e.\ c_1 => 2$) in order to satisfy the requirements of the application-compositions the following constraint must be considered:

$$\sum_k x_{k,t} \geq AC \quad \text{for all } t\,. \tag{7.3}$$

Our specific objective is to minimize the maximum load, max $\{\theta_k\}$. Subject to satisfying the requirements of the function-composition by guaranteeing enough active sensors per time slot to provide the required number of functions. Ultimately, this objective results in an extended lifespan of the WSN in the mine.

7.5.2 Second Optimization Problem Formulation (Power-Up Energy Minimization)

At the second stage of the optimization, the objective of minimizing the *Power-Up Energy is considered.* The Power-Up Energy (E_w) is the extra energy consumption when a sensor switches from the sleep mode to the active mode. Normally, E_w , is very small in magnitude in comparison to E_{ac}. As mentioned before the normalized power-up energy consumption E_{up} is the ratio of the actual energy consumed by the sensor to switch from the sleep mode to the active mode to that when the sensor is in the active mode (i.e. $E_{up} = E_w/E_{ac}$). Therefore, if we normalize the energy consumption for an active sensor (E_{ac}) in one time slot to be 1, then we can assume E_{up} <<1. However, in the case when the length of a time slot is short, i.e., all of the sensors' functions can be finished in a short time, for example, in a low data rate WSN, E_{up} could be relatively large with respect to the actual energy consumption for a full time slot. Thus, it is important to consider the power-up energy consumption and merge active time slots as much as possible to reduce the energy consumption while satisfying the requirements of having enough active sensors in each time slot.

Given a sleep schedule $[X]$ from the first stage of the optimization, we can use a binary variable $y_{k,t}$ to indicate such a mode switch at the beginning of time slot t, where;

$$y_{k,t} = \begin{cases} 1 & \text{When } x_{k,t} < x_{k,t+1} \\ 0 & \text{Otherwise} \end{cases}. \tag{7.4}$$

If we assume that the energy consumed by the sensor to switch from the sleep mode to the active mode is E_{up}, then the total energy consumed by each sensor for the number of times switching

from sleep to active mode for the entire length of time-cycle, T, can be calculated as in the following:

$$\varphi_k = E_{up} \sum_{t=1}^{T} y_{k,t} \, . \tag{7.5}$$

Therefore, considering the two types of energy consumptions, the total energy for each sensor, r_k, in the WSN for a period of one time-cycle, T, can be calculated as in the following.

$$E_k = \theta_k + \varphi_k \, , \tag{7.6}$$

$$E_k = \sum_{t=1}^{T} x_{k,t} + E_{up} \sum_{t=1}^{T} y_{k,t} \, . \tag{7.7}$$

Of course, this objective is subject to the constraint of guaranteeing enough number of functions per time slot to guarantee all the requirements of the application-compositions. For any function f_j at any time slot t, we need to guarantee that:

$$\sum_{k} x_{k,t} \geq AC \quad \text{for all } t \, . \tag{7.8}$$

where;

θ_k: is the total energy consumed by the sensor r_k for being active for a number of time slot for a complete time-cycle, T.

φ_k : is the total Power-Up energy consumed by the sensor r_k for a complete time- cycle, T.

E_k: is the total energy consumed by the sensor r_k for a complete time-cycle, T.

AC : Application composition.

7.5.3 Optimizations Formulation Summary

In stage one we minimize the Lost Opportunity (Active-Mode) energy consumption for each sensor over time-cycle T. In stage two we minimize the Power-Up energy consumed by each sensor over time-cycle T:

Objective functions:

$$\text{Minimize} \qquad (\theta_k = E_{ac} \sum_{t=1}^{T} x_{k,t}), \tag{7.9}$$

$$\text{Minimize} \qquad (\varphi_k = E_{up} \sum_{t=1}^{T} y_{k,t}). \tag{7.10}$$

By normalizing E_{ac} to 1, the multi objective cost function becomes;

$$\text{Minimize} \qquad (E_k = \sum_{t=1}^{T} x_{k,t} + E_{up} \sum_{t=1}^{T} y_{k,t}), \tag{7.11}$$

subject to:

$$\sum_{k} x_{k,t} \geq AC \quad \text{for all } t. \tag{7.12}$$

The constraint of this optimization is to guarantee enough active sensors all the time (at each time slot) that are capable of performing the requirements of the application compositions.

7.6 Resources- Aware Sleep Schedule Algorithm (RASSA)

Based on linear programming (LP), our developed algorithm introduces a new approach in Multi-objectives optimization where we introduced an approach based on prioritizing the objectives in the cost function in a hierarchical fashion.

The optimization is conducted in two stages. The first stage, which is the most critical, is the minimization of the power wasted due to idle listing of the sensors; this is the case when the sensor is active but not utilized by any application-consumption or not doing any useful activity. We also can refer to this wasted energy as "Wasted Opportunity" where the sensors are active but not used by the WSN to participate in any useful application- composition. In this stage, we try to turn the sensors into sleep mode as much as possible but still guaranteeing enough number of active sensors to provide the required functions and services.

The second objective in the cost function is to minimize the Power-Up energy consumption of the sensors. This is the power consumed by the sensors during the switch from the sleep mode to the active mode mainly due the power crystal and oscillator stabilization in the transmitter circuit of the sensor. This objective is considered to be less important than the first one since the Power-Up energy is a small fraction of the power consumed when the sensor is active. The optimization of the Power-Up energy consumption is achieved by trying to switch the sensors from the sleep mode to the active mode less frequently.

In our algorithm, the Multi-Objective optimization problem follows a priority or hierarchical technique, where the optimization is solved in two stages. In the first stage we relax the optimization by considering only the first objective of minimizing the power consumption as it is more critical and important than the second objective of Power-Up energy optimization. This technique results in a most optimized solution for the first objective which is more critical. Once the optimized sleep schedule is obtained, we can further optimize the solution by additional optimization (or ordering the solution) for optimized and less frequent sensors' switching from sleep to active mode. The two stages of the algorithm are explained in the following sections in more details.

7.6.1 Sleep Schedule Generations.

As mentioned before, the algorithm contains two stages. In the first stage, we generate the sleep schedule for all the sensors in the WSN. In fact, the generation of the schedule happens at the sink (gateway) nodes' levels. The schedule will then be delivered to all the nodes in the cluster of that sink gateway nose.

In our RASSA we consider the sleep schedule time slot by time slot. In each time slot, t_s, we select a sensor that we refer to as the "anchor" sensor of that time slot. The anchor sensor is active regardless of the number of services or functions that the sensor can perform and can contribute to the application. The selection of the anchor sensor follows certain criteria that guide the process of generating the sleep schedule to contain the minimum number of active sensors per time slot. At the same time it is guaranteeing an adequate number of active sensors to provide the required application composition. The sensors in the WSN cluster are identified with their unique ID address; that can be mapped to certain qualification criteria such as the remaining power in the sensor's battery and its K factor. The schedule assigns the anchor sensor at each time slot based upon these criteria in the network. At each time slot the selected anchor sensor may be inadequate for all the functions required in the application- composition, therefore, more sensors are required to be active at the same time (time slot) to satisfy the requirements of the application. We can refer to this process as "Building the Composition Matrix, CM, of the application".

$$CM = r_1 \cup r_2 \cup ..... \cup r_{n-1} \cup r_n \,, \tag{7.13}$$

where;

CM : Composition Matrix of the Application

r_n: Sensors in the WSN

Building this matrix involves activating more sensors until the Composing Matrix satisfies or exceeds the requirements of the application.

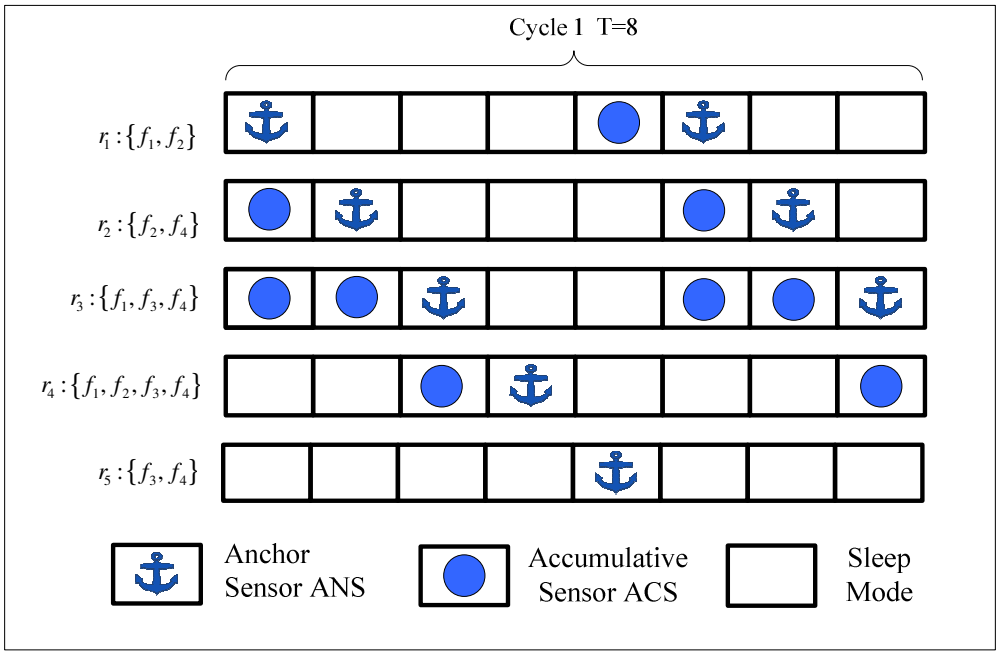

Figure 7.8: RASSA Example

However, in doing this, we may have set too many sensors in active mode because we have ignored the fact that each active sensor can perform multiple functions. As a result, there may be more active sensors providing the same function than needed. Figure 7.8 shows an example for a sleep schedule generated by the RASSA algorithm. In this example, suppose that function f_1 is required only once ($f_1 = 1$), after selecting r_1 to be the anchor sensor, the application Composition Matrix has only two functions $CM = \{f_1, f_2\}$, and therefore it is missing two more functions (f_3, f_4) to complete the application-composition requirements. In this case the schedule activates r_2 to add more functions to the CM. After r_2 is added, the Composition Matrix becomes $CM = \{f_1, f_2, f_4\}$. Obviously, CM is still not complete as it does not contain f_3 and therefore additional sensors are yet needed to complete the function composition matrix. After adding r_2 the Composition Matrix is $\{f_1, f_2, f_3, f_4\}$. Therefore, the CM is completed and satisfies the requirements of the application. It is obvious, that sensor r_2 could be skipped and only two sensors r_1 and r_3 could be selected to satisfy the application Compositor Matrix. We refer to the unnecessary selection of the additional sensor as the relative Error (E_o) in the sleep schedule. This is the error of RASSA when it is generating an optimized schedule in comparison to the schedule generated by a benchmark optimized solution.

To improve the algorithm's behavior and to reduce the relative error(E_o), further modification can be added to the algorithm. A history matrix could be created to analyze all the possible combinations of additional accumulative sensors after the anchor sensor. The best solution can then be selected for the minimum number of active sensors per time slot. However it is demonstrated in the simulation and performance analyses, that the relative error (E_o) might be an acceptable and tolerated trade-off to achieve faster schedule generations. The process of generating a sleep schedule by RASSA is demonstrated in the flowchart of Figure 7.9.

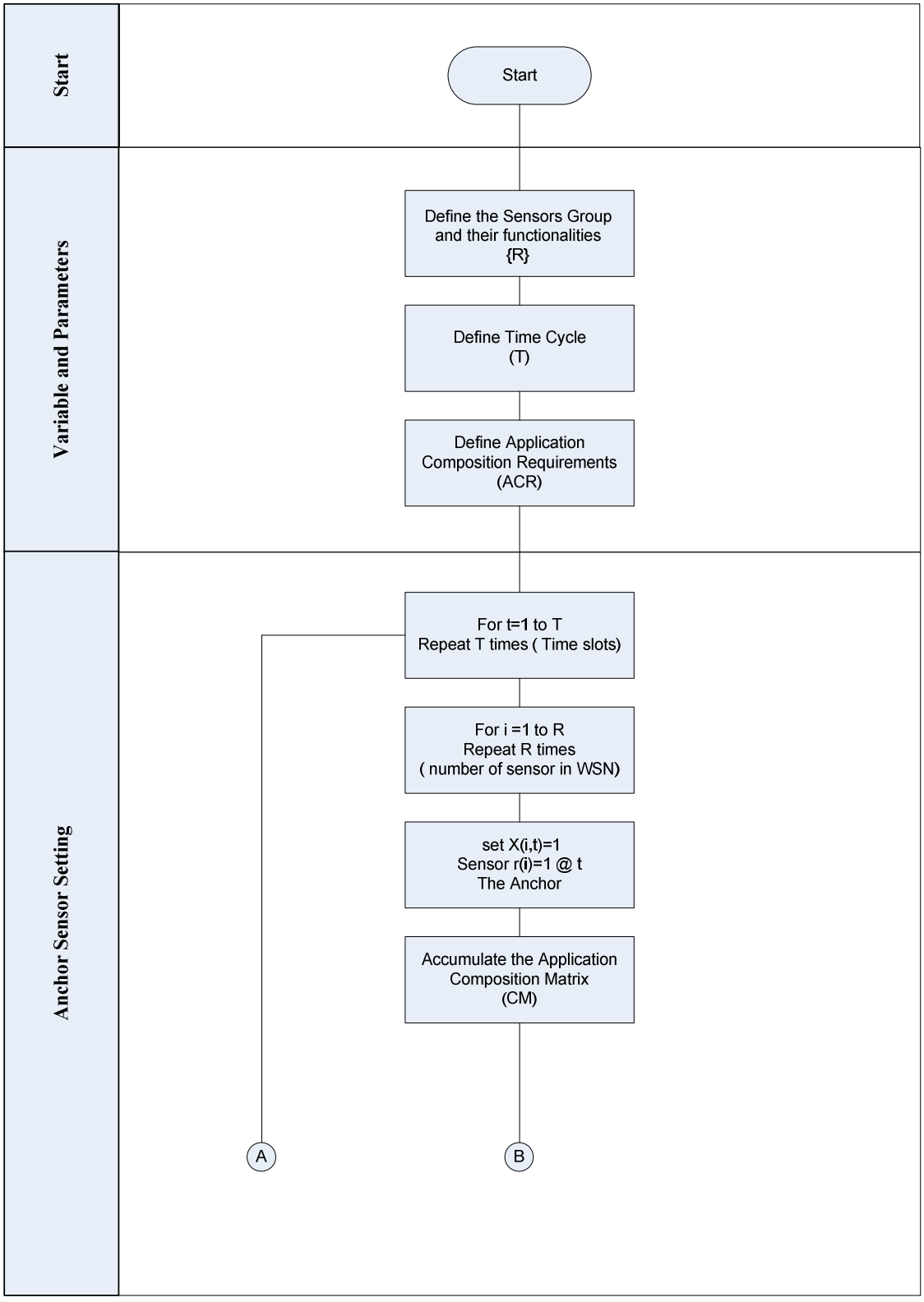

Figure 7.9 : RASSA Flowchart
Section A

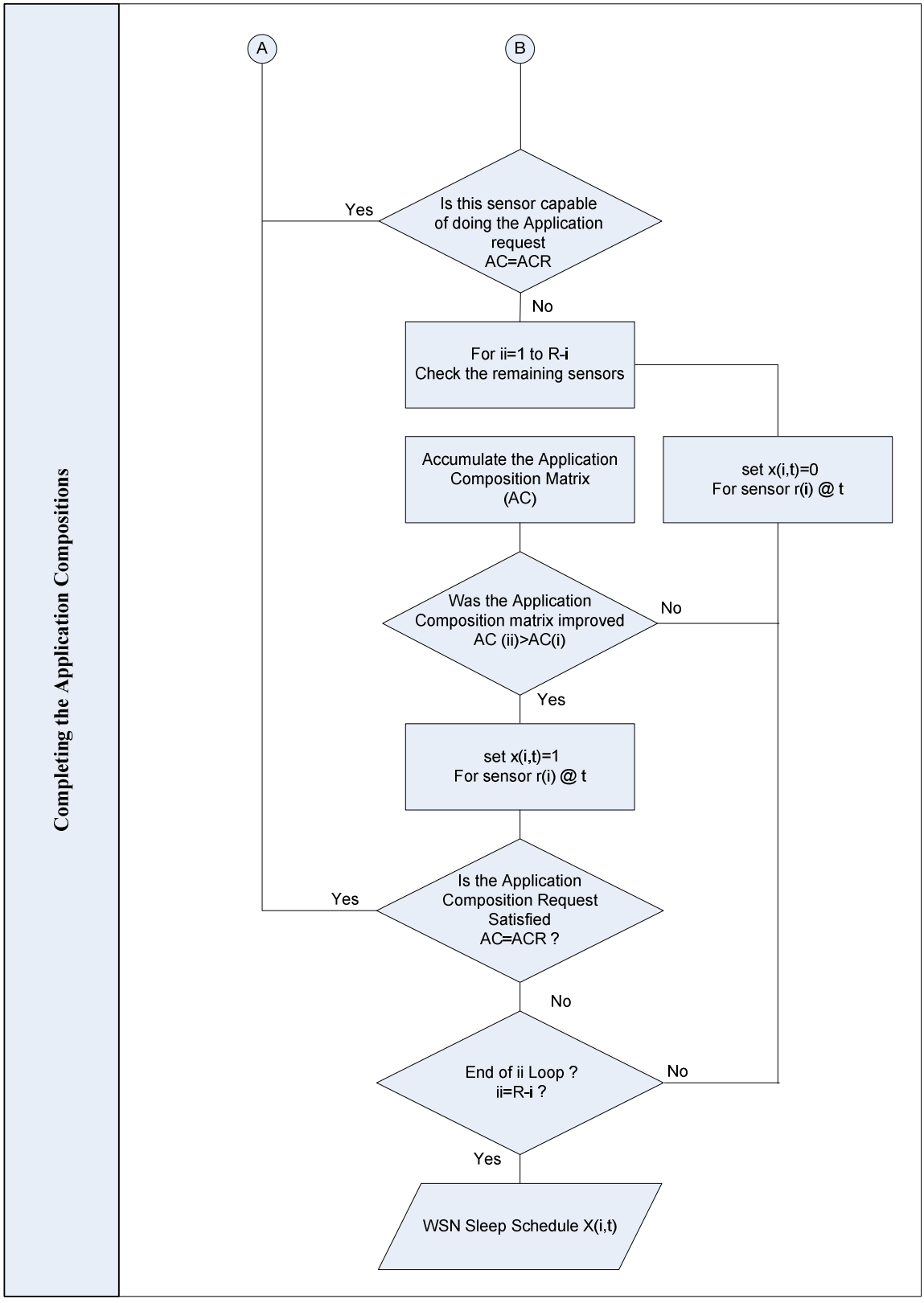

Figure 7.9: RASSA Flowchart
Section B

7.6.2 Power-Up Energy Consumption Minimizations

In the second stage of our optimization, RASSA algorithm is improved to include ordering technique to find an optimized order of the schedule and reduce the wasted power consumed when the sensors switch from sleep mode to active mode (wake-up power consumption). In the first stage, we have assumed that the energy consumed by the sensor when it is in the active mode for one time slot is one unit. In the second stage we assume the normalized power-up energy consumption E_{up} is the ratio of the actual energy consumed by the sensor to switch from the sleep mode to the active mode to that when the sensor is in the active mode (i.e. $E_{up} = E_w/E_{ac}$). Therefore, the total energy consumed by each sensor for a full time cycle, T, is the sum of the number of active time slots and the total power-up energy consumption.

$$E_k = \sum_{t=1}^{T} x(k,t) + E_{up} \cdot y(k,t), \tag{7.14}$$

$$x_{k,t} = \begin{cases} 1 & \text{When } r_k \text{ is active at time slot } t \\ 0 & \text{When } r_k \text{ is asleep at time slot } t \end{cases}, \tag{7.15}$$

$$y_{k,t} = \begin{cases} 1 & \text{When } x_{k,t} < x_{k,t+1} \\ 0 & \text{Otherwise} \end{cases}, \tag{7.16}$$

where;

E_k: The total energy consumed by the sensor r_k for a complete time-cycle, T. (normalized unit energy)

E_{up}: The normalized Power-Up energy consumed by the sensor when switching from sleep to active mode,

x: Binary variable referring to the sensor mode being active or asleep,

y: Binary variable referring to the mode of the sensor transition between two time slots.

Our objective is to minimize the maximum energy consumption among all sensors in a full time-cycle, T. We assume that the energy consumption for each active time slot is much larger than one power-up energy consumption, i.e. $E_{up} \ll 1$. For this reason, the objective of minimizing

E_{UP} is considered secondary in importance with respect to the first objective of minimizing the load of sensors by reducing the number of active time slots per full time-cycle, T.

In this stage, we will reorder the schedule generated in the first stage to reduce the power-up energy. We refer to this stage as the Sleep Scheduled Ordering Algorithm. Our algorithm will process the schedule as shown in the flowchart of Figure 7.10. Nevertheless, the ordering can be easily obtained by evaluating all the combinations of the schedule column and then selecting the best combination that gives the minimized power-up energy consumption. However, this technique is very time consuming. To calculate all the rows' combinations of the sleep schedule matrix, it requires calculating the factorial of the number under the column in the matrix. For example, if we have 64 time-slots in the sleep schedule, it takes ($64! = 1.26886932\ X\ 10^{89}$) trials. This number of trials requires excessive computing time; therefore, a faster approximated technique is required.

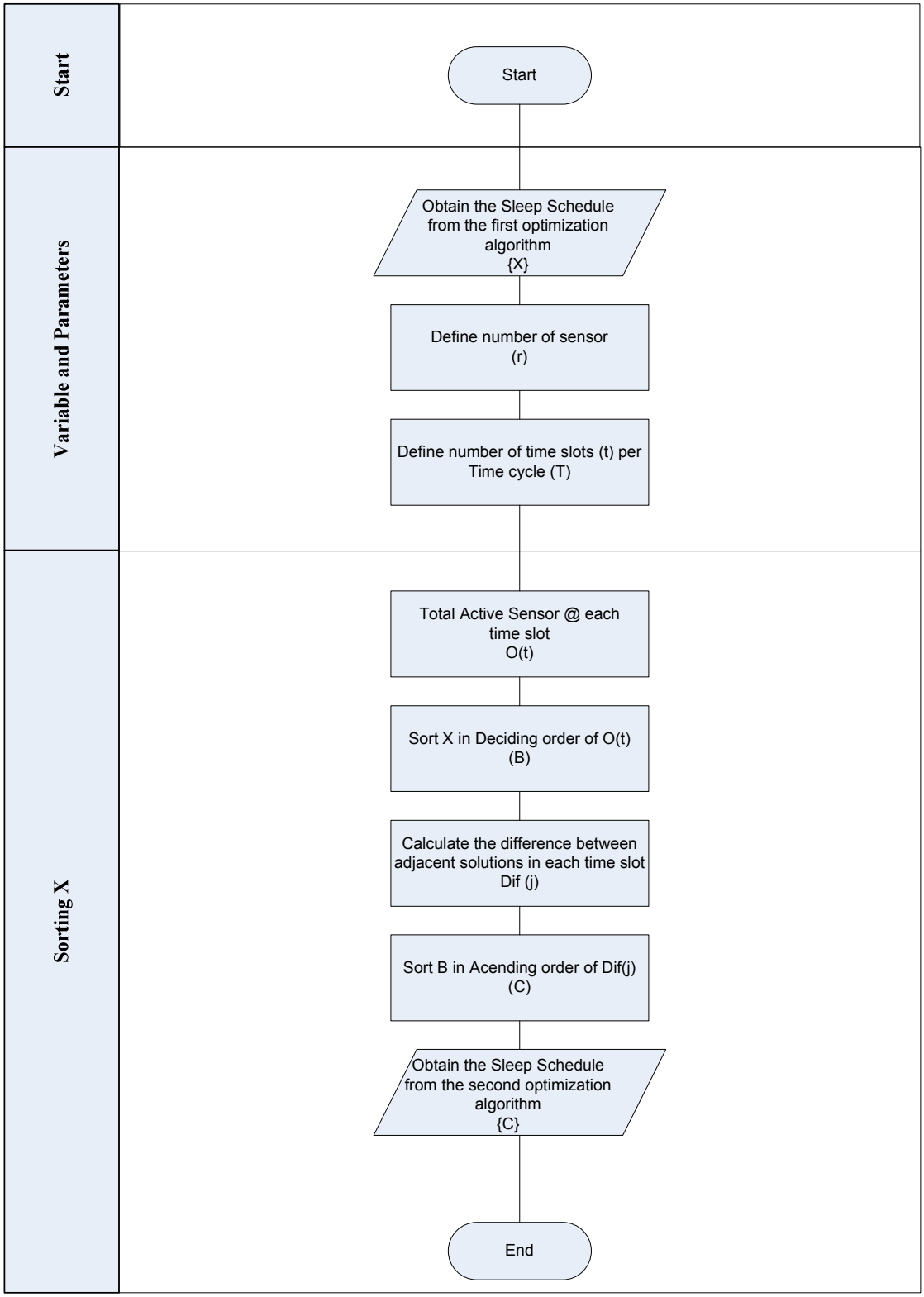

Figure 7.10: Sleep Schedule Ordering Algorithm

Our sleep schedule ordering algorithm is based on two stages, the first is to perform preliminary ordering routine on the optimized sleep schedule generated by the Resources-Aware Sleep Schedule Algorithm (RASSA) in the first stage. We first count the number of ones in each column and sort the sleep schedule [X] in descending order. The result of the preliminary ordering routine is a new matrix [B]. The position of columns in [X] is swapped to produce [B] as a preliminary ordered matrix in descending order with respect to the number of ones per column. In the second stage of the ordering algorithm, we try to organize [B] in a way that similar columns is next to each other. We calculate the differences between each adjacent column in matrix [B] and sort the matrix in an ascending order with respect to the differences between the adjacent columns. The result of the second stage of ordering algorithm will be a new matrix [C] that is optimized to have less frequent transitional switching from zeros to ones. Figure 7.11 shows an example of sorting a sleep schedule to produce an optimized minimum number of switching from sleep mode to active mode for each sensor in the network.

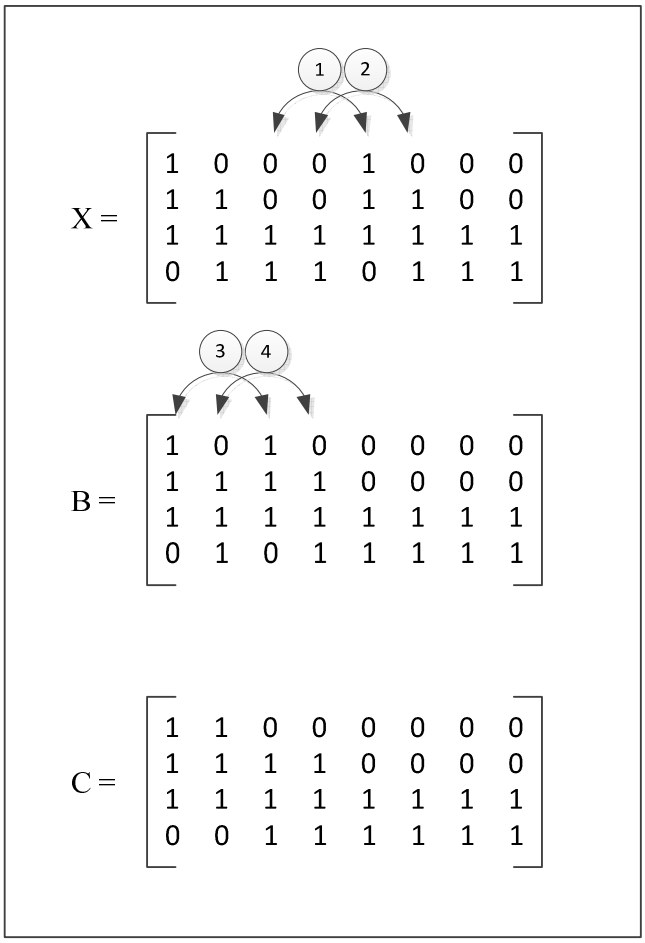

Figure 7.11: Sleep schedule ordering technique

In the example of Figure 7-11, [X] is the sleep schedule obtained at the first stage of the optimization. As a first step, [X] is primarily sorted in a descending order with respect to the number of ones in each column. Therefore, in step #1 the third and fifth column are swapped together. In step #2 columns number 4 and 6 will be swapped together. At the end of the preliminary sorting, matrix [B] is compiled in a descending order with respect to the number of ones in each column. In the second stage of the ordering algorithm [C] is produced by ordering [B] with respect to the similarities between adjust columns in [B]. Matrix [C] is the optimized and ordered solution for the WSN sleep schedule.

7.7 AIMMS Optimization Software

It is required to establish benchmarks that can be used to compare the results of our optimization as per the Resources-Aware Sleep Schedule Algorithm (RASSA). The AIMMS is used to generate an optimization sleep schedule that satisfies the requirements of the application composition of the WSN. AIMMS is advanced optimization software for building operations research applications and advanced planning systems for decision support.

AIMMS supports a good number of algorithms and solvers that can be manually or automatically selected by the software to generate the best optimized results. Figure 7.12 shows the Page Manager for an optimized sleep schedule for a case of WSN with 4 sensors scheduled in eight time-slots.

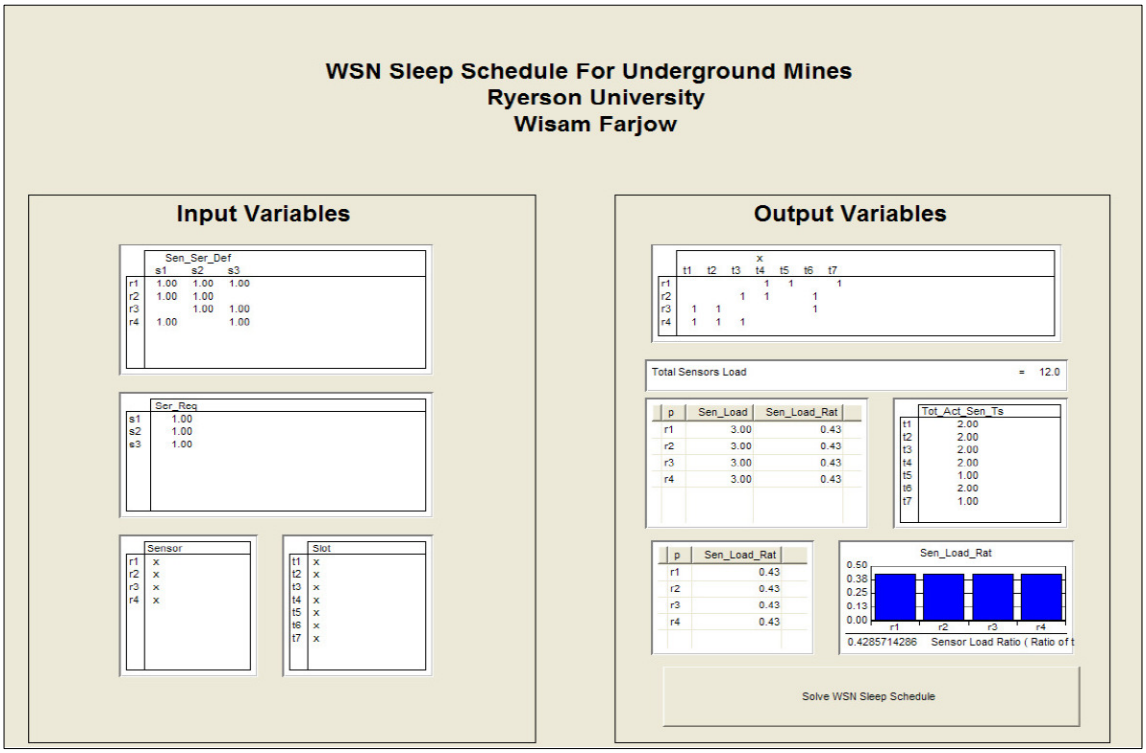

Figure 7.12: AIMMS Optimized sleep schedule

7.8 Simulation results

7.8.1 Schedule Generation

In this Section, simulation results are presented for the developed Resources-Aware Algorithm. The generated schedule guarantees the availability of adequate number of active sensors in the cluster of the WSN where the application composition is required. The first stage of the algorithm is concerned with generating a sleep schedule that is optimized for a minimum number of active sensors while satisfying the applications-compositions requirements.

We start by defining a two dimensional matrix, which identifies the profile of the available sensors in the WSN cluster and the function each sensor can provide. The algorithm is required to compose the application by utilizing this profile. In this simulation we have assumed a WSN cluster made of four sensors capable in providing certain functions. The four sensors in the given profile can perform $\{f_1\}$, $\{f_2, f_3\}$, $\{f_1, f_2, f_3\}$, and $\{f_1, f_3\}$, respectively. The WSN sensor profile is shown in Table 7.1.

	f_1	f_2	f_3
r_1	1	0	0
r_2	0	1	1
r_3	1	1	1
r_4	1	0	1

Table 7.1: WSN senses profile

In the simulation we assumed the length of a complete Time-cycle $T = 4$. (i.e. there are four time slots, t_s, in each time-cycle). We also have assumed that the application composition requires at least one function of each type to be available at any given time. In other words, the application requires at least one of each type of the functions (f_1, f_2 and f_3) at each time slot during T.

Figure 7.13 shows the sleep schedule generated by the algorithm with cycle length T = 4. Under this sleep schedule, r_1 needs to be active in one time slot of a cycle, r_2 needs to be active in three separate time slots of a cycle, r_3 needs to be active in two consecutive time slots of a cycle, and r_4 needs to be active in one time slot of a cycle. This schedule guarantees continuous availability for all the services required by the application composition.

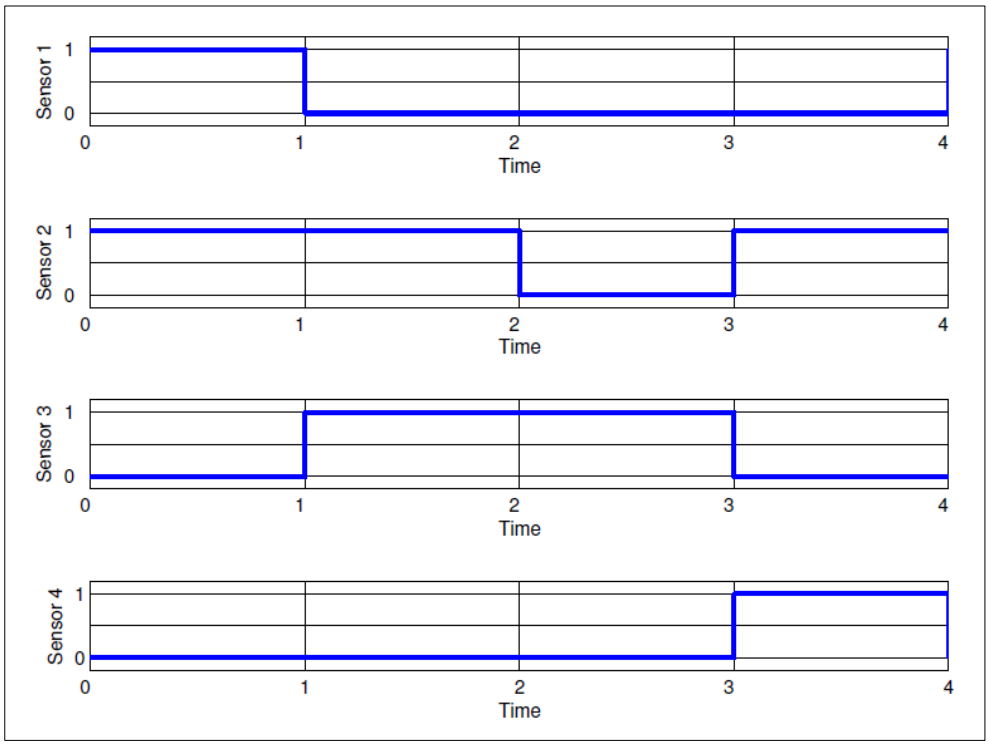

Figure 7.13: RASSA optimized sleep schedule

7.8.2 Algorithm Performance

In this Section we compare the simulation results generated by our algorithm, RASSA, with the results obtained from the AIMMS optimization software. The result obtained from the AIMMS establishes a benchmark that can be utilized to compare the performance of our algorithm outcomes. In these analyses, the AIMMS was configured to automatically select the best algorithm among number of available algorithms within the AIMMS portfolio. That way we could consider the results generated by the AIMMS as the most optimized schedule results for the WSN. In these comparison analyses, we calculated the Average Relative Error (E_{ave}) by comparing the WSN schedule as generated by the AIMMS optimizer and our RASSA Sleep Schedule Algorithm. The Average Relative Error (E_{ave}) can be calculated as follows:

$$E_{ave} = (1 - \frac{L_{AIMMS}}{L_{RASSA}}) \cdot 100\% \,, \tag{7.17}$$

where;

E_{ave}: Average relative error of the RASSA algorithm,
L_{AIMMS} : Sensor's load optimized by AIMMS, and
L_{RASSA} : Sensor's load optimized by ARASSA.

In the simulation the number of time slots, t_s, per time cycle, T , were varied from $T = 4$ to 64 time slots. The loads of the wireless sensors in the WSN were calculated for each time-cycle T. These simulations were repeated for three sizes of WSN clusters ($R = 10, 20\ and\ 30$) sensors. The results of average relative error analyses are listed in Table 7.2.

T	E% (R=10)	E% (R=20)	E% (R=30)
4	0.052	0.105	0.156
8	0.044	0.085	0.113
16	0.038	0.062	0.080
32	0.031	0.042	0.055
64	0.027	0.036	0.046

Table 7.2: Average Relative Error analyses.

It is not expected for the size of the WSN to be more than 30 sensors per a cluster in the mine. Therefore, we have focused our analyses in these sizes of WSN. Also the length of the time cycle is not expected to exceed 64 time slots per cycle. Otherwise, excessive time cycles do not lend themselves to adaptive schedules.

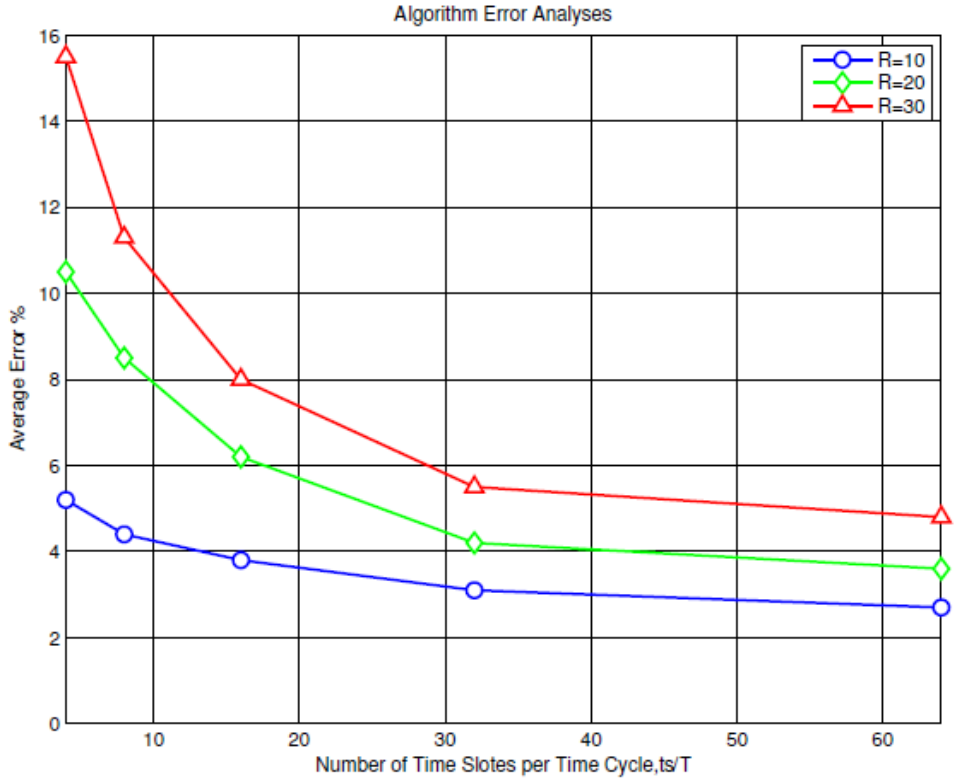

Figure 7.14: Average Relative Error analyses

It is obvious from Figure 7.14, that the Average Relative Error decreases when the number of time slots, t_s, increases. When T is small, the optimal solution is also small. Thus, a small difference leads to a large relative error. For example, when we have 30 sensors in the WSN (R=30) and T = 4, the optimal solution from AIMMS may be 5 and the solution from our RASSA maybe 6. In such a case, one active time slot difference in the RASSA solution leads to a relative error of 16.67 % when compared with the AIMMS optimized solutions. For higher value of T such as when $T = 64$, the optimal solution may be 14 active time slots for each sensor in the WSN and the solution from our RASSA algorithm maybe 15 active sensors. In such a case, one active time slot difference in the RASSA solution leads to a relative error of 6.67 % when compared with the AIMMS optimized solutions.

It is also obvious that the Average Relative Errors increase with the number of sensors R. With the increase of the number of sensors in the WSN, there is higher possibility of making a mistake when deciding on activating or waking up anchor sensors regardless of its effectiveness in the schedule in terms of its suitability to be selected at that time slot to conduct an optimized number of functions Thus, the relative error increases with the increase of R.

7.8.3 Individual Sensor Load vs. T

As was proven in the previous Section, the average load (L_s) of the sensors is the total energy consumed by the sensor r_k for the entire length of the time-cycle, T:

$$L_S = \theta_k = E_{ac} \sum_{t=1}^{T} x_{k,t} \, . \tag{7.18}$$

To simplify the calculations, E_{ac} is normalized to one energy unit. In our analyses, we have simulated the effect of the sleep schedule on reducing the sensor load to an optimized minimum value. This optimization is achieved with the constraint of guaranteeing enough active sensors to satisfy the application composition requirements. Therefore;

$$\sum_{k} x_{k,t} \geq AC \quad \text{for all } t, \tag{7.19}$$

where;

L_s: The total energy consumed by the sensor r_k for being active for a number of time slots for a complete time-cycle, T. It is also can be referred to as the load of the sensor,

E_{ac}: Energy consumed by the sensor during one time slot,

AC: Application-composition.

The simulation was repeated for different lengths of the time-cycle, T. We have analysed the effect of increasing the number of sensors in the WSN on minimizing the sensor load and therefore the power consumption of the sensor. The numbers of sensors were increased from 1 to 30 sensors for the cases of $T = 4, 8, 16 \text{ and } 32$. The simulation showed that the loads of the sensors decreased when increasing the number of sensors. This is because a larger number of sensors means that the sensors need to work less (i.e. fewer active time slots for a complete time-

cycle) . In this simulation it was assumed that the three functions are required to complete the application $= \{f_1, f_2, f_3\}$. It is also assumed that one of each type of the three functions is required all the time (every time slot) $\{f_1 = 1,\ f_2 = 1,\ f_3 = 1\}$. Figure 7.15 shows the simulation results of Average Sensor Load when varying the number of sensors.

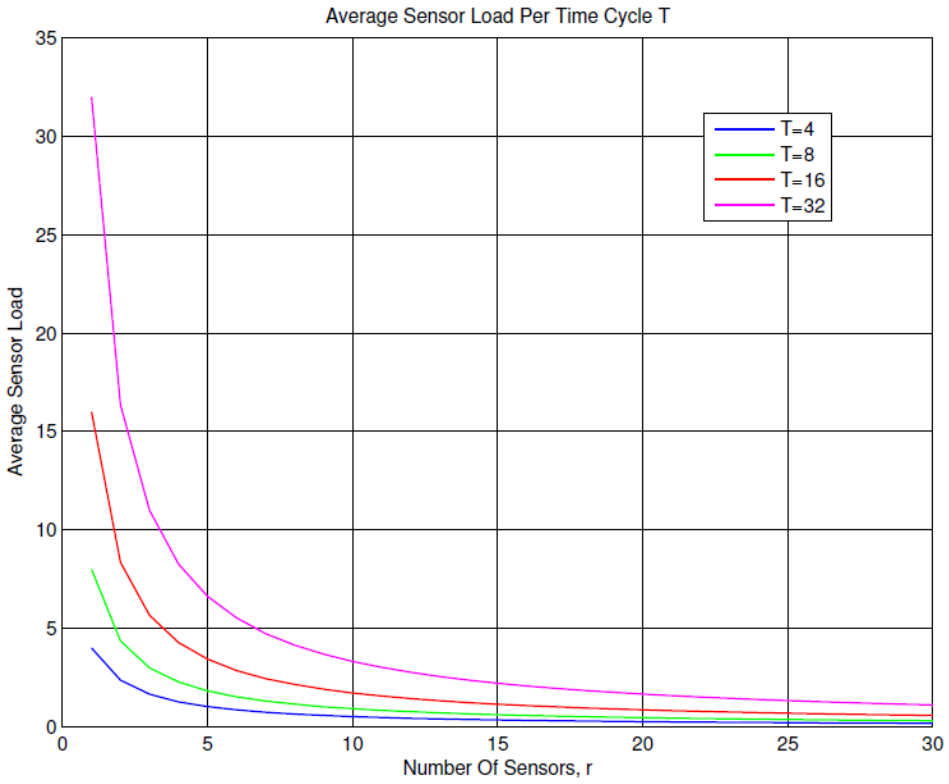

Figure 7.15: Average sensors load for different WSN sizes

7.8.4 Effect of increasing the Number of Services

It might be necessary to have more than one service or function (of the same type) available at every time slot. It is also possible that the WSN has more than one application running at the same time, thus requiring more than one applications-composition. This is the case when the WSN is performing more than one application simultaneously. When applications like localizations, ventilation on demand and environmental monitoring are all required at the same time, we have to guarantee enough services and resources to provide the three applications. This means more sensors that are capable of providing the same function must be active at the same time.

To simulate the effect of increasing the number of required functions or services at each time slot, we have analyzed the effect of increasing the number of functions per time slot on the average sensor load. We have assumed that there are three types of functions that are required by any Application Composition. $F = \{f_1, f_2, f_3\}$. In the simulation we have increased the number of these individual functions from $1\ to\ 5$ $\{f_1 = 1\ to\ 5,\ f_2 = 1\ to\ 5,\ f_3 = 1\ to\ 5\}$.

When the number of required services increases, the average sensor load also increases. This is because more sensors are required in the active mode to accommodate the requirements of the applications-compositions. Therefore the power consumption increases for each sensor in the WSN.

Figure 7.16, shows the simulation analyses for a WSN with 30 sensors. The simulation was repeated for $T = 4,\ 8$ and 16 time slots. It is obvious that the average sensor load increases when increasing the number of the functions required in the application-composition.

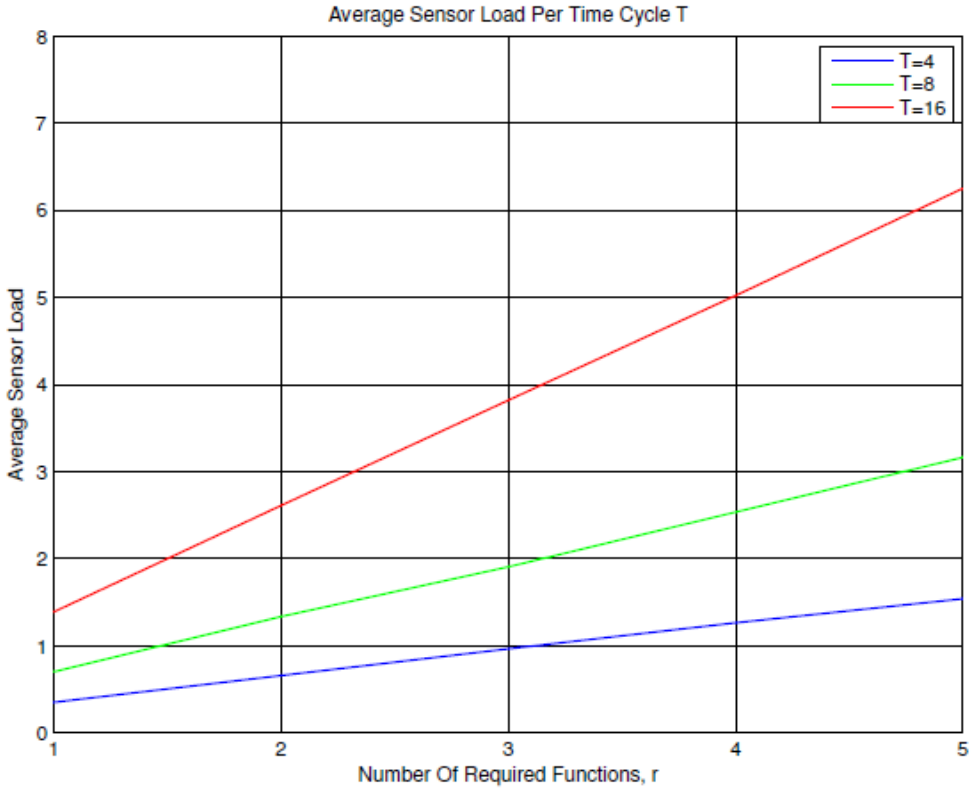

Figure 7.16: Average sensors load and number of required functions analyses

7.8.5 RASSA Ordering Improvement

The sleep schedule generated by our algorithm, RASSA, can be improved by ordering the columns of the schedule to an optimized order that minimizes the power-up energy consumed by the sensor. Figure 7.17, shows the simulation result for the ordering algorithm when applied to a cluster of four sensors with an application-composition of three functions that requires one of each function at each time slot.

In this example, it was observed that the frequency of switching from the sleep mode to the active mode in first sensor, r_1 , was reduced from three times to only once. Therefore, the power-up energy was reduced by an order of three times. The power-up energy consumption is reduced by an order of two for the second sensor, r_2 , as the frequency of switching from the sleep to the active mode was reduced from two times in the unordered sleep schedule to only one time in the sleep schedule after applying the ordering algorithm.

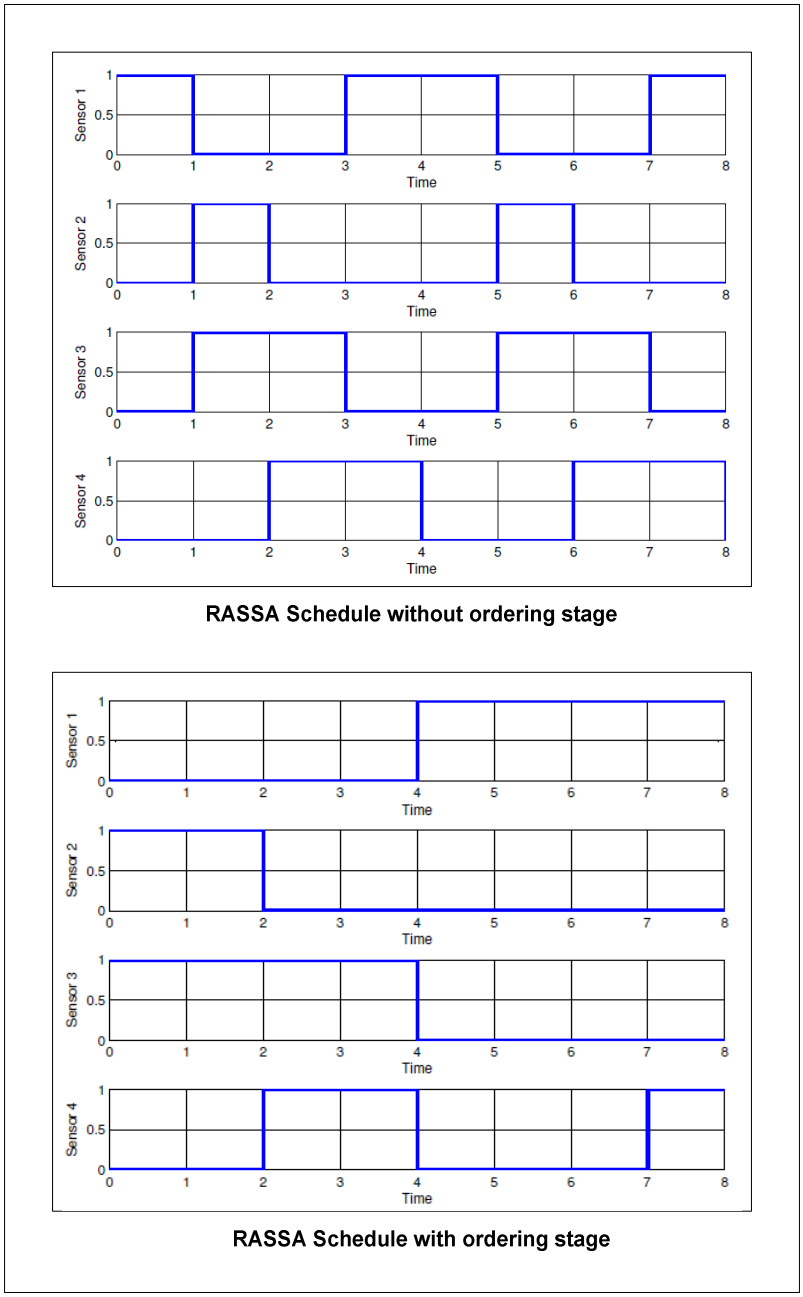

Figure 7.17: RASSA improved ordering algorithm

The same for the third sensor, r_3, as the frequency of switching to the active mode was reduced from two times to only one time in the ordered sleep schedule. The fourth sensor, r_4, however, did not enjoy any further power saving as the power-up energy (E_{up}) in the ordered sleep schedule remained the same as that in the unordered schedule.

As mentioned earlier, our objective here is to optimize the power-up energy consumption of the sensors by reducing the frequency of switching from the sleep to active mode. The power-up consumption energy is relatively small in comparison with the power consumed by the sensor when it is in active mode. However, in such case when the length of a time-slot is short, E_{up} could be relatively large with respect to the actual energy consumption for a full time slot. Therefore, it is important to consider the power-up energy consumption and merge active time slots as much as possible to reduce E_{up} and therefore, increase the life of the sensor.

The performance of the ordering algorithm on a cluster of four sensors was simulated as shown in Figure 7.18. In this simulation, the application-composition required three functions. One type of each function must be available all the time (every time slot). In the simulation we have analyzed the effects of the ordering algorithm on reducing the power-up energy consumption of the sensors. It has been observed that the power-up energy increases linearly with increasing the number of time slots. However, the increase in the power-up consumption is much less when applying the ordering algorithm.

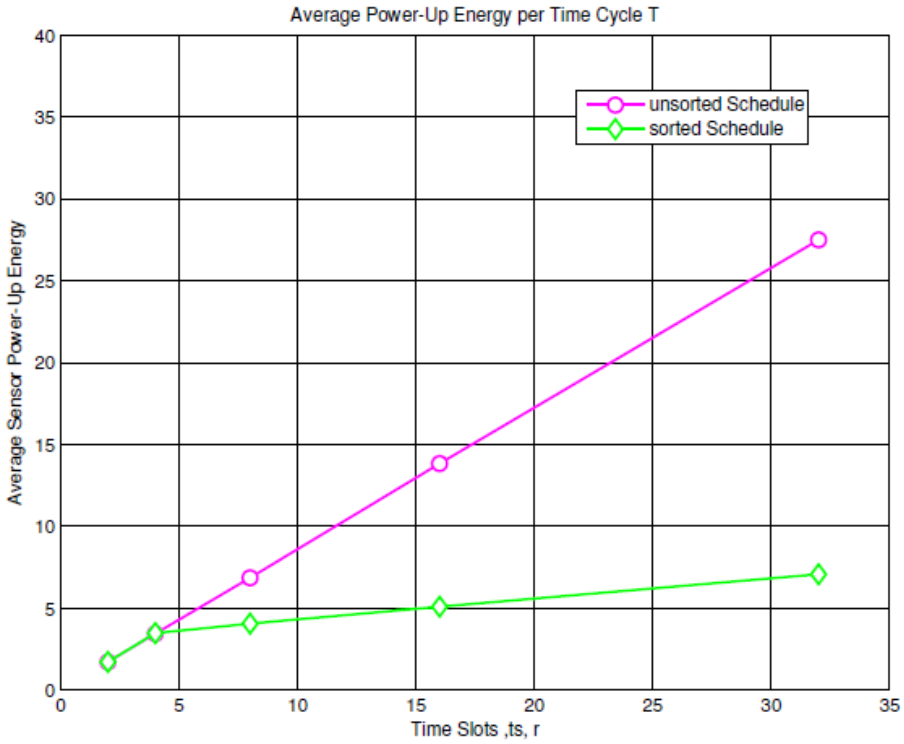

Figure 7.18: Ordering algorithm simulations

7.8.6 Effects of K factors

For further power saving and longer network life the Resources-Aware Sleep Schedule can be further improved. The sensors in the underground WSN have the intelligence to adaptively modify their transmission power to an optimized minimum level. Nonetheless, the sensors still need to maintain acceptable link performance (i.e. minimum BER). The wireless channel model (Mine Segmenting Wireless Channels Model) that was developed in Chapter 6 is used by the sleep schedule algorithm to provide additional power saving. The sensors in the network will know their wireless channel characteristics (i.e. which performance curve they belong to at any given time). Figure 7.19 shows the simulation results for different wireless channel conditions (i.e. different K factors). For each K factor (or curve) we can relate the performance of the link measured in BER to the SNR. Moving up and down on a specific curve, the sensors in the WSN are able to adjust their transmission power and SNR to arrive at the target BER of acceptable performance. Therefore, the sensors are not required to transmit at full power during the active time slot of the sleep schedule.

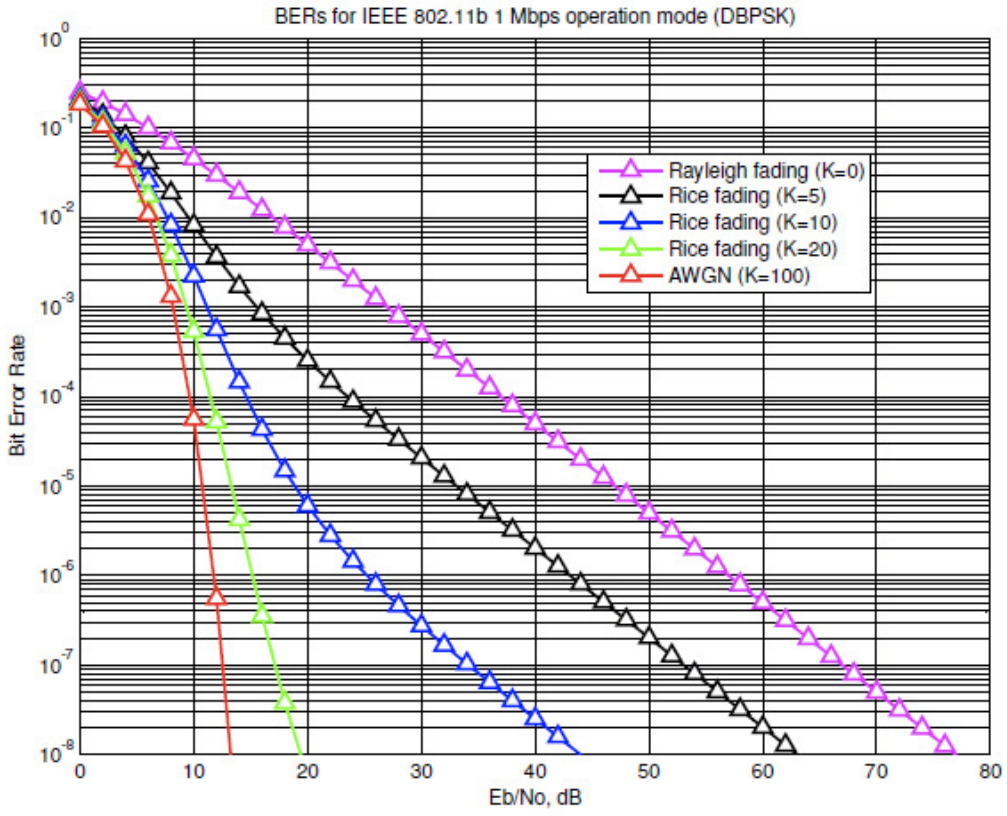

Figure 7.19: Wireless channels characteristics in confined areas

Typically, the sensor's transmitter can transmit RF level at different values. The power consumed by the RF transmitter is the most dominant source for power consumption in the sensors. Table 7.3 shows typical sensor's power consumption for different RF levels of transmission. In this analysis we have used a Wi-Fi based sensor, SenSiFi™ 802.11b Wi-Fi® Sensor from Redpine Signal. The same principles can be applied to any other type of sensors such as Zigbee sensors. The amount of power shown on the table represents the total amount of power consumed by the sensors when in active mode of the schedule.

RF Power	Current (mA) @	Power %
10 dBm	18	100%
5 dBm	14	78%
0 dBm	9	50%
-5 dBm	7	39%
-10 dBm	5	28%

Table 7.3: Sensors power consumption table

In mine environments the sensors are able to estimate their channel's characteristics or more precisely their performance curves. The sensors can then adjust the transmitted power to a minimized optimum value that guarantees the required BER of the wireless links. As per our developed "Mine Segmenting Wireless Channel Model" the confined areas within the mine are divided into a number of segments with different channel characteristics. The model is based on a statistical combination of different distribution functions related to the type of channel fading conditions. Figure 7.20 shows an example for an area in a mine divided into three segments. Each segment has different fading channel distribution function and, therefore, has a K factor that can be mapped to a performance curve. Once the proper curve is determined by the sensors, it is possible for the sensor to estimate its wireless channels characteristics and, therefore, obtain the required SNR that guarantees certain link performance in terms of BER. In the example, the fading channels of the three areas changes from LOS with Rayleigh fading channel and high K factor ($K > 20$) to PLOS with Rician channel and $K = 10$ and then to NLOS with a low value of K factor $K = 4$.

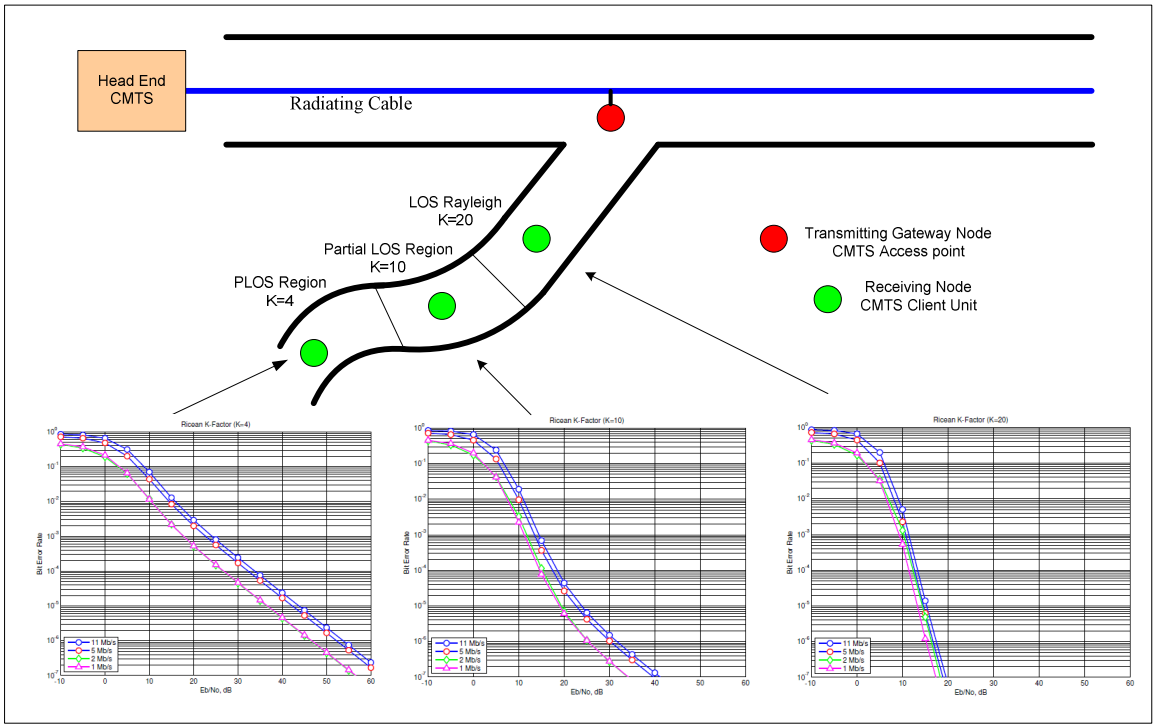

Figure 7.20: Typical mine layout

Figure 7.19 shows the simulation results for Wi-Fi Based sensors communicating over DBPSK modulated link with data speed of 1 Mbps. It is obvious that when operating in higher values of K (i.e. closer to the LOS condition) it is much easier with lower SNR to obtain acceptable BER performance value. For example, assuming the BER requirement for the wireless link is $BER \geq 10^{-6}$, it requires the sensors to have SNR= 12 dB to achieve the required BER. However, a higher SNR is required to achieve the same BER if the sensors are in areas of lower K factors. This, of course, requires higher RF transmission power and therefore higher DC power consumption and shorter network life in comparison to operating in areas of higher K factors.

Figure 7.21 shows the simulation results of sensors transmitting at a different percentage of RF power level. This simulation mimics the scenarios when the sensors in the WSN are aware of their wireless channel (K factor). In these analyses, the numbers of sensors were increased from 1 to 30 sensors to simulate the effect of different network scale on the average power consumed by a sensor in the mine. It is obvious that the average power consumed by each sensor decreases when increasing the number of sensors in the WSN. The sensors are expected to work less (fewer

active time slots) when the total number of sensors in the WSN is bigger since the tasks of the application-consumption are shared with a larger number of sensors.

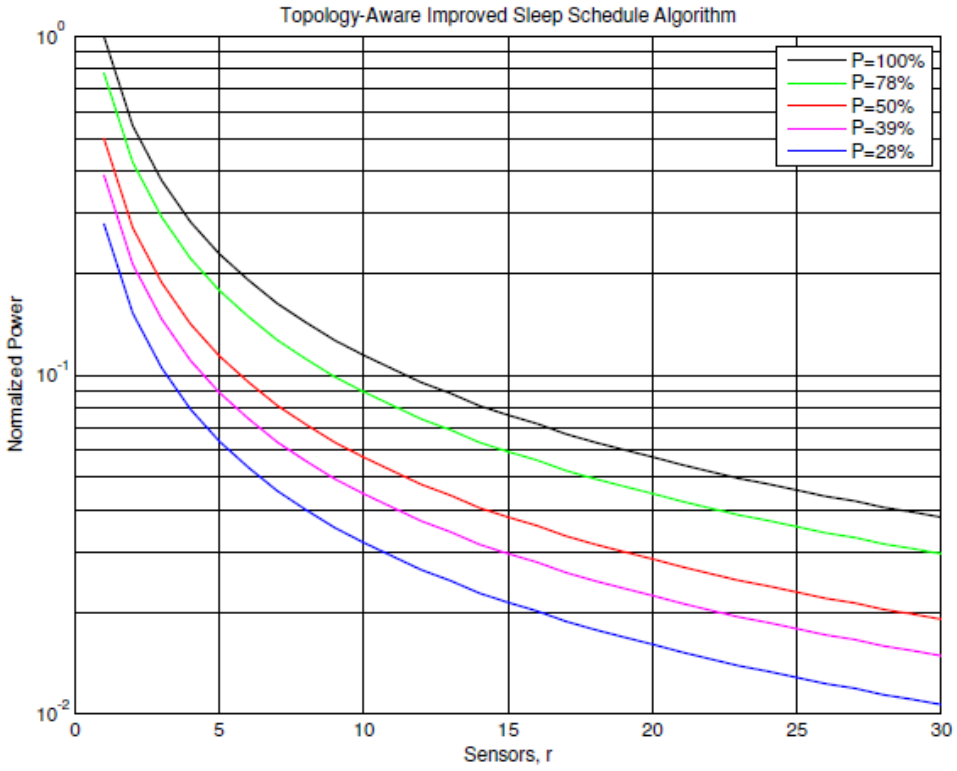

Figure 7.21: Role of K factor in improving the network power consumption

7.9 Analyzing Algorithm's Impact on Sensors' Batteries Life.

Prolonging battery life is a principal objective in the design of wireless sensor networks due to the difficulty and high cost associated with replacing or recharging exhausted batteries in a deployed network. This has, in large part, driven the research and development of numerous technologies that aim at minimizing WSN energy consumption. However, for many electronic systems the battery life is a function not only of the energy consumed by the system, but also of the manner in which the system drains the battery. Recently, this observation has led to research in the area of "battery-driven" system design, which encompasses a set of technologies that aim at exploiting battery characteristics in order to achieve lifetime extensions beyond what can be achieved through low-power or energy-efficient design alone.

7.9.1 Typical Model Discharge Curve

The standard or rated capacity of a battery (usually expressed in current-time units, e.g. mAh) is a measure of the total charge that can be extracted from a battery when discharged under standard load conditions. Manufacturers may specify the current rating, as a constant discharge rate that corresponds to the standard load conditions. For example, a battery may be rated at 500 mAh capacity under a rated current of 100 mA, at 25°C. The delivered capacity of a battery is the capacity that the battery supplies under a given load and operating environment. A typical discharge curve of Li-Ion battery is shown in Figure 7.22. The model shows the battery discharge curve made of three regions. These are the exponential region, nominal region and the cut-off region. The operational regain of the battery starts from the beginning of the exponential region till the end of the nominal region of the discharge curve. The battery voltage is given by [65]:

$$V_{batt} = E_o - K\frac{Q}{Q-it}\cdot it - R\cdot i + A\exp(-B\cdot it) - K\frac{Q}{Q-it}\cdot i^* , \tag{7.20}$$

where;

V_{batt} = Battery voltage (V)

E_o = Battery constant voltage (V)

K = polarisation constant (V/Ah) or polarisation resistance (Ω)

Q = battery capacity (Ah)

$it = \int idt$ = $actual\ battery\ charge\ (Ah)$

A = $exponential\ zone\ amplitude\ (V)$

B = $exponential\ zone\ time\ constant\ inverse\ (Ah)^{-1}$

R = $internal\ resistance\ (\Omega)$

i = $battery\ current\ (A)$

i^* = $filtered\ current\ (A)$

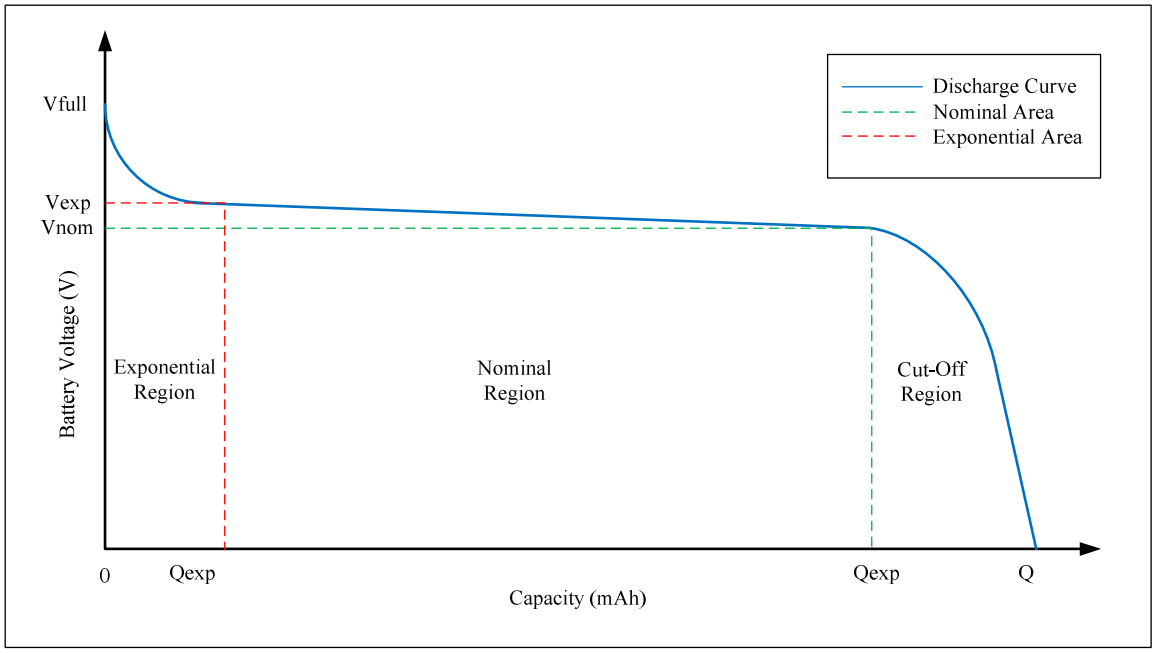

Figure 7.22: Typical discharge curve of Li-Ion battery

We consider Lithium-Ion batteries because they are commonly used within the domain of portable electronics, including sensor networks. Table 7.4 shows the most common battery parameters for the Li-Ion battery used in our analyses.

Parameters	Li-Ion 3.7V 2.8Ah
$E_o(V)$	3.7
$R(\Omega)$	0.01
$\mathrm{K}\left(\text{ or } \mathrm{V} = (\mathrm{Ah})\right)$	0.0076
A (V)	0.26422
$B\ (Ah)^{-1}$	26.5487

Table 7.4: Battery parameters table

As shown in Figure 7.23, a simple numeric model can be generated by dividing the discharge curve into two phases: normal operation and post-cut-off [66]. The title “normal operation” is given to the slightly decreasing slope. Post-cut-off describes the region just before the battery is empty.

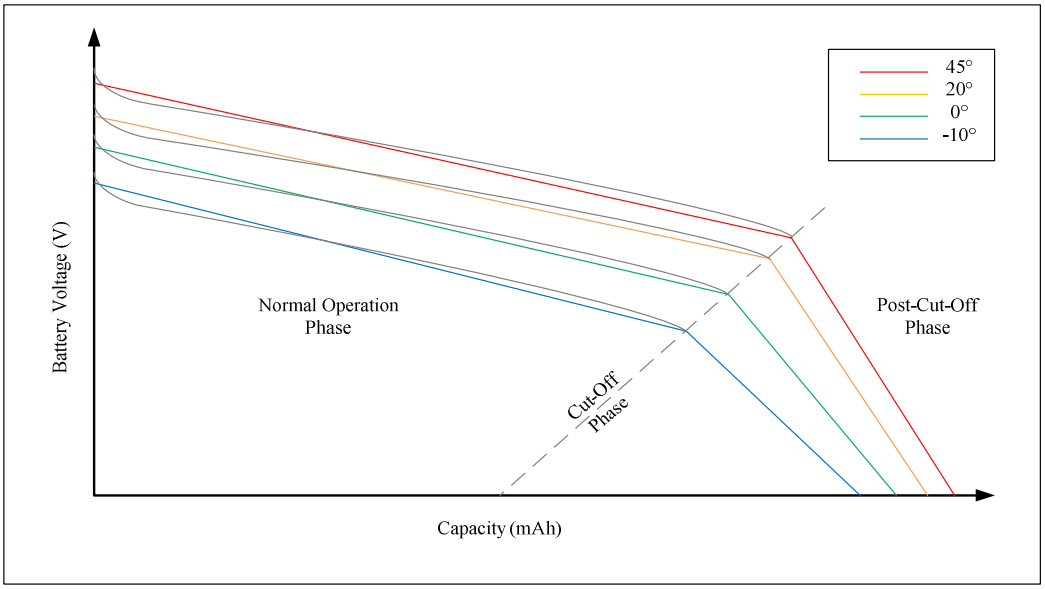

Figure 7.23: Approximated discharge characteristics with varying temperature

7.9.2 Sleep Seclude Simulations Impact on Battery Life

To demonstrate the effects of various operation parameters on the battery life we have simulated different cases of sensors operations. When the sensors were operating full time with no sleep schedule to optimize their power consumption, we could operate the sensors for only 5.5 days of continuous operation from a single battery charge. The average sensor's life increased significantly to 23.9 days when we applied our RASS algorithm for a cluster of 30 sensors operating at T=30 time slots. Longer average life could be obtained when we applied the RASS algorithm along with the ordering improvement. The simulation results are tabulated in Table 7.5. This table shows the impact of WSN operating parameters of sensors life.

Parameters	Sensor Life (Days)
Full Time (No Sleep Schedule)	5.50
Recourse Aware Sleep Schedule Algorithm (No Ordering)	23.90
Recourse Aware Sleep Schedule Algorithm (With Ordering)	34.25
RASS with Ordering at P50%	68.50
RASS with Ordering at P28%	122.30

Table 7.5: Impact of WSN operating parameters of sensors life

As it was demonstrated in the previous Sections, when the sensors in the WSN have information about the mine wireless channel characteristics (i.e. the K factor of the channel), they can adjust their transmit RF power to an optimized level that meets the BER and link performance requirements. It is simulated that when the transmitted power was reduced to 28%, the sensor's life can increase up to 122.3 days from a single battery charge. This is a case when the sensors are in an area in the mine where LOS is available and it is operating in a less multi-path environment (i.e. Rician fading channel with higher K factor). The simulation results of operating the WSN in different configuration scenarios are shown in Figure 7.24.

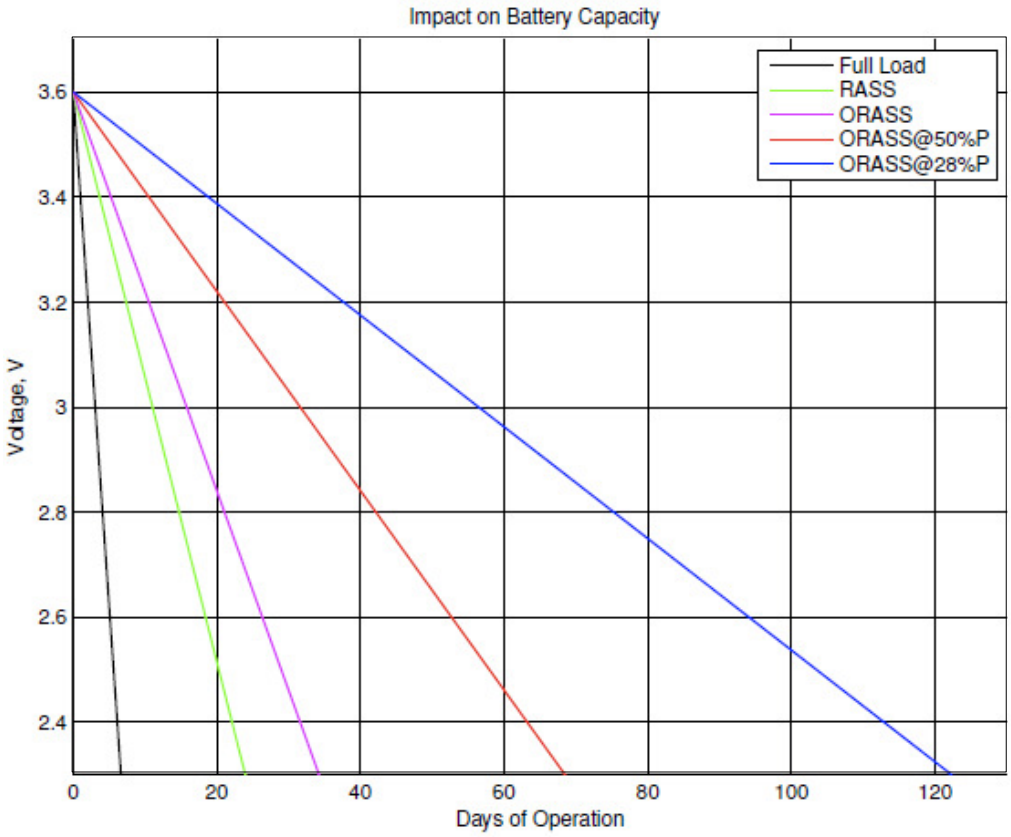

Figure 7.24: RASSA impact on prolonging the battery life of the sensors

7.10 Summary

In this Chapter we have presented a novel approach for deploying WSN in the mines. The proposed algorithm, RASSA, offered solutions for efficient WSN deployments that are optimized for power efficiency, scalability and rapid development of applications. The RASSA algorithm presented a new approach of Cross-Layer architecture where sensors in the WSN can be rapidly configured to provide new applications by composing a number of available functions provided by groups of sensors in WSN of the mine. Sensors' functions such as data processing functions, time synchronization functions, wireless characterization functions, node localization functions and data aggregation functions can be composed to a number of applications that can adaptively change to suit the operational requirements of the mine.

It was demonstrated in this Chapter that wireless sensors in the mine could utilize the proposed "Mine Segmenting Wireless Channel Model" to estimate their environmental locations with respect to reflections, scatterings and other multi-path phenomena. Therefore, further optimization could be obtained while maintaining acceptable performance characteristics.

The effectiveness of the RASSA algorithm in generating an optimized sleep schedule was compared to a bench mark solution generated by advanced optimization software called AIMMS. It was concluded that the sleep schedule of the algorithm was optimized with very small relative error. It was also demonstrated that the RASSA algorithm could guarantee the availability of an adequate number of active sensors in the cluster of the WSN where the application composition is required.

The RASSA algorithm was further optimized by providing an ordering scheme for the sleep schedule. This scheme offered optimized power-up consumption where the sensors in the WSN are switched less frequently from the sleep to the active modes. It was also demonstrated that further power minimization can be obtained when the sensors have information about the mine's wireless channel characteristics (i.e. the K factor of the channel). Therefore, they can adjust their transmit RF power to an optimized level, which meets the BER and link performance requirements.

Chapter 8

8. Conclusions and Future Work

The communication networks in underground mines can be a very complicated structure made of a number of elements that are required to interact. For comprehensive enhanced performance, the entire network needed to be optimized for improved reliability, scalability and efficient power utilization. The following Sections height a few conclusions determined by this research.

8.1 New Optimized Self-Organized Backbone Network in Underground Mines

It was demonstrated that algorithm, PAEA, could enhance the stability and scalability of the backbone networks in the mines. In particular the backbone network was optimized within the overall scheme of the Self-Organized Network (SON) in two stages. These are the Network Self Recognition (NSR), where the network could discover its own parameters, and Network Self Configuration (NSC), where the network optimized its performance by adjusting the network parameters and configurations.

It was concluded from the simulation analyses that the PAEA algorithm could align the system and produces the proper gain and slope for each amplifier in both directions of the communication. It was also concluded that the PAEA algorithm could produce certain amounts of errors that affect the output of the algorithm. Three types of errors were identified as factors potentially affecting the accuracy of the algorithms in calculating and predicting the gains and slopes of the amplifiers in the system. It was demonstrated through the errors analyses that our suggested remedies and modifications have mitigated the effects of errors in the system.

For the first type of error analysis called, “Pilot’s Levels Precision Errors (LPE),” it was concluded that the proposed averaging technique in the PAEA algorithm could produce accurate

results averaging the pilots' level and therefore provide precise inputs to the algorithm. An ideal number of samples could be determined. The simulation analysis showed an ideal number of N = 20 samples where the precision of the pilot level reached a limit of a little or no further improvements.

The second type of error that was analyzed is the Components Tolerance Errors (CTE). It was concluded that this type of error could affect the performance of the algorithm in generating adequate equalization parameters that ultimately could result in gain accumulations and system instability. It was concluded from the simulation analyses that systematic corrections of up to 100% could be obtained when utilizing the algorithm's suggested correction scheme.

The third type of error that was analyzed is the Gain Estimation Errors (GEE). This is the error that the algorithm can produce when predicating the equalization parameters in the upstream direction of the mine's network. It was concluded from the simulation analyses that the proposed correction schemes could enhance the operation of the algorithm to ensure the required level of system stability is provided.

The proposed algorithm was prototyped with a hardware system and software applications. It was concluded from the system test in the lab that the algorithm could accurately respond to any variation in the network and could produce the required equalization parameters for the network stability and scalability. Furthermore, the algorithm was also tested in a real mine environment in NORCAT Mine, Sudbury, Ontario, Canada. From the comparison tests and analyses, it was determined that the PAEA algorithm could be used effectively to enhance the stability and scalability of the mines' backbone networks.

8.2 New Optimized Power-Aware Algorithm for Green Communication in Mines

It was concluded that the definition of green communication in underground mines requires further expansion. Within mines, the permissible amount of power must be minimized to levels that ensure safe operation, especially in the areas where gases are present that could be ignited from sparks caused by high power signals in the networks. It was demonstrated that our proposed algorithm, PACSA, could improve the utilization of power by the network in the mine. This

optimization has considered the need for operating the networks with a minimum amount of power to ensure safe power distribution in addition to providing power savings and reduced cost.

It was concluded that the proposed algorithm, PACSA, could generate charging schedules that are optimized for minimum duration of T. A Global Satisfaction Ratio of 100% could be obtained to fully satisfy the power demand of the network given the limitations and constraints of power availability. It was also concluded that the proposed ordering scheme could offer further improvement to the PACSA algorithm by optimizing the number of switches between the active and sleep modes during the power delivery cycle. Ultimately, this ordering scheme results in more effective power utilization and longer battery life in the network's units.

When the effect of the number of devices in the network on the length of T was analyzed, it was concluded that the larger the network, the longer it takes to satisfy the network power requirements. It was also concluded that the average duration of the optimized Time-Cycle of the sleep schedule decreases when the amount of the permissible power in the network, P_{MAX} , increases. Therefore, there is a trade-off between the allowed amount of P_{MAX} and the acceptable duration of the sleep schedule to keep the network operative continuously.

8.3 Novel Mine Segmenting Wireless Channel Model

For reliable wireless communication in an underground mine, the channel predictions are crucial in optimizing the performance of the networks. Although there are several channel prediction techniques, most of these approaches are very difficult and time consuming. Our proposed "Mine Segmenting Wireless Channels Model" has demonstrated a generalized approach that can be applied in any underground mine, regardless of the mine's topology. In this model, we could divide the general areas of a mine into a number of segments. Each of these segments has different wireless channel characteristics that we could combine statistically into a unified model.

It was concluded when utilizing the probability of bit error (p_e) to indicate the performance of different modulation techniques associated with each 802.11b that the wireless channels in different segments of the mine had unique and different characteristics that affected the performance in these areas accordingly. It was also concluded that when changing the K factor in the model from one extreme to the other, (such as K=0 to K=20), the representation of the fading

channels was also changing from the extreme Rayleigh fading channel to the extreme of the Rician fading channel.

From the simulation analyses, we could determine the effects of the mine's environment and layout on the performance communication links of the wireless network. It was demonstrated that the transitions in the statistical models could be mapped to the mine's topology in moving from one area of NLOS to areas of PLOS and finally to areas with LOS. The model was evaluated in a real underground mine (NORCAT Mine, Sudbury, Ontario, Canada). The filed test results showed very similar outcomes when compared to the model simulation.

8.4 Proposed Adaptive Resources-Aware Scheme for Sleep Schedule Optimizations

The proposed algorithm, RASSA, demonstrated effective outcomes in optimizing the performance of the WSN in mines. Notably, the power efficiency, scalability and rapid application developments aspects were offered by this optimized algorithm. It was demonstrated that wireless sensors in the mine could utilize the proposed "Mine Segmenting Wireless Channel Model" to estimate their environmental locations with respect to reflections, scatterings and other multi-path phenomena. Therefore, further optimization could be obtained while maintaining acceptable performance characteristics.

The simulation results presented the effectiveness of the developed algorithm, RASSA, in generating an optimized sleep schedule that guarantees the availability of an adequate number of active sensors in the cluster of the WSN where the application composition is required.

The effectiveness of the optimized algorithm was compared to a bench mark solution generated by advanced optimization software called AIMMS. It was noted in our proposed algorithm that Average Relative Error decreases when the number of time slots increases. In other words, when T is small, the optimal solution is also small. Thus, a small difference leads to a large relative error.

When the effect of increasing the number of sensors in the WSN was analyzed, it was concluded that it caused the loads of the sensors to decrease. More sensors mean that each of them needs to work less. It was also concluded that when the number of required services increases, the average

sensor load also increases. This occurs because more sensors are required in the active mode to accommodate the requirements of the applications-compositions. Therefore the power consumption will increase for each sensor in the WSN.

During the simulation of the ordering algorithm, it has been observed that the power-up energy increases linearly when increasing the time slots. However, the increase in the power-up consumption is much less when applying the ordering algorithm.

The simulation analyses have demonstrated that when the sensors have information about the mine wireless channel characteristics (i.e. the K factor of the channel), they can adjust their transmit RF power to an optimized level, which meets the BER and link performance requirements. It is simulated that when the transmission power was reduced to 28% of full load, the sensor's life can increase up to 122.3 days compared to only 5.5 days when the algorithm is not utilized.

8.5 Future Work

Some of the suggested future work is listed below.

- PAEA Algorithm: PAEA can be further improved by considering the approach of part-time equalization. Through this approach the equalization pilots can be scheduled in part-time bases. Therefore, the carriers of the reference pilots might not need to be present in the system all the time. Instead, the pilots will be available only when needed by the amplifier circuit. This will help to maximize the channel capacity of the system and to reduce the power consumption of the amplifiers when the equalization is not needed.

- PACSA Algorithm: To validate the performance of PACSA, the algorithm can be prototyped in hardware. This will allow the test of the proposed scheme in a real mine environment. Test data can be collected and compared with the simulation analyses results.

- Wireless Channels Model: The Mine Segmenting Wireless Channel Model can be further expanded by considering different Probability Density Functions. The model can also be tested over large areas and in different mine layouts to validate its comprehensiveness.

- RASSA Algorithm: The RASSA algorithm can be improved further by considering other constraints such as sensing coverage range, delay efficiency, and network connectivity. The algorithm can also be prototyped to validate its operation over a longer time and under different conditions.

9. Appendix A: Patents and Publications

- W. Farjow, and X. Fernando, "System and Method to Control Amplifier Gain in a Radiating Line Communication System," *Canadian patent*, serial number 2789768, September 2012.

- W. Farjow, X. Fernando, A. Chehri, and H. Mouftah, " An Energy-Efficient Routing Protocol for Wireless Sensor Networks through Non-Linear Optimization," *Proceedings of the 3rd IEEE ICWCUCA for Underground Mines Communications Conference*, Clermont, France, 28-30 August 2012.

- W. Farjow, X. Fernando, and K. Raahemifar, "Mine Segmenting Wireless Channel Model," *IEEE Transactions on Consumer Electronics*, submitted, October 2012.

- A. Chehri, H. Mouftah, W. Farjow, and X. Fernando, "A Joint Power and Rate Allocation Algorithm for Wireless Sensor Networks," *Elsevier Journal of Computer Communications*, submitted, July 2012.

- W. Farjow, and X. Fernando, "Wireless Sensor Networks in Underground Mines," *World Coal Journal* , Volume 21 number 2, February 2012.

- A. Chehri, M. Hussein, and W. Farjow, "Indoor Cooperative Positioning Based on Fingerprinting and Support Vector Machines," *Book Chapter, in Mobile and Ubiquitous Systems: Computing, Networking, and Services,* editors: Ozgur Akan, Volume 73, 2012, *pp. 114-124*, June 2012.

- W. Farjow, A. Chehri, H. Mouftah, and X. Fernando, "Support Vector Machines for Indoor Sensor Node Localization," *Proceedings of the IEEE Wireless Communications & Networking Conference*, *pp. 779-783*, Cancun, Mexico, March 2011.

- W. Farjow, A. Chehri, H. Mouftah, and X. Fernando, "Design of Wireless Sensor Network for Mine Safety Monitoring," *Proceedings of the IEEE CCECE / CCGÉI 2011, pp 1532-1535*, Niagara Falls, Ontario, May 2011.

- W. Farjow, and X. Fernando, "Post Disaster Underground Communications," *Proceedings of the Third International Tunnel Safety Forum, pp. 165-173,* Nice, France, April 2011.

□ W. Farjow, A. Chehri, H. Mouftah, and X. Fernando, "An Empirical Link-Quality Analysis for Wireless Sensor Networks," *Proceedings of the IEEE International Conference on Distributed Computing in Sensor Systems (IEEE DCOSS '11)*, Barcelona, Spain, June 2011.

□ K. Krishanth, T. Kirubarajan1, and X. Fernando, W. Farjow, "Destination Prediction for Localizing Underground Miners," *Proceedings of the annual IEEE International Symposium on Personal, Indoor and Mobile Radio Communications (PIMRC),* Toronto, Ontario, Canada, September 2011.

□ M. Daoud ,W. Farjow, and X. Fernando, " A Novel Diagnostic System for Adding Reliability to Communication Networks in Underground Mines," *Proceedings of the IEEE CCECE / CCGÉI 2011, pp. 1342-1346*, Niagara Falls, Ontario, May 2011.

□ W. Farjow, M. Daoud, and X. Fernando, "Diagnostic System with Ventilation on Demand for Underground Mines," *Proceedings of the SARNOFF 2011: 34th IEEE Sarnoff Symposium,* Princeton, USA, May 2011.

□ W. Farjow, and X. Fernando, "Transmitting Radio Signals through the Earth," *Proceedings of the World Tunnel Conference - 36 General Assembly* , Vancouver, Canada, May 2010.

□ A. Chehri, W. Farjow, H. Mouftah, and X. Fernando, "Link-Quality Measurement and Reporting in Wireless Sensor Networks," *Proceedings of the 2nd ICST International Conference on Sensor Systems, Sensor Systems and Software*, Miami, FL. USA, December 2010.

□ A. Chehri, H. Mouftah, and W. Farjow, "Indoor Cooperative Positioning based on Fingerprinting and Support Vector Machines," *Proceedings of the 7th ICST International Conference on Mobile and Ubiquitous Systems: Computing, Networking and Services*, Sydney, Australia , 6-9 December 2010.

□ W. Farjow, and X. Fernando, "Technological Advancements for Safety in Confined Spaces," *Proceedings of the Mining Magazine Congress,* Niagara Falls, Ontario, Canada, October 2009.

10. References

[1] W. Farjow and X. Fernando, "Transmitting Radio Signals through the Earth," *Proceedings of the World Tunnel Conference - 36 General Assembly* , Vancouver, Canada, May 2010.

[2] W. Farjow and X. Fernando, "Technological Advancements for Safety in Confined Spaces," *Proceedings of the Mining Magazine Congress,* Niagara Falls, Ontario, Canada, October 2009.

[3] W. Farjow, and X. Fernando, "Post Disaster Underground Communications," *Proceedings of the Third International Tunnel Safety Forum, pp. 165-173*, Nice, France, April 2011.

[4] W. Farjow, A. Chehri, H. Mouftah, and X. Fernando, "An Empirical Link-Quality Analysis for Wireless Sensor Networks," *Proceedings of the IEEE International Conference on Distributed Computing in Sensor Systems (IEEE DCOSS '11)*, Barcelona, Spain, June 2011.

[5] A. Abdi, C. Tepedelenlioglu, M. Kaveh, and G.Giannakis, "On the estimation of the K parameter for the Rice fading distribution," *IEEE Communications Letters*, p. 92 -94 , March 2003.

[6] W. Farjow, X. Fernando, A. Chehri, and H. Mouftah, " An Energy-Efficient Routing Protocol for Wireless Sensor Networks through Non-Linear Optimization," *Proceedings of the 3rd IEEE ICWCUCA for Underground Mines Communications Conference*, Clermont, France, 28-30 August 2012.

[7] Z. Sun, and F. Akyildiz, "Modeling and Analysis for Wireless Networks in Underground Mines and Road Tunnels," *IEEE Transaction on Communications, VOL. 58, NO. 6*, June 2010.

[8] Y. Hwang, Y. Zhang, and R. Kouyoumjian, "Ray-optical prediction of radio-wave propagation characteristics in tunnel environments: theory, analysis and measurements," *IEEE Transaction on Antenna and Propagations*, vol. 46, no. 9, pp. 1328-1345, September 1998.

[9] Y. Zhang, and H. Hong, "Ray-optical modeling of simulcast radio propagation channels in tunnels," *IEEE Transaction on Vehicular Technology*, vol. 53, no. 6, pp. 1800-1808, November 2004.

[10] S. Zhang, "The multipath propagation model of rectangular tunnel channel," *Proceedings IEEE 10 Annual International Conference TENCON 2002, vol. 2, pp. 1016-1019*, October 2002.

[11] Y. Zhang, "Novel model for propagation loss prediction in tunnels," *IEEE Transaction on Vehicular Technology*, vol. 52, no. 5, pp. 1308-1314, September 2003.

[12] I. Akyildiz, Z. Sun, and M. Vuran, "Signal propagation techniques for wireless underground communication networks," *IEEE Transaction on Physical communication, vol.2 iss.3 pg.167 - 183,* 2009.

[13] M. Asif, Y. Zeng, B. Memari, H. Ahmad, and B. Honary, "A Ray-Tracing Technique for Ultra Wideband Channel Modelling," *10 th International Symposium on Communication Theory and Applications (ISCTA'09),* July 2009.

[14] G.Y. Delisle, "Propagation Characteristics for Modern Wireless System Networks in Underground Mine Galleries," *First IEEE International Workshop on Wireless Communication in Underground and Confined Area,* Val d'Or, QC, Canada, August 2005.

[15] A. Emslie, R. Lagace and P. Strong, "Theory of the propagation of UHF radio waves in coal mine tunnels," *IEEE Transaction on Antenna and Propagation, Vol. 23, pp. 192-205,* March 1975.

[16] Z. Sun, and I. Akyildiz, "Channel Modeling of Wireless Networks in Tunnels," *in Proceedings of IEEE Globecom 08*, New Orleans, USA, November 2008.

[17] Z. Sun, and I. Akyildiz, "Influences of Vehicles on Signal Propagation in Road Tunnels," *IEEE ICC 2010*, Cape Town, South Africa, May 2010.

[18] Y. P. Zhang, G. X. Zheng, and J. H. Sheng, "Radio propagation at 900 MHz in underground coal mines," *IEEE Transaction on Antennas Propagation., vol. 49, no. 5, pp. 757–762*, May 2001.

[19] L. K. Bandyopadhyay, S. K. Chaulya, and P. K. Mishra, "*Wireless Communication in Underground Mines: RFID-based Sensor Networking*," Springer Editions, 2009.

[20] H. Hettstedt, "Development and Applications of Leaky Feeders," *Reference papers RFS,* Hannover-Germany, May 2000.

[21] H. Hettstedt, and M. Davies "Coverage Evaluations In Tunnels Applying Radiating Cable," *Proceedings of the ITC Conference Amsterdam*, March 2002.

[22] A. Caraiola, H. G. Haag, Karl SchuPze-Buxloh and G. Thoennessen, "Leaky Coaxial Cable with Length Independent Antenna Receiving Level," *Proceedings of the RFS International Wire cable Symposium,* Hannover, Germany, June 1992.

[23] M. Daoud ,W. Farjow, and X. Fernando, " A Novel Diagnostic System for Adding Reliability to Communication Networks in Underground Mines," *Proceedings of the IEEE CCECE / CCGÉI 2011,* pp. 1342-1346, Niagara Falls, Ontario, May 2011.

[24] W. Farjow, M. Daoud, and X. Fernando, "Diagnostic System with Ventilation on Demand for Underground Mines," *Proceedings of the SARNOFF 2011: 34th IEEE Sarnoff Symposium,* Princeton, USA, May 2011.

[25] A. Chehri, W. Farjow, H. Mouftah, and X. Fernando, "Link-Quality Measurement and Reporting in Wireless Sensor Networks," *Proceedings of the 2nd ICST International Conference on Sensor Systems, Sensor Systems and Software*, Miami, FL. USA, December 2010.

[26] Z. Zheng, "*Research Challenges Involving Cross-layered Communication Protocol Design for Underground WSN,*" Institute of Intelligent Information Processing, Guizhou Normal University, Guiyang, China, August 2010.

[27] W. Farjow, A. Chehri, H. Mouftah, and X. Fernando, "Support Vector Machines for Indoor Sensor Node Localization," *Proceedings of the IEEE Wireless Communications & Networking Conference*, Cancun, pp. 779-783, Mexico, March 2011.

[28] W. Farjow, A. Chehri, H. Mouftah, and X. Fernando, "Design of Wireless Sensor Network for Mine Safety Monitoring," *Proceedings of the IEEE CCECE / CCGÉI 2011,* pp.1532-1535, Niagara Falls, Ontario, May 2011.

[29] G. Samakovitis, "Impact of Mobility in Ad Hoc Protocol Design," *World Congress on Computer Science and Information Engineering,* Athens, June 2009.

[30] A. Qaimkhani, and E. Hossain, "Contention-free approaches for WiFi MAC design for VoIP services: performance analysis and comparison," *Proceedings of the International Conference on Wireless Communications and Mobile Computing*, IWCMC 2009, Leipzig, Germany, June 2009.

[31] K. Krishanth, T. Kirubarajan1, X. Fernando, and W. Farjow, "Destination Prediction for Localizing Underground Miners," *Proceedings of the annual IEEE International Symposium on Personal, Indoor and Mobile Radio Communications (PIMRC),* Toronto, Ontario, Canada, September 2011.

[32] A. Chehri, P. Fortier, and P.-M. Tardif, "Application of Ad-hoc sensor networks for localization in underground mines," *IEEE Wireless and Microwave Technology Conference, 2006. WAMICON '06, pp. 1-4*, December 2006.

[33] A. Chehri, M. Hussein, and W. Farjow, "Indoor Cooperative Positioning Based on Fingerprinting and Support Vector Machines," *Book Chapter, in Mobile and Ubiquitous Systems: Computing, Networking, and Services,* editors: Ozgur Akan, Volume 73, 2012, pp 114-124, June 2012.

[34] A. Chehri, H. Mouftah, and W. Farjow, "Indoor Cooperative Positioning based on Fingerprinting and Support Vector Machines," *Proceedings of the 7th ICST International Conference on Mobile and Ubiquitous Systems: Computing, Networking and Services*, Sydney, Australia , 6-9 December 2010.

[35] L. K. Bandyopadhyay, S. K. Chaulya and P. K. Mishra, "Wireless Communication In Underground Mines: RFID-Based Sensor Networking," *Springer*, ISBN: 978-0-387-98164-2 September 2009.

[36] M. Boutin, A. Benzakour, and C. Despins, "Radio Wave Characterization and Modeling in Underground Mine Tunnels," *Proceedings of the IEEE Transactions on Antennas and Propagation, Vol. 56, No. 2, pp. 540- 549*, February 2008.

[37] D.Niculescu and B.Nath, "Error Characteristics of Ad Hoc Positionning Systems (APS)," *MobiHoc'04*, May 2004.

[38] B. Krishnamachari, "Networking Wireless Sensors," *Cambridge University Press*, ISBN-13 978-0-521-83847-4 , United Kingdom, 2005.

[39] Y. Yu, B. Krishnamachari, and V. K. Prasanna, "Issues in Designing Middleware for Wireless Sensor Networks," *IEEE Network Magazine*, Special Issue on Middleware Technologies for Future Communication Networks, p 18, January 2004.

[40] T. Rappaport, "*Wireless Communications, Principles and Practices,*" Second Edition, Prentice Hall PTR, ISBN 0-13-042232-0.

[41] T. Kaur and B. Jinsuk, "A strategic deployment and cluster-header selection for wireless sensor networks," *IEEE Transactions Consumer Electron.*, vol. 55, no. 4, pp. 1890-1897, November, 2009.

[42] S. Cui, A. J. Goldsmith and A. Bahai, "Energy-constrained modulation optimization," *IEEE Transactions on Wireless Communication*, Vol.4, no. 5, pp. 2349-2360, September 2005.

[43] A. Chehri, H. Mouftah, W. Farjow, and X. Fernando, "A Joint Power and Rate Allocation Algorithm for Wireless Sensor Networks," *Elsevier Journal of Computer Communications*, submitted, July 2012.

[44] C. Schurgers, V. Tsiatsis, S. Ganeriwal and M. Srivastava, "Topology Management for Sensor Networks: Exploiting Latency and Density," *Proceedings of the of ACM Mobihoc*, Lausanne, Switzerland, 2002.

[45] Y. Xu, J. Heidemann and D. Estrin, "Geography-informed Energy Conservation for Ad Hoc Routing ," *Proceedings of MOBICOM 2001*, Rome, Italy, May 2001.

[46] K. Xu, H Hassanein, and G. Takahara, "Relay node deployment strategies in heterogeneous wireless sensor networks: multi-hop communication case," *IEEE Communications Society Conference on Sensors and Ad Hoc Communications, pp. 575-585,* September 2005.

[47] K. Xu, H. Hassanein, G. Takahara, and Q. Wang, "Relay node deployment strategies in heterogeneous wireless sensor networks," *IEEE Transactions on Mobile Computing, Vol. 9, No. 2, pp. 145-159,* February 2010.

[48] W. Farjow, and X. Fernando, "Wireless Sensor Networks in Underground Mines," *World Coal Journal* , Volume 21 number 2, February 2012

[49] K. Akkaya and M. Younis, "A survey on routing protocols for wireless sensor networks," *Ad Hoc Networks (Elsevier)*, Vol. 3, pp. 325-349, 2005.

[50] S. Dulman, T. Nieberg, J. Wu and P. Havinga, "Trade-off between Traffic Overhead and Reliability in Multipath Routing for Wireless Sensor Networks," *WCNC Workshops, New Orleans, Louisiana,* USA, March 2003.

[51] W. Farjow and X. Fernando, "System and Method to Control Amplifier Gain in a Radiating Line Communication System," *Canadian patent*, serial number 2789768, September 2012.

[52] J.D. Brown, J. Abouei, "Adaptive demodulation in differentially coherent phase systems: Design and performance analysis," *IEEE Transactions on Communications, Volume 59, Issue 7, Article number 5772067, Pages 1772-1778*, July 2011.

[53] W. Farjow, X. Fernando, and K. Raahemifar, "Mine Segmenting Wireless Channel Model," *IEEE Transactions on Consumer Electronics*, submitted, October 2012.

[54] P. Mahasukhon, and M. Hempel, "BER Analysis of 802.11b Networks under Mobility," *Proceedings of the USAICC*, Lincoln, NE,USA 2007.

[55] S.Qu, and Y. Xin, "Distribution of SNR and error probability of a two-hop relay link in Rayleigh fading," *IEEE 70th Vehicular Technology Conference*, Anchorage, Alaska, USA, September 2009.

[56] S. Datta, "Performance analysis of distributed selection combining with dual-hop relay link in Rayleigh fading channel," *IEEE International Conference on Communication* Systems, Singapore 17-19 November 2010.

[57] R. Ha, P. Ho, and X.S. Shen, "SS-Trees: A Cross-Layer Organizational Approach for Mesh-Based Wide-Area Wireless Sensor Networks," *Proceedings of the IEEE Int'l Conf. Broadband Networks (BroadNets), pp. 885-894*, October 2005.

[58] J. Jin and K. Nahrstedt, "Source-Based QoS Service Routing in Distributed Service Networks," *Proceedings of the IEEE Int'l Conf. Comm., pp. 20-24,* June 2004.

[59] J. Ma, W. Lou, Y. Wu, X. Li, and G. Chen, "Energy Efficient TDMA Sleep Scheduling in Wireless Sensor Networks," *Proceedings of the IEEE INFOCOM*, June 2009.

[60] K. Kredo and P. Mohapatra, "Medium access control in wireless sensor networks," *The International Journal of Computer and Telecommunications Networking*, Vol. 51, Issue 4, pp. 961-994, March 2007.

[61] B. Krishnamachari, Y. Mourtada, and S. Wicker, "The energy-robustness tradeoff for routing in wireless sensor networks," *Proceedings of the IEEE ICC, Vol. 3 , pp. 1833-1837*, May 2003.

[62] J. Liu, and F. Zhao, "Towards Semantic Services for Sensor-Rich Information Systems," *Proceedings of the Second IEEE/CreateNet Int'l Workshop Broadband Advanced Sensor Networks*, Boston, MA, October 2005.

[63] X. Chu and R. Buyya, "Service Oriented Sensor Web, Sensor Network and Configuration: Fundamentals, Techniques, Platforms, and Applications," *N.P. Mahalik, Springer-Verlag*, 2006.

[64] J.Wang, and D. Li, "Cross-Layer Sleep Scheduling Design in Service-Oriented Wireless Sensor Networks," *IEEE Transactions on Mobile, VOL. 9, NO. 11,* November 2010.

[65] O. Tremblay and A. Louis "Dessaint Experimental Validation of a Battery Dynamic Model for EV Applications," World Electric Vehicle Journal Vol. 3 , issue 1, 2009.

[66] C. Behrens, O. Bischoff, M. Lueders, and R. Laur , "Energy-efficient topology control for wireless sensor networks using online battery monitoring," *Advances in Radio Science, pp. 205-208* ,2007.